Dosimetry studies for brachytherapy sources

By

Sridhar Sahoo

HLTH 09 2011 04 004

Tata Memorial Centre, Mumbai

A thesis submitted to the

Board of Studies in Health Sciences

In partial fulfillment of requirements

for the Degree of

DOCTOR OF PHILOSOPHY

of

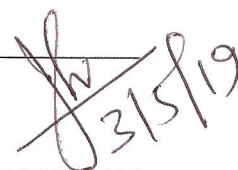**HOMI BHABHA NATIONAL INSTITUTE**

August, 2018

Homi Bhabha National Institute[1]

Recommendations of the Viva Voce Committee

As members of the Viva Voce Committee, we certify that we have read the dissertation prepared by Sridhar Sahoo entitled "Dosimetry studies for brachytherapy sources" and recommend that it may be accepted as fulfilling the thesis requirement for the award of Degree of Doctor of Philosophy.
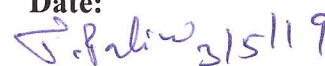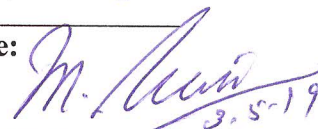
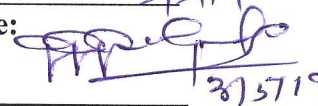|	
Chairman - Dr. J. P. Agarwal	**Date:** 3/5/19
Guide / Convener - Dr. T. Palani Selvam	**Date:** 3/5/19
Examiner - Dr. M. Ravikumar	**Date:** 3.5.19
Member 1- Dr. S. D. Sharma	**Date:** 3/5/19
Member 2- Dr. D. D. Deshpande	**Date:** 3/5/19
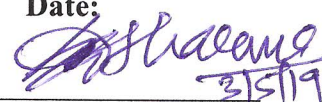
Final approval and acceptance of this thesis is contingent upon the candidate's submission of the final copies of the thesis to HBNI.

I/We hereby certify that I/we have read this thesis prepared under my/our direction and recommend that it may be accepted as fulfilling the thesis requirement.

Date: 3/5/19

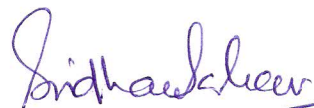**Place: Mumbai, India**

(Dr. T. Palani Selvam)

Guide

---

[1] This page is to be included only for final submission after successful completion of viva voce.

Version approved during the meeting of Standing Committee of Deans held during 29-30 Nov 2013

STATEMENT BY AUTHOR

This dissertation has been submitted in partial fulfillment of requirements for an advanced degree at Homi Bhabha National Institute (HBNI) and is deposited in the Library to be made available to borrowers under rules of the HBNI.

Brief quotations from this dissertation are allowable without special permission, provided that accurate acknowledgement of source is made. Requests for permission for extended quotation from or reproduction of this manuscript in whole or in part may be granted by the Competent Authority of HBNI when in his or her judgment the proposed use of the material is in the interests of scholarship. In all other instances, however, permission must be obtained from the author.

(Sridhar Sahoo)

DECLARATION

I, hereby declare that the investigation presented in the thesis has been carried out by me. The work is original and has not been submitted earlier as a whole or in part for a degree / diploma at this or any other Institution / University.
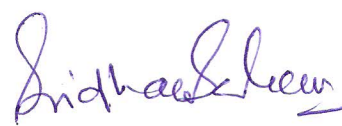
(Sridhar Sahoo)

Version approved during the meeting of Standing Committee of Deans held during 29-30 Nov 2013

CERTIFICATION ON ACADEMIC INTEGRITY
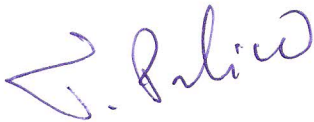
1. I, Sridhar Sahoo, HBNI Enrolment No. **HLTH 09 2011 04 004** hereby undertake that, the Thesis titled **"Dosimetry studies for brachytherapy sources"** is prepared by me and is the original work undertaken by me and free of any plagiarism. The document has been duly checked through a plagiarism detection tool and the document is plagiarism free.

2. I am aware and undertake that if plagiarism is detected in my thesis at any stage in future, suitable penalty will be imposed as per the applicable guidelines of the Institute/UGC.

(Sridhar Sahoo)

Signature of the Student

(with date)

Endorsed by the PhD Supervisor

(I certify that the work done by the Researcher is plagiarism free)

Signature:

Name: Dr. T. Palani Selvam

Designation: Associate Professor, HBNI

Department/Centre: RP&AD, BARC

Name of the CI/OCC: TMC

List of Publications arising from the thesis

Journal

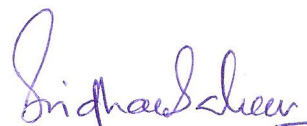1. "Dosimetry of indigenously developed ^{177}Lu patch source for surface brachytherapy - Experimental and Monte Carlo methods", **Sridhar Sahoo**, Vandana Srivastava, T Palani Selvam, A K Bakshi, Rajesh Kumar, Rama P, D Datta, Chinnaesakki S, Saxena S K, Yogendra Kumar and A Dash, *Journal of Radiological Protection,* **2019***, 39,* 54-70.

2. "Dosimetry of indigenously developed ^{192}Ir HDR brachytherapy source - An EGSnrc Monte Carlo study", **Sridhar Sahoo**, T. Palani Selvam, S. D. Sharma, Trupti Das, A. C. Dey, B. N. Patil and K. V. S. Shastry, *Journal of Medical Physics*, **2016**, *41,*115-122.

3. "Monte Carlo-based dose calculation for ^{32}P patch source for superficial brachytherapy applications" **Sridhar Sahoo,** T. Palani Selvam, S. K. Saxena, D. A. R. Babu, A. Dash, *Journal of Medical Physics*, **2015**, *40,* 13-17.

4. "Comment on "Design and bioevaluation of a ^{32}P-patch for brachytherapy of skin diseases" [Appl. Radiat. Iso. 66 (2008) 303-309]", **Sridhar Sahoo**, T. Palani Selvam, *Applied Radiation and Isotopes*, **2014**, *91*, 62-63.

Conferences

1. "Calibration of EBT films for its use at ^{125}I energies", **Sridhar Sahoo**, Vandana S, Rajesh Kumar, T. Palani Selvam, Sunil Singh and D. Datta. *Journal of Medical Physics*, **2018**, *Vol 43, Supplement 1, Page S82-83 (Proceedings of 39th Annual conference of the Association of Medical Physicists of India (AMPI), 2018).*

2. "The response of well chamber to pressure variations at high altitudes - A Monte Carlo study for ^{169}Yb source", **Sridhar Sahoo**, T. Palani Selvam, Arghya Chattaraj, D. Datta, *Proceedings of 17thAsia Oceania Congress of Medical Physics (AOCMP)and 38th Annual Conference of Association of Medical Physicists of India (AMPI),* **2017**, *42,* s200-201.

3. "Beta-gamma spectrometry of indigenously developed ^{177}Lu patch source for superficial brachytherapy", **Sridhar Sahoo**, T. Palani Selvam, Rahul Tripathi, Rama P., Gupta A. M., Saxena S. K. and Yogendra Kumar, *Proceedings of 32nd International conference of Indian Association for Radiation Protection,* **2016**, *Page-155.*

4. "Dosimetry of indigenous developed ^{169}Yb brachytherapy seed source", **Sridhar Sahoo**, T. Palani Selvam, S. K. Saxena and A. Dash, *Proceedings of 35th Annual conference of the Association of Medical Physicists of India,* **2014**, *39,* 305-306.

(Sridhar Sahoo)

Version approved during the meeting of Standing Committee of Deans held during 29-30 Nov 2013

DEDICATED TO

LORD JAGANNATH

&

MY FRIENDS AND WELL-WISHERS

ACKNOWLEDGEMENTS

CONTENTS

Chapter 2. Interaction of radiation with matter, Monte Carlo techniques and their applications in brachytherapy

Chapter 3. Dosimetry of indigenously developed ^{192}Ir HDR brachytherapy source

Chapter 4. Dosimetry of ^{32}P and ^{177}Lu patch sources used in superficial brachytherapy applications

Chapter 5. Dosimetry of indigenously developed ^{125}I source for intraocular tumours

Chapter 6. Dosimetry of ^{125}I and ^{131}Cs brachytherapy sources due to non-uniform scatter condition

Chapter 7. The response of well chamber to pressure variations at high altitudes for ^{131}Cs and ^{169}Yb sources using Monte Carlo simulation techniques

Chapter 8. Summary, conclusions and future scope

References

First page of publications

ABSTRACT

Brachytherapy is plays an important role in the treatment of gynaecologic cancers, oral cancers, sarcomas, breast and prostate cancers etc. The success of a brachytherapy depends on accurate dosimetry of sources and dose delivery. Dosimetry is the accurate calculation of the absorbed dose rate distribution in a medium, usually water, around the source which depends strongly on the geometry, material and medium around the source. American Association of Physicists in Medicine Task Group report (AAPM TG-43) recommended that dose distribution for individual brachytherapy sources should be made available in water medium and published in reviewed literature before its use.

BARC and BRIT play an important role on development of radiotherapy machine, sources and methodologies for their use in medicine. BARC / BRIT has developed a ^{192}Ir HDR source for indigenous Karknidon HDR machine; ^{125}I source (OcuProsta) for ocular and prostate cancers; ^{32}P and ^{177}Lu skin patch sources for skin applications.

The dosimetry parameters of the ^{192}Ir HDR source were generated using the EGSnrc Monte Carlo code and the results are compared with similar sources. These data are utilized for the development of the brachytherapy treatment planning software. Dose profiles of ^{32}P and ^{177}Lu patch sources were calculated using Monte Carlo code and compared with measurements. Dose parameters for ^{125}I source (single seed) and silver eye plaque embedded with 13 ^{125}I seeds were measured using EBT3 Gafchromic film. Dosimetry of ^{125}I and ^{131}Cs sources in non-uniform scatter condition was carried out. The response of Well chamber to pressure variations at high altitudes for ^{131}Cs and ^{169}Yb sources was studied using Monte Carlo simulation techniques.

SYNOPSIS

The modalities of cancer treatment are surgery, radiotherapy and chemotherapy. Radiotherapy is the use of ionizing radiation for the treatment of cancer. The goal of radiotherapy is to kill the cancer cells by delivering a prescribed dose to a tumour, and sparing the normal surrounding organs and tissues. Radiotherapy is classified in to external beam therapy and brachytherapy. In brachytherapy, sealed radioactive sources are placed directly into or near the tumour volume. Brachytherapy delivers a high radiation dose to the tumour keeping the dose to surrounding normal tissues to a minimum. In a radiotherapy department, about 10 - 20% of radiotherapy patients are treated using brachytherapy (Suntharalingam et al 2005). Brachytherapy has an important role in treating various tumours such as gynaecologic malignancies, oral cancers, sarcomas, breast and prostate cancers etc.

The clinical outcomes of the radiotherapy treatment depend on accurate dosimetry of individual sources and dose delivery. Dosimetry of a source strongly depends on its design, encapsulation material and the surrounding medium around the source. American Association of Physicists in Medicine (AAPM) Task Group report (TG-43 and TG-43U1) recommended that dose distribution and dosimetry parameters for individual brachytherapy sources should be made available in water medium and published in reviewed literature before its use (Nath et al 1995, Rivard et al 2004).

Bhabha Atomic Research Centre (BARC), India plays an important role on development of ^{60}Co-based radiotherapy treatment machine, radiation sources and methodologies for their use in medicine. BARC / BRIT has indigenously developed a ^{192}Ir HDR source for

Karknidon (Karknidon is an indigenously developed HDR treatment machine) for brachytherapy treatments. BARC has also developed: (a) ^{125}I source (Ocuprosta) for the treatment of ocular cancer and (b) ^{32}P and ^{177}Lu skin patch sources for the treatment of skin cancers.

Objectives of the work undertaken in this thesis are:

- Dosimetric study of HDR ^{192}Ir brachytherapy source indigenously developed by BARC / BRIT using Monte Carlo-based EGSnrc code system.

- Dosimetric study of indigenously developed ^{32}P and ^{177}Lu patch sources for skin applications.

- Dosimetry of indigenously developed ^{125}I source for intraocular tumours.

- Dosimetry of ^{125}I and ^{131}Cs brachytherapy sources due to non-uniform scatter condition.

- The response of Well chamber to pressure variations at high altitudes for ^{131}Cs and ^{169}Yb sources using Monte Carlo simulation techniques.

The thesis comprises of eight chapters as described below.

Chapter 1: Introduction to brachytherapy and literature survey

This chapter discusses classification of brachytherapy, sources used in brachytherapy, dosimetry methods followed in different eras, and dosimetry of various sources reported in literature involving experimental and Monte Carlo methods. Brachytherapy treatment involves the placement of radioactive sources directly into or near the tumour volume. It

is classified into six categories: Intracavitary, Interstitial, Superficial, Intraluminal, Intraoperative and Intravascular brachytherapy.

High dose rate (HDR) remote afterloading is a widely accepted technology, where high activity ^{192}Ir or ^{60}Co source is automatically loaded in to the patient by a computer-controlled device. This technology reduces exposure to hospital personnel, high dose delivered in short time and more important is comfort to patient (Das and Thomadsen 2005). A lot of clinical results have been published in terms of survival rates, early and late tissue complication rates which prove HDR as an acceptable treatment modality. Brachytherapy procedures today are performed in one-day without the need for hospitalization. It is a very cost effective and patient friendly procedure compared to teletherapy. Low energy and short half-life radionuclides such as ^{125}I and ^{103}Pd are used for permanent implants for prostate cancer.

Radiation dosimetry is the quantitative determination of energy deposited or the dose rate at a point in a given medium, usually water. It is measured using detectors and calculated using empirical dose-calculation formalism. Since, the absorbed dose strongly depends on source strength, it is essential that source strength should be accurately determined.

In the past, the strength of a source was specified in terms of the apparent activity, the milligram radium equivalence, exposure rate constant, gamma ray constant etc. There are always some amount uncertainties due to use of certain correction factors. Hence, they are no longer recommended quantities for dosimetry. Brachytherapy dosimetry based on Sievert integral formula was found to be accurate enough for ^{137}Cs tubes, but fail to

provide dosimetric accuracy to the acceptable level for ^{192}Ir and low-energy sources (Williamson et al 1983, Williamson 1996).

In the modern era, the above semi-empirical models have been replaced by Monte Carlo techniques and measurements. As per the recommendations given in AAPM TG-43 and TG-43U1 report (Nath et al 1995, Rivard et al 2004), the dosimetry parameters around each source model should be determined by both experimental and Monte Carlo-based radiation transport calculations and published in the peer-reviewed literature before using in routine clinical practice.

Chapter 2: Interaction of radiation with matter, Monte Carlo techniques and their applications in brachytherapy

This chapter discusses interaction of photons and electrons with matter, Monte Carlo techniques and their application in brachytherapy dosimetry. Monte Carlo technique is a random sampling technique to simulate statistical processes. Simulation begins with the exact description of the medium, geometry and sources and the accuracy depends on the precise modelling of the problem, cross-sections and number of particles simulated. There are several Monte Carlo codes such as MCNP, EGSnrc, GEANT4 and FLUKA which are available for dosimetry studies in medical physics. Monte Carlo methods have found extensive use in brachytherapy radiation dosimetry, due to difficulties and complications involved in direct measurement near the sources.

High Energy Brachytherapy Source Dosimetry (HEBD) Working Group of AAPM and the European Society for Radiotherapy and Oncology (ESTRO) recommended methods

for evaluating consensus dosimetry datasets for high-energy photon sources with average energy higher than 50 keV (Perez-Calatayud et al 2012). Recommendations include choice of detectors, phantom materials, phantom size and grid size and the guidelines given in the TG-43U1 report for low-energy brachytherapy sources (Rivard et al 2004).

Chapter 3: Dosimetry of indigenously developed ^{192}Ir HDR brachytherapy source

The clinical use of new sources requires generation of extensive, accurate dosimetry data using computational and experimental methods. The Monte Carlo techniques can significantly reduce the experimental uncertainties, provide the required accuracy and the desired precision in the dosimetry data. Several HDR ^{192}Ir sources such as microSelectron, BEBIG, VariSource, Flexisource are used worldwide. These sources are different in geometry, encapsulation dimensions as well as structural details.

Board of Radiation & Isotope Technology (BRIT) and BARC, India, developed a ^{192}Ir HDR source for remote afterloading HDR machine (Karknidon). The dosimetry parameters of this source were generated using Monte Carlo-based EGSnrc code system (Kawrakow et al 2013) in a 40 cm diameter x 40 cm height cylindrical water phantom. The calculated value of air-kerma strength per unit activity for BRIT HDR source is 9.894×10^{-8} U Bq^{-1}. The calculated value of dose rate constant (Λ) for BRIT HDR source is 1.112 cGy h^{-1} U^{-1}.

The AAPM and the ESTRO recommended that the dose rate should be computed in a liquid spherical water phantom of 80 cm diameter or (the equivalent cylindrical phantom) for ^{192}Ir, ^{137}Cs, and ^{169}Yb sources (Perez-Calatayud et al 2012). Simulations were carried

out to calculate radial dose function, $g_L(r)$ for BRIT HDR ^{192}Ir source in 80 cm diameter x 80 cm height and 40 cm diameter x 40 cm height water phantoms. A comparison of $g_L(r)$ values in the above two phantoms does not show significant difference up to r = 10 cm. However, for r = 10 - 15 cm, $g_L(r)$ values calculated in 80 cm diameter x 80 cm height phantom are higher by about 2 - 6% than the values obtained in 40 cm diameter x 40 cm height phantom.

The $g_L(r)$ values of BRIT ^{192}Ir HDR source calculated in an 80 cm diameter and 80 cm height cylindrical water phantom are almost same with that of the BEBIG, Flexisource and GammaMed 12i source models. The $g_L(r)$ values for VariSource (classic and VS2000), microSelectron (vl-classic and v2) source models fall rapidly as compared to BRIT source model, as these are based on 30 cm diameter spherical water phantom (Williamson and Li 1995, Wang and Sloboda 1998, Angelopoulos et al 2000).

In this chapter, the 2D dose distribution data of the ^{192}Ir HDR source are presented and compared with other commercially HDR ^{192}Ir sources clinically used worldwide. The calculated data of the ^{192}Ir HDR source are utilized for the indigenous development of the brachytherapy treatment planning software.

Chapter 4: Dosimetry of ^{32}P and ^{177}Lu patch sources used in superficial brachytherapy applications

Superficial brachytherapy uses beta or beta-gamma isotopes for treatment of skin cancers because this treatment is simple, less trauma to patients, and less expensive as compared to external beam therapy. This chapter discusses dosimetric studies of ^{32}P and ^{177}Lu patch sources.

Central axis depth dose and dose profiles in water phantom for a ^{32}P-nafion-based patch source indigenously developed by BARC using the EGSnrc-based Monte Carlo code system were calculated. For an initial activity of 1 Bq distributed in 1 cm^2 surface area of the source, the calculated surface dose is 3.62 x 10^{-10} Gy and dose at 1 mm from the source surface is 8.41 x 10^{-11} Gy. The treatment time calculated for delivering 30 Gy dose at 1 mm depth along the central axis of the source involving 37 MBq activity is 2.7 hours.

The surface dose rate at 5 μm depth in water of an in-house developed ^{177}Lu skin patch source containing 3.46 ± 0.01 mCi was measured using an extrapolation chamber, EBT3 film and compared against Monte Carlo methods. The source uniformity was measured using EBT3 films and found to be 2.2%, which is much less than 20% limit for planar and concave sources (ICRU report 2004). EBT3 films were also used to measure surface dose rate using electron beam calibration. Activity of the source was measured using HPGe detector. The Bragg-Gray stopping power ratio of water-to-air and wall correction factors were calculated using Monte Carlo method (Kawrakow et al 2013).

The Monte Carlo-calculated value of surface dose rate is 8.7 ± 0.2 Gy h^{-1} mCi^{-1}, which agrees to within 6% with the EBT3 film-based measurement and 14% with the extrapolation chamber-based measurement. The large deviations in extrapolation chamber-based result may be attributed to systematic uncertainty present in the extrapolation chamber measurements as the source size is smaller than sensitive volume of the chamber.

Chapter 5: Dosimetry of indigenously developed ^{125}I source for intraocular tumours

BARC has developed ^{125}I source (OcuProsta) for treatment of ocular tumours. This chapter presents measured dose distributions using EBT3 Gafchromic film. In this study, EBT3 films were used for measurement of absorbed dose rate, central axis depth dose and isodose lines. EBT3 films were calibrated both in 70 kV x-ray beam in dose range 0.5 – 5.1 Gy and ^{60}Co beam in dose range 0.5 - 30 Gy. The ratio of optical density is within 8% for dose of 50 cGy and 2% for dose range of 100 - 510 cGy, which shows that the EBT3 film has negligible energy dependence for doses more than 100 cGy. Dose was measured for a single ^{125}I seed in solid water phantom using films and compared with the Monte Carlo values, which agrees within 11%. Experimental dosimetry for a 14 mm diameter silver eye plaque embedded with 13 ^{125}I seeds was also carried out using stack of EBT3 films of size 3 x 3 cm^2. Depth dose and dose profiles were analyzed.

Chapter 6: Dosimetry of ^{125}I and ^{131}Cs brachytherapy sources due to non-uniform scatter condition

This chapter discusses the effect of tissue in-homogeneity, non-uniform scatter condition and interseed attenuation on dose distribution for ^{125}I and ^{131}Cs sources. The AAPM TG-43 dosimetry data calculated around a single source positioned at the centre of a liquid water or solid phantom using Monte Carlo code or measurements were strictly valid for a homogeneous water phantom of same size used in the simulation or measurement. During planning, dose differences occur because of tissue heterogeneities differing from water, less scatter due to finite patient size and interseed attenuation.

Dose distribution was calculated in water and three different types of prostate tissue compositions for ^{125}I and ^{131}Cs sources using FLUKA Monte Carlo code (Ferrari et al 2005).This simulation involved single seed. Differences up to 4% for ^{125}I source and 3% for ^{131}Cs source were observed for distances 0.1 - 2 cm from these sources.

In another simulation, thirty nine seeds (^{125}I or ^{131}Cs) were embedded in the prostate along with critical organs such as bladder and rectum. Doses at various points in prostate, bladder, bladder wall, rectum and rectum wall were estimated. Effect of interseed attenuation on dose distribution was also calculated using the superposition principle and found to be about 6 - 9% at points lying inside the implant volume and about 16% at points lying in the prostate boundary.

In order to estimate the dose differences between uniform scatter and non-uniform scatter condition, the ^{125}I / ^{131}Cs source was simulated, (i) at the centre of the water phantom and (ii) at distances of 0.5, 1, 1.5, 2 cm from the surface of the water phantom. Dose variations up to 10% and 8% were observed for ^{125}I and ^{131}Cs sources respectively.

Chapter 7: The response of Well chamber to pressure variations at high altitudes for ^{131}Cs and ^{169}Yb sources using Monte Carlo simulation techniques

Calibrated well-type ionization chambers are routinely used in hospitals to measure air-kerma strength of brachytherapy sources. A temperature and pressure correction factor (K_{TP}) is applied during routine measurements. The air pressure falls exponentially with height (Bohm et al 2005). For example, air density at Shimla (h = 2276 m) is 0.94 kg m^{-3}, which is 78% of standard air density (1.197 kg m^{-3}).

The K_{TP} corrected normalized response of a well chamber to air density variations at high altitudes was studied using EGSnrc and FLUKA Monte Carlo codes. Sources studied were ^{131}Cs and ^{169}Yb source. Simulations were carried out for air densities from 0.862 kg m^{-3} (3048 m) to 1.197 kg m^{-3} which cover Shimla, Darjeeling (2042 m) and Srinagar (1585 m) as well as Mexico (2240 m).

For ^{131}Cs source, the response was about 13% higher than unity for Shimla and Mexico. This is due to the range of electrons in the active volume and the cavity dimension are of same order and all electrons generated in the cavity, stop in the cavity and the well chamber do not behave as a small cavity dosimeter. For ^{169}Yb source, this response was about 1 - 3% higher than unity, which is due to the range of electrons is higher than cavity dimension and few electrons will stop in the cavity. The K_{TP} corrected normalized response was higher for aluminium, copper chamber than graphite, C-552 chamber. This is due to high atomic number material and higher photon cross section in aluminium and copper than for C-552 and graphite.

Chapter 8: Summary, conclusion and future scope

This chapter highlights the major contributions and achievements made in the research works. These are listed as follows:

- Dosimetric study of HDR ^{192}Ir brachytherapy source indigenously developed by BARC / BRIT using Monte Carlo-based EGSnrc code system.
- Dosimetric study of indigenously developed ^{32}P and ^{177}Lu patch sources for skin applications.

- Dosimetry of indigenously developed ^{125}I seed source for intraocular tumours.

- Dosimetry of ^{125}I and ^{131}Cs brachytherapy sources due to non-uniform scatter condition.

- The response of Well chamber to pressure variations at high altitudes for ^{131}Cs and ^{169}Yb sources using Monte Carlo simulation techniques.

The ^{32}P and ^{177}Lu patch sources were prepared by immersing the nafion membrane in a solution of known activity. The activity of the these sources was estimated using NaI(Tl) counter by subtracting the residual activity in the reaction volume from the initial added ^{177}Lu activity in the reaction volume.

Significant research studies were already carried out in the field of brachytherapy dosimetry using Monte Carlo techniques. It is important to state the future requirements in this area. Accordingly, following studies can be initiated as continuation of the works presented in this thesis:

- Patient-specific dose distributions based upon the actual locations of the sources, applicator heterogeneities, interseed attenuation, patient size, and can account for tissue heterogeneities using Monte Carlo techniques. Such detailed studies may be clinically useful.

- Development of calibration standard for ^{32}P and ^{177}Lu patch sources.

LIST OF FIGURES

Figure 5.4. A 14 mm diameter silver plaque embedded with 13 ^{125}I OcuProsta sources. S_K of each seed is 2.94 U.

Figure 5.5. 14 mm diameter silver plaque embedded with 13 ^{125}I OcuProsta seeds, placed over Gafchromic film. Films are in the centre of wax phantom. S_K of each seed is 2.94 U.

Figure 5.6. Dose response of EBT3 Gafchromic films for ^{60}Co energy and 70 kV x-ray.

Figure 5.7. The central axis depth dose for 14 mm diameter silver plaque embedded with 13 seeds measured using EBT3 Gafchromic film. The fitted dose is estimated using 12th order orthogonal polynomial fit.

Figure 5.8. The isodose plot for 14 mm diameter silver plaque measured using EBT3 film at 4 mm from the surface of the plaque.

Figure 5.9. The isodose plot for 14 mm diameter silver plaque measured using EBT3 film at 5.9 mm from the surface of the plaque.

Figure 5.10. The isodose plot for 14 mm diameter silver plaque measured using EBT3 film at 7.2 mm from the surface of the plaque.

Figure 6.1. Schematic diagram of (a) ^{125}I source (OcuProsta) and (b) ^{131}Cs source (Cs-1 Rev-2 model) (Picture courtesy: Tailor et al 2008) with the Cartesian co-ordinate system used in the FLUKA Monte Carlo simulation. Dimensions shown are in millimeters (not to scale). The origin of the co-ordinate system is chosen at the center of the active source.

Figure 6.2. (a) Cross sectional view of prostate implant in the MC simulation along with bladder and rectum using 39 seeds. Origin of the co-ordinate system coincides with centre of prostate and contains one seed. (b) Magnified picture of prostate. Five seeds in the central plane and three seeds each in top and bottom plane are visible.

Figure 6.3. Figure represents transverse plane. (a) 21 seeds (9 inner circle + 12 outer circle) in the central XY-plane (Z = 0). (b) 9 seeds each were arranged at Z = 1 cm and Z = -1 cm. This makes 39 seeds.

LIST OF TABLES

GLOSSARY

AAPM	American Association of Physicists in Medicine
ABS	American Brachytherapy Society
AKS	Air-kerma strength
BARC	Bhabha Atomic Research Centre
BCRU	British Committee on Radiation Units and Measurements
BRIT	Board of Radiation isotope and Technology
BTE	Boltzmann transport equation
CH	Condensed history
COMS	Collaborative Ocular Melanoma Study
CPE	Charged particle equilibrium
CT	Computed tomography
DRC	Dose rate constant
ECUT	Electron transport cut-off energy
ESTRO	European Society for Radiotherapy and Oncology
HDR	High dose rate
HEBD	High Energy Brachytherapy Source Dosimetry
HPGe	High purity germanium
IAEA	International Atomic Energy Agency
ICRU	International Commission on Radiation Units and Measurements
IORT	Intraoperative radiotherapy
LDR	Low dose rate
NICPR	National Institute of Cancer Prevention and Research
NIST	National Institute of Standards and Technology
NNDC	National Nuclear Data Center

NTCP   Normal tissue complication probability

OP   Orthogonal polynomial

PCUT   Photon transport cut-off energy

PDF   Probability density functions

PDR   Pulse dose rate

PMMA   Polymethyl methacrylate

PTV   Planning target volume

RAKR   Reference air-kerma rate

ROPES   Radiation Oncology Physics and Engineering Services Australia

SPR   Stopping-power ratio

TCP   Tumour control probability

TLD   Thermo luminescence dosimeter

TPS   Treatment planning system

TSD   Target to skin distance

WAFAC   Wide angle free air chamber

WHO   World Health Organization

CHAPTER 1

INTRODUCTION TO BRACHYTHERAPY AND LITERATURE REVIEW

1.1. Cancer incidence

Cancer is one of the leading causes of deaths in India (NICPR2018). Every year about seven lakhs new cancer cases are detected. As per the data in 2010 by cancer registry of India, annually more than five lakhs people die due to this disease (NICPR2018). The recorded incidence of cancer in India is at 94 per lakhs people (Mallath et al 2014). According to World Health Organisation, lung, oral, throat and neck cancers were the most common among men while cervix, breast and ovarian cancer were common in women (WHO 2017a). Cancers of oral cavity and lungs in males and cervix and breast in females account for over 50% of all cancer deaths in India (NICPR2018). However, if cancer is detected in its early stages, it can be treated with radiotherapy and an individual can lead a healthy life. Brachytherapy treatment may play a very important role in the management of these cancers.

1.2. Radiotherapy

The aim of radiotherapy is to deliver a uniform prescribed dose to the predetermined target volume (tumour) while sparing the surrounding critical structures and normal tissues (ICRU 24 1976). The radiotherapy principle is mainly based on two sigmoid curves (Figure 1.1). Curve-A is the tumour control probability (TCP) curves and Curve-B is the normal tissue complication probability (NTCP) curve. The best radiation therapy has maximum TCP and minimum NTCP. For a good radiotherapy treatment, TCP ≥ 0.5

and NTCP $\leq$ 0.05. The therapeutic ratio is the ratio of the TCP and NTCP at a specified level of response (usually 0.05) for normal tissue. The more is the therapeutic ratio, there will be less complications. Radiotherapy is divided two categories, (a) External beam therapy and (b) Brachytherapy.
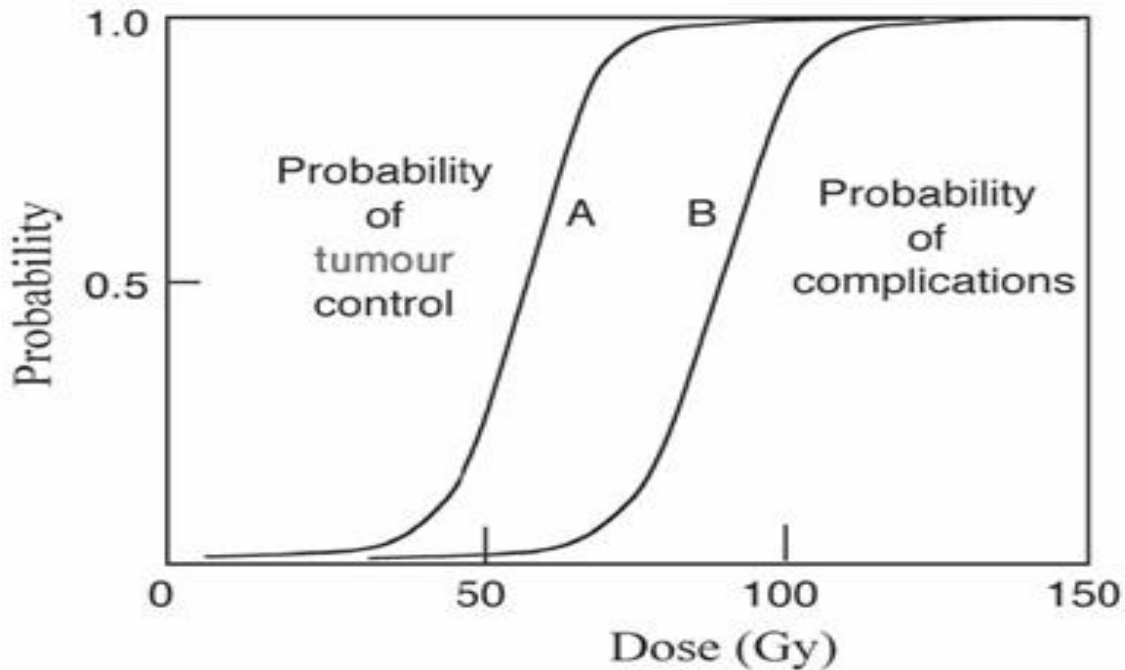
Figure 1.1. The principle of therapeutic ratio. Curve A represents the TCP, curve B the probability of complications. The total clinical dose is usually delivered in 2 Gy fractions. (Courtesy: Radiation Oncology Physics: A handbook for teachers and students edited by EB Podgorsak)

1.3. Brachytherapy

In brachytherapy treatment, sealed radioactive sources are placed directly into or near the tumour volume (Hendee 1999, Khan 2010, Williamson et al 1995). Brachytherapy uses the inhomogeneous dose distributions around the radiation sources. Due to the sharp fall

of radiation dose, brachytherapy delivers a high radiation dose to the tumour keeping the dose to surrounding normal tissues to a minimum.

1.3.1. Classifications of brachytherapy based on source insertion or type of implant

Brachytherapy treatments are classified depending upon the method of source insertion in the tumour site or type of implant.

Intracavitary application: In intracavitary application, the radioactive sources (in form of tubes or pellets) are placed inside the natural body cavities. The best example is the use of radioactive sources within applicators in the uterus and vaginal cavity.

Interstitial implant: In interstitial implant, the sources are inserted or implanted into the tumour through surgical incision for cancers such as oral cavity, oropharynx, breast, prostate etc. The example would be the use of radioactive needles in the treatment of carcinoma of the tongue (Meridith 1947).

Intraluminal brachytherapy: Intraluminal brachytherapy uses high dose rate micro-sources, which need only remain within the lumen for a few minutes. It is used for tumours that obstruct the opening of a pulmonary bronchus, biliary duct, esophagus, etc. Catheters placed by endoscopy are afterloaded with radioactive sources to deliver a dose that can relieve the obstruction.

Superficial brachytherapy: In superficial brachytherapy, beta sources are placed over the tissue to be treated e.g. for tumours of the skin.

Intraoperative radiotherapy: Intraoperative radiotherapy (IORT) uses low-energy x-rays (30 - 50 KV), where a single high dose of radiation (10 - 20 Gy) can be given to the tumour bed during surgery (Podgorsak E B and Podgorsak M B 2005). IORT mostly used for breast cancer.

Intravascular brachytherapy: In intravascular brachytherapy a single source is placed in to arteries during angioplasty. After opening of a blocked blood vessel by angioplasty there is a high likelihood that the restenosis will occur. Clinical studies indicate that irradiation of 15 - 30 Gy dose during angioplasty reduces the occurrence of restenosis (Nath et al 1999a). It is estimated that the restenosis rate may drop from roughly 35 - 40% to well below 10% if radiation is delivered during angioplasty (Waksman and Crocker 1996). Radiation is a proven agent to prevent growth of cells and is effective in preventing restenosis. ^{192}Ir HDR, ^{32}P, ^{90}Sr/Y, ^{188}Re beta sources are currently used in vascular treatment (Roa et al 2004).

Temporary implant: In temporary implants, the sources are inserted in the tumour for a short time. The sources are removed after the prescribed dose has been delivered. Treatment time of temporary implants are order of few minutes in case of high dose rate treatment using ^{192}Ir and ^{60}Co HDR sources and order of few days in case of low dose rate treatments using ^{137}Cs source.

Permanent implant: In permanent implants, the sources are inserted into the patient permanently. The radiation dose is delivered continuously for its whole lifetime.

Generally low energy and short half-life radionuclides (^{125}I and ^{103}Pd) are used in permanent implants treatment (Nag et al 1999 and 2000). Example is prostate cancer.

1.3.2. Classification based on dose rate

Brachytherapy treatments are also categorized with respect to dose rates or rate of irradiation (ICRU 38 1985). They are

1. Low dose rate (LDR: 0.4 - 2 Gy h^{-1})

2. Medium dose rate (MDR: 2 - 12 Gy h^{-1})

3. High dose rate (HDR: More than 12 Gy h^{-1})

In low dose-rate application, ^{137}Cs or ^{60}Co sources with spacers are used to deliver dose-rates of about 0.4 - 2 Gy h^{-1}. Pulsed Dose Rate (PDR) treatment is a new modality that combines physical advantages of HDR technology with radiobiological advantages (repair) of LDR brachytherapy. PDR uses a single ^{192}Ir source (activity about 0.5 - 1 Ci) and the dose rate is up to about 3 Gy h^{-1}. A series of short exposures (10 - 30 minutes duration) every hour are delivered amounting to approximately the same total dose in the same overall time delivered in the LDR treatment (Skowronek et al 2001) .

1.3.3. HDR treatment using remote afterloading technique

HDR remote afterloading systems use a single source of ^{192}Ir, with a typical activity of about 10 Ci or a ^{60}Co with a typical activity 2 Ci. Initially, the applicator is inserted in to the target position and the radioactive sources are loaded later by a computer-controlled device / machine is known as remote afterloading unit. The advantages of the remote

afterloading technique are (1) dose distributions will be optimized using TPS, (2) dose reduction to normal tissue is possible by pushing them away from source due to short treatment time, (3) reduction of exposure to hospital staff, (4) treatments are reproducible, (5) sources can be retracted into shielded condition in emergency conditions, and (6) comfort and convenient to patient due to outpatient treatment (Das and Thomadsen 2005). The disadvantages are (1) the treatment units are expensive and requires well shielded room, (2) need frequent source replacement (in case of ^{192}Ir source) and (3) stringent quality assurance tests are required (4) potential for accidental high exposures and serious errors and (5) radiobiology.

1.4. Radioisotopes used in brachytherapy

Artificially produced gamma sources (^{137}Cs, ^{192}Ir, ^{60}Co, ^{125}I and ^{103}Pd) and beta sources (^{32}P, ^{90}Sr/Y, ^{188}Re) available from nuclear reactors and particle accelerators are used in brachytherapy practice. ^{192}Ir and ^{60}Co sources are popular in intracavitary applications and ^{125}I and ^{103}Pd sources are used for permanent implants. ^{169}Yb, ^{198}Au and ^{131}Cs sources are emerging sources and limited applications are available in literature.

1.4.1. Gamma emitting brachytherapy sources

^{137}Cs: ^{137}Cs source is a fission by-product with a long half-life (30 year) and its gamma energy is 0.662 MeV. ^{137}Cs in the form of insoluble powder or ceramic microspheres, is doubly encapsulated in iridium-platinum alloy and finally sealed in stainless steel encapsulation. ^{137}Cs sources are popular during 1940 - 1990 for intracavitary LDR

treatment using manual afterloading. Their use has been diminished due to introduction of remote afterloading HDR technique using ^{192}Ir sources.

^{192}Ir: ^{192}Ir is produced by neutron activation of stable ^{191}Ir using the (n,γ) reaction. It decays to excited states of platinum-192 and osmium-192, followed by a wide spectrum of gamma rays. Internal conversion and electron capture give rise to a significant amount of characteristic x-rays. It has a complicated gamma ray spectrum with average energy of 0.38 MeV and half life of 73.83 days (Nath 2005). The main advantages of ^{192}Ir are its low energy gamma and high specific activity which allows fabrication of miniature sources. ^{192}Ir HDR sources are widely used in remote afterloading system.

^{60}Co: ^{60}Co is a gamma emitting source, which is produced by neutron activation of stable ^{59}Co in a nuclear reactor, which has reasonably long half-life (5.26 years). It emits two gamma photon of energy, 1.17 MeV and 1.33 MeV and beta particle with energy 0.313 MeV. These ^{60}Co sources are usually encapsulated in stainless steel. Its high gamma energy requires thicker shielding. ^{60}Co isotope is used in HDR remote afterloading units, because of high specific activity.

^{125}I: ^{125}I is produced in a nuclear reactor by neutron activation of ^{124}Xe to ^{125}Xe which decays, via electron capture to ^{125}I with a half-life of 18 hours. ^{125}I decays by electron capture to an excited state of ^{125}Te and emission of 35.5 keV gamma rays. Characteristic x-rays in the range of 27 - 35 keV are also emitted due to electron capture and internal conversion processes. Half life of ^{125}I is 60 days. Silver spheres or rods are used to absorb the ^{125}I on its surface and it is encapsulated in titanium. Fluorescent x-rays of 22.1 and

25.2 keV resulting from silver source core are also emitted. Its main advantage is its low energy photon, which requires lesser shielding.

103Pd: ^{103}Pd isotope is produced by neutron capture in the stable ^{102}Pd nucleus using (n,γ) reaction. ^{103}Pd also decays by electron capture with the emission of characteristic x-rays in the range of 20 - 23 keV (mean energy 21 keV). The initial delivered dose rate is higher due to its shorter half-life (17 days) than that of ^{125}I. The dose to the surrounding organs is also lower due to its lesser mean energy in comparison to ^{125}I or ^{192}Ir sources.

198Au: ^{198}Au is produced in nuclear reactor by neutron activation of ^{197}Au. It has a half-life of 2.7 days and emits monoenergetic gamma of 0.412 MeV. They are used for permanent implants and replaced ^{222}Rn in early 50's. Its high energy gamma-rays give higher dose to normal tissue and needs more shielding.

169Yb: ^{169}Yb isotope (half-life is 32 days), is produced by neutron activation during the irradiation of ^{168}Yb in nuclear reactors. The ^{169}Yb source decays to ^{169}Tm by electron capture. The average energy is 92.7 keV (Medich et al 2006).

131Cs: ^{131}Cs is a pure electron capture isotope and it is a suitable for permanent interstitial implants. ^{131}Cs is produced by neutron capture in ^{130}Ba. ^{131}Cs decays by electron capture to ^{131}Xe yielding gamma rays (33.6 keV), K_α x-rays (29.5 and 29.8 keV) and K_β x-rays (33.6, 44.4 keV) with a mean photon energy of approximately 30.4 keV (Wittman and Fisher 2007). The half-life of ^{131}Cs source is 9.7 days. The short half-life enables production of higher dose rate sources and shortening the dose delivery time.

1.4.2. Beta emitting brachytherapy sources

These are many β-ray emitting nuclides available for treatment such as ^{32}P, ^{90}Sr, ^{90}Y, ^{177}Lu etc. β-rays have the advantage of delivering high doses in the vicinity of the emitting source, they have finite range and they are easily shielded by a few millimeters of plastic or tissue.

^{32}P: ^{32}P is a pure beta emitter. It emits beta particles with $E_{\beta,max} = 1.71$ MeV and its half-life is 14 days. Recently, ^{32}P source has been used in many intravascular brachytherapy system, as temporary implants (catheter based radioactive seeds, wires, or liquid filled balloons) or permanent implant as ^{32}P stent (Bohm et al 2001). Continuous irradiation delivered by a radioactive ^{32}P stent reduces restenosis during percutaneous transluminal coronary angioplasty (PTCA) (Janicki et al 1997). The ^{32}P eye applicator is also used to deliver therapeutic doses to the surface of the conjunctiva, during surgery of primary pterygium to reduce the risk of local recurrence of pterygium.

^{90}Sr/^{90}Y: ^{90}Sr decays with a half-life of 29 years to ^{90}Y and yields only beta particles with $E_{\beta,max} = 0.5$ MeV. The daughter isotope ^{90}Y is a nearly pure beta emitter with a 64-hours half life, and emits beta particles with a maximum energy of 2.27 MeV. This radionuclide is suitable for treatment of superficial lesions, e.g., a ^{90}Sr ophthalmic applicator is used for treatment of lesions in the eye where the depth of penetration needed is a few millimeters. ^{90}Sr and ^{90}Y sources are used in intravascular brachytherapy for prevention of restenosis in coronary or peripheral arteries (Roa et al 2004).

177Lu: 177Lu is a favorite isotope for treatment of superficial tumour. It emits beta particles with end-point energies 498 (79.4 %), 385 (9 %) and 177 keV (11.6 %) along with 113 (6.6 %) and 208 keV (11 %) gamma photons (NNDC 2003). Its half-life is 6.7 days.

1.5. Source strength specifications in brachytherapy

The term dosimetry is the method of calculating the dose rate at a specific point in a given medium, which is usually considered as water. The absorbed dose of a brachytherapy source is strongly depends on source strength. Hence, it is absolutely essential that source strength of a source can be accurately estimated.

In the early years of the twentieth century, known as biological dosimetry era or Radium era (1900 - 1940), only radium tubes and needles were used for brachytherapy. The strength of a source was specified in terms of milligram-hours (mgh) for radium. The Sievert integral, introduced by Rolf Sievert (Sievert 1921), was used to calculate one-dimensional (1-D) integration of the point-source dose kernel over the active length of a radium needle.

During classical era (1940 - 1990), many new brachytherapy source models such 125I, 103Pd, 192Ir and 137Cs were developed. The dosimetry of such sources, e.g. 137Cs tubes and 125I seeds (Krishnaswamy 1972 and 1979) were estimated using Sievert integral-type analytic models.

In modern era (1990 - present), the semi-empirical models used in brachytherapy planning, have been replaced in by Monte Carlo transport calculations and measurement-

based methodologies. The dosimetry relies on dose-rate measurements around each specific source model. An empirical dose-calculation formalism known as the AAPM TG-43 protocol was published in 1995 (Nath et al 1995) and revised in 2004 as AAPM TG-43U1 (Rivard et al 2004). 2-Dimensional dose distribution and dosimetry parameters of brachytherapy sources were calculated using this protocol.

1.5.1. Quantities used for source strength specification

The strength of a brachytherapy source has been specified based on many recommendations and standards developed in different periods and for different radionuclides. They are, (a) Mass of radium (MgRa), (b) Activity (A), (c) milligram-radium equivalent (mgRaEq), (d) Apparent activity (A_{app}), (e) Specific gamma ray constant (Γ_{γ}) and exposure rate constant ($\Gamma_{x, \delta}$), (f) Reference air-kerma rate (RAKR, $\left(\dot{K}_{air}(d_{ref})\right)_{air}$ and (g) Air-kerma strength (AKS, S_K).

The activity of a source is not easy to measure. It cannot be easily applied to brachytherapy source strength specifications because the dose distribution around an encapsulated brachytherapy source depends on the form, dimensions of the source, the attenuation and scattering of the photons by the encapsulation material. For this reason, the term apparent activity was introduced. Apparent activity is defined as the activity of a hypothetical unfiltered point source of the same radio-nuclide which will give the same exposure rate in air at the same distance on the transverse axis of the given sealed source. The apparent activity includes the effects of self absorption, attenuation, and production of bremsstrahlung X–rays in the source and its encapsulation.

When the source strength is expressed in units of activity, the dose rate at any point is calculated using either the specific gamma ray constant or exposure rate constant of the source. Specific gamma ray constant, Γ_γ is defined as the exposure rate at a reference distance per unit activity from a point source, in air under scatter free condition, evaluated on the basis of photons emitted from the radio-nuclide. The specific gamma ray constant includes exposure contribution due to only the primary gamma.

Exposure rate constant and specific gamma ray constant are both sensitive to the method of calculation, defined for unshielded point source, depends upon photon energy spectrum, characteristic of the radionuclides, except for radium. Actual sources are not point and there is absorption and filtration of the radiation in its encapsulation. Prior to 1978, different values of $\Gamma_{X,\delta}$ were quoted for ^{192}Ir source (with many photon energies) in the literature i.e. 3.9 to 5.0 R cm^2 mCi^{-1} h^{-1} (Nath et al 1995). This may introduce errors due to choosing different values of $\Gamma_{X,\delta}$ during calculation by the source suppliers and the source users (Nath et al 1995). In order to overcome these errors, output based quantities or measurable quantities have been recommended.

1.5.1.1. Reference air-kerma rate $\left(\dot{K}_{air}\left(d_{ref}\right)\right)_{air}$

The quantity recommended for the specification of gamma ray brachytherapy sources is the reference air-kerma rate (RAKR), $\left(\dot{K}_{air}\left(d_{ref}\right)\right)_{air}$ (ICRU 38 1985, ICRU 58 1997, CFMRI 1983, BCRU 1984).

It is defined as the air-kerma rate in air at a reference distance of 1 m from the center of the source, along its perpendicular bisector axis, corrected for attenuation and scattering in air. The original unit proposed by ICRU 38 is μGy h^{-1} at 1 m. Its unit is μGy h^{-1} for LDR sources and mGy h^{-1} or μGy s^{-1} for HDR sources. IAEA (1999 and 2002a) and ESTRO (2004) also recommended the use of $\left(\dot{K}_{air}(d_{ref})\right)_{air}$ for brachytherapy source strength specification.

1.5.1.2. Air-kerma strength (S_K)

The AAPM Task Group No 32 in 1987 introduced the term "air-kerma strength (AKS), S_K" to specify the strength of a brachytherapy source (AAPM TG-32 1987). It is defined as the product of the air-kerma rate in free space at a measurement distance d from the source center along the perpendicular bisector, $\dot{K}_{air}(d)$ and the square of the distance, d.

$$S_K = \dot{K}_{air}(d) . d^2 \tag{1.1}$$

It can be noticed that the two quantities, $\left(\dot{K}_{air}(d_{ref})\right)_{air}$ and S_K, are numerically same (ICRU 38 1985, ICRU 60 1998) and differ only in the unit in which the source strength is expressed.

1.6.   Dose calculation formalisms in brachytherapy

Brachytherapy sources are mostly cylindrical, encapsulated and emit spectrum of photons with energies ranging from a few keV to MeV. Attenuation and scattering occur in the source, encapsulation material, applicator and the surrounding tissue. Due to large dose

gradient exists close to the source, dose measurement is difficult and which only relies on theoretical calculations.

1.6.1. Dose rate for a point source of strength S_K

The cylindrical sources, assumed as a group of many point isotropic source or linear type depending upon the dimensions of the source and the distance of interest in dose calculation. The simple example is the case of an ideal point source with a spherical symmetry of the radiation field around it.

Let us consider an unencapsulated point source of strength, S_K, is placed in air. The quantity S_K describes source strength in terms of air-kerma, K_{air} which is the total kinetic energy transferred to charged particles by photon interactions with atoms per unit mass of air (Williamson 2005).

Under charged particle equilibrium (CPE), the rates of energy absorption and energy transfer are approximately equal. The collision-kerma in air, $(K_{col})_{air}$ is approximately equal to the absorbed dose (Attix 1986) and givenby following equation,

$$D_{air} \cong (K_{col})_{air} = K_{air}(1 - g) \qquad (1.2)$$

The collisional kerma refers to the component of the transferred energy which is ultimately absorbed by the medium due to charged particle collisions. g is the fraction of the energy lost to bremsstrahlung radiation and its value is less than 0.001 at brachytherapy energies. This radiative correction is usually ignored in tissue (Boutilon and Perroche-Rous A M 1987, Williamson 2005).

Hence the dose to air in free space is equal to air-kerma. Similarly dose rate to air is equal to air-kerma rate.

$$\dot{D}_{air}(d) \; = \; \dot{K}_{air}(d) \tag{1.3}$$

From equation (1.1)

$$\dot{D}_{air}(d) = \frac{S_K}{d^2} \tag{1.4}$$

Dose rate in water can be obtained from above equation (1.4) by multiplying the mass

energy absorption coefficient of water to that of air $\left(\mu_{en}/\rho\right)_{air}^{wat}$ and the absorption and

scatter correction factor for photons in water, $f_w(d)$.

$$\dot{D}_{wat}(d) = \frac{S_K \cdot \left(\mu_{en}/\rho\right)_{air}^{wat} \cdot f_w(d)}{d^2} \tag{1.5}$$

For all photon-emitting radionuclides with energies greater than 200 keV, $\left(\mu_{en}/\rho\right)_{air}^{wat}$,

has the value 1.11 in water. The absorption and scatter correction factor $f_w(d)$ is

dependent on distance and energy of the source. Use of S_K for clinical source-strength

specification eliminates the error in choosing different inconsistent values of exposure

rate constant by vendor and hospital physicist, which increases the accuracy in the dose

measurement.

1.6.2. Dose rate for a line source using Sievert integral

Sources used in brachytherapy treatment have finite dimensions, are cylindrical in shape

and encapsulated in stainless steel, platinum, or titanium. Dose distributions around such

sources are calculated by dividing the line source into large number of point sources and

correcting for distance, oblique filtration, attenuation, and scattering in the encapsulation materials. This is an extension of the point source model.

Rolf Sievert (1921) was first introduced the 1-D path length model (Williamson et al 1983, Williamson 1996, Karaiskos et al 2000b) for dosimetry of line sources. The Sievert integral considers the effect of distribution of radioactivity within the encapsulated source on the dose distribution by integrating over the active length of source. The dose rate in water at any point P, $\dot{D}(r, \theta)$ from a linear source of length L (Figure 1.2) is given by,

$$\dot{D}(r, \theta) = \frac{S_K \cdot \left(\mu_{en}/\rho\right)_{air}^{wat} e^{\mu d}}{h \cdot L} \int_{\theta_1}^{\theta_2} e^{-\mu d \sec\theta} f_w(h \sec\theta) d\theta \qquad (1.6)$$
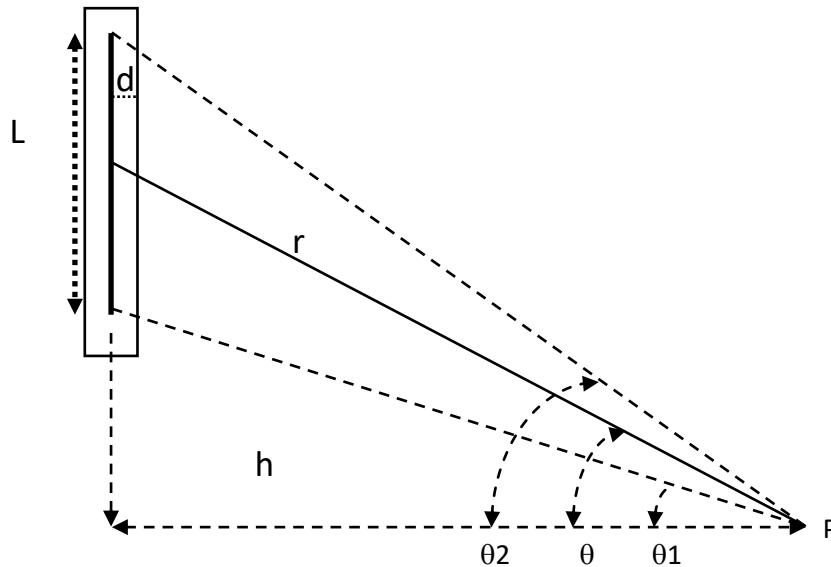
Figure 1.2. Dose rate calculation at a point due to a linear source of length L using Sievert integral.

Where h is the perpendicular distance between the source axis and the point P, θ_1 & θ_2 are the angles subtended by the active ends of the source at point P, μ is the linear attenuation

coefficient and d is the encapsulation thickness of the source. f_w is the absorption and scatter correction factor. The integrals of eq. (1.6) can be readily calculated with computer algorithms that carry out the calculations by summation over a large number of source segments.

The use of Sievert integral has been shown to be highly accurate for ^{137}Cs tubes (Williamson 1996), allowing its use in commercial brachytherapy TPS. However, for ^{192}Ir sources, which has complex photon energy spectra and ^{125}I and [103]Pd low-energy sources, this Sievert integral results in significant dose calculation errors. Monte Carlo simulations have also shown that beyond the active source region, the Sievert integral method introduces significant errors and breaks down in the extreme oblique directions (Williamson et al 1983). Modified forms of Sievert integral have been proposed by Williamson (1996) and Karaiskos et al (2000b) to improve the accuracy of Sievert integral for ^{192}Ir sources.

1.7. TG-43 dose calculation model

In 1995, the American Association of Physicists in Medicine (AAPM) Radiation Therapy Committee Task Group 43 published its report (Nath et al 1995) entitled "Dosimetry of Interstitial Brachytherapy Sources," specially for low energy brachytherapy sources, such as [103]Pd and [125]I.

TG-43 recommended to derive the dosimetry parameters directly calculated or measured in water medium for the actual source. Some of these parameters are dose rate constant,

Λ, radial dose function, $g_X(r)$, anisotropy function, F(r,θ), and geometry factor, G_L(r,θ). The differences between the dosimetry constants calculated using traditional method and recommended by TG-43 were as large as 17% for some sources (Nath et al 1995).

About 20 new low-energy interstitial brachytherapy seed sources have been introduced during 1995 and 2004 and significant advances have taken place in the brachytherapy dosimetry. In view of this, AAPM in 2004 revised the TG-43 report to TG43U1 report (Rivard et al 2004). This report also recommends for a single dosimetry document for all low-energy brachytherapy sources to complement the joint AAPM (Rivard et al 2009b) / RPC Brachytherapy Source Registry (RPC 2005).

The AAPM in 1998, recommended that at least one experimental and one Monte Carlo determination of the TG-43 dosimetry parameters be published in the peer-reviewed literature before using new low-energy photon-emitting sources (average photon energies less than 50 keV) in routine clinical practice (Williamson et al 1998).

1.7.1. 2-D Dose calculation formalism

The two-dimensional dose rate at polar coordinates (r,θ) for a line source $\dot{D}(r,\theta)$ is given by,

$$\dot{D}(r,\theta) = S_K \cdot \Lambda \cdot \frac{G_L(r, \theta)}{G_L(r_0,\theta_0)} \cdot g_L(r) \cdot F(r,\theta) \qquad (1.7)$$

Where r is the distance (in cm) from the center of the active source to the point P, r_0 is the reference distance (= 1 cm) in this protocol, and θ denotes the polar angle specifying the point P, P(r,θ), relative to the source longitudinal-axis. The reference angle, $\theta_0 = 90°$.
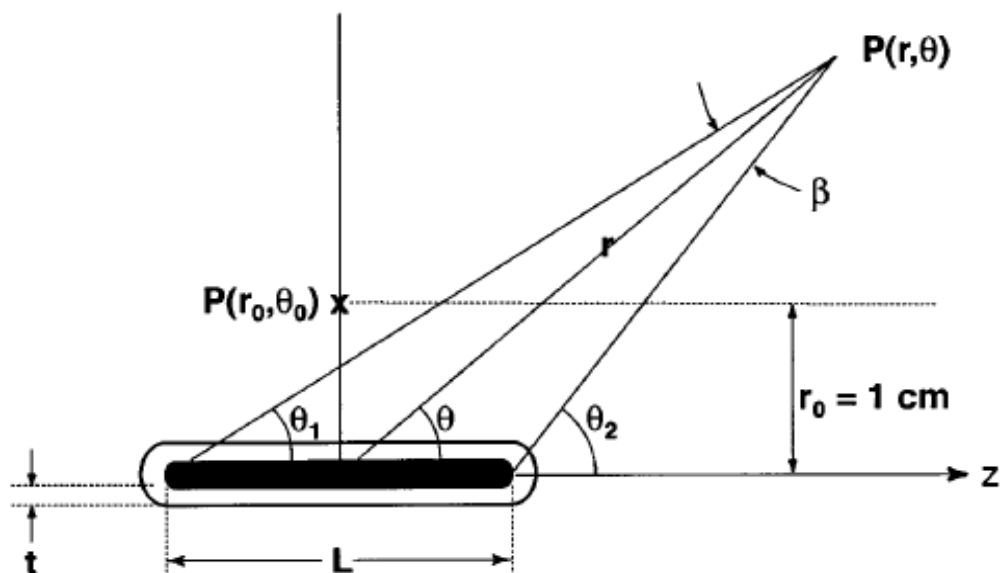
Figure 1.3. Coordinate system used for brachytherapy dosimetry calculations for a line source.

Equation (1.7) includes additional subscript L, which is the line source approximation used for the geometry function. This report applies to cylindrical sources i.e, dose distribution is symmetric with respect to the source longitudinal-axis.

1.7.1.1. Air-kerma strength

A minor revision was made in the definition of S_K by AAPM TG-43U1 (Rivard et al 2004). The air-kerma rate $\dot{K}_\delta(d)$, was calculated in vacuum due to photons of energy greater than δ. The cut-off energy δ (typically 5 keV) excludes all low-energy and contaminant photons i.e. characteristic x-rays originating in the encapsulation material of the source. These characteristic x-rays increases S_K without contributing significantly to dose at distances greater than 1 mm in tissue.

$$S_K = \dot{K}_\delta(d) . d^2 \qquad\qquad (1.8)$$

The d is the distance from the source center to the point of $K_\delta(d)$ specification, should be located on the transverse-plane of the source. The d should large relative to the active length of the source, so that S_K is independent of d. S_K denoted by the symbol U, where 1 U = 1 μGy m^2 h^{-1} = 1 cGy cm^2 h^{-1}.

The qualification in vacuum means that the measurements should be corrected for photon attenuation and scattering in air and any other medium interposed between the source and detector, as well as photon scattering from nearby objects such as walls, floors and ceilings.

1.7.1.2. Dose rate constant

The Λ is defined as the ratio of dose rate in water at ($r_0 = 1$ cm, $\theta_0 = 90^0$) on the transverse axis $\dot{D}(r_0, \theta_0)$ and S_K. It has units of cGy h^{-1} U^{-1}.

$$\Lambda = \frac{\dot{D}(r_0, \theta_0)}{S_K} \qquad\qquad (1.9)$$

It includes the effects of source geometry, the spatial distribution of radioactivity within the source, self-filtration within the source and scattering in water surrounding the source. The Λ depends on both the radionuclide and source model.

1.7.1.3. Geometry function

The $G_L(r,\theta)$ accounts for the variation of relative dose distribution due to the spatial distribution of activity within the source. It neglects scattering and attenuation in the source itself and provides an effective inverse square-law. Therefore, the AAPM TG-

43U1 report recommends use of point- and line-source models giving rise to the following geometry functions:

$$G_P = r^{-2} \qquad\qquad \text{Point source approximation}$$

$$G_L(r,\theta) = \begin{cases} \dfrac{\beta}{Lr\sin\theta} & if\ \theta \neq 0 \\[2mm] \left(r^2 - \dfrac{L^2}{4}\right)^{-1} & if\ \theta = 0 \end{cases} \qquad Line\ source\ approximation \quad (1.10)$$

where β is the angle, in radians, subtended by the tips of the line source at P(r,0).

1.7.1.4. Radial dose function

The $g_X(r)$ accounts for dose fall-off on the transverse-plane due to photon scattering and attenuation, i.e., excluding fall-off included by the geometry function. The subscript X to the $g_X(r)$, either (a) P for a point-source, or (b) L for line-source.

$$g_X(r) = \frac{\dot{D}(r,\theta_0)G_X(r_0,\theta_0)}{\dot{D}(r_0,\theta_0)G_X(r,\theta_0)} \qquad\qquad (1.11)$$

1.7.1.5. Anisotropy function

The F(r,0) accounts for the anisotropy of dose distribution around the source including the effects of absorption and scatter in water. This function describes the variation in dose as a function of polar angle relative to the transverse plane. The 2D anisotropy function, $F(r,\theta)$, is defined as

$$F(r,\theta) = \frac{\dot{D}(r,\ \theta)G_L(r,\theta_0)}{\dot{D}(r,\theta_0)G_L(r,\ \theta)} \qquad\qquad (1.12)$$

The value of $F(r,\theta)$ on the transverse plane is 1. The value of $F(r,\theta)$ off the transverse plane typically decreases as (i) r decreases, (ii) as θ approaches 0° or 180°, (iii) as encapsulation thickness increases, and (iv) as photon energy decreases.

1.8. Literature survey on dosimetry of brachytherapy sources

1.8.1. HDR ^{192}Ir and ^{60}Co sources

A number of HDR ^{192}Ir and ^{60}Co source models are available worldwide for brachytherapy applications. Experimental measurement using thermoluminescence detectors (TLDs) and Monte Carlo transport techniques are normally used to generate dosimetry dataset for individual seeds as required by treatment planning system.

Williamson and Li (1995) and Daskalov et al (1998) calculated dosimetry parameters in water for Microselectron ^{192}Ir HDR and PDR source using Monte Carlo photon transport (MCPT) code. The calculations made by Williamson and Li (1995) became the basis of a TG43 dosimetry protocol for brachytherapy (Nath et al 1995). Dosimetry data for the VariSource HDR source in a water medium were calculated by Wang and Sloboda (1998) using the EGS4 Monte Carlo code. GEANT3 Monte Carlo particle transport code was used to study the dosimetric evaluation for the Plus and 12i Gammamed PDR ^{192}Ir sources (Perez-Calatyud et al 2001).

Anagnostopoulos et al (2004) utilised MCNPX Monte Carlo code to study the effect of patient inhomogeneities on the dosimetry planning in ^{192}Ir HDR treatment. Taylor and Rogers (2008) used the EGSnrc based BrachyDose code to calculate TG-43 dosimetry parameters for 15 high dose rate ^{192}Ir and ^{169}Yb brachytherapy sources using state-of-the art XCOM photon cross sections.

Granero et al (2011) used MCNP5, PENELOPE, and GEANT4 Monte Carlo code and compared the dose-rate distributions of HDR ^{192}Ir model mHDR-v2 brachytherapy

source. Karaiskos et al (2003) and Angelopoulos et al (2000) also used Monte Carlo codes to investigate the dosimetric properties of HDR ^{192}Ir brachytherapy source models. Several investigators, Nath et al (1993), Wang and Sloboda (1996), Ballester et al (1997), Karaiskos et al (2000b) and Capote et al (2001a) reported 2-D dosimetry of LDR ^{192}Ir sources using the Monte Carlo simulation code.

^{60}Co HDR source is not as widespread like ^{192}Ir HDR source. Two ^{60}Co HDR remote afterloading systems are currently used in the treatment of gynaecological lesions (Ballester et al 2005). Many investigators (Ballester et al 2005, Selvam and Bhola 2010, Sahoo et al 2010 and Bhola et al 2012) calculated dosimetry parameters around the BEBIG ^{60}Co HDR brachytherapy source in an unbounded liquid water phantom using Monte Carlo code and analytical methods.

Similarly, Papagiannis et al (2003) compared the dosimetry parameters of three HDR ^{60}Co source models used in the Ralstron remote afterloader (Shimadzu Corporation, Japan) using Monte Carlo MCNP4C code. Enger et al (2012) explored the feasibility of ^{57}Co source in brachytherapy using the Geant4 Monte Carlo code.

1.8.2. Surface brachytherapy applications

Superficial brachytherapy is a promising treatment method for skin cancers using beta or beta-gamma sources such as ^{32}P, ^{90}Sr/^{90}Y, ^{188}Re and ^{177}Lu. These sources are capable of delivering therapeutic doses to the disease site with their short range (few mm) in tissue (Mukherjee et al 2002 and 2003, Salgueiro et al 2008a 2008b, Saxena et al 2012 and 2014 and Koneru et al 2016).

Lee et al (1997) first introduced the treatment of skin cancer using beta emitting ^{165}Ho-impregnated patch sources. Mukherjee et al evaluated ^{90}Y skin patches and ^{188}Re radioactive bandages for therapy of superficial tumuors in mice (Mukherjee et al 2002 and 2003). Treatment of skin cancer using ^{188}Re-labeled paper patches has been reported by Jeong et al (2003).

Pandey et al reported the use of ^{32}P cellulose-based adsorbent paper skin patches to control the tumour regression in C57BL6 mice bearing melanoma (Pandey et al 2008). Park et al (2008) studied the use of ^{32}P ophthalmic applicator after pterygium and glaucoma surgeries. Xu et al (2012) investigated the therapeutic effects of the chromic phosphate particle-based ^{32}P source in a rabbit VX2 lung tumour animal model. Salguerio et al (2008b) designed ^{32}P brachytherapy patch source for skin diseases using phosphoric acid and chromic phosphate in combination with natural rubber or silicone and evaluated its therapeutic efficacy. Gupta et al (2009) studied the efficacy of ^{32}P patch source for treatment of basal cell carcinoma and they concluded that this treatment modality is a suitable alternative against surgery.

^{177}Lu source labeled with radiopharmaceuticals are being used as a therapeutic radionuclide in nuclear medicine to treat many cancers. ^{177}Lu-DOTATATE is also an appropriate treatment option for patients with inoperable or metastatic neuro-endocrine tumour (Danthala et al 2014). Saxena et al (2015) has indigenously developed Nafion-115 based ^{177}Lu patch source to explore its suitability in the clinical treatment of skin cancer. Recently, Baum et al (2016) also studied the safety and efficacy of ^{177}Lu source labeled

with Prostate-Specific Membrane Antigen Radioligand Therapy for treatment of Metastatic Prostate Cancer.

^{90}Sr/^{90}Y applicators are commonly used in the treatment of restenosis, superficial lesions of the eyes and skin. Roa et al (2004) reported the dosimetric characteristics of the Novoste Beta-Cath ^{90}Sr/Y source trains using MD55-2 Gafchromic films in a Solid Water phantom and presented the necessary dose distributions as per TG-60 guidelines. The surface dose rate of ^{90}Sr or ^{90}Sr/^{90}Y ophthalmic applicator was measured using extrapolation chamber (Goetsch and Sunderland 1991b, Deasy and Soares 1994) and TLD's (Ali and Khan 1990). They concluded that the absorbed dose rate is strongly depends on size of collecting electrode of extrapolation chamber (Goetsch and Sunderland 1991b) and proposed calibration procedure including effect of measurement gap width, entrance window and stopping power ratio (Deasy and Soares 1994). Gleckler et al (1998) estimated the dose to the most radiosensitive areas of the lens during pterygium irradiation treatments for an ideal ^{90}Sr(^{90}Y) ophthalmic applicator using Monte Carlo simulations. They reported the dose rates to the lens ranging from 8.8 to 15.52 cGy s^{-1} for the applicator containing an activity of 55 mCi.

Soares et al (2001) reported the dosimetry intercomparison of three beta particle emitting ophthalmic applicators containing ^{90}Sr–^{90}Y, ^{106}Ru–^{106}Rh and ^{106}Ru–^{106}Rh sources at 1 mm from the source surface using several detector. Cohen et al (2013) studied the safety and efficacy of ^{90}Sr beta radiotherapy as adjuvant treatment of conjunctival melanoma for 20 patients. They concluded that this treatment is a very effective adjuvant

treatment with a local success rate of 90% and is not associated with significant side effects and visual acuity is not affected.

1.8.3. Low energy ^{125}I, ^{103}Pd and ^{131}Cs sources

Many investigators (Williamson 1991, Mainegra et al 1998, Kirov and Williamson 2001, Capote et al 2001b, Duggan and Johnson 2004) reported the dosimetric parameters of commercial ^{125}I sources using different Monte Carlo codes. Taylor et al (2007) presented a complete set of TG-43 data for 18 ^{125}I and 9 ^{103}Pd sources using the BrachyDose code. Murphy et al (2004), Wittman and Fisher (2007) and Rivard (2007) generated TG43 parameters and dose distributions for IsoRay Medical CS-1 ^{131}Cs brachytherapy source using MCNP5 Monte Carlo code. Sahoo and Selvam (2009) also investigated the influence of Ti K-shell x-rays on S_k, Λ and radial dose function for five ^{125}I seed models using the EGSnrc code system.

Plaque brachytherapy for eye treatment uses about 12 - 16 low energy seeds such as ^{125}I, ^{103}Pd and kept in the close contact with tumours. A number of dosimetry studies of different plaque designs have been reported in literatures using measurements and Monte Carlo simulations. Thomson and Rogers (2010) and Acar et al (2013) calculated and compared the dose distributions for ^{125}I seed models in the COMS eye plaque using the Monte Carlo code.

Dosimetry data for standard COMS-plaques using ^{125}I sources were generated by Chiu-Tsao et al (1993), Rivard et al (2008) and Knutsen et al (2001). Krintz et al (2002) also

measured the dose distribution for COMS plaques, loaded with ^{125}I seeds in a solid water phantom using radiochromic model MD55-2 film.

Dosimetric studies were carried out for ROPES eye plaque design loaded with ^{125}I seeds using the GEANT4 Monte Carlo code, Gafchromic EBT3 films, PRESAGE$^{\mathrm{m}}$ 3-D type dosimeter and results were compared with 3D treatment planning system (Granero et al 2004, Poder and Corde 2013a, Poder et al 2013b). Chiu-Tsao et al (2008), Acar et al (2013), Morrison et al (2014) and Heilemann et al (2015) used EBT3 Gafchromic film for dosimetry of ^{125}I sources. Chaudhary et al (2008) studied the dosimetry of OcuProsta source, treatment planning and quality assurance of a patient treated for ocular metastasis in eye plaque therapy.

1.8.4. Inhomogeneity correction in low energy brachytherapy sources due to non-uniform scatter condition

The TG-43 formalism calculates the dose distribution and dosimetry parameters around a single brachytherapy source positioned at the centre of a spherical liquid water phantom. In treatment planning, the doses are calculated by superposing the pre-calculated dose distributions according to the pattern of the source placement and the source dwell-time (Beaulieua et al 2012). However, the influence of tissue composition and applicator heterogeneities differing from liquid water, interseed attenuation, and finite patient dimensions are all ignored. It also cannot account for the reduced photon backscatter near the skin.

Rivard et al (2009a) reported the effect of the inhomogeneities such as applicator shielding, interseed attenuation and concluded that the effect would be greater for low-energy photon emitters, such as ^{125}I compared with ^{192}Ir. Lee (2014) found the differences in the absorbed dose to water compared with tissue are −4% for low-energy emitters and +2% for high-energy emitters.

Various research groups reported the dose differences between dose to the medium by accounting all inhomogeneities present and dose to water. The estimated dose to the medium is always lower than the dose in water due to inhomogeneity except for lung treatment. Tissue inhomogeneity correction factor for brachytherapy sources in a homogeneous phantom was calculated by Meigooni and Nath (1992b). Taylor found 10% difference for ^{125}I and ^{103}Pd sources for prostate tissue (Taylor 2006). Similarly Thomson et al obtained a difference of 9% for different eye tissues for ^{125}I or ^{103}Pd seeds in the standardized eye plaque therapy (Thomson et al 2008). In an another dose-volume histograms study for ^{125}I and ^{103}Pd idealized implants, Chibani and Williamson (2005b) found 6% lower dose to 100% of the prostate volume when prostate modeled as soft tissue than water.

In a Monte Carlo study of prostate implant using ^{125}I seeds, Carrier et al (2006) reported dose differences of 4 - 5% between the dose deposited in 90% of the prostate volume and water. In an another Monte Carlo simulation study using 28 patient CT data, Carrier et al (2007) reported 7% dose difference between the dose to water and the dose to medium, of which 3% is due to tissue composition and the remaining 4% to interseed attenuation.

Sutherland et al (2012) estimated the dose to medium in intraoperative ^{125}I lung brachytherapy using patient CT data in BrachyDose Monte Carlo code. They reported that TG-43 underestimates the dose by up to 36% in larger volumes containing higher proportions of healthy lung tissue.

In lung brachytherapy, Yang and Rivard (2011) investigated the effect of non-water tissues using Monte Carlo simulations of a phantom comprised of soft tissue, lung, and cortical bone for photon sources for energies 20 - 400 keV, they concluded that TG-43 overestimates PTV dose and underestimates dose to bone and healthy tissue.

1.8.5. Response of well chamber to pressure variations at high altitudes

Well-type ionization chambers are routinely used to measure air-kerma strength of brachytherapy sources. During routine measurements, a temperature and pressure correction factor (K_{TP}) is applied to account for the change of air density in chamber volume. This K_{TP} correction factor breaks down for low energy photon sources at low air pressures observed at high altitude cities.

Response of the well chamber to pressure difference at high altitudes is studied by Bohm et al (2005, 2007) using Monte Carlo calculations. Bohm et al (2005) concluded that normalized K_{TP} correction factor produces 10 - 20% over-response at the reduced air pressure corresponding to altitudes of 3048 m above sea level for photon energies 20 - 40 keV. Bohm et al (2005) modeled well chamber with graphite, copper, C-552 plastic and aluminum and concluded that the response is dependent on atomic number and photon cross section of the chamber wall material.

Griffin et al (2005) also designed a pressure vessel for range of pressure corresponding to height 2590 m above sea level to 610 m below sea level. He measured the over-response for three models of air-communicating well chambers (SI model HDR1000 Plus, IVB1000 and PRM WC-2 chamber) for low-energy photon sources at various elevations above sea level. Additional correction factor for ambient pressure was proposed by them for aluminum walled well chambers (Griffen et al 2005).

Russa and Rogers (2006, 2007) also investigated the validity of the K_{TP} correction factor for kilovoltage x-rays for different ion chambers using the EGSnrc Monte Carlo code and measurements. A 2% deviation over expected value when measured in graphite thimble chamber and 16% deviation over expected value measured in a large spherical graphite chamber are observed for a 40 kV spectrum corresponding to air density of Mexico.

1.9. Objectives of the work undertaken in this thesis

- Dosimetric study of HDR ^{192}Ir brachytherapy source indigenously developed by BARC / BRIT using Monte Carlo-based EGSnrc code system in a 40 cm diameter x 40 cm height cylindrical water phantom and compared with other commercially available HDR ^{192}Ir sources. The calculated data are utilized for the indigenous development of the brachytherapy TPS which will be used for planning of brachytherapy patients.

- Dosimetric study of indigenously developed ^{32}P and ^{177}Lu patch sources for skin applications. Central axis depth dose and dose profiles in water phantom were

calculated ^{32}P patch sources using the EGSnrc-based Monte Carlo code system. The surface dose rate of an in-house developed ^{177}Lu skin patch source was measured using an extrapolation chamber, EBT3 Gafchromic film and compared against Monte Carlo methods.

- Dosimetry of indigenously developed ^{125}I source for intraocular tumours. Experimental dosimetry for a 14 mm diameter silver eye plaque embedded with 13 ^{125}I seeds was carried out using EBT3 films to determine absorbed dose rate and central axis depth dose.

- Dosimetry of ^{125}I and ^{131}Cs brachytherapy sources due to non-uniform scatter condition such as the effect of tissue in-homogeneity and interseed attenuation.

- The K_{TP} corrected normalized response of Well chamber to pressure variations at high altitudes for ^{131}Cs and ^{169}Yb sources using EGSnrc and FLUKA Monte Carlo codes. Simulations were carried out for air densities from 0.862 kg m^{-3} (3048 m) to 1.197 kg m^{-3} which cover high altitude cities like Shimla, Darjeeling, Srinagar and Mexico.

CHAPTER 2

INTERACTION OF RADIATION WITH MATTER, MONTE CARLO

TECHNIQUES AND THEIR APPLICATIONS IN BRACHYTHERAPY

2.1. Interaction of radiation with matter

Radiation emitted by a radioisotope cannot be seen or felt by any human senses. Radiation when incident on matter, interact with the atoms and depending on its energy, produce excitation or ionization of atoms along its path. Excitation is a process in which the orbital electron of an atom is raised to a higher energy state. Ionization is responsible for the physical, chemical and biological effects in the medium. Both these processes lead to transfer of energy from radiation to matter. Ionizing radiation can be divided into directly ionizing radiation (charge particles such as alpha and beta) and indirectly ionizing radiation (x-ray, gamma rays and neutron).

2.1.1. Interaction of beta particles with matter

Beta particles are light particles. They get scattered in the presence of electrons in the medium and undergo a tortuous path. The range of beta particles is expressed in g cm^{-2} which is the product of the density and the linear thickness of the absorber. The relationship between energy and range is given by the empirical equations (Cember and Johnson 2009):

$$R = 0.407 \, (E)^{1.38} \, , \quad E \leq 0.8 \text{ MeV} \tag{2.1}$$

$$R = 0.542 \, E - 0.133, \quad E \geq 0.8 \text{ MeV} \tag{2.2}$$

Where R = range in g cm^{-2} and E = maximum beta energy in MeV

Beta particles loose energy by radiative processes and by collisional losses. Coulomb interaction with the orbital electrons leads to excitation and ionization and the amount energy loss is known as collisional loss. The ejected electron with sufficient kinetic energy also produces delta ray.

When a fast moving charged particle passes close to a nucleus, it experiences deceleration and travel in a new direction with reduced speed. The energy loss in this process appears as electromagnetic radiation and radiation emitted is termed as bremsstrahlung radiation. The intensity of bremsstrahlung radiation increases with the atomic number of the medium and decreases with increase in the mass of the particle.

2.1.2. Interaction of electromagnetic radiation with matter

Electromagnetic radiations (X and gamma rays) commonly known as photons are referred to as indirectly ionizing radiation. The electron produced during the first interaction further carries out the ionization process and transfer the energy received from the photon into the medium. The interactions of these radiations with matter are (1) Photoelectric absorption, (2) Compton scattering and (3) Pair production and these interactions are discussed below.

2.1.2.1. Photoelectric absorption

In photoelectric absorption, an incoming photon transfers its entire energy to a bound electron and disappears. A photon of energy E will release an electron with kinetic energy E_e equal to $E - \phi$, where ϕ is the binding energy of the orbital electron. The electron moves out of the atom leaving a vacancy in the shell. An electron from an outer shell will

occupy this vacancy, releasing its excess energy in the form of characteristic x-rays or by emission of auger electron.

Photoelectric absorption is more likely to happen when the energy of the photons is equal or just above the binding energy of the inner most orbital electrons of the interacting medium. The probability of the photoelectric interaction is proportional to $Z^3 E^{-3}$, where Z is the atomic number of the medium.

2.1.2.2. Compton scattering

In Compton scattering, an incoming photon interacts with a relatively free or outermost electron. During the interaction, photon transfers only a part of its energy and deviates from original path with reduced energy as a scattered photon. The recoil electron produced in this process, interacts with the medium by excitation and ionization.

Compton scattering depends on the electron density of the medium. Since almost all elements have same number of electrons per gram of the material except hydrogen, Compton scattering is independent of the Z of the medium. The probability of this interaction decreases with the increase in the energy of the incident photon. In soft tissues, in the energy of 100 keV to 10 MeV, this interaction is more predominant than photo electric or pair production process.

2.1.2.3. Pair production

It is an interaction between a high energy photon and the strong electromagnetic field surrounding the nucleus. In this process the photon in the presence of nuclear field gets converted into a pair of electron and positron. As the rest mass energy of an electron is

0.511 MeV, the minimum energy of photon required to create an electron positron pair is 1.02 MeV is known as threshold energy. Energy in excess of this threshold energy is shared as the kinetic energy between the electron and positron. Positrons when comes to rest combines with an electron resulting in the release of annihilation radiation in the form of two photons, each of energy 0.511 MeV, moving in opposite direction.

2.1.2.4. Attenuation of x-rays and gamma rays in the medium

When a photon beam interacts with the medium some photons are absorbed in the medium (photoelectric effect), some are scattered from the medium (Compton scattering, pair production) and the remaining photons which do not undergo interactions, emerge out of the medium as transmitted photons. In another words, interacting medium attenuates a photon beam.

The attenuation per unit path length in the medium is termed as linear attenuation coefficient (μ) and unit is cm^{-1}. Linear attenuation coefficient depends upon the energy of photon and the atomic number or density of the medium.

The attenuation coefficients or cross sections give the probabilities of removal of a photon from a beam. The total attenuation coefficient is the sum of the coefficients for each of the three interactions discussed above. Higher the energy of photons, lesser will be the attenuation and higher the atomic number or density of the medium, more will be the attenuation.

Attenuation of photons in the medium is governed by following exponential law:

$$I = I_0 \, e^{-\mu x} \qquad\qquad\qquad (2.3)$$

Where, I_0 is the intensity of the incident beam, I is the intensity of the beam emerging out after traversing a thickness x cm of the medium and μ is the linear attenuation coefficient of photon.

2.2. Monte Carlo techniques in radiation transport

The radiation transport theory, being statistical in nature, can be used to solve dosimetric problems in radiotherapy. Deterministic methods and Monte Carlo techniques are used to model the radiation transport of photons, electrons, neutrons etc. in a medium. Monte Carlo method is a well known stochastic method that uses Boltzmann transport equations to simulate particle transport in a medium (Boman 2005, Andreo 1991, Lorence and Beutler 1997). The Monte Carlo method was first introduced by Neuman & Ulam (Eckhardt 1987).

The Monte Carlo simulation begins with the exact description of the medium, geometry and radiation sources. This technique involves the computation of the average of probable behaviour of a system by observing the outcomes of a large number of trials. The accuracy depends on the modelling of the problem, cross-sections and number of simulations performed. There are many Monte Carlo codes such as MCNP (Briesmeister 1993), EGSnrc (Kawrakow et al 2013), BrachyDose (Taylor et al 2007), GEANT4 (Agostinelliae et al 2003), PTRAN (Berger 1993), PENELOPE (Baro et al 1995, Salvat et al 1996) etc available for radiation transport applications. Monte Carlo radiation transport codes have been widely used for dose calculations at the vicinity of the brachytherapy sources and because of the large potential errors associated with experimental measurements (Wallace et al 2002, Perez-Calatayud et al 2009).

In Monte Carlo techniques, the physical systems and phenomena are simulated by statistical methods employing random numbers. The general idea is to create a model, which is similar as possible to the real physical system of interest, and to create interactions within that system based on known probabilities of occurrence. The behavior of physical system can be described by probability density functions and the Monte Carlo simulation can proceed by sampling from these probability density functions. As the number of individual events (called histories) is increased, the quality of the reported average behavior of the system improves, meaning that the statistical uncertainty decreases. Particles are generated within the source region and are transported by sampling from probability density functions (PDF) through the scattering media until they are absorbed or escaped the volume of interest. The outcomes of these random samplings or trials (known as Scoring), must be accumulated or tallied in an appropriate manner to produce the desired result. The essential characteristic of Monte Carlo is the use of random sampling techniques to arrive at a solution of the physical problem.

2.2.1. Random sampling in Monte Carlo techniques

Monte Carlo techniques utilize sequences of random numbers to perform the simulation. For any statistical simulation, where only probability of occurrence of a certain process is known, random numbers are used.

The linear congruential random number generator is a deterministic algorithm, most commonly used to generate a sequence of random numbers from a seed (Gentle 1998). It is given in the form of

$$X_{i+1} = (a\,X_i + c)\,mod\,m \tag{2.4}$$

Where i is the sequence label and *a, c* and *m* are the magic numbers. Note X_i can't be truly random as they are generated using deterministic algorithm and two sequences from the same seed are identical. These random numbers pass through many tests of randomness. They are often termed pseudo-random numbers and they are used for all practical purposes as if they were truly random.

A random number 'R' is a number, uniformly distributed between 0 and 1 such that probability $p(R)$ of finding any particular value of R is independent of the value of R;

i.e. $p(R) = 1, 0 \leq R \leq 1$

and probability of selecting a number from a certain gap is equal to the gap width (Figure 2.1); i.e. $p(R) \, dR = dR$
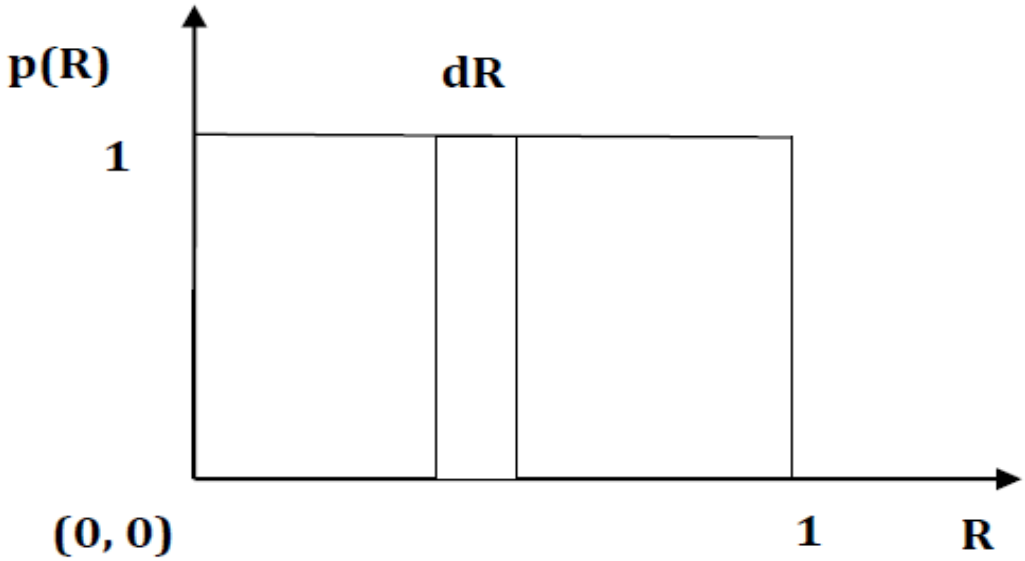
Figure 2.1. The probability density function of random numbers.

The cumulative distribution function P(R) is given by (Figure 2.2),

$$P(R) = \int_0^R p(R)dR = R, \quad \text{with P(R)} = 0, \text{ for } R < 0, \text{ and}$$

P(R) = R, $0 \leq R \leq 1$ and P(R) =1 , R>1
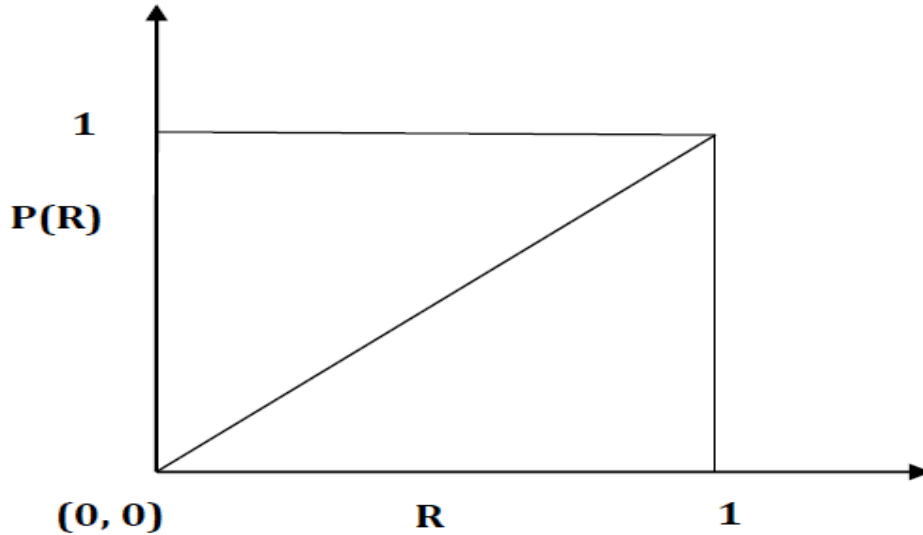
Figure 2.2. The cumulative distribution functions of random numbers.

The uniformly distributed random number R in the interval (0,1) can be simply denoted as U(0,1). The random sampling techniques help us to convert a sequence of random numbers (R_i), uniformly distributed in the interval (0,1) to a sequence (x_i) having the desired density, say f(x). Inversion sampling technique is widely used in Monte Carlo simulation. The distance travelled by the photon or path length before first collision in a medium is determined by this technique using random numbers.

Particles are emitted from the source, travel in the medium and their interaction such as collision, absorption, scattering, escape from the medium etc. are recorded. The events

associated with one particle constitute the history of that particle. Finally, the Monte Carlo result or score (tally output) represents an average of the contributions from all the events, sampled during the course of the problem. The tally output comes with the required result and a statistical error associated with the result. To get better statistical uncertainty, more number of histories is required. The statistical error in the Monte Carlo simulation is proportional to $\frac{1}{\sqrt{N}}$ where N is the number of histories i.e. the total number of histories to be increased to 4 times to make error to half.

2.2.2.   Physics of Monte Carlo code system

2.2.2.1.   Physics of photon transport

Basically, the photon transport algorithms used in any Monte Carlo simulation technique consists of four routines given below. The logic flow diagram (Rogers and Bielajew 1990) is shown in Figure 2.3:

1. **Source routine:** Source routine generates photons and places them in STACK along with their energy, position and directions.

2. **Path length routine:** If the energy of the photon is above cut-off energy, then distance to photons next interaction (path length) is determined by exponential probability law.

    The probability of transmission of photon traveling a distance x is $e^{-\mu x}$

    The probability of interaction of photon in the medium in dx is μdx

    Probability of interaction between x and x + dx = $\mu dx\, e^{-\mu x}$

    Required PDF of path length (x) = p(x) dx = $\mu\, e^{-\mu x}\, dx$

Sampling for distance x from the cumulative probability P(x):-

$$R = P(x) = \int_0^x p(x)dx$$

$$R = \mu \left| \frac{e^{-\mu x}}{-\mu} \right|_0^x = 1 - e^{-\mu x}$$

$$x = \frac{\ln(1-R)}{-\mu} = \frac{-\ln R}{\mu}$$

Where R is the random number distributed between 0 and 1.

3. **Photon interaction routine:** The type of interaction of a photon is determined by random sampling from their individual relative interaction probabilities (μ_i/μ_T). The sum of individual relative interaction probabilities is given by:

$$\frac{\mu_{PE}}{\mu_T} + \frac{\mu_c}{\mu_T} + \frac{\mu_{Pp}}{\mu_T} = 1 \tag{2.5}$$

Where $\mu_{pe} + \mu_c + \mu_{pp} = \mu_T$. Here, μ_T is the total cross-section or linear attenuation coefficient, μ_{pe} is photo electric interaction cross-section, μ_c is Compton scattering cross-section and μ_{pp} is pair production cross-section. All these are macroscopic cross sections and have the unit of cm^{-1}.

Let us assume an interaction of photon, where probability of photo electric effect is 20%, probability of Compton scattering is 75% and probability of pair production is 5% (Figure 2.4). Sample a random number, R. If its value is ≤ 0.20, then the interaction is photo electric effect. If the value of R > 0.20 and ≤ 0.95, then it is Compton scattering and if R is ≥ 0.95 then it is pair production.
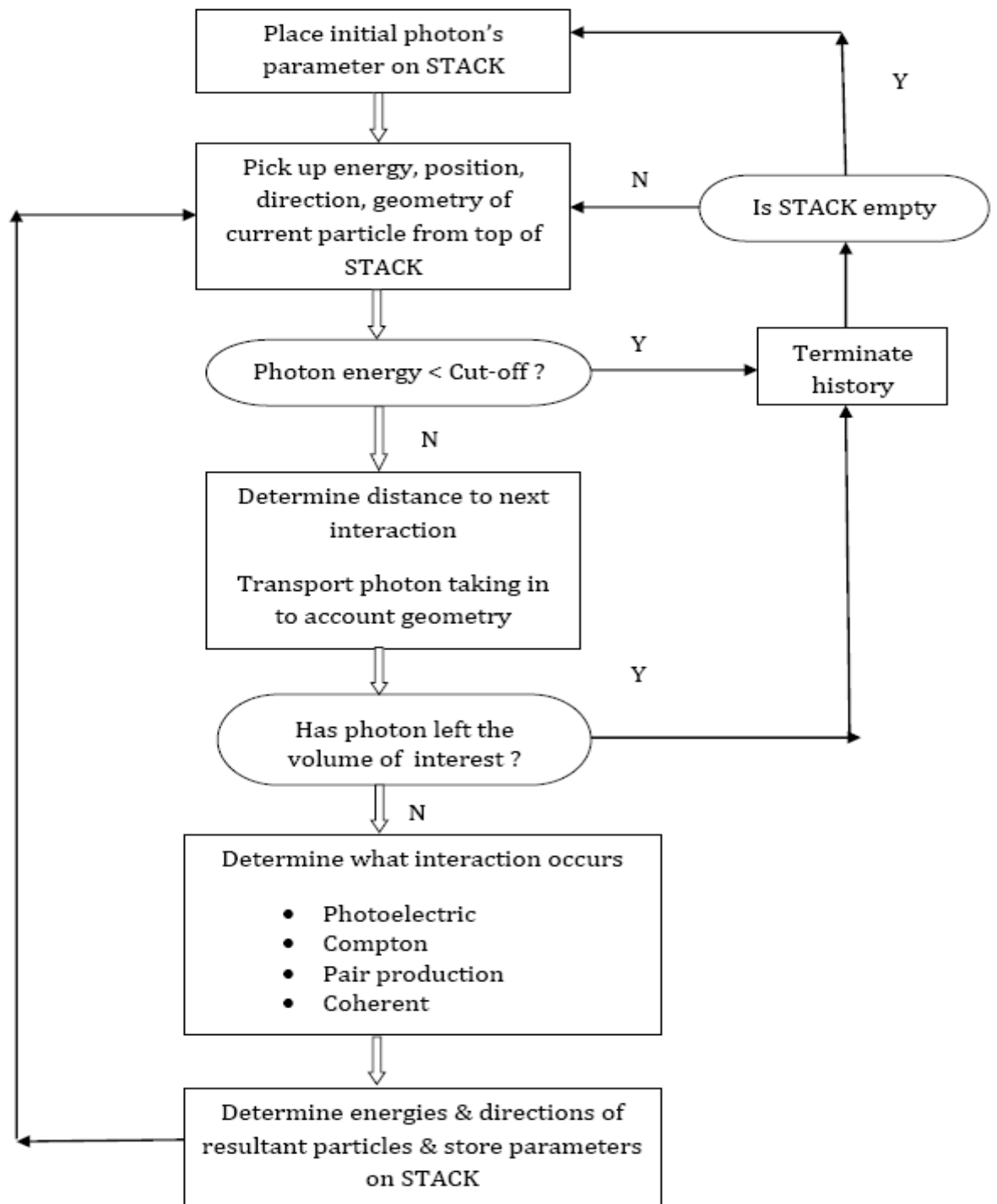
Figure 2.3. Flow of a Monte Carlo simulation of photon transport (Ref. Rogers &

Bielajew 1990*).*

0   0.20   0.95   1.0

Figure 2.4. Determination of type of interaction of photon using random number sampling.

4. **Geometry and scoring routine:** A geometric routine is designed to decide whether a photon, during its transport is (a) inside the medium, (b) escaped into another medium or system, (c) deflected from the original direction, or (d) entered the region of interest and particle scored with specified parameters. Scoring a physical quantity means keeping track of the particle. For example, to find out absorbed dose, we score the energy deposited in a particular geometric region.

2.2.2.2. Physics of electron transport

The predominant modes of interaction of electrons through matter are inelastic collision with atomic electrons (collision loss) and inelastic collision with nucleus (radiation loss). In addition, electrons also participate in elastic collisions with nuclei, which lead to deflection and electron does not radiate nor it excites the nucleus.

It is known that a fast electron and its secondary particles undergo very large number of interactions (order of 10^4 - 10^5) with surrounding matter during slowing down process (Berger 1963). Hence it is difficult to track the event-by-event simulation of electrons and photons produced during successive interactions, which takes lot of computing time.

65

Berger (1963) developed the condensed history (CH) technique, where, large numbers transport and collision processes are condensed to a single step. The cumulative effect of the individual interactions is taken into account by sampling the change of the particle's energy, direction of motion, and position, at the end of the step from appropriate multiple scattering distributions. Berger (1963) divided the CH technique in to Class I and Class II techniques.

Class I CH technique groups all the interactions and uses a predetermined set of path lengths, the random sampling of interactions being performed at the end of the step. Class II technique is a mixed procedure in which (a) collisions with small energy losses and deflections, resulting in emission of bremsstrahlung above an energy threshold, are grouped together and (b) occasional catastrophic collisions, in which the loss or deflection are very large, that produces delta rays, are treated separately over the entire CH step.

2.3. EGSnrc Monte Carlo code system

The EGSnrc code system is a general purpose package for the Monte Carlo simulation and transport of electrons and photons in an arbitrary geometry for particles with energies of few keV up to several hundreds of GeV (Kawrakow et al 2013). It is an enhanced version of EGS4 system (Kawrakow 2000) and it includes many improvements in electron-transport algorithms. EGSnrc code system employs the Class II CH Monte Carlo model for electron energy loss. It uses Moliere multiple scattering theory and electron-step algorithm (PRESTA-II).

Cross sections included with the EGSnrc code system are: 1) The Evaluated Photon Data Library (Cullen et al 1990), 2) XCOM data from Berger & Hubbell (1987), and 3) Storm & Israel (1970). PEGS4 is the program which prepares the material dependent cross section data sets required by EGSnrc code system to do the simulations. The code allows the user to score any parameter of interest and track the simulation step-by-step. The outputs information is given in the user-written subroutine called AUSGAB. The code system allows importance sampling and other variance reduction techniques (eg., particle biasing, splitting, path length biasing, Russian roulette, etc.).

The EGSnrc code system consists of many user-codes such as DOSRZnrc, FLURZnrc, CAVRZnrc, DOSXYZnrc, BEAMnrc and SPRRZnrc for scoring different quantity of interest (Rogers et al 2010). DOSRZnrc user-code scores dose in a generalised cylindrical geometry. FLURZnrc scores particle fluence in the cylindrical geometry. CAVRZnrc scores a variety of quantities which are of specific interest to dosimetry calculations for an ion chamber. SPRRZnrc calculates Spencer-Attix spectrum averaged stopping-power ratios for arbitrary media. DOSXYZnrc user-code calculates dose distributions in a rectilinear voxel phantom. The user-codes were discussed below.

2.3.1. DOSRZnrc user-code

DOSRZnrc user-code (Rogers et al 2010) simulates the passage of an electron or photon beam in a finite, right cylindrical geometry. It also scores pulse height distributions in an arbitrary volume made up of any number of regions. The energy deposited within various user defined regions are scored and analyzed statistically. This user-code scores dose per

incidence particle in a user defined cylindrical geometry. Important routines where the user will define the geometry, materials and transport parameters are described below;

Geometry description and material inputs: The geometry in the DOSRZ user-code is described by numbering the cylinders / rings and planar regions / slabs. Each geometrical region needs a material to be associated with it. The names of the materials must be entered through the MEDIA input and must match that in the PEGS4 dataset.

Source routine inputs: In this routine, user will select incident particle and its energy (either mono-energetic or spectrum). For spectrum, user will create a spectrum file (file extension ends with .SPECTRUM) consisting of energy bins and corresponding probabilities. The RZ user-code has 16 source options (point, parallel beam, disk source, etc.) to specify various sources. User will enter the source number and source dimensions (height, radius, position etc.).

In the present work, DOSRZnrc user-code is utilized for dose calculation of (i) BRIT ^{192}Ir HDR source (Chapter 3), (ii) ^{177}Lu skin patch source (Chapter 4), and (iii) ^{125}I OcuProsta source (Chapter 5).

2.3.2. CAVRZnrc user-code

The CAVRZnrc user-code (Rogers et al 2010) scores a variety of quantities of dosimetric interest for an ion chamber. All the scoring regions comprising the cavity are entered in the cavity block of the user-code. The material described in the cavity is air. This user-code gives the total energy deposited in the cavity by electrons generated by primary photons and the energy deposited in the cavity by the scatter component that contains the

dose due to scattered photons as well as the dose due to bremsstrahlung, fluorescent and annihilation photons, whatever their origin (Bielajew1986). The output of this user-code is normalized to per starting particle.This user-code is utilized for estimation of response of a well-type ionisation chamber at high altitudes for ^{131}Cs and ^{169}Yb source (Chapter 7).

2.3.3. DOSXYZnrc user-code

DOSXYZnrc is a user-code for 3-dimensional absorbed dose calculations (Walters et al 2009). DOSXYZnrc simulates the transport of photons and electrons in a cartesian volume and scores the energy deposition in the designated voxels. Voxel dimensions are completely variable in all three directions. Every voxel can have different materials and/or varying densities. DOSXYZnrc user-code has a number of unique features such as dose component calculations, 10 source configurations and beam reconstruction techniques, CT to phantom conversion using ctcreate, restart capabilities, phase-space redistribution, *etc*. In the present work, DOSXYZnrc user-code is utilized for dose calculation of ^{32}P skin patch source (Chapter 4).

2.3.4. Transport parameters required in the EGSnrc simulations

The transport parameters defined by the user during the simulations are: (1) Electron-step algorithm (ESA), (2) Global electron and photon transport cut-off energy (ECUT, PCUT), (3) Global maximum step size restriction (SMAX) (4) Boundary Crossing Algorithm (BCA), (5) Skin depth for BCA, and (6) Low-energy threshold for secondary electron production (AE). The user is to specify the number of histories, time limit and statistical limit in the Monte Carlo routine. Variance reduction techniques are also available for the user.

The EGSnrc Monte Carlo calculations for the dosimetry of brachytherapy sources in this thesis utilized the PRESTA-II algorithm for electron step length and EXACT boundary-crossing algorithms. The electron step-size parameter was set at ESTEP = 0.25. The PEGS4 dataset needed for the Monte Carlo calculations was based on XCOM compilations (Berger and Hubbell 1987). To increase the speed of the calculations, for all simulations, electron range rejection technique is used by setting ESAVE = 2 MeV.

In the Monte Carlo calculations for low energy sources (^{125}I, ^{131}Cs and ^{169}Yb, ^{177}Lu skin patch source), the transport cut off energy for photon, PCUT and for electron, ECUT were chosen at 1 keV and 0.512 MeV, respectively. The values of AE, AP set in the PEGS4 programme were 0.512 MeV and 1 keV, respectively. The parameters AE and AP are the low energy thresholds for the production of knock-on electrons and secondary bremsstrahlung photons, respectively.

Similarly, the transport parameters in the simulations of high energy sources (^{192}Ir HDR source and ^{32}P patch source), the values of AE and AP were set at 521 keV and 10 keV respectively. The value of photon transport cutoff parameter PCUT used in all simulations was 10 keV. The value of ECUT used in absorbed dose calculations was 521 keV.

2.4. FLUKA Monte Carlo code

FLUKA is general purpose Monte Carlo code capable of transporting about 60 different particles accurately in matter including photons and electrons from 1 keV to thousands of

TeV (Ferrari et al 2005). FLUKA version 2011.2c is used in present study. This code has the capability to handle complex geometries using an improved version of the Combinatorial Geometry (CG) package. FLUKA can score many dosimetric quantities, (a) energy density in a region (b) energy and momentum transfer density and specific activity in a geometry averaged over event by event, (c) energy deposition weighted by a quenching factor (Birks law), (d) fluence, current and dose equivalent scoring via boundary crossing, collision and track-length estimators.

2.4.1. Electrons and Photons transport in FLUKA code

Following is based on FLUKA manual (Ferrari et al 2005). FLUKA code uses an original transport algorithm for charged particles, including a complete multiple coulomb scattering treatment giving the correct lateral displacement even near a boundary. The variations with energy of the discrete event cross sections and of the continuous energy loss in each transport step are taken into account exactly. Differences between positrons and electrons are taken into account concerning both stopping power and bremsstrahlung. The bremsstrahlung differential cross sections of Seltzer and Berger have been extended to include the finite value at "tip" energy, and the angular distribution of bremsstrahlung photons is sampled accurately (Seltzer and Berger 1985). The Landau-Pomeranchuk-Migdal suppression effect (Landau and Pomeranchuk 1953) and the Ter-Mikaelyan polarisation effect (Ter-Mikaelyan 1954) in the soft part of the bremsstrahlung spectrum are also implemented. Positron annihilation in flight and at rest and delta-ray production via Bhabha and Møller scattering are incorporated (Bhabha 1935, Moller 1932).

Pair production is treated with actual angular distribution of electrons and positrons. Compton effect is incorporated with Doppler broadening using a fit of the Compton profiles, and account for atomic bonds through use of inelastic Hartree-Fock form factors (Biggs et al 1975). Photoelectric effect uses actual photoelectron angular distribution, according to the fully relativistic theory of Sauter (Sauter 1931). Interactions sampled separately for each component element and for each edge. The edge fine structure is taken into account.

The present lowest transport limit for electrons is 1 keV. Although in high-Z materials the Molière multiple scattering model becomes unreliable below 20 - 30 keV, a single-scattering option is available which allows to obtain satisfactory results in any material also in this low energy range. The minimum recommended energy for primary electrons is about 50 to 100 keV for low-Z materials and 100 - 200 keV for heavy materials, unless the single scattering algorithm is used. Single scattering transport allows overcoming most of the limitations at low energy for the heaviest materials at the price of some increase in CPU time.

2.5. Monte Carlo techniques in brachytherapy dosimetry

Monte Carlo methods have found extensive use in brachytherapy radiation dosimetry, due to difficulties and complications involved in direct measurement near the sources (Chibani and Williamson 2005a). Due to the inverse square law dominance, there is a high dose gradient around brachytherapy sources. For example, dose at 2 mm from the source is 25 times of dose at 1 cm. To limit the dose uncertainty up to 2%, the position

uncertainty of the detectors in the phantom should be less than 50 μm and 20 μm at 5 mm and 2 mm from the source respectively (Williamson, 2005). Positioning the detectors at such micron distance is difficult in measurements. Detectors have also other issues like linearity of dose response, spatial resolution, energy dependence, sensitivity, volume averaging artefacts, etc. The second disadvantage of experimental dosimetry is the poor signal-noise ratio in the detector for large distances from the source.

1-dimensional Monte Carlo simulations and transport equation have been used since the 1960s to calculate radial dose distributions for isotropic point sources in medium, using buildup factors (Berger 1968), and the tissue-attenuation and scatter buildup factors (Meisberger et al 1968). The recent developed Monte Carlo codes use accurate cross section tables (Hubbell 2006) and can able to simulate complex geometries and calculate dose distribution within mm range from the sources with desired accuracy. Monte Carlo code has become a powerful and valuable tool in brachytherapy dosimetry and constituting one of the dosimetry prerequisites for routine clinical use of new low and high energy photon sources (Rogers 2006, Baltas et al 2007, Thomadsen et al 2005).

The Monte Carlo method has its own limitations. It is a time consuming technique, because for a precise and accurate result, simulation will run for millions of histories. Also, there is a need for accurate knowledge of the source, spectrum, geometry, atomic composition of materials, the uncertainties involved in the cross sections and the modelling of the physical processes.

2.6. Recommendations for Monte Carlo dosimetry (low energy sources)

AAPM recommends that the Monte Carlo investigators should utilize well-benchmarked Monte Carlo codes such as EGSnrc, MCNP, Geant4, PTRAN etc. with modern / updated cross-section libraries to model 3D geometry of the source and generate reference-quality dose distribution (Kawrakow et al 2013, Williamson 1987). Monte Carlo investigators should able to reproduce previously published dose distributions for at least one widely used brachytherapy source model and they should rigorously test new radiation transport codes for brachytherapy dosimetry and publish in the peer-reviewed literature before their use in clinics.

2.6.1. Requirements in the Monte Carlo calculations

The requirements for calculating dosimetry parameters for low energy sources are, (1) The phantom must be a 30 cm diameter liquid water sphere (Rivard et al 2004), (2) Enough histories should be calculated such that the statistical uncertainty should be $\leq 2\%$ at r $\leq$ 5 cm, and $\leq$ 1 % in the derivation of S_K with k = 1, (3) Modern cross-section libraries equivalent to the current NIST XCOM database should be used. The use of older cross sections libraries could produce errors of up to 5 - 10% in low energy sources (Bohm et al 2003), (4) Source dimensions and compositions of encapsulation and internal components should be verified through the use of physical measurements, transmission radiography, and autoradiography, (5) Use of the appropriate choice of tallies and scoring voxels, and (6) A simulation of the WAFAC (Wide Angle Free Air Chamber) must be mandatory for comparison of S_k.

2.7. Guidance on dosimetry for high energy brachytherapy sources – need of a new TG report

The AAPM has reviewed its 1995 and 2004 TG dosimetry reports TG-43 and TG-43U1 (Nath et al 1995, Rivard et al 2004) for low-energy brachytherapy sources and its supplement reports TG-43U1S1 (Rivard et al 2007 and 2010). In the last decade several new ^{192}Ir source designs for the HDR delivery systems have been introduced (Williamson and Li 1995, Daskalav et al 1998, Karaiskos et al 2003, Angeopoulos et al 2000, Ballester et al 2001, Perez-Calatayud et al 2001). Many new brachytherapy sources, such as ^{60}Co (Papagiannis et al 2003, Ballester et al 2005, Granero et al 2007), ^{169}Yb (Medich et al 2006, Medich and Munro 2010), and ^{170}Tm (Ballester et al 2010, Enger et al 2011, Munro et al 2008) are also being actively investigated.

Similar recommendations and guidelines are not available for high energy sources. To fill this void, the High Energy Brachytherapy Source Dosimetry (HEBD) Working Group of AAPM recommended methods for evaluating consensus dosimetry datasets for high-energy photon sources with average energy higher than 50 keV (Perez-Calatayud et al 2012). Li et al (2007) recommends that the dosimetric studies should be approved by the U.S. Federal Drug Administration (FDA) and Nuclear Regulatory Commission (NRC) for sources with average energy higher than 50 keV intended for clinical use.

All TG-43U1 guidelines and recommendations given in the TG-43U1 report (Rivard et al 2004) on low-energy brachytherapy are also applicable to high energy sources, with few exceptions such as dependence of dosimetry parameters on (a) effect of phantom

dimension, (b) grid size and interpolation accuracy, (c) source active length, and (d) disequilibrium near the source. These four parameters are discussed below.

(a) Effect of phantom dimensions

Treatment Planning System calculations are generally based on dosimetry parameters, dose rate tables for cylindrically symmetric sources in a uniform water or water-equivalent medium and negligible inter source attenuation effects. The absorbed dose rate to water should be computed in an unbounded liquid water phantom. For ^{192}Ir, ^{137}Cs, and ^{169}Yb sources, a spherical phantom with radius R = 40 cm (or the equivalent cylindrical phantom), while R = 80 cm should be used for ^{60}Co sources (Perez-Calatayud et al 2012).

Williamson (1991) compared the dose values for ^{192}Ir source in unbounded water phantom and a 15 cm radius spherical phantom with measured data for a (20 cm)^3 cubic phantom. Agreement in dose values within 5% was observed up to 5 cm from the source, but differences of 5 - 10% were noted for r > 5 cm. A difference of 12% at r = 12 cm was observed for a PDR ^{192}Ir source between the dose calculated in an unbounded phantom and a spherical phantom of radius R = 15 cm (Williamson and Li 1995). Perez-Calatayud et al (2004) showed that dose differences between phantom of R = 40 cm (unbounded phantom) and R = 15 cm, reached 7% (^{192}Ir) and 4.5% (^{137}Cs) at r = 10 cm.

For ^{60}Co source a spherical water phantom of 50-cm radius (Ballester et al 2005, Papagianis et al 2003) or a cylindrical water phantom of 100-cm diameter and 100-cm height (Sahoo et al 2010) acts as an unbound phantom and provide full scatter up to a distance of 20 cm. These differences in the dose parameters for different phantom size are

due to the different scatter conditions caused by a lack of backscattered photons at the border of the phantom.

(b) Dose calculation grid size and interpolation accuracy

Current TPS allow direct entry of tabulated dosimetry parameters, in rectangular format (y,z) or polar coordinates (r,θ). During changing from rectangular to polar coordinates, mathematical functions are required to fit and smooth tabulated data, and extrapolating data outside of the available data range. Hence, the TG-43 data should be presented with adequate range and spatial resolution. Dose scored in voxels is a volume averaged estimate of the dose at the center of a voxel.

To minimize systematic error, voxel sizes are chosen: $(0.1 \text{ mm})^3$ for distances $0 < r \leq 1$ cm, $(0.5 \text{ mm})^3$ voxels for $1 \text{ cm} < r \leq 5 \text{ cm}$, $(1 \text{ mm})^3$ voxels for $5 \text{ cm} < r \leq 10 \text{ cm}$, and $(2 \text{ mm})^3$ voxels for $10 \text{ cm} < r \leq 20 \text{ cm}$, where r is de fined as the distance from the center of the source. The magnitude of error introduced by voxel size effects is typically less than 0.25% (Taylor and Rogers 2008).

(c) Dosimetry parameter dependence on source active length

The TG-43 dosimetry parameters for high-energy sources (^{192}Ir, ^{60}Co and ^{137}Cs) containing the same radionuclide and having comparable dimensions are similar. Williamson and Li in 1995 compared the Λ values of microSelectron Classic, PDR source and VariSource ^{192}Ir HDR models and revealed that they have nearly identical Λ values, and their $g_L(r)$ data agreed within $\leq 1\%$ for $r > 0.5$ cm.

Papagiannis et al in 2002 performed a dosimetry comparison of five HDR ^{192}Ir sources and suggested the expression,

$$\Lambda = 1.12 \times G_L(r_0,\theta_0) \text{ cGy h}^{-1}\text{U}^{-1} , \tag{2.6}$$

Where $G_L(r_0,\theta_0)$ is the geometry function and $\Lambda = 1.12$ for a point ^{192}Ir source (Chen and Nath 2001).

Similarly, Papagiannis et al in 2003 compared the dosimetry parameters of three HDR ^{60}Co source models. The main influence on Λ once again proved to be the spatial distribution of activity, represented by $G_L(r, \theta)$ and the relation is given by

$$\Lambda = 1.094 \times G_L(r_0,\theta_0) \text{ cGy h}^{-1}\text{U}^{-1} \tag{2.7}$$

Where $\Lambda = 1.094$ for a ^{60}Co point source (Chen and Nath 2001).

The value of Λ for the BEBIG ^{60}Co source, using the above equation is 1.083 cGy h^{-1} U^{-1}, which closely matches with the Monte Carlo estimated value of 1.086 cGy h^{-1} U^{-1} for water (Sahoo et al 2010).

(d) Electronic equilibrium

In Monte Carlo codes, many investigators approximate collision-kerma with absorbed dose, at distances from the source surface where electronic equilibrium is reached to save computation time.

Ballester et al in 2009 concluded that electronic equilibrium is reached to within 1% for ^{192}Ir, ^{137}Cs, ^{60}Co, and [169]Yb at distances greater than 2, 3.5, 7, and 1 mm from the source

center, respectively. Errors exceeding 2% will occur for distances at or below 1.6, 3, and 7 mm for ^{192}Ir, ^{137}Cs and ^{60}Co sources, respectively.

For the ^{192}Ir energies, electronic equilibrium is assumed only at distances greater than 1 mm from the sources (Wang and Li 2000, Baltas et al 2001). At distances less than 1 mm this approximation introduces errors of up to 6%.

The investigations by Selvam et al (2009) on the D/K for the stainless steel encapsulated ^{137}Cs sources suggests that for distances ≥ 2 mm from source capsules, collision kerma is approximately equal to absorbed dose.

Selvam and Bhola (2010) investigated the dose to collision kerma (D/K) ratio in water for point isotropic ^{60}Co and new ^{60}Co BEBIG HDR sources using EGSnrc code system. The authors concluded that the value of D/K = 1.04 at about 4 mm for the point source and 1.076 at about 3 mm for the BEBIG HDR source. The authors also concluded charged particle equilibrium exists at 1 cm from the source.

CHAPTER 3

DOSIMETRY OF INDIGENOUSLY DEVELOPED ^{192}Ir HDR

BRACHYTHERAPY SOURCE

3.1. Introduction

The use of remote afterloading HDR systems has increased in recent years. This is because of better dose optimization, improved radiation control, patient comfort and lesser radiation exposure to hospital personnel (Das and Thomadsen, 2005). Similarly several ^{192}Ir HDR brachytherapy sources for such systems are commercially available. The clinical use of a HDR sources requires an extensive dosimetric data and these data should be generated for every new source design introduced in clinical practice (Li et al 2007, Perez-Calatayud et al 2012).

The recommendations on dose calculations for photon emitting brachytherapy sources with average energy higher than 50 keV are presented by AAPM and ESTRO (Perez-Calatayud et al 2012) and Li et al (2007). For commercially distributed sources, single source-based dose distribution used for clinical treatment planning should be based on two dose-rate determinations, one of which is theoretical method such as Monte Carlo method, and the other an experimental measurement (Li et al 2007, Rivard et al 2004). However, for conventionally encapsulated ^{192}Ir sources similar in design to existing ones, a single dosimetric study, either Monte Carlo simulation techniques, or other transport equation solutions, or experimental dosimetry methods is sufficient (Perez-Calatayud et al 2012, Nath et al 1995). These reference dosimetry datasets must be independently

verified for its accuracy and are readily available in a format accepted by treatment planning system. The recommendations given by AAPM and ESTRO also includes the TG-43U1 dosimetry guidelines along with attention to phantom size effects, grid size, and dosimetry parameter dependence on source active length (Perez-Calatayud et al 2012).

The experimental determination of dosimetry data at short distances of clinical interest may involve large uncertainties mainly due to the large dose-rate gradients in the vicinity of the source. The Monte Carlo simulation can significantly reduce these experimental uncertainties and can provide the required accuracy and the desired precision in the dosimetry calculations (Williamson 1991).

Several HDR ^{192}Ir source models such as, microSelectron-v1(classic) (Williamson and Li 1995), microSelectron-v2 (Daskalov et al 1998), BEBIG (Granero et al 2005), VariSource (classic) (Wang and Sloboda 1998), VariSource (VS2000) (Angelopoulos et al 2000), Flexisource (Granero et al 2006) and GammaMed 12i (Ballester et al 2001) are used worldwide in brachytherapy applications. These sources are different in geometry, encapsulation dimensions as well as structural details. A number of publications related to Monte Carlo and experimental dosimetry of these ^{192}Ir sources are available in the literature. The differences in dosimetric parameters are already investigated by several authors.

Board of Radiation & Isotope Technology (BRIT) and Bhabha Atomic Research Centre (BARC), India, jointly, indigenously developed a remote afterloading HDR machine

(Karknidon) shown in figure (Figure 3.1 (a)). This machine will utilize indigenously developed ^{192}Ir HDR source (Figure 3.1 (b)).

(a)
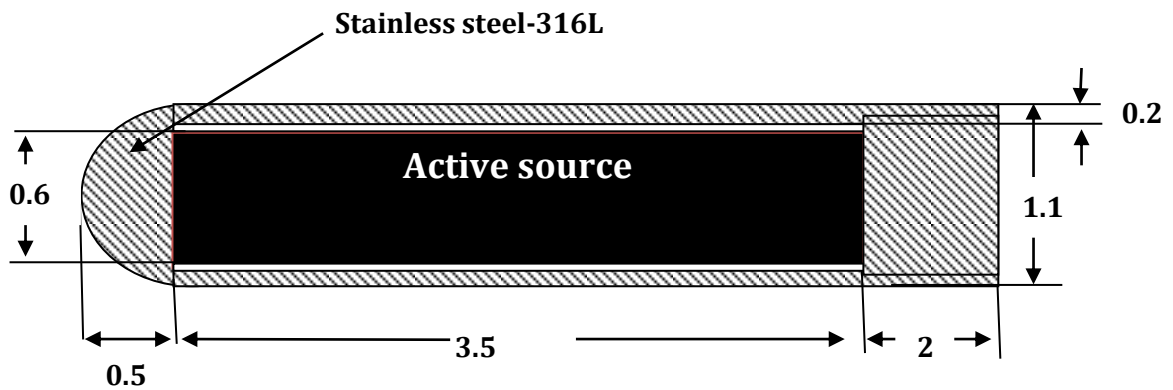
(b)

Figure 3.1. (a) Remote afterloading HDR brachytherapy unit (Karknidon) (b) Schematic diagram of the ^{192}Ir HDR source capsule jointly developed by BRIT and BARC, India. Dimensions shown are in millimeters (not to scale).

The objective of this work is to calculate AAPM TG-43 dosimetry parameters and dose distribution in liquid water for the BRIT ^{192}Ir HDR source (Figure 3.1 (b)) and utilize the same for the indigenous development of treatment planning software (Nath et al 1995, Rivard et al 2004). DOSRZnrc and FLURZnrc user-codes (Rogers et al 2010) of the EGSnrc Monte Carlo code system (Kawrakow et al 2013) are used for this purpose. The calculated dosimetry parameters are compared with published results of other ^{192}Ir HDR sources (Williamson and Li 1995, Daskalov et al 1998, Granero et al 2005, Wang and Sloboda 1998, Angelopoulos et al 2000, Granero et al 2006 and Ballester et al 2001).

3.2. Description of BRIT ^{192}Ir HDR source

The radioactive material in the ^{192}Ir HDR source is in the form of ^{192}Ir slugs (density = 22.42 g cm^{-3}) of 0.6-mm-diameter x 3.5-mm-length. The active source is encapsulated in stainless steel-316L (density = 7.8 g cm^{-3}) capsule of thickness 0.2 mm, which is welded remotely by argon gas laser welding process. The distal end of the capsule is spherical in shape with radius of 0.55 mm and length of the proximal end is 2 mm. The total length of the capsule is 6 mm and diameter is 1.1 mm (Figure 3.1 (b)).

Table 3.1 compares the source geometries, which includes encapsulation material / thickness and distal, and proximal end thicknesses of different ^{192}Ir HDR sources including BRIT ^{192}Ir HDR source, including the details of cable length modeled in the Monte Carlo calculations. The proximal and distal end thickness of BRIT ^{192}Ir HDR source is different from the other HDR source models.

Table 3.1. Comparison of source designs, encapsulation material / thickness and cable length modeled in Monte Carlo calculations of different ^{192}Ir HDR sources. All dimensions are in mm.

Source model	Active length	Active diameter	Total length	Total diameter	Encapsulation Material and thickness	Distal end thickness	Proximal end thickness + cable length in the simulation
BRIT ^{192}Ir HDR [This study]	3.5	0.6	6	1.1	SS316L, 0.2	0.5	2 + 1
BEBIG GmbH (Granero et al 2005)	3.5	0.6	4.9	1	SS316L, 0.15	0.84	0.55 *
Flexisource (Granero et al 2006)	3.5	0.6	4.6	0.85	SS304,	0.65	0.45 + 5
microSelectron-v1 (classic) (Willamson and Li 1995)	3.5	0.6	5	1.1	SS304, 0.2	0.35	1.15 + 1.85
VariSource (classic) (Wang and Sloboda 1998)	10	0.35		0.61	Ni/Ti Alloy	1	3 *
microSelectron-v2 (Daskalov et al 1998)	3.6	0.65	4.5	0.9	SS316L, 0.1	0.2	0.70 + 2
VariSource (VS2000) (Angelopoulos et al 2000)	5	0.34		0.61	Ni/Ti Wire	1	*
GammaMed 12i (Ballester et al 2001)	3.5	0.6	4.96	1.1	SS316L, 0.2	0.86	0.5 + 60

*Cable length in the simulation is not reported.

3.2.1. Decay scheme of ^{192}Ir source

^{192}Ir is produced from enriched ^{191}Ir targets (37% natural abundance) in a reactor by the (n,γ) reaction, creating HDR ^{192}Ir sources (typically 1 mm diameter by 3.5 mm length

cylinders) with activities about 4.4 TBq (Perez-Calatayud et al 2012). Its high specific activity makes it practical to deliver sources of activities of as much as hundreds of GBq. It's a half life 74 days allows it to be easily used for temporary implants.

It decays to several excited states of ^{192}Pt via beta decay (95%) and ^{192}Os via electron capture (5%) and emit about 30 x-rays and gamma rays with a range of energies 61.49 - 884.548 keV (Figure 3.2). The higher energy excited state of ^{192}Pt (1.061, 1.089 and 1.378 MeV) are neglected because of negligible intensity.

The average energy of the emitted photons from an unencapsulated source is about 365 keV. The sum of intensities is 2.24. The beta rays emitted have a maximum energy of 0.675 MeV and an average energy of 0.1807 MeV. HDR ^{192}Ir sources are encapsulated in a thin titanium or stainless steel capsule and laser welded to the end of a flexible wire. Electrons from beta decay are absorbed by the core and the capsule (Baltas et al 2001, Nath et al 1999b, Wang and Li al 2002, Ballester et al 2009). The photon energy spectrum of ^{192}Ir used in Monte Carlo simulations was taken from literature (Ballester et al 1997) given below in Table 3.2.

Table 3.2. Spectrum of photons emitted in the decay of ^{192}Ir. The intensity is expressed as the number of photons emitted per decay. The sum of intensities is 2.24 (Ballester et al 1997).

Sr. No.	E(MeV)	Intensity
1	0.06149	0.016
2	0.063	0.0203
3	0.0713	0.006629
4	0.0734	0.001732

5	0.11009	0.000127
6	0.13634	0.001836
7	0.17698	4.29E-05
8	0.20131	0.004719
9	0.2058	0.03303
10	0.28004	0.000233
11	0.28327	0.002627
12	0.29596	0.2867
13	0.30847	0.3269
14	0.31651	0.8286
15	0.32931	0.000186
16	0.37449	0.007208
17	0.41647	0.006644
18	0.42053	0.000734
19	0.46807	0.4783
20	0.48458	0.03187
21	0.4853	0.000022
22	0.48904	0.004433
23	0.58859	0.04515
24	0.59337	0.000425
25	0.5994	3.88E-05
26	0.60442	0.08232
27	0.61247	0.05309
28	0.70398	5.34E-05
29	0.766	1.49E-05
30	0.88454	0.002919
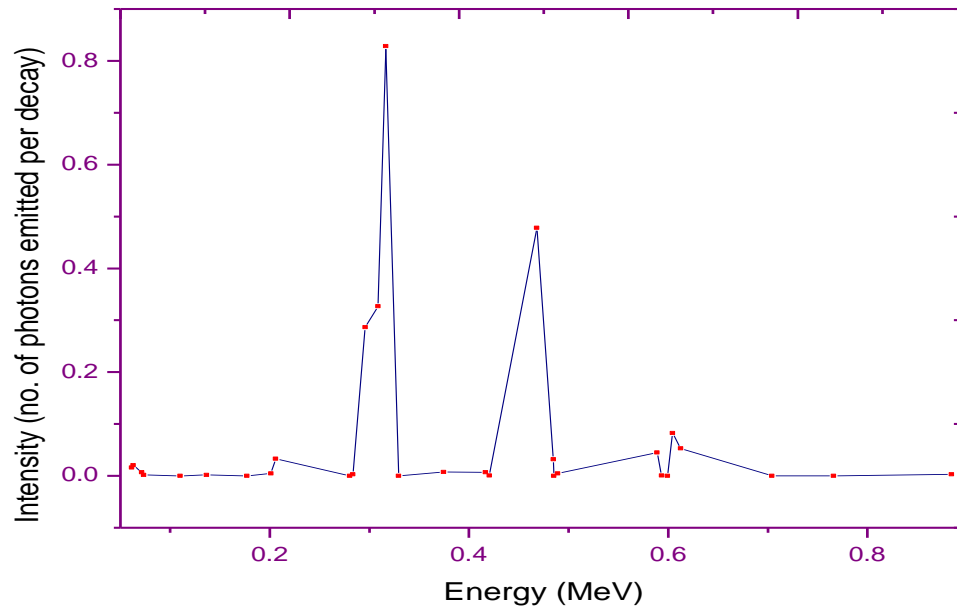
Figure 3.2. Spectrum of photons emitted in the decay of ^{192}Ir. The intensity is expressed as the number of photons emitted per decay. The sum of intensities is 2.24 (Ballester et al 1997).

3.3. Monte Carlo Calculations

DOSRZnrc user-code (Rogers et al 2010) of the EGSnrc Monte Carlo code system (Kawrakow et al 2013) is used for modeling of the BRIT ^{192}Ir HDR source in liquid water. The DOSRZnrc user-code calculates absorbed dose and kerma in cylindrical regions in an RZ cylindrical geometry. The material, mass density, and geometric details of the source needed for simulations are taken from source supplier. Figure 3.3 shows the co-ordinate system used in the DOSRZnrc simulations. In the Monte Carlo calculations, the source is immersed in a 40 cm diameter x 40 cm height cylindrical water phantom. The density of water was taken as 0.998 g cm^{-3} at 22 °C, consistent with AAPM TG-43U1 formalism (Rivard et al 2004). A grid system was simulated with thin cylindrical

shells of different thickness (δR, δZ) around source axis, where δR represents radial distance and δZ represents axial distance. The thickness of shells, $\delta R = \delta Z$ is 0.5 mm (up to R = Z = 5 cm), 1 mm (up to R = Z = 10 cm) and 2 mm (up to R = Z = 14 cm).
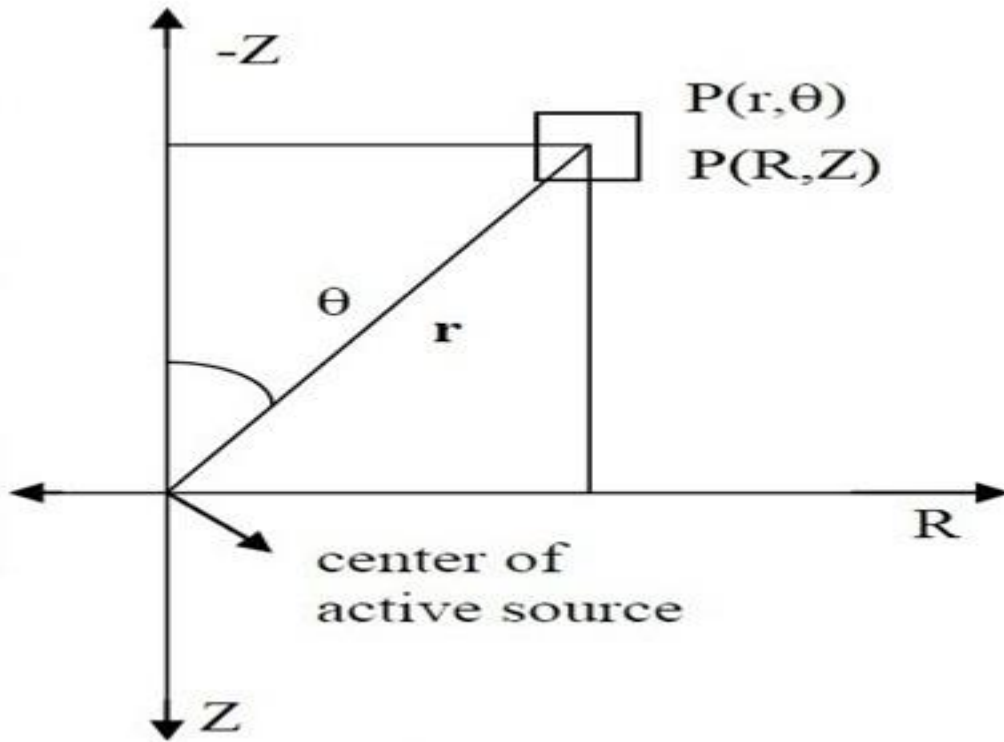
Figure.3.3. The Cartesian co-ordinate system, P(R,Z) used in the EGSnrc simulations. The co-ordinate of P will be (r, θ) in polar co-ordinate system. The origin of the co-ordinate system is chosen at the center of the active source.

The origin of the co-ordinate system is chosen at the geometric center of the active core. In the simulation, we modeled 1 mm long stainless steel-316L cable at proximal end of the source. The distal end of the source is a rounded tip of 0.5-mm-thickness and 0.55-mm-radius, which cannot be simulated in DOSRZnrc code. The thickness part (0.5 mm) is divided in to 10 slabs each of thickness 0.05 mm and the radius (0.55 mm) is divided

into 11 cylinders each of radius 0.055 mm. This geometrical modeling makes a step like shape, which tries to mimic the real rounded tip.

The geometry factor, $G(r,\theta)$ accounts for the distribution of radioactivity in the active source volume, which is calculated either by point or line source approximation. TG-43U1 report recommends the use of line source based geometry factors for evaluation of 2D dose distributions. This approximation is suitable for dose estimation at larger distances from the source. But this approximation introduces errors up to 3% at radial distances close to the sources (Karaiskos et al 2000a). Therefore, we have calculated the exact geometry factor, up to 1 cm distances around the source. Difference of 0.8% at 0.2 cm and 0.3% at 0.5 cm along transverse axis, are observed between exact and line source based geometry factor.

The dose value for a particular location in polar coordinate (r,θ), is estimated by converting the polar coordinate in to corresponding cartesian co-ordinate (R,Z). When this co-ordinate (R,Z) is not falling with in the centre of voxel, dose is estimated from dose values of four nearest points, (R_1,Z_1), (R_2,Z_2), (R_3,Z_3) and (R_4,Z_4) using bilinear interpolation. Accuracy of the interpolation is improved by dividing the dose values with the exact geometry function, up to a distance of 1 cm from the active center of the source and line source-based geometry function thereafter. These dose values in polar coordinate are used to estimate anisotropy function for this source. The above-described interpolation approach has been also applied elsewhere (Selvam et al 2009, Taylor et al 2007).

Air-kerma strength per Bq (U Bq^{-1}) is calculated for the BRIT ^{192}Ir source by using the FLURZnrc code (Rogers et al 2010). In this calculation, the source was in vacuum. This is consistent with the updated TG-43U1 formalism. As detailed secondary electrons transport is not important, ECUT=1 MeV (kinetic energy) is set in the FLURZnrc simulations. The photon fluence energy spectrum in 10 keV interval, along the transverse axis, at 100 cm is scored and subsequently converted into air-kerma per initial photon, k_{air} (Gy/initial photon) using the mass-energy-absorption coefficient of air (Hubbell and Seltzer 1995) The composition of air considered is as recommended by the TG-43U1 protocol (40% humidity) (Rivard et al 2004). The k_{air} values were then converted to S_k per unit activity (cGy cm^2 h^{-1} Bq^{-1} or U Bq^{-1}).

The Monte Carlo transport parameters are discussed in Chapter 2. We set AE = 521 keV and AP = 10 keV while creating PEGS4 dataset. The value of photon transport cutoff parameter PCUT used in all simulations is 10 keV. The value of ECUT used in absorbed dose calculations is 521 keV. Up to 2 x 10^9 primary photon histories are simulated. All Monte Carlo simulations were run on a 32-bit Intel (R) Core i3, 3.2 GHz computer. The statistical uncertainties on the calculated estimates have a coverage factor k=1. The uncertainties on the dose values varies between 0.1 - 1% for the regions up to Z = 2 cm, R = 0.2 - 14 cm. For regions Z = 2 - 5 cm and R = 0.2 - 0.5 cm, the uncertainties varied between 1 - 2%. For regions Z = 5 - 15 cm and R = 0.2 - 0.5 cm, the uncertainties varied between 2 - 3%. The uncertainty on air-kerma calculation is less than 0.10%.

3.4. Results and discussion

3.4.1. 2-D dose rate distribution

Absorbed dose per unit air-kerma strength (in cGy h^{-1} U^{-1}) is presented along both axial and radial distances up to 14 cm from the centre of the active source in Table 3.3.

3.4.2. Dose rate constant

The value of air-kerma strength is 9.894 x 10^{-8} ± 0.06% U Bq^{-1}. The calculated value of Λ for BRIT ^{192}Ir HDR source is 1.112 ± 0.11% cGy h^{-1} U^{-1} and is in excellent agreement with the published values of Λ for other ^{192}Ir HDR source models (see Table 3.4) other than VariSource (classic). This is due to same active length (3.5 mm) of the ^{192}Ir HDR sources.

The value of Λ for BRIT ^{192}Ir HDR source is higher by 6.5% when compared to VariSource (classic) (Wang and Sloboda 1998). This is because, the active length of VariSource (classic) is 1 cm. For a given radionuclide, the main influencing factor which affects Λ is the geometry factor. The values of Λ when corrected for geometry factor are comparable (see Table 3.4).

3.4.3. Radial dose function

The AAPM and the ESTRO recommended that the dose rate should be computed in a liquid spherical water phantom of 80 cm diameter or (the equivalent cylindrical phantom) for ^{192}Ir, ^{137}Cs, and ^{169}Yb sources (Perez-Calatayud et al 2012).

Table 3.3. Dose rate per unit air-kerma strength (cGy h⁻¹ U⁻¹) around the BRIT ¹⁹²Ir HDR source in a 40 cm diameter x 40 cm height cylindrical liquid water phantom of density 0.998 g cm⁻³. The positive z-axis is towards the proximal end. The origin is taken at the active center of the source.

Distance along, Z (cm)	Distance away, R (cm)											
	0	0.2	0.5	1	1.5	2	3	4	5	7	10	14
-14	0.00377	0.00381	0.0038	0.00391	0.00389	0.00388	0.00388	0.00376	0.00367	0.00325	0.00258	0.00171
-10	0.00798	0.00825	0.00827	0.00844	0.00839	0.00849	0.00828	0.00803	0.0075	0.00626	0.00445	0.00264
-7	0.0164	0.017	0.0172	0.0177	0.0179	0.0178	0.017	0.0156	0.0138	0.0103	0.00648	0.00345
-5	0.0313	0.0324	0.0339	0.0348	0.0352	0.0345	0.0307	0.0259	0.0213	0.0143	0.008	0.00397
-4	0.0478	0.05	0.052	0.0545	0.0543	0.0511	0.0425	0.0337	0.0266	0.0165	0.00879	0.0042
-3	0.0822	0.0871	0.0929	0.0959	0.0908	0.081	0.0605	0.044	0.0325	0.0187	0.00944	0.00441
-2	0.18	0.196	0.213	0.203	0.17	0.136	0.0857	0.0557	0.0384	0.0207	0.00998	0.00453
-1.5	0.318	0.355	0.379	0.323	0.241	0.177	0.0996	0.0617	0.041	0.0215	0.0102	0.00458
-1	0.724	0.836	0.814	0.543	0.341	0.223	0.113	0.0662	0.0431	0.022	0.0103	0.00465
-0.5	3.373	3.632	2.192	0.889	0.448	0.264	0.122	0.0694	0.0445	0.0224	0.0103	0.00464
-0.25	27.0159	11.73	3.514	1.047	0.485	0.277	0.125	0.0703	0.045	0.0225	0.0104	0.00463
0	--	22.862	4.308	1.1	0.498	0.281	0.125	0.0705	0.045	0.0225	0.0104	0.00467
0.25	--	11.74	3.514	1.0452	0.484	0.277	0.125	0.0705	0.0448	0.0224	0.0104	0.00465
0.5	3.019	3.619	2.191	0.886	0.448	0.264	0.122	0.0695	0.0444	0.0224	0.0104	0.00464

1	0.639	0.803	0.812	0.543	0.34	0.224	0.113	0.0664	0.0431	0.022	0.0103	0.00463
1.5	0.282	0.325	0.376	0.323	0.242	0.177	0.0995	0.0614	0.0411	0.0215	0.0101	0.00459
2	0.161	0.177	0.209	0.202	0.17	0.136	0.0853	0.0559	0.0385	0.0207	0.00993	0.00457
3	0.075	0.0786	0.0884	0.0954	0.0901	0.0811	0.0605	0.0441	0.0324	0.0187	0.00942	0.00439
4	0.0439	0.0452	0.0492	0.0537	0.0535	0.0507	0.0425	0.0338	0.0264	0.0165	0.00873	0.00422
5	0.0289	0.0302	0.0311	0.0338	0.0345	0.034	0.0305	0.0257	0.0214	0.0143	0.00802	0.00398
7	0.0154	0.0158	0.0158	0.0169	0.0175	0.0175	0.017	0.0155	0.0137	0.0103	0.00646	0.00344
10	0.00765	0.00744	0.00777	0.00793	0.00803	0.00821	0.00821	0.00795	0.00744	0.00623	0.00445	0.00265
14	0.00362	0.00361	0.00378	0.0037	0.00377	0.00378	0.00381	0.00372	0.00367	0.00326	0.00258	0.00171

Hence, simulation was carried out to calculate $g_L(r)$ in 80 cm diameter x 80 cm height water phantom for BRIT HDR ^{192}Ir source.

Table 3.4. Dose rate constant, Λ of ^{192}Ir HDR brachytherapy sources.

Source model	Active length	DRC (cGy h^{-1} U^{-1})	DRC / G (1, 90^0) (cGy h^{-1} U^{-1} cm^2)
BRIT ^{192}Ir HDR (This study)	3.5	1.112	1.123
BEBIG GmbH (Granero et al 2005)	3.5	1.108	1.119
Flexisource GmbH (Granero et al 2006)	3.5	1.109	1.120
microSelectron-v1 (classic) (Williamson and Li 1995)	3.5	1.115	1.126
VariSource (classic) (Wang and Sloboda 1998)	10	1.044	1.126
microSelectron-v2 (Daskalov et al 1998)	3.6	1.108	1.120
VariSource (VS2000) (Angelopoulos et al 2000)	5	1.101	1.123
GammaMed 12i (Ballester et al 2001)	3.5	1.118	1.129

Table 3.5 presents the values of $g_L(r)$ for BRIT ^{192}Ir HDR source (for phantom dimensions 40 cm diameter x 40 cm height and 80 cm diameter x 80 cm height) and

other commercial source models for distances r = 0.25 - 20 cm. Phantom dimensions used for other commercial model of the ^{192}Ir source also mentioned in this Table.

A comparison of $g_L(r)$ values for BRIT ^{192}Ir HDR source in the above two phantoms does not show significant difference up to r = 10 cm. This is because up to r = 10 cm above two phantom dimensions offer full scattering conditions. However, for r = 10 - 15 cm from the source, $g_L(r)$ values calculated in 80 cm diameter x 80 cm height phantom are higher by about 2 - 6% when compared to the values obtained in 40 cm diameter x 40 cm height phantom. This is due to lack of additional scattering in the case of 40 cm diameter x 40 cm height phantom.

The $g_L(r)$ values of BRIT ^{192}Ir HDR source calculated in an 80 cm diameter and 80 cm height cylindrical water phantom are almost same with that of the BEBIG, Flexisource and GammaMed 12i source models. This is due to similar active lengths and comparable phantom dimensions used in the calculations. The BEBIG and Flexisource models utilized 40 cm radius spherical water phantom, while the GammaMed 12i source utilized a 40 cm diameter x 40 cm height cylindrical water phantom to calculate the $g_L(r)$ up to 15 cm distance using a third-order polynomial fitting (Ballester et al 2001).

Granero et al (2008) observed 1% difference in $g_L(r)$ values, for ^{192}Ir point source, at r = 10 cm, between an unbounded spherical phantom of 40 cm in radius and cylindrical phantom of 40 cm in diameter and 40 cm in height.

Table 3.5. Radial dose function, $g_L(r)$ for the BRIT ^{192}Ir and other ^{192}Ir HDR source models.

r (cm)	BRIT[a]	BRIT[b]	BEBIG[c]	Flexi source[c]	*mS- v1[d]	Vari source (classic)[e]	*mS- v2[d]	Vari Source (VS2000)[d]	Gamma Med 12i[f]
0.25	0.994	0.993	0.99	0.991	-	-	-	-	0.995
0.5	0.995	0.995	0.996	0.997	0.997	0.989	1	0.995	0.997
0.75	0.998	0.998	0.998	0.998	-	-	-	-	0.998
1	1	1	1	1	1	1	1	1	1
1.5	1.002	1.004	1.003	1.002	1.002	1.005	1.003	1.002	1.002
2	1.006	1.006	1.004	1.004	1.003	1.007	1.007	1.005	1.004
3	1.008	1.009	1.005	1.005	1.002	1.006	1.008	1.006	1.005
4	1.007	1.008	1.004	1.003	0.997	1.003	1.004	1.002	1.003
5	1.002	1.004	0.999	0.999	0.987	0.998	0.995	0.993	0.997
6	0.995	0.999	0.992	0.991	0.973	0.984	0.981	0.981	0.989
7	0.982	0.988	0.981	0.981	0.956	0.967	0.964	-	0.979
8	0.968	0.977	0.968	0.968	0.933	0.947	0.94	0.941	0.966
10	0.928	0.945	0.935	0.935	0.871	0.885	0.882	0.881	0.933
12	0.875	0.902	0.894	0.894	0.795	0.807	0.799	0.803	0.893
15	0.776	0.828	0.821	0.821	-	-	-	0.609	0.822
20		0.688	0.687	0.686	-	-	-	-	0.684

[a]40 cm diameter x 40 cm height cylindrical water phantom

[b]80 cm diameter x 80 cm height cylindrical water phantom

[c]80 cm diameter spherical water phantom

*microSelectron

[d]30 cm diameter spherical water phantom

[e]30 cm diameter x 30 cm height cylindrical water phantom

[f]40 cm diameter x 40 cm height cylindrical water phantom and fitted to a third-order polynomial

Figure 3.4 compares the plot of $g_L(r)$ with distance for different HDR ^{192}Ir sources. The $g_L(r)$ values for VariSource (classic and VS2000), microSelectron (vl-classic and v2) source models are based on 30 cm diameter spherical water phantom. Hence, the values of $g_L(r)$ fall rapidly for these models as compared to BRIT source model (80 cm diameter and 80 cm height water phantom), due to lack of back scattering of photons. A comparison of $g_L(r)$ values of BRIT and source models of VariSource and microSelectron-V1 show differences by about 2% at r = 6 cm and up to 13% at r = 12 cm. This difference is due to 30 cm diameter spherical water phantom used in the dosimetry calculations of microSelectron-v1 (classic) (Williamson and Li 1995) and VariSource models (Wang and Sloboda 1998, Angelopoulos et al 2000). The difference in $g_L(r)$ values were negligible when microSelectron-v1 and VariSource models were simulated in 80 cm diameter x and 80 cm height water phantom.

3.4.4. Anisotropy function

The anisotropy function, $F(r,\theta)$ data, at radial distances r = 0.25 - 10 cm, at polar angles $\theta = 0^0$ - 180^0 relative to long axis of the source are presented in Table 3.6. Figure 3.5 presents the plot of $F(r,\theta)$ of the BRIT ^{192}Ir HDR source for radial distance 1 cm. The ratio of $F(r,\theta)$ of the other HDR sources to the BRIT ^{192}Ir HDR source, $\frac{F_i(r, \theta)}{F_{BRIT}(r, \theta)}$ is plotted for radial distances r = 1, 5 cm (Figures 3.6 and 3.7), where i denotes other HDR source models used for comparison.
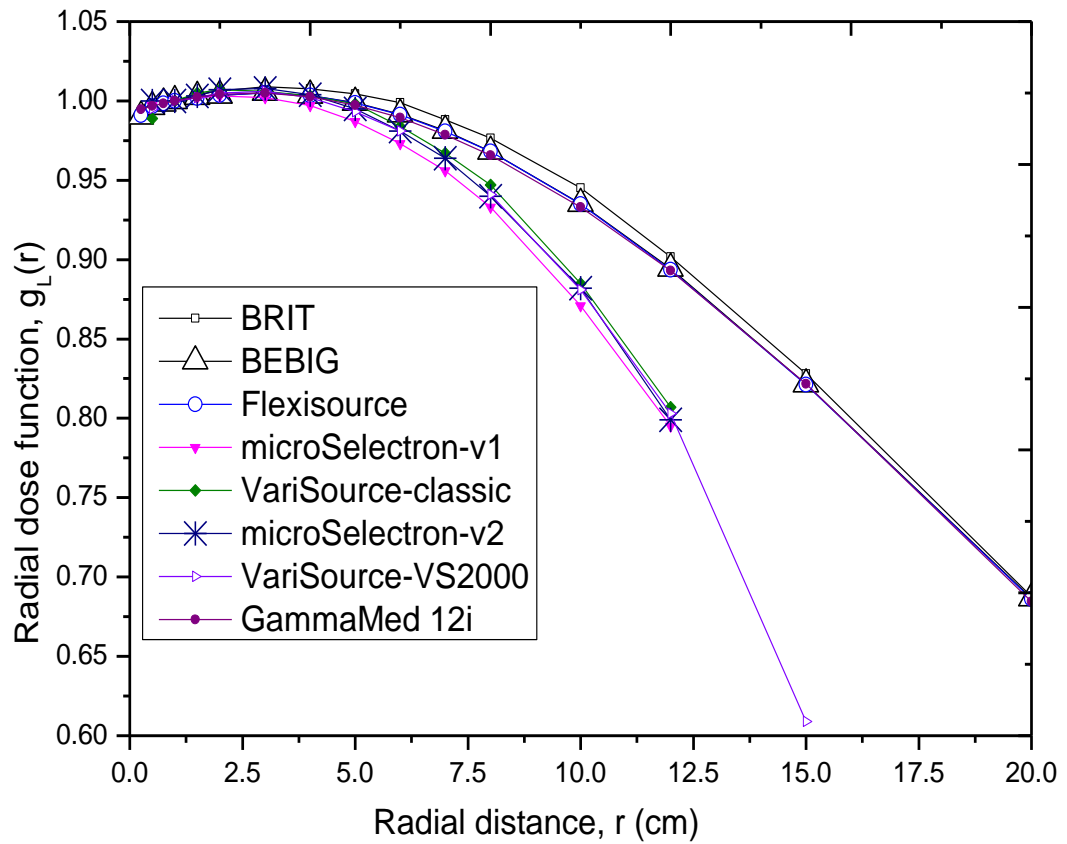
Figure 3.4. Comparison of the radial dose functions of various ^{192}Ir HDR sources.

It is observed from the figures 3.6 and 3.7 that for polar angles from 20^0 to 140^0, the $\frac{F_i(r,\ \theta)}{F_{BRIT}(r,\ \theta)}$ ratio is nearly independent of r and similar for all HDR sources. However, at polar angles close to the longitudinal axis of the source, (0^0 - 20^0 and 140^0 - 180^0), i.e. proximal and distal end of the source, greater differences in $\frac{F_i(r,\ \theta)}{F_{BRIT}(r,\ \theta)}$ ratio are observed. This is mainly due to the different encapsulation thickness at proximal and distal end of the source.

Due to similar design, F(r,θ) values of BRIT ^{192}Ir HDR source and microSelectron-v1 (classic) source are comparable. Small difference in the distal end thickness of these sources did not show observable differences in the anisotropy.
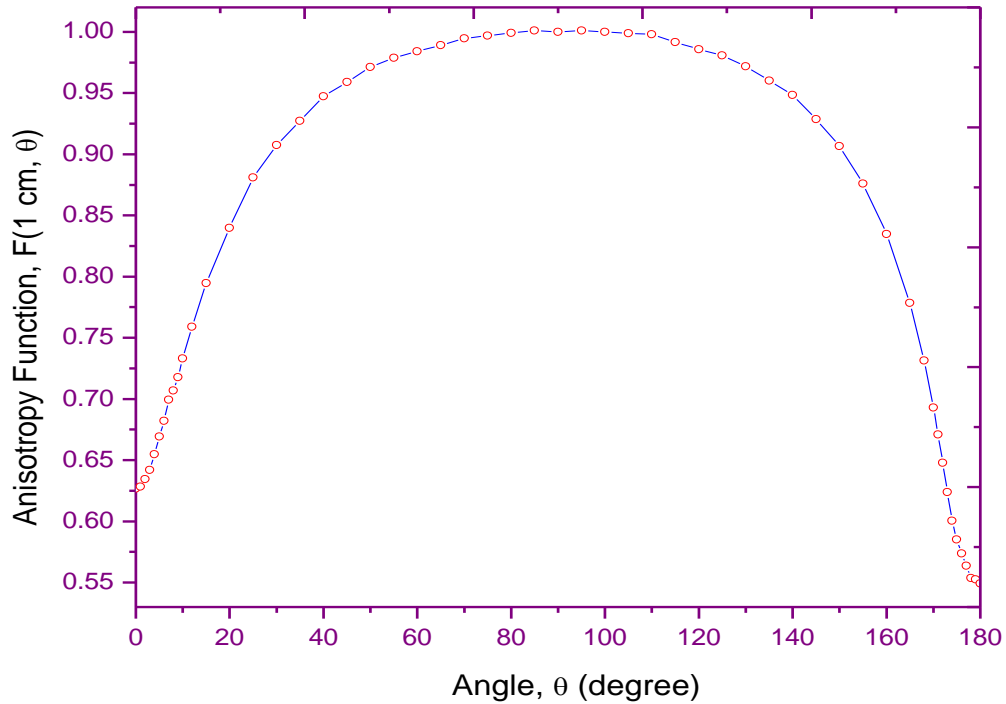
Figure 3.5. Anisotropy function of BRIT ^{192}Ir HDR source for radial distance r = 1 cm.

The F(r,θ) values of BRIT source compares well with microSelectron-v2 source for θ = 0 - 165[0] and for angles greater than 165[0] significant differences up to 6% are observed. The microSelectron-v2 source shows more anisotropy than BRIT source. This is due to differences in the geometry in the proximal end. The VariSource (classic) source shows more anisotropy due to its longer active length (10 mm). Anisotropy is 30 % higher than BRIT source along source axis for r = 1 cm.
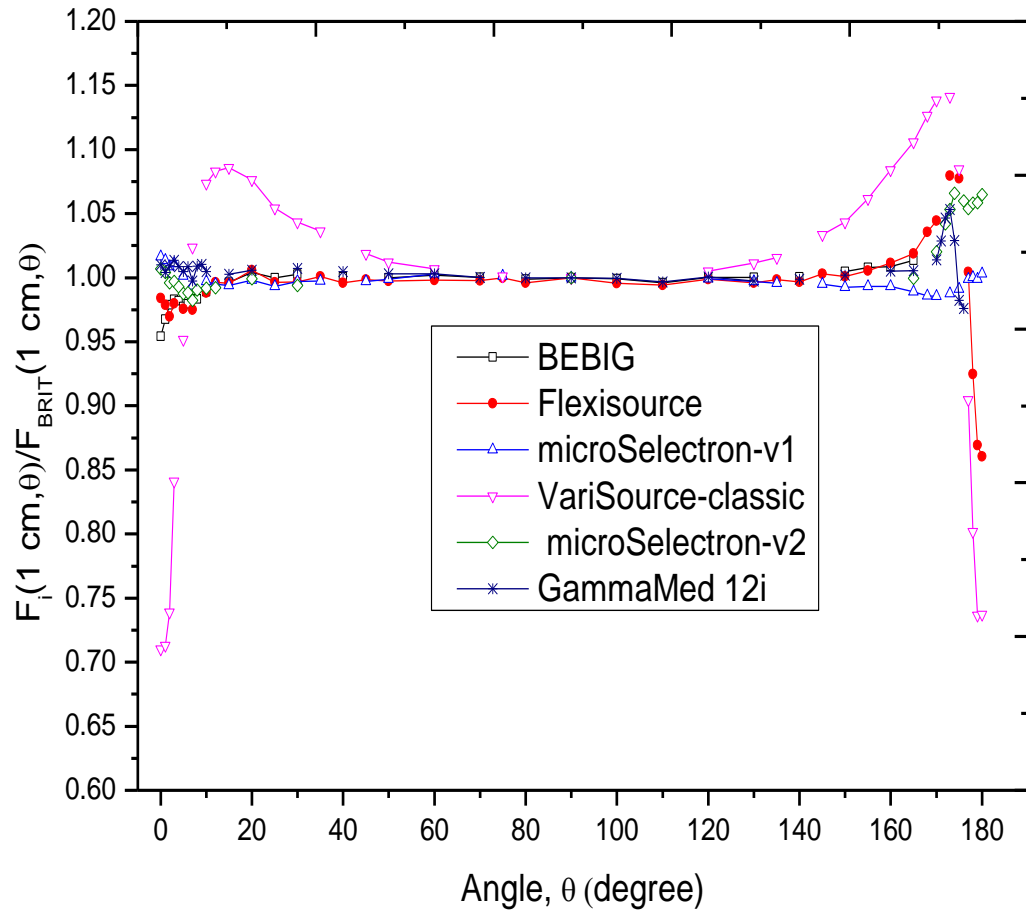
Figure 3.6. Ratio of anisotropy function of ^{192}Ir clinical HDR sources to BRIT ^{192}Ir HDR source for radial distance r = 1 cm.

A difference of about 5% at r = 1 cm and 2% at r = 5, 10 cm, in F(r,θ) values along distal end (θ = 0^0) are observed between BRIT and BEBIG source. This is due to difference in distal end thickness, which is 0.5 mm for BRIT source and 0.84 mm for BEBIG source. Similarly, significant differences up to 20% along proximal end are observed between two sources, which are also due to the difference in end thickness.
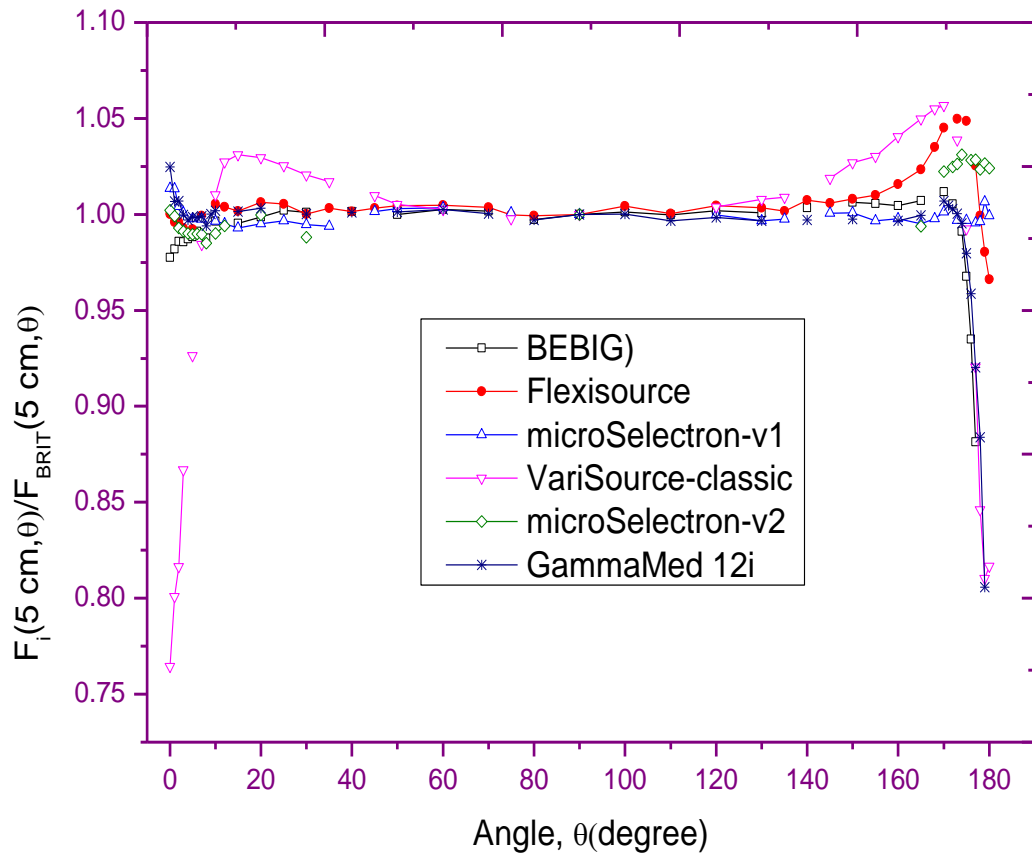
Figure 3.7. Ratio of anisotropy function of ^{192}Ir clinical sources with BRIT ^{192}Ir HDR source for radial distance r = 5 cm.

A significant difference of up to 15% along proximal end is observed between BRIT and Flexisource models. This is due to 0.45 mm end thickness and 5 mm steel cable considered in the Flexisource simulations. A difference of up to 20% along proximal end is also observed between BRIT and GammaMed 12i source models as the later source utilized 0.5 mm end thickness and 60 mm stainless steel cable in the Monte Carlo calculations.

Table 3.6. Anisotropy function, F(r, θ) of the BRIT ^{192}Ir HDR Source calculated in a 40 cm diameter x 40 cm height cylindrical liquid water phantom of density 0.998 g cm^{-3}. The origin is taken at the active centre of the source and the origin of the polar angle is at the tip side (distal end) of the source.

θ (deg)	Radial distance, r (cm)												
	0.25	0.5	0.75	1	1.5	2	3	4	5	6	7	8	10
0	0.774	0.662	0.636	0.627	0.628	0.634	0.654	0.673	0.695	0.723	0.733	0.739	0.783
1	0.783	0.662	0.636	0.628	0.625	0.635	0.660	0.691	0.702	0.731	0.739	0.751	0.768
2	0.773	0.663	0.636	0.634	0.638	0.658	0.678	0.695	0.714	0.737	0.750	0.758	0.780
3	0.770	0.662	0.638	0.642	0.652	0.664	0.687	0.703	0.724	0.743	0.755	0.758	0.795
4	0.769	0.664	0.652	0.655	0.661	0.675	0.697	0.715	0.733	0.749	0.761	0.772	0.793
5	0.774	0.676	0.666	0.669	0.677	0.687	0.710	0.726	0.743	0.757	0.770	0.776	0.801
6	0.771	0.688	0.679	0.682	0.687	0.698	0.717	0.734	0.751	0.762	0.779	0.785	0.803
7	0.772	0.699	0.691	0.699	0.700	0.712	0.732	0.744	0.761	0.770	0.793	0.795	0.818
8	0.777	0.713	0.704	0.707	0.714	0.723	0.741	0.752	0.775	0.782	0.799	0.802	0.822
9	0.793	0.726	0.717	0.718	0.725	0.734	0.753	0.763	0.781	0.791	0.802	0.812	0.829
10	0.799	0.737	0.730	0.733	0.739	0.748	0.767	0.779	0.790	0.801	0.811	0.821	0.833
12	0.820	0.762	0.758	0.759	0.766	0.773	0.787	0.798	0.809	0.820	0.839	0.838	0.852
15	0.845	0.797	0.790	0.795	0.798	0.806	0.818	0.826	0.838	0.841	0.856	0.858	0.874
20	0.886	0.845	0.842	0.840	0.845	0.848	0.857	0.866	0.872	0.878	0.885	0.885	0.897

25	0.917	0.883	0.879	0.881	0.882	0.882	0.891	0.894	0.899	0.907	0.911	0.908	0.920
30	0.937	0.910	0.907	0.908	0.907	0.910	0.915	0.918	0.922	0.927	0.931	0.927	0.930
35	0.952	0.929	0.926	0.927	0.929	0.931	0.931	0.935	0.940	0.938	0.945	0.943	0.947
40	0.964	0.947	0.953	0.947	0.946	0.946	0.949	0.952	0.954	0.955	0.956	0.951	0.957
45	0.972	0.960	0.959	0.959	0.958	0.960	0.962	0.963	0.964	0.967	0.968	0.965	0.969
50	0.978	0.972	0.971	0.971	0.972	0.971	0.973	0.974	0.974	0.975	0.977	0.974	0.976
55	0.985	0.976	0.975	0.979	0.978	0.980	0.981	0.982	0.982	0.981	0.987	0.982	0.982
60	0.989	0.983	0.981	0.984	0.986	0.986	0.985	0.985	0.986	0.986	0.992	0.984	0.984
65	0.993	0.989	0.989	0.989	0.998	0.989	0.988	0.989	0.990	0.990	0.995	0.987	0.990
70	0.995	0.992	0.992	0.995	0.994	0.995	0.994	0.996	0.994	0.994	1.001	0.992	0.995
75	0.997	0.995	0.995	0.997	0.997	0.997	0.998	0.997	0.999	0.998	1.001	0.993	0.993
80	1.001	0.997	0.998	0.999	0.998	0.998	0.999	1.002	1.002	1.000	1.000	1.000	0.999
85	1.003	1.001	0.999	1.001	1.000	1.002	1.002	0.999	0.999	0.999	1.003	0.998	1.001
90	1.000	1.000	1.000	1.000	1.000	1.000	1.000	1.000	1.000	1.000	1.000	1.000	1.000
95	1.000	1.000	0.999	1.001	1.002	1.001	0.999	1.000	1.000	0.999	1.004	1.000	1.001
100	0.998	0.996	0.997	1.000	0.999	0.998	0.997	0.998	0.998	1.000	0.999	0.997	0.998
105	0.998	0.998	0.999	0.999	0.998	0.998	0.995	0.995	0.996	0.996	0.997	0.996	0.999
110	0.995	0.993	0.993	0.998	0.993	0.996	0.996	0.995	0.995	0.993	0.998	0.990	0.993
115	0.992	0.990	0.988	0.992	0.989	0.991	0.995	0.987	0.993	0.988	0.994	0.991	0.991

120	0.991	0.984	0.983	0.986	0.984	0.987	0.987	0.985	0.985	0.984	0.990	0.983	0.990
125	0.985	0.980	0.978	0.981	0.980	0.980	0.979	0.979	0.982	0.982	0.982	0.980	0.981
130	0.981	0.970	0.969	0.972	0.969	0.971	0.972	0.971	0.973	0.975	0.976	0.970	0.975
135	0.975	0.962	0.957	0.960	0.959	0.960	0.962	0.960	0.965	0.963	0.969	0.962	0.969
140	0.965	0.949	0.945	0.948	0.946	0.948	0.948	0.958	0.952	0.952	0.960	0.955	0.962
145	0.953	0.933	0.929	0.929	0.930	0.930	0.932	0.933	0.937	0.939	0.943	0.941	0.947
150	0.940	0.910	0.905	0.907	0.905	0.908	0.911	0.914	0.917	0.922	0.925	0.923	0.939
155	0.920	0.881	0.875	0.876	0.876	0.882	0.885	0.888	0.896	0.898	0.902	0.909	0.917
160	0.892	0.845	0.836	0.835	0.840	0.841	0.848	0.855	0.864	0.873	0.875	0.879	0.893
165	0.844	0.792	0.781	0.778	0.785	0.788	0.799	0.810	0.821	0.832	0.838	0.844	0.858
168	-	0.739	0.730	0.731	0.737	0.746	0.761	0.770	0.785	0.800	0.808	0.820	0.835
170	-	0.701	0.687	0.693	0.698	0.709	0.725	0.742	0.757	0.772	0.783	0.795	0.822
171	-	0.679	0.664	0.671	0.678	0.690	0.711	0.725	0.744	0.760	0.776	0.782	0.800
172	-	0.650	0.641	0.648	0.656	0.670	0.689	0.713	0.730	0.747	0.756	0.772	0.789
173	-	0.621	0.614	0.624	0.634	0.652	0.673	0.697	0.714	0.737	0.747	0.754	0.783
174	-	0.606	0.595	0.601	0.613	0.628	0.654	0.678	0.698	0.720	0.735	0.747	0.778
175	-	0.598	0.582	0.585	0.597	0.612	0.640	0.663	0.686	0.714	0.723	0.742	0.773
176	-	0.585	0.569	0.574	0.580	0.597	0.627	0.650	0.676	0.699	0.708	0.727	0.757
177	-	0.585	0.560	0.564	0.571	0.588	0.620	0.641	0.667	0.688	0.703	0.712	0.742

178	-	0.586	0.555	0.554	0.560	0.576	0.605	0.634	0.660	0.682	0.693	0.711	0.740
179	-	0.585	0.557	0.553	0.554	0.567	0.595	0.623	0.648	0.676	0.678	0.701	0.733
180	-	0.586	0.559	0.549	0.556	0.568	0.597	0.616	0.646	0.671	0.680	0.689	0.728

3.5. Conclusions

In this Chapter, the 2D dose distribution and the AAPM TG-43 dosimetry parameters of the BRIT ^{192}Ir HDR source are generated using the EGSnrc Monte Carlo code system. The dosimetry data of the BRIT ^{192}Ir HDR source are presented and compared with other commercially HDR ^{192}Ir sources clinically used worldwide. The calculated dose rate constant of BRIT ^{192}Ir HDR source is in excellent agreement with the published values of other commercially HDR ^{192}Ir sources, which have similar active length of 3.5 mm.

The values of radial dose function of BRIT ^{192}Ir HDR source compares well with the corresponding values of BEBIG, Flexisource and GammaMed-12i sources due to similar active lengths and comparable phantom dimensions used in the calculations. The sources such as VariSource (classic, VS2000) and microSelectron (classic and v2) exhibit significant deviations in the values of radial dose function as compared to the BRIT source which is attributed to the size of water phantom employed in the simulations.

The anisotropy function of BRIT ^{192}Ir HDR source is comparable with the corresponding values of microSelectron-v1 (classic) HDR source. Significant differences along source axis are observed, when compared with other ^{192}Ir HDR source models.

The calculated data of the ^{192}Ir HDR source are utilized for the indigenous development of the brachytherapy treatment planning software which will be used for treatment planning of brachytherapy patients. For clinical use, independent validation of this Monte Carlo data generated in this work, either through experimental measurements and/or Monte Carlo simulation using a different code would be helpful in ascertaining its reliability.

CHAPTER 4

DOSIMETRY OF ^{32}P AND ^{177}LU PATCH SOURCES USED IN SUPERFICIAL BRACHYTHERAPY APPLICATIONS

4.1. Introduction on superficial brachytherapy

Skin cancer has emerged as one of the most common diagnosed cancers affecting fair-skinned populations with about 1,32,000 new cases of melanoma and 2 - 3 million cases of non-melanoma skin cancers worldwide each year (WHO 2017b). Basal cell carcinoma and squamous cell carcinoma known collectively as non-melanoma skin cancer are the most common forms of malignancy that usually develop on sun-exposed areas of the body (Panda 2010). Basal cell carcinoma is also more probable for middle aged people and fair complexion people (Kopf 1979). While the incidence of skin cancer has been high among white skinned people, it remains relatively low in colored people owing to the ability of epidermal melanin to offer photo-protection, which filters twice as much ultraviolet radiation as does that in the epidermis of Caucasians (Montagna and Carlisle 1991).

The treatment modalities for skin cancers are surgical excision, radiotherapy and chemotherapy. Removing the affected area by surgical excision is usually preferred in many cases, but the recurrence rates after treatment are high (Panda 2010). Chemotherapy is costly and has its own side effects. Radiotherapy seems to be an attractive option. It offers the scope for treating not only the visible tumour but also potential subclinical disease around the macroscopically visible tumour (Griep et al 1995, Guix et al 2000).

The external beam therapy is (a) expensive, (b) difficulties in treating tumours close to critical structures, (c) adverse effects of radiation into underlying bone and soft tissues.

Mould or superficial brachytherapy is a promising alternative treatment method for such skin cancers, where high-energy beta emitting radio-nuclides such as ^{32}P, ^{90}Sr/^{90}Y, ^{188}Re, ^{177}Lu etc. are used to overcome the disadvantages of radiotherapy and surgery. In superficial brachytherapy, prescribed dose can be delivered to the affected area without excessive damage to the neighboring normal tissues. The advantage of superficial brachytherapy is that high energy radiation can be delivered to superficial tumours with a very rapid fall-off within the tissue beneath, due to the inverse-square law. This technique is simple, less trauma to patients, and less expensive as compared to external beam therapy.

Many published studies based on above mentioned beta sources were available in literature. They were successfully used for tumour control both in animal and human studies (Lee et al 1997, Mukherjee et al 2002 and 2003, Salgueiro et al 2008a 2008b, Saxena et al 2012, Sahoo et al 2015). Superficial brachytherapy is still widely used for treatment of ocular tumours using a ^{106}Ru or ^{90}Sr applicator.

This Chapter presents central axis depth dose and dose profiles in water phantom for the indigenously developed ^{32}P and ^{177}Lu skin patch source using EGSnrc-based Monte Carlo code system (Kawrakow et al 2013). Based on the calculated dose rate, the treatment time to deliver a therapeutic dose at reference depth (1 mm) is calculated (ICRU report 2004, IAEA 2002b).

This Chapter also includes measurement of surface dose rate of the in-house developed ^{177}Lu patch source using three methods (i) an extrapolation chamber, (ii) EBT3 Gafchromic film and (iii) EGSnrc-based Monte Carlo code system (Kawrakow et al 2013) to compare against the measured values. EBT3 films were used to estimate the source uniformity by taking auto-radiographs (ICRU report 2004) and measure surface dose using electron beam calibration.

The study also includes (i) determination of activity of the ^{177}Lu patch source using the HPGe detector, (ii) estimation of Bragg-Gray stopping power ratio of water-to-air and chamber wall correction factor needed to be applied on measurements for establishing the dose rate at 5 µm depth using the Monte Carlo methods. The efficiencies of the HPGe detector for standard sources were fitted using an orthogonal polynomial function.

Surface dose rate was the parameter used to specify the strength of beta emitting brachytherapy sources (Soares 1991, Gleckler et al 1998, Pruitt 1987, Sudhir et al 2015). NIST also defined surface dose rate as the dose rate to an infinitesimal layer of water at the exact surface of the source (Gleckler et al 1998, Pruitt 1987, Sudhir et al 2015).

An extrapolation chamber (entrance window thickness is about 5 µm) was used for surface dose rate $\left(\dot{D}_w\right)$ measurement of ^{177}Lu source. Secondly, the absorbed-dose rate at 1 mm is 0.2% of the dose rate at surface, which is negligible. Therefore the absorbed-dose rate at 5 µm with extrapolation chamber is termed as surface dose rate.

4.2. Materials and methods

4.2.1. Specification of beta sources used in brachytherapy

The radiation intensity of beta sources used in brachytherapy is specified in terms of reference absorbed-dose rate, contained activity and source uniformity (ICRU report 2004).

4.2.1.1. Reference absorbed-dose rate

The reference absorbed-dose rate is the absorbed-dose rate to water at a reference point in water. For planar source, the reference point is located at a distance of 1 mm measured from the center of source surface, along the axis of symmetry of the source.

In the present study we choose to determine the absorbed dose rate at 5 μm depth owing to the lower range of the beta rays of this source with respect to other therapeutic sources such as ^{32}P. Hence the absorbed dose rate at 1 mm is expected to be much lower with respect to surface (5 μm) dose rate.

4.2.1.2. Contained activity

Traditionally activity of beta sources have been specified in terms of contained activity. Activity incorporated into a source is depends on source-binding method and source thickness. The relationship between the contained activity and the reference absorbed-dose rate can be established using Monte Carlo calculations and absorbed-dose rate measurements. This relation can be used to obtain reference absorbed-dose rate for other sources of that type, once the contained activity is known.

4.2.1.3. Source uniformity

In beta sources, we assume that the radioactive material is distributed uniformly in the source matrix. Source uniformity is specified as the uniformity of the absorbed-dose rate over the source area, measured at a depth of 1 mm in a water-equivalent medium. This source uniformity can be estimated by a parameter called source non-uniformity (U), which is equal to the difference of the maximum and minimum values of relative absorbed-dose rate at the specified depth over a specified area of the source, given in percentage of average absorbed-dose rate (ICRU report 2004, Soares and McLaughlin, 1993).

The value of U, is estimated by the formula given in equation (4.1):

$$U(\%) = \frac{\dot{D}_{max} - \dot{D}_{min}}{\dot{D}_{avg}} * 100 \qquad (4.1)$$

Here $\dot{D}_{max}$ and $\dot{D}_{min}$ are the maximum and minimum dose rates for any radius $< 0.8\ R_{50}$, and $\dot{D}_{avg}$ is the average dose rate. R_{50} is the average radius for the area bounded by the 50% isodose line. The value of U for planar and concave sources should be less than 20% (ICRU report 2004). In the present study the non-uniformity was measured using Gafchromic film.

4.2.2. Description of ^{32}P patch source

Radiopharmaceuticals Division, BARC has indigenously developed nafion–zirconium phosphate film-based ^{32}P patch source for superficial brachytherapy applications (Saxena

et al 2012). A nafion-117 membrane of thickness 100 µm is treated with $ZrOCl_2$ solution, and subsequently dipped in orthophosphoric acid. These radioactive ^{32}P patches are cut in to 1 cm x 1 cm sizes and then subsequently laminated with thermoplastic polyurethane sheets of thickness 40 µm. The above preparation method is robust, inexpensive and reproducible and complies with the safety standard stipulated by Atomic Energy Regulatory Board, India (AERB 2001). The detailed preparation of nafion-117 patches is explained in literature (Saxena et al 2012).

[32]P is a pure beta emitter with maximum energy of 1.71 MeV. Its half-life is 14.2 days. The maximum and average range of ^{32}P beta particle in soft tissue is 8 and 3 mm respectively (Gao et al 2009).

4.2.2.1. Monte Carlo calculations

DOSXYZnrc user-code (Walters et al 2009) of the EGSnrc-code system (Kawrakow et al 2013) is used to calculate central axis depth doses and dose profiles in the unit density water medium for simulating the 1 cm x 1 cm ^{32}P-nafion-patch source. The 1 cm x 1 cm ^{32}P-nafion-patch source is positioned on 2 x 2 x 2 cm^3 water phantom. The thickness of source is 100 µm.

The geometry and co-ordinate system used in the Monte Carlo calculations is shown in Figure 4.1.   The elemental composition of phosphorous-loaded zirconium-nafion-117 composite membrane used in the Monte Carlo calculation are given in Table 4.1 (Saxena et al 2012). The density of nafion-117 membrane is 1620 kg m^{-3}.
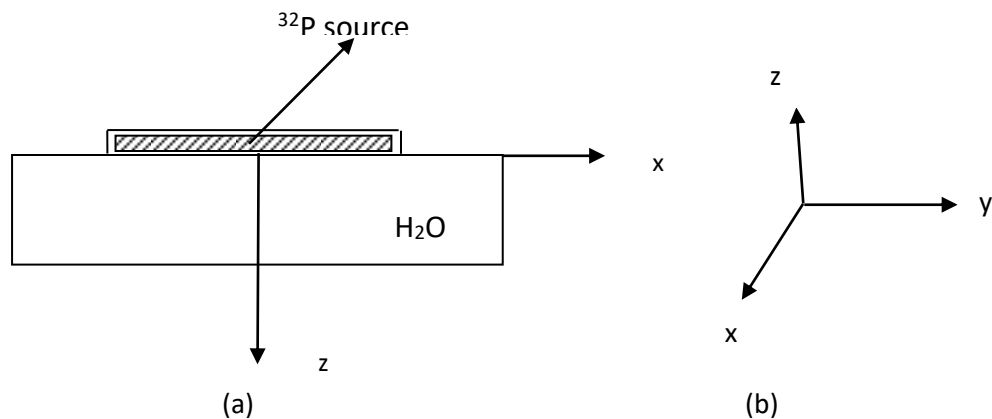
Figure 4.1. (a) Schematic diagram of the ^{32}P-nafion-patch source and water phantom used in the DOSXYZnrc Monte Carlo simulation. (b) Co-ordinate system used in the simulation.

The ^{32}P beta spectrum (Figure 4.2) needed for the Monte Carlo calculation is based on ICRU Report No. 56 (ICRU 56, 1997). In the Monte Carlo calculations, it is considered that the source particles are uniformly distributed in the nafion patch of dimensions 1 cm x 1 cm x 100 μm.

Table 4.1. Elemental composition of phosphorous-loaded zirconium-nafion-117 composite membrane (density = 1620 kg m^{-3}).

Element	C	F	O	S	P	Zr
Atom (%)	22.5	67.15	8.1	1.8	0.29	0.16

The water phantom was divided in to voxels of dimension of 0.25 x 0.25 x 0.25 mm^3 for generating dose profiles. The Monte Carlo transport parameters required for this simulation were discussed in Chapter 2. Dose distributions in water are scored in these

voxels. Separate simulation is carried out to score central axis depth dose by using bigger voxel dimensions (2 x 2 x 0.25 mm^3).
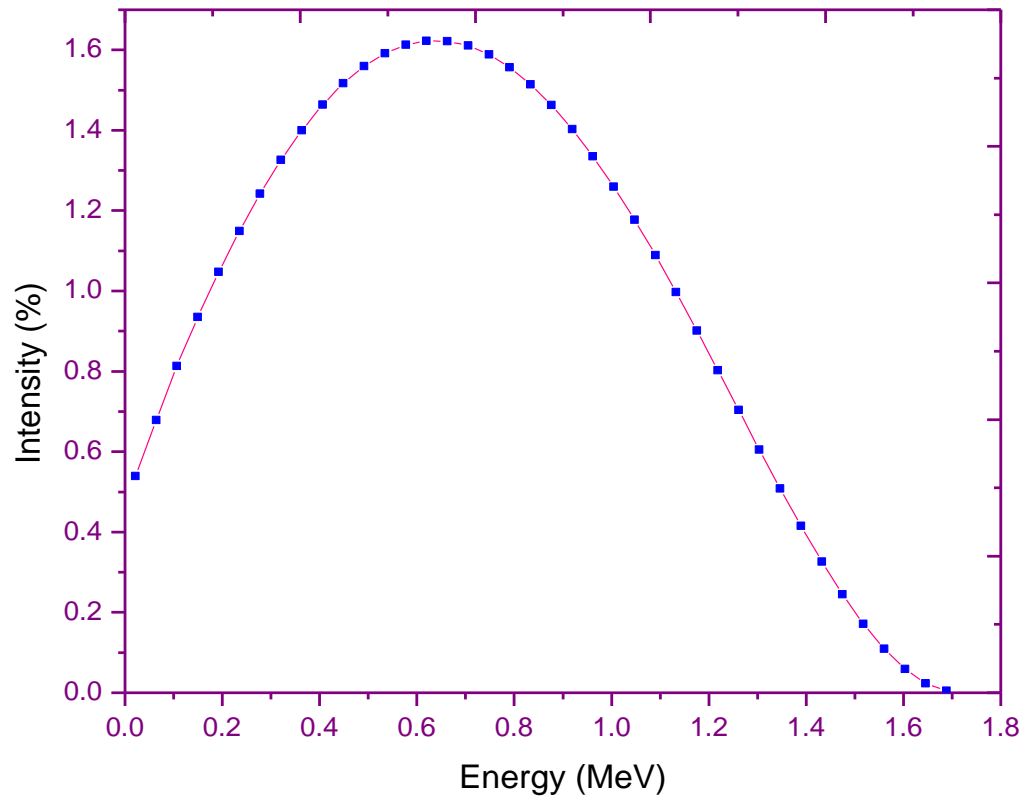
Figure 4.2. ^{32}P beta spectrum from ICRU 56 used in the Monte Carlo simulation.

4.2.3. ^{177}Lu skin patch source and measurements

4.2.3.1. Description of ^{177}Lu skin patch source

^{177}Lu was produced by neutron irradiation of inactive lutetium targets (^{176}LuO$_3$) in this research centre. Nafion-115 membrane of 2 cm diameter and 130 μm thickness was treated with pre-calculated amounts of ^{177}Lu under suitable laboratory conditions. The radioactive source was entrenched between thin sheets of cellofin tape (thickness 35 μm).

Leakage and surface contamination tests were conducted on the patch source (AERB 2001). A contamination free ^{177}Lu patch source of activity 3.46 ± 0.01 mCi was prepared for further measurements. Table 4.2 presents the major gamma lines and major end-point energies of beta of the bare ^{177}Lu source along with their intensity (NNDC 2003).

Table 4.2. Major beta and gamma energies emitted from ^{177}Lu source (NNDC 2003).

Beta end point energy (MeV)	Intensity (%)	Gamma energy (MeV)	Intensity (%)
0.498	79.4	0.113	6.6
0.385	9.0	0.208	11.0
0.177	11.6		

4.2.3.2. Measurement of activity of ^{177}Lu skin patch source using HPGe detector

Coaxial P-type HPGe detector was used to obtain the gamma spectrum of ^{177}Lu source and thereby estimate the radioactivity. The detector comes with an active volume of about 150 cm^3 (the detector has diameter and height 5.72 cm and 5.78 cm, respectively) and is covered with an aluminum cap of thickness 0.7 mm (Bakshi et al 2014). The spacing between the detector face and the end cap aluminum window is 0.6 cm. The measurement setup, consisting of the detector and source, is surrounded by about 3" thick lead to reduce the contribution of background radiation. The ^{177}Lu source in the disk geometry was counted for 700 seconds by placing it on to the centre of a perspex source holder at a distance of 30 cm from the detector. Earlier, the background spectrum was acquired using the same perspex source holder at the same distance. The background was subtracted

from the sample's spectrum before estimating the activity. Prior to that, the energy and efficiency calibration of the system corresponding to a particular radionuclide/gamma line was determined at the same distance by using the standard disc sources. The photo peak efficiency, calibration of the detector was carried out using standard disc sources ([241]Am, [133]Ba, [152]Eu, ^{137}Cs and ^{60}Co) by placing them at 30 cm from the detector. The photo peaks of 60 keV of [241]Am, 81 keV, 302 keV, 356 keV of [133]Ba, 121.78 keV and 244.7 keV of [152]Eu, 662 keV of ^{137}Cs and 1173 keV and 1332 keV of ^{60}Co sources were used for efficiency calibration. The output from the detector was analyzed using an 8K PC-based multichannel analyzer. The absolute efficiency ε (in %) of the HPGe detector at a particular gamma energy, E_γ was derived using the following equation (4.2) (IAEA 1989):

$$\varepsilon = \frac{N}{A * P_\gamma} \qquad (4.2)$$

where N is the background-subtracted net count rate (counts per second) of the full energy peak, A is the activity (in Bq) of standard source and P_γ is the gamma emission probability (in %).

The absolute efficiencies obtained for standard sources were fitted using orthogonal polynomial, discussed in the next section.

4.2.3.3. Efficiency calculation of HPGe detector using orthogonal polynomial

The accuracy of gamma spectroscopy used in a wide range of applications is related to the efficiency calibration of the detector system. The experimental efficiency of the HPGe detector was determined using the ratio of the number of gamma counts per second

measured in the detector to the true activity of the source. The experimental data points for efficiency function were fitted by a 10th order orthogonal polynomial.

Orthogonal polynomial

Orthogonal polynomials (OPs) provide solutions for mathematical and physical problems. The classical OPs are those named after Jacobi, Laguerre, and Hermite. They can be characterized in a number of ways; their weight functions satisfy first-order differential equations with polynomial coefficients, their derivatives are OPs of the same family. The main properties of OPs considered in the literature are related to zeros, generating functions, asymptotic behaviour, expansion problems, connection coefficients, kernel polynomials, integral representations, continued fractions, spectral measures, Rodrigues' formula, etc. As a secondary effect of the computer revolution and the heightened activity in approximation theory and numerical analysis, we have applied OPs to fit the experimental efficiency function of HPGe detector. It is always better to introduce the mathematical behavior of orthogonal polynomials before its usage in any application.

Algorithm developed for efficiency function

In this method, two functions $g(x)$ and $h(x)$ are orthogonal (to each other) if they satisfy the relations, the inner product of g and h as $\langle g, h \rangle = 0$. We can write this explicitly as given below in equation (4.3):

$$\langle g, h \rangle \ = \ \int_{-1}^{1} g(x) \ h(x) \ dx \qquad\qquad (4.3)$$

Further, we say that $P_0(x)$, $P_1(x)$, $P_2(x)$, . . . is a (finite or infinite) sequence of orthogonal polynomials provided the $P_i(x)$ are all orthogonal to each other and each $P_i(x)$ is a polynomial of exact degree i. In other words, for each i,

(i) $P_i(x) = \alpha_i x^i +$ a polynomial of degree $<i$, with $\alpha_i \neq 0$

(ii)   Whenever $i \neq j$, then $<P_i, P_j> = 0$, i and j are indices

One of the very important properties of OPs is that the sequences of OPs satisfy a three-term recurrence relation and this can be used to generate the sequence further. That is the reason, experimental efficiency function can be fitted using orthogonal polynomial in the sense that orthogonal polynomial can be generated from the data point itself which at the same time reduce the oscillation at the data point.

Mathematical formulation of generating an orthogonal polynomial is based on the three term recurrence relations which can be written as

$$P_{n+1}(x) = A_i (x - B_i) P_i(x) - C_i P_{i-1}(x), \qquad i = 0,1,\dots\dots, k-1 \text{ for all } A_i = 1$$

Where $B_i = \frac{\langle x P_i(x), P_i(x) \rangle}{S_i}, i = 1, \dots, k-1$ and $C_i = \begin{cases} \text{arbitrary, } i = 0 \\ \frac{A_i S_i}{A_{i-1} S_{i-1}} \end{cases}$

For the purpose of fitting experimental efficiency function of HPGe detector, the least square method of approximation technique has been adopted and the structure of the fitted polynomial is given below in equation (4.4):

$$p(x) = d_0 p_0(x) + d_1 p_1(x) + d_2 p_2(x) + \dots\dots + d_k p_k(x) \qquad (4.4)$$

Where, d's are suitable coefficients to be determined during fitting. An algorithm has been developed to compute the coefficients, B, C and d.

The measured absolute efficiency data were fitted to an orthogonal polynomial function. The efficiency calibration plot is shown in the Figure 4.3. The coefficients obtained by

fitting the efficiency verses various energies using a ten-order orthogonal polynomial are given in Table 4.3.
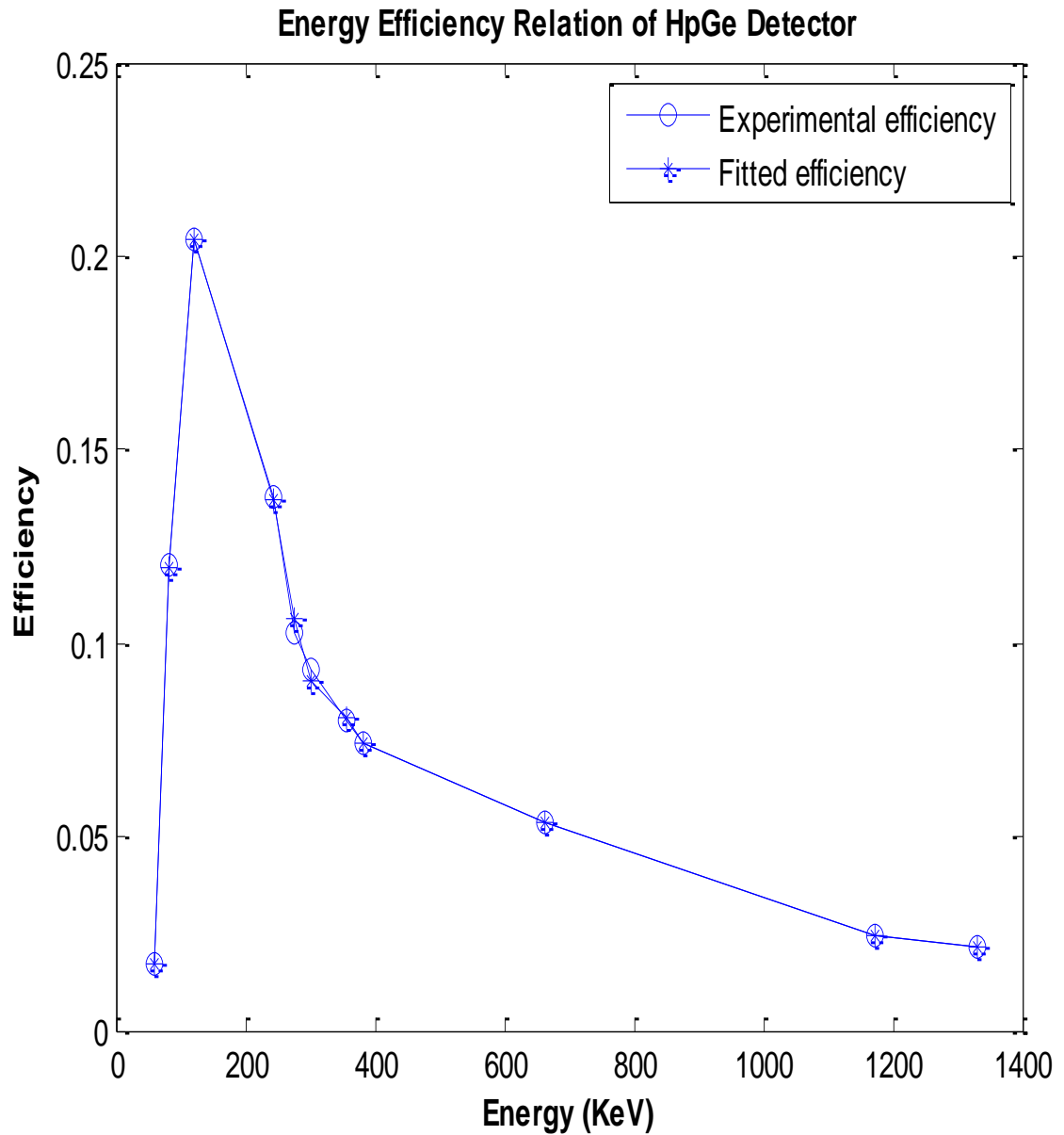
Figure 4.3. The energy versus efficiency calibration curve for an HPGe detector for disc source geometry. The figure also presents fitted efficiency using ten-order orthogonal polynomial.

Table 4.3. The coefficients obtained by fitting the efficiency of HPGe detector for various energies using a ten-order orthogonal polynomial.

	B	C	d
1	4.54E+02	0.00E+00	8.45E-02
2	9.35E+02	1.68E+05	-7.88E-05
3	5.15E+02	1.00E+05	-5.89E-10
4	7.76E+02	9.60E+04	2.77E-10
5	8.02E+02	1.31E+05	-1.02E-12
6	2.97E+02	3.80E+04	1.12E-14
7	2.13E+02	1.28E+04	-6.93E-17
8	2.49E+02	3.48E+03	9.41E-20
9	1.79E+02	8.99E+03	9.75E-23
10	2.85E+02	6.86E+03	1.25E-23

4.2.3.4. EBT3 film-based measurements

Gafchromic EBT3 (Ashland ISP Advanced Materials, NJ, USA) is a self-developing radiochromic film. It is composed of an active radiochromic layer of thickness 30 μm, which is laminated between two 125 μm matte polyester layers and makes a symmetric structure, different to the asymmetric structure of its predecessor EBT2. The physical density of EBT3 film is about 1.33 g cm^{-3}. The total physical thickness and water equivalent thickness of the film are 0.28 mm and 0.32 mm respectively. The matte polyester contains microscopic silica spheres at the surface to eliminate Newton's Rings scanner artifacts in images obtained using a flatbed scanner. The yellow colour of the film arises from the presence of a yellow dye incorporated in the active layer. A marker dye

within the active layer is included for the correction of small thickness variations, using multiple colour channels (wavelengths) to correct for the film non-uniformity. The effective atomic number, Z_{eff} of EBT3 film is 6.84 and it is close to Z_{eff} of water ($Z_{eff,water}$= 7.3). Gafchromic EBT3 film incorporates the lithium salt of pentacosa-10, 12-diynoate (LiPAD) as active monomer.

Characteristics and applications of Gafchromic EBT3 film for radiotherapy dosimetry have been studied in detail by a number of researchers (Crijns et al 2013, Borca et al 2013, Sorriaux et al 2013, Lewis et al 2012). EBT3 Gafchromic films were used to study the uniformity of activity distribution of the source (Villarreal-Barajas and Khan 2014).

Estimation of the uniformity of activity distribution in the source

In order to estimate the uniformity of activity distribution of ^{177}Lu patch source, an autoradiograph of the source was taken on the EBT3 film by keeping the source in contact with the film for 15 min. The irradiated film was scanned using the EPSON Expression 10000 XL scanner with a resolution of 72 dpi and the image was analyzed with commercial software (FilmQA Pro Ashland ISP Advanced Materials, NJ, USA).

The software has features such as flatness and symmetry etc. to measure the radiation field size and other beam parameter of a teletherapy machine. This software eliminates film and scanner artifacts by detecting errors during scanning. The same feature was used to quantify the separation between 50% of normalized pixel value.

Calibration of EBT3 films at electron energy

The EBT3 films of size 3 cm x 20 cm were calibrated using 4 MeV electron beam from a linear accelerator. The output of the linear accelerator (D_w) at Z_{ref} (6 mm) was 0.963 MU cGy^{-1} for 100 cm target to surface of detector distance (TSD) measured with a plane parallel chamber. The EBT3 films were kept below a Solid Water slab of 6 mm thickness to give necessary build up. Dimension of Solid Water phantom was 30 cm x 30 cm x 7 cm. The films were irradiated to doses of 279, 705, 1439 and 3000 cGy and were analyzed using the EPSON Expression 10000 XL scanner. This calibration (Figure 4.4) was used to estimate the surface dose of ^{177}Lu source that involved Gafchromic film.
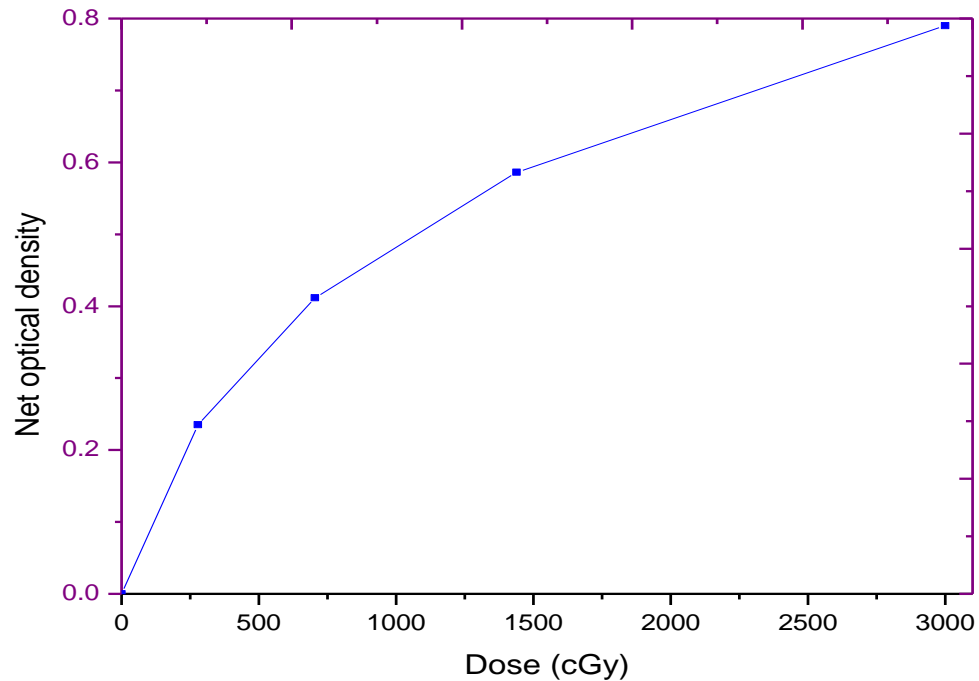
Figure 4.4. Dose response of EBT3 Gafchromic film for 4MeV electron beam. The films were irradiated to doses of 279, 705, 1439 and 3000 cGy.

4.2.3.5. Surface dose measurements using an extrapolation chamber

An extrapolation chamber made by PTW-Freiburg, Germany was used in this study. It is a parallel plate ionization chamber having collecting electrode made from polymethyl methacrylate (PMMA) coated with 0.02 mm graphite. It has a 30 mm diameter graphite collecting electrode surrounded by a 30 mm annular guard electrode mounted on a 25 mm long movable piston with micrometer gauge.

The entrance window is made of graphite-coated polyethylene terephalate film (Mylar®) having thickness (3.5 µm of Mylar® and 1.57 µm of graphite) approximately 0.75 mg cm^{-2}. The Mylar® foil is stretched by a ring on the electrode housing made up of PMMA. The leakage current of the chamber was less than 10^{-14} A. The details of the chamber are available in literatures (Bakshi et al 2013, Sudhir et al 2015, Vandana et al 2016).

The ^{177}Lu patch source mounted on a 5-mm-thick PMMA circular disc was placed on the entrance window of the extrapolation chamber (Figure 4.5). The UNIDOS electrometer was used to measure the output current of the extrapolation chamber with a resolution down to a few pA. The electric field strength was maintained at 50 V mm^{-1} by changing applied voltage and cavity length (l) during the experiment.

Minimum five readings for each polarity (positive and negative) were recorded, to observe the polarity effect on chamber current. The average current was corrected for variation in temperature and pressure (reference temperature=20°C, reference pressure=1013.15 mbar). In order to measure the surface dose rate, the charge (nC) was collected by varying the plate separation from 0.7 mm to 2.5 mm.
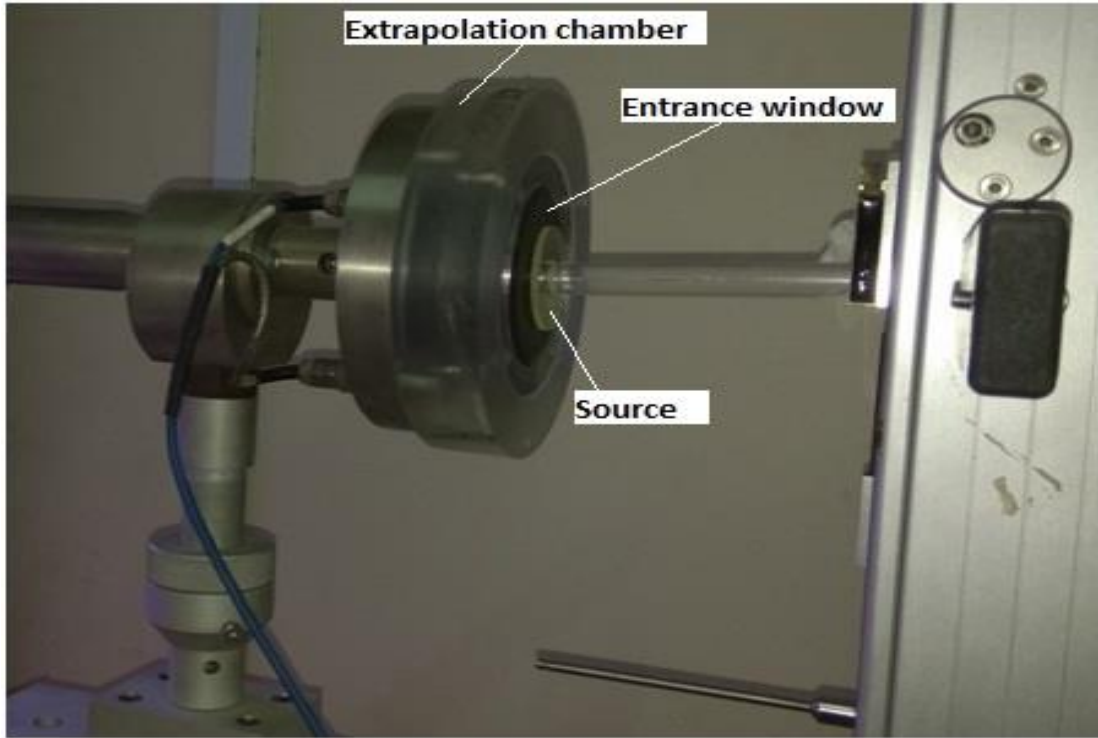
Figure 4.5. Photograph of measurement set up of ^{177}Lu patch source with extrapolation chamber.

The surface dose rate $\dot{D}_w$ (at 5 µm depth) in water, using the extrapolation chamber was obtained based on equation (4.5) given below (IAEA 2002b, ICRU report 2004, Chang et al 2016):

$$\dot{D}_w = \left[\left(\frac{w}{e}\right)\frac{1}{a_{eff}\rho_0}\left\{\frac{dI}{dl}\right\}k_{wall}\right](S/\rho)_a^w \qquad (4.5)$$

where w/e is the average energy required to produce an ion pair in air, which is equal to 33.97 J C^{-1}, a_{eff} (in cm^2) is the effective collector area of the charge collection, density of

air is $\rho_0 =1.18$ x10^{-3} g cm^{-3} at reference conditions, dI/dl is the slope of an extrapolation curve obtained through the plot between corrected current and l. k_{wall} corrects for the chamber wall materials being different from water.

$(S/\rho)_a^w$ is the Bragg-Gray stopping power ratio of water-to-air. The term in square bracket of equation (4.5) measures the dose rate in air cavity of the extrapolation chamber. The dose rate in water is obtained by multiplying the dose rate in air cavity with $(S/\rho)_a^w$.

a_{eff} was taken as the area enclosed by the 50% normalized pixel value at the source surface (Prutt 1987, Soares 1991, Goetsch and Sunderland 1991b, Deasy and Soares 1994). This method of defining the a_{eff} can be adopted when collector electrode diameter (30 mm) is larger than the source diameter (20 mm).

It may be noted that in the published literature (IAEA 2002b, ICRU report 2004, Chang et al 2016), the effect due to back wall being different from water was addressed through a correction factor, k_{back}. Whereas in the present study, all the wall materials of the extrapolation chamber (front, side and back walls) being different from water is accounted through k_{wall}.

4.2.3.6. Monte Carlo calculations

The DOSRZnrc user-code (Rogers et al 2010) of the EGSnrc code system (Kawrakow et al 2013) is utilized in this work. The extrapolation chamber (all the mechanical dimension and materials of entrance window, collecting electrode, guard ring etc.) and the ^{177}Lu skin

patch source were simulated in the DOSRZnrc user-code as per its design and geometry to estimate k_{wall}. The Monte Carlo transport parameters required for this simulation were discussed in Chapter 2.

Calculation of $(S/\rho)_a^w$

The calculation of $(S/\rho)_a^w$ was carried out using the modified version of SPRRZnrc user-code (Selvam and Rogers 2008). For this purpose, in the preparation of PEGS4 data sets for Bragg-Gray (BG) stopping-power ratios, the IUNRST was set as 1 in the PEGS4 input file. The IUNRST = 1 option provides a cross section data set (PEGS4 output) that includes just the unrestricted collision stopping powers. $(S/\rho)_a^w$ is calculated at 5 μm depth in a cylindrical unit density water phantom of 7 cm radius and 3 cm thick. In the calculations, the disc source was positioned on the top of the water phantom. Both the disc source and the water phantom had a common axis. The scoring radius and thickness used in the calculations were 1 cm and 1 μm, respectively. Up to 10^6 particle histories were simulated. The 1σ statistical uncertainties on the calculated values of $(S/\rho)_a^w$ were 0.01%.

Calculation of k_{wall}

The factor k_{wall} was calculated for $l = 0.75$, 2 and 2.5 mm using the DOSRZnrc user-code (Rogers et al 2010). The value of k_{wall} corrects for the fact that not all the materials in the extrapolation chamber are water and its value is calculated as the ratio of the absorbed dose to air in a homogeneous water-walled chamber to the absorbed dose to air in the PTW extrapolation chamber. Up to 10^7 particle histories were simulated

Dose calculations in water phantom

Absorbed dose to water in the water phantom was calculated using the DOSRZnrc user-code (Rogers et al 2010). The calculations include on-axis depth doses and lateral dose profiles at depths of 5 µm and 1 mm. In these calculations, the ^{177}Lu patch source was positioned on the surface of a 7 cm radius x 3 cm height cylindrical water phantom. For depth dose calculations, scoring radius was 1.5 mm radius. For depths up to 10 µm, the scoring height was 1 µm thereafter, it was 10 µm. For lateral dose profile at 5 µm depth, the dose was scored in cylindrical shell segments of thickness 1 mm and height 1 µm. At 1 mm depth, the scoring was done in cylindrical shell segments of thickness 1 mm and height 10 µm. Up to 10^9 particle histories were simulated.

4.3. Results and discussion

4.3.1. ^{32}P brachytherapy patch source

Salguerio et al (2008a, 2008 b) designed ^{32}P brachytherapy patch source (1 mm in height x 5 mm in diameter) for skin diseases using phosphoric acid and chromic phosphate in combination with natural rubber or silicone and evaluated its therapeutic efficacy. They reported arrest of tumour growth and complete regression of tumour in some cases with 40 Gy of single-dose scheme in animal studies. They estimated the dose rate at selected depths (0.0001, 0.01, 4 and 7.5 mm) using the Monte Carlo code (Salguerio et al 2008b, MCNP5 2003). The activity per unit area considered in their calculations was 10.6 MBq cm^{-2}. The surface area of the source was 0.196 cm^2. Hence, the total activity of the source considered in their work was 2.081 MBq. We repeated their study using the DOSRZnrc

user-code (Rogers et al 2010). The dose rate values showed a good agreement for 0.0001 and 0.01 mm depths. For 4 and 7.5 mm depths, the published values were higher by a factor of about 22 and 3.6 x 10^4, respectively. We concluded that this large discrepancy in the dose rate values at 4 and 7.5 mm depths published by Salguerio et al (2008b) was due to possible systematic error in their Monte Carlo calculations (Sahoo and Selvam, 2014).

The variation of the dose values per unit activity (Gy Bq^{-1}) as a function of depth (mm) in water for the ^{32}P-nafion-patch source is shown in Figure 4.6. The dose decreases rapidly with increasing depth in water. Central axis dose at 4 mm depth in water is only 0.08% of the central axis surface dose. Such a rapid decrease in dose will result in better sparing of the normal tissues.
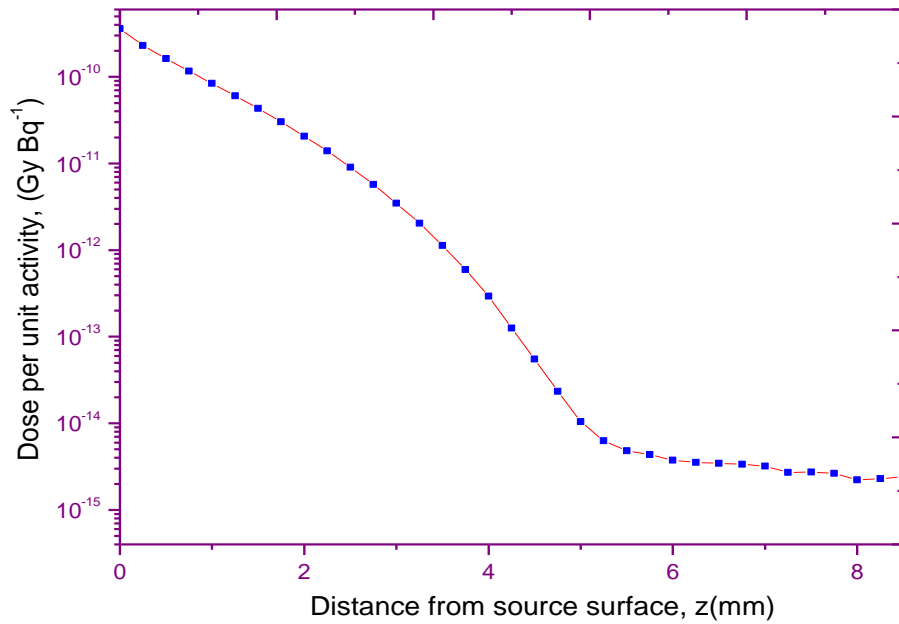
Figure 4.6. Depth dose distribution of ^{32}P-nafion-patch source along the central axis of the source.

Table 4.4 compares the values of central axis depth dose per unit activity (Gy Bq^{-1}) of ^{32}P-nafion-patch source with the corresponding values of ^{32}P-silicon-patch (Salgueiro et al 2008b) for different depths in water. Higher dose rate values are observed in the case of ^{32}P-silicon-patch source, because the radioactivity is distributed in lesser surface area (0.196 cm^2) as compared to ^{32}P-nafion-patch source, where surface area is 1 cm^2.

For treatment time calculation, 1 mm depth from the surface along the central axis of the source is considered as reference depth (IAEA 2002b, ICRU report 2004). The value of dose in water calculated at 1 mm from the source surface is 8.41 x 10^{-11} Gy Bq^{-1}. Hence, the time required to deliver a therapeutic dose of 30 Gy for a 37 MBq of radioactivity distributed in 1 cm^2 of ^{32}P-nafion-patch source is about 2.7 hours.

Table 4.4. Comparison of dose values per unit activity (Gy Bq^{-1}) presented as a function of depth in water. The number shown in the parenthesis against the dose values is the percentage error (1 σ).

Depth in water (mm)	Dose values per unit activity (Gy Bq^{-1})	
	^{32}P-nafion-patch source [a] (this work)	^{32}P-silicone-patch source [b] (Sahoo & Selvam 2014)
0.0125	3.62 x 10^{-10}(0.05%)	1.51 x 10^{-9} (0.30%)[c]
1	8.41 x 10^{-11} (0.10%)	--
4	2.93 x 10^{-13} (1.30%)	1.41 x 10^{-11} (0.40%)
7.5	2.74 x 10^{-15} (7.40%)	3.5 x 10^{-15} (24%)

[a]Source dimensions: 1cm x 1 cm x 100 µm.

[b]Source dimensions: 5 mm diameter x 1 mm height

[c]depth is 0.01 mm

Figure 4.7 presents the dose rate profiles along the x-axis of ^{32}P-nafion-patch source for three different depths z = 0.5, 1 and 2 mm from the source surface. Figure 4.8 presents normalized dose values along the x-axis at depth 1 mm. The central axis dose value at 1 mm depth is used for normalization. Dose rate value at 3.5 mm away from the central axis is about 91% of the central axis value. Whereas dose rate at 5 mm away from the central axis is only 50% of the central axis value.

Figures 4.9 - 4.11 show isodose profiles of the ^{32}P-nafion-patch source at depths of 0.5, 1, and 2 mm. About 3.25 - 3.5 mm distance around the central axis is covered by about 90% isodose line for depths of 0.5, 1, and 2 mm. Hence, the ^{32}P-nafion-patch source (1 cm x 1 cm) is effective for treatment of skin lesions approximately of size 6.5 - 7.0 mm.
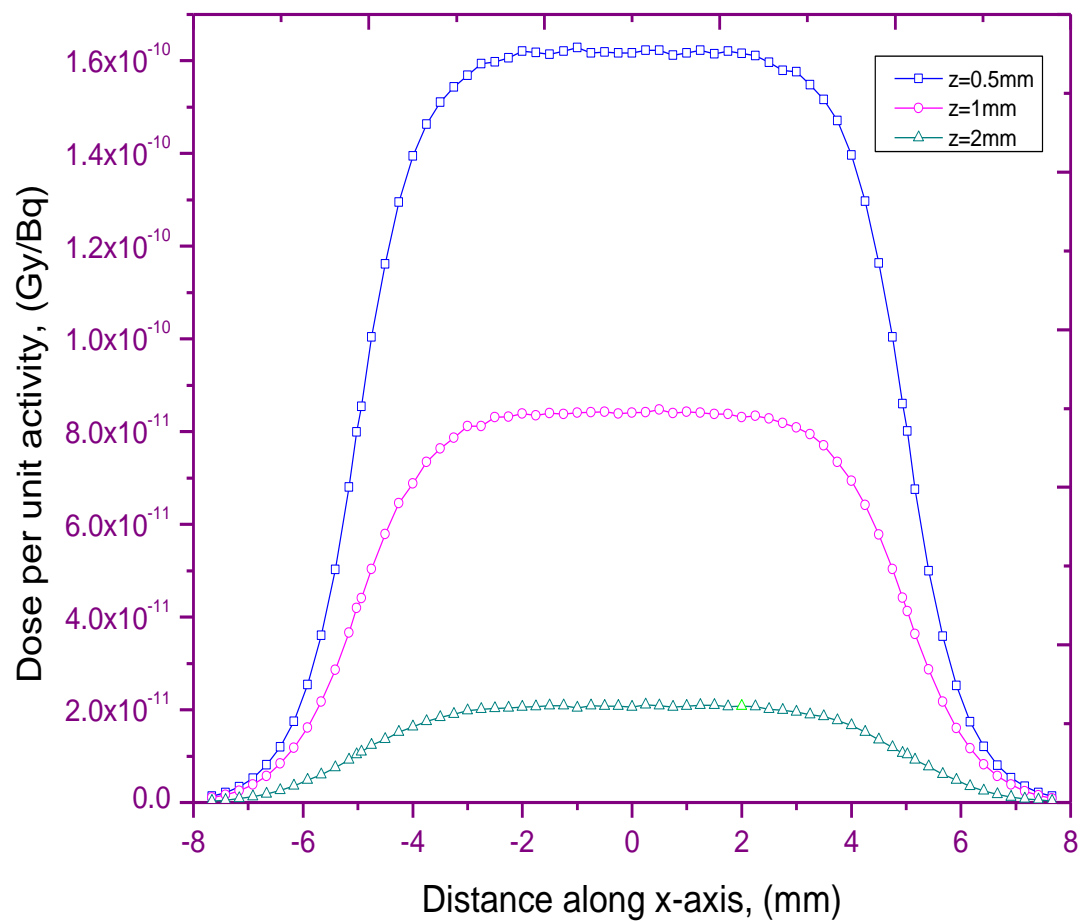
Figure 4.7. Dose profile along the x-axis of ^{32}P-nafion-patch source for different depths, z = 0.5 mm, z = 1 mm and z = 2 mm.
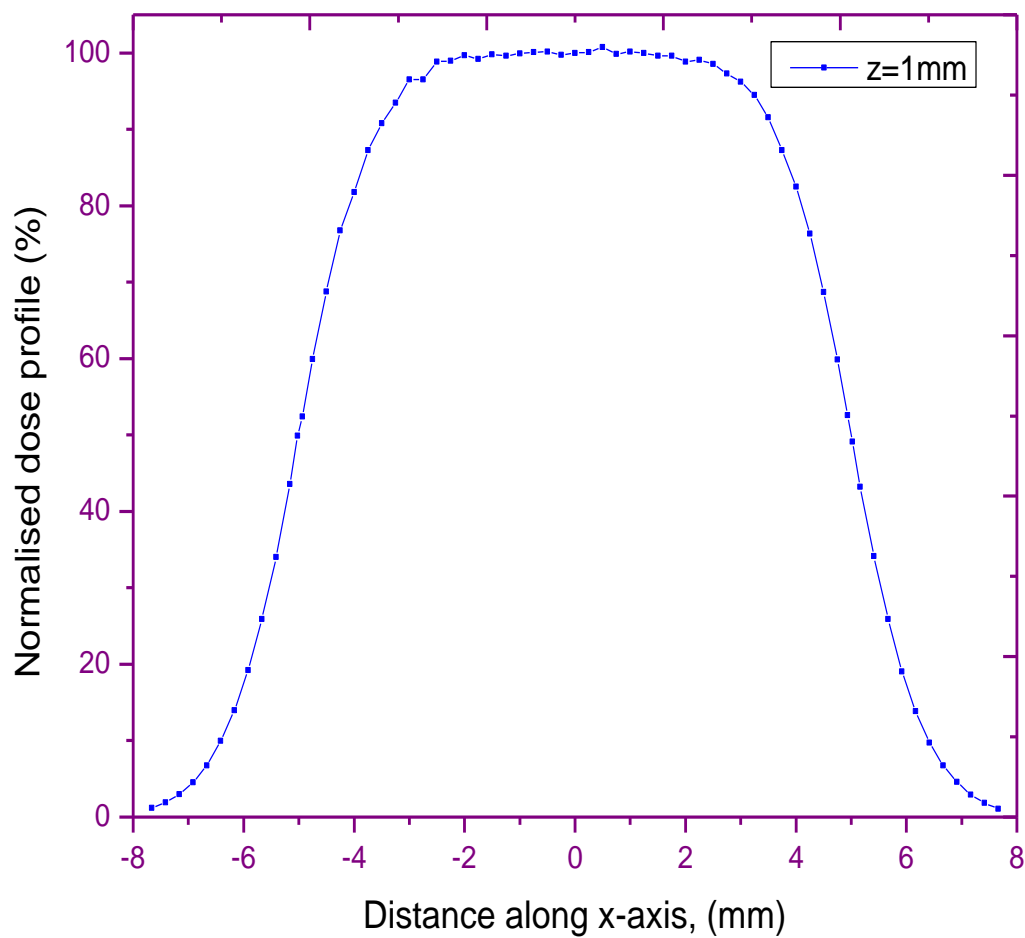
Figure 4.8. Normalised dose profile along the x-axis of ^{32}P-nafion-patch source for depth z = 1 mm.
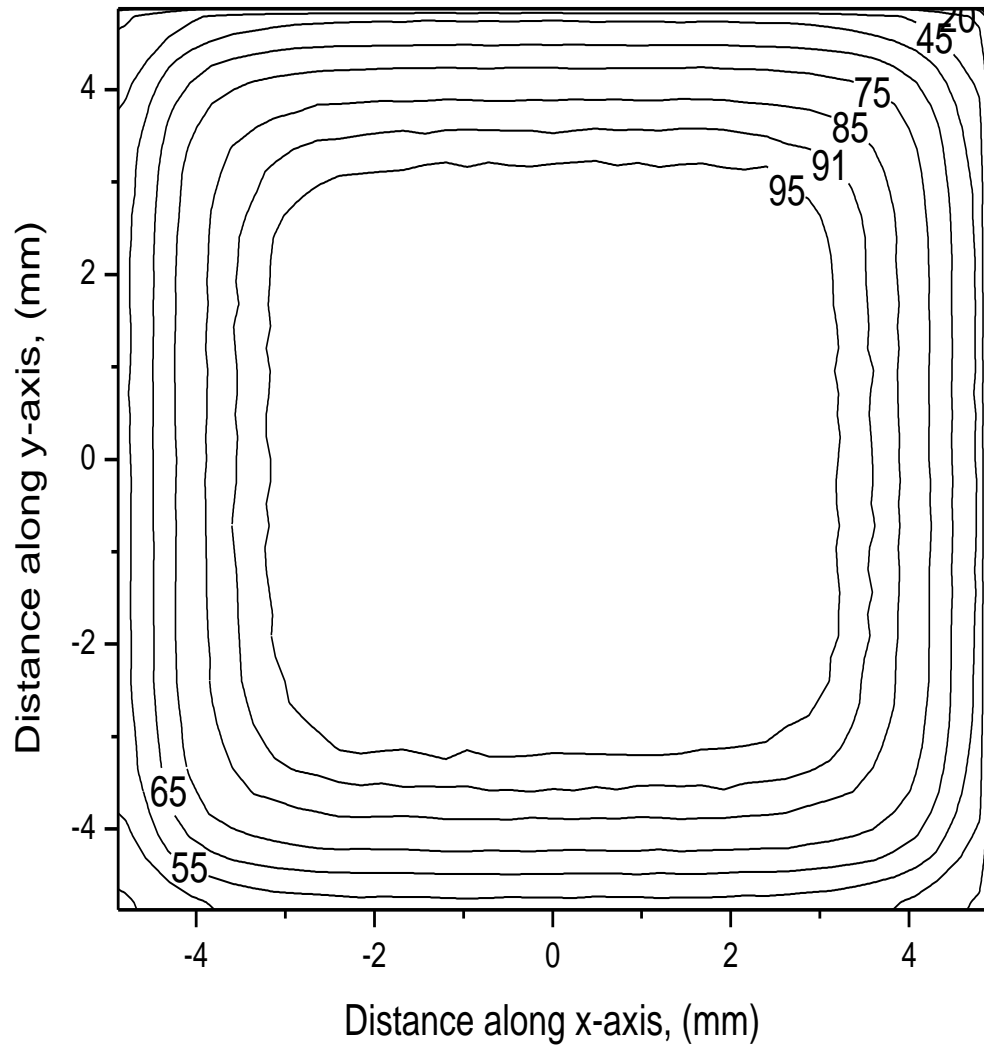
Figure 4.9. Isodose profiles of the ^{32}P skin patch source on xy-plane at a depth of 0.5 mm.
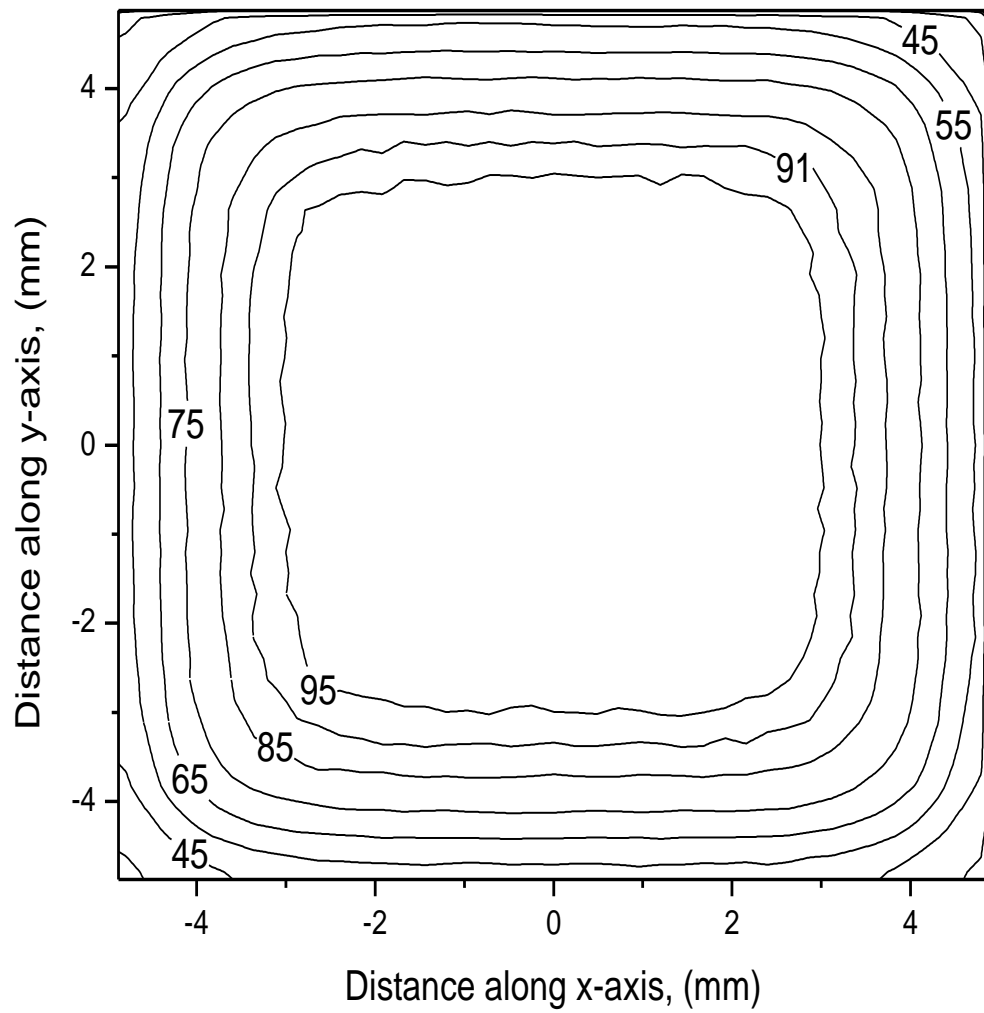
Figure 4.10. Isodose profiles of the ^{32}P skin patch source on xy-plane at a depth of 1mm.
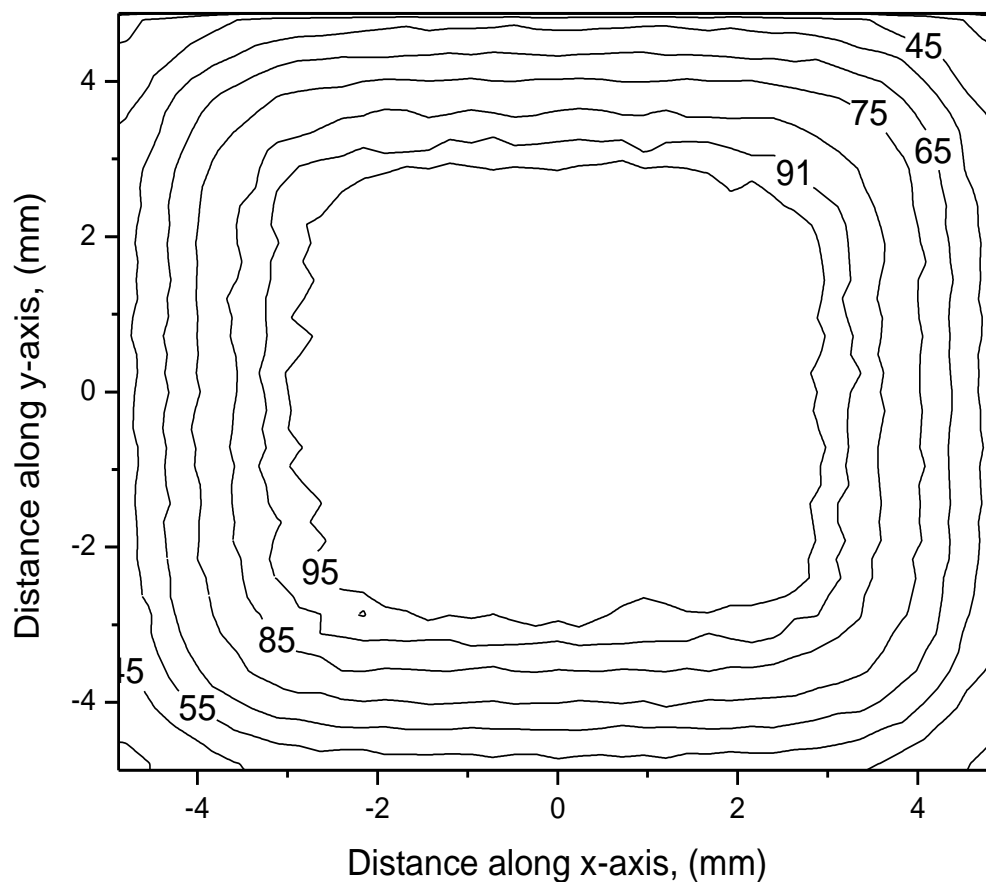
Figure 4.11. Isodose profiles of the ^{32}P skin patch source on xy-plane at a depth of 2 mm.

4.3.2. ^{177}Lu skin patch source

4.3.2.1. Activity and gamma ray spectrum of ^{177}Lu skin patch source

The gamma ray spectrum of the ^{177}Lu source measured by the HPGe detector is shown in Figure 4.12. The prominent low energy photons emitted by ^{177}Lu are 113 keV (6.6%) and 208 keV (11%). The efficiencies obtained using a ten-order orthogonal polynomial fitting were 0.194%, and 0.178% for gamma energies 113 keV and 208 keV respectively.

The activity of ^{177}Lu source estimated by substituting the background subtracted net count rate (N in counts per second), efficiency (ε in %) and the emission probability (Pγ in %) of 113 and 208 keV gamma energy lines in equation (4.2). The activity of ^{177}Lu source was found to be 3.46 ± 0.01 mCi. The uncertainty in the activity measurement was calculated as discussed in the literature (IAEA 2004, Bakshi *et al* 2017).
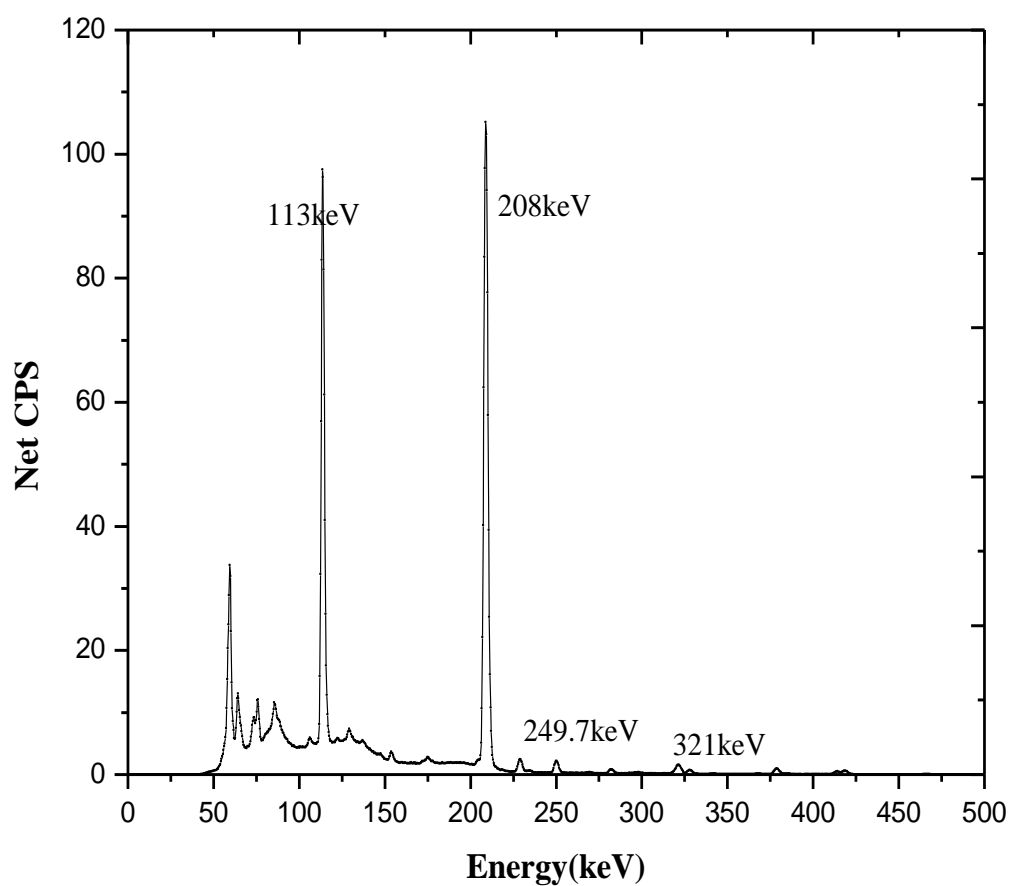
Figure 4.12. Gamma ray spectrum of a ^{177}Lu patch source recorded on a coaxial HPGe detector.

4.3.2.2. Uniformity of activity distribution of ^{177}Lu patch source

Figure 4.13 presents the scanned image of autoradiograph of ^{177}Lu patch source. Normalized pixel values (%) with respect to the central position of the autoradiograph were determined. The variation of activity distribution in central region of 11.5 mm diameter is within 5% (Figure 4.14). The source diameter corresponding to 50% normalized pixel value is obtained as 21 mm (Prutt 1987, Soares 1991, Deasy and Soares 1994). The autoradiograph is scanned in an EPSON scanner with a resolution of 72 dpi.

During the analysis for width of 50% normalized pixel value, an error of 1 pixel may occur, which corresponds to 0.35 mm. This means radius of the source is 10.5 ± 0.35 mm and the uncertainty in a_{eff} estimation is 6.6%. An effective collector area ($a_{eff} = \pi r^2$) is calculated as 3.46 cm^2 which is used in the surface dose rate calculation (equation 4.5).
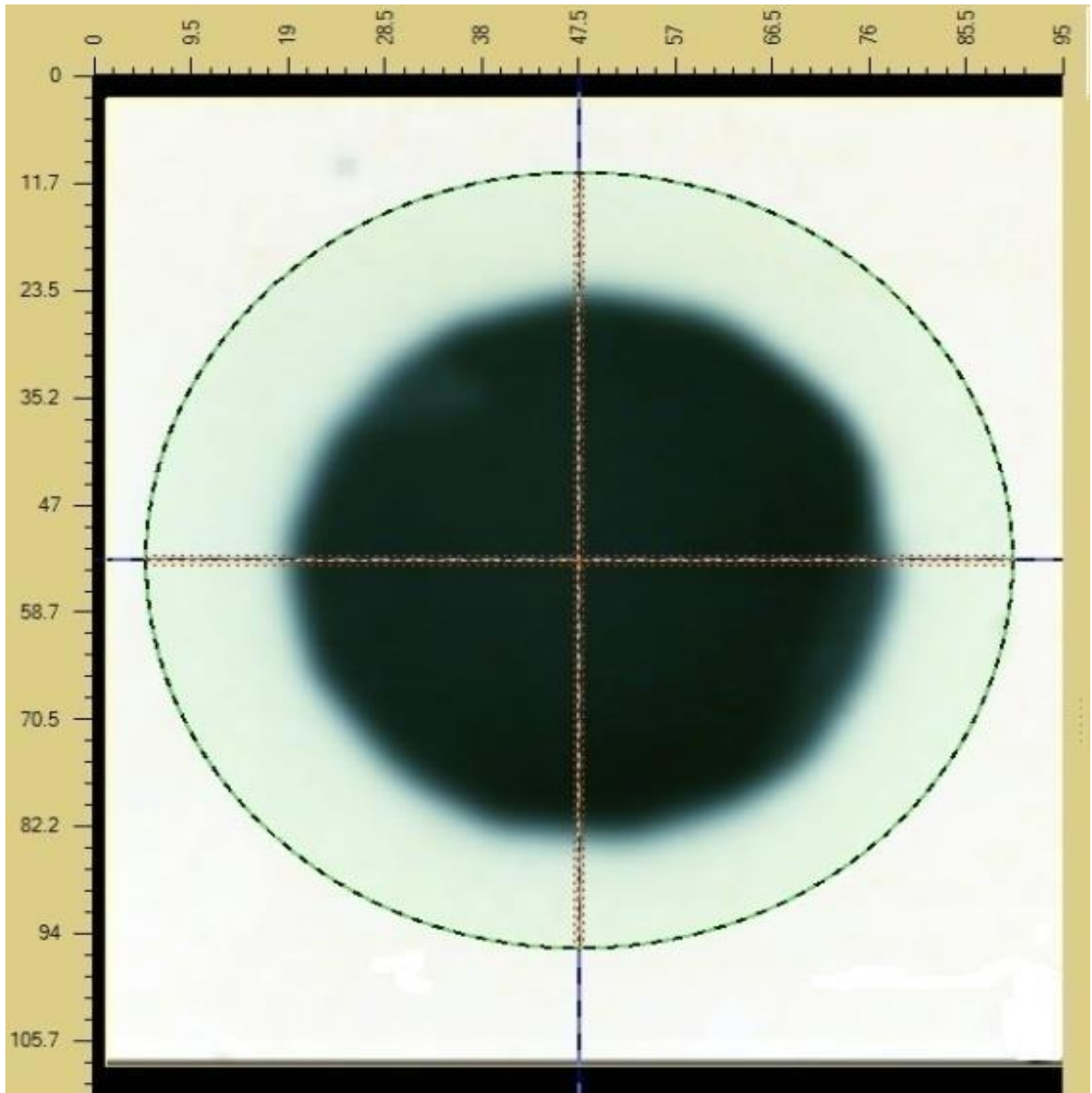
Figure 4.13. Scanned image of autoradiograph of ^{177}Lu patch source taken on EBT3 film.
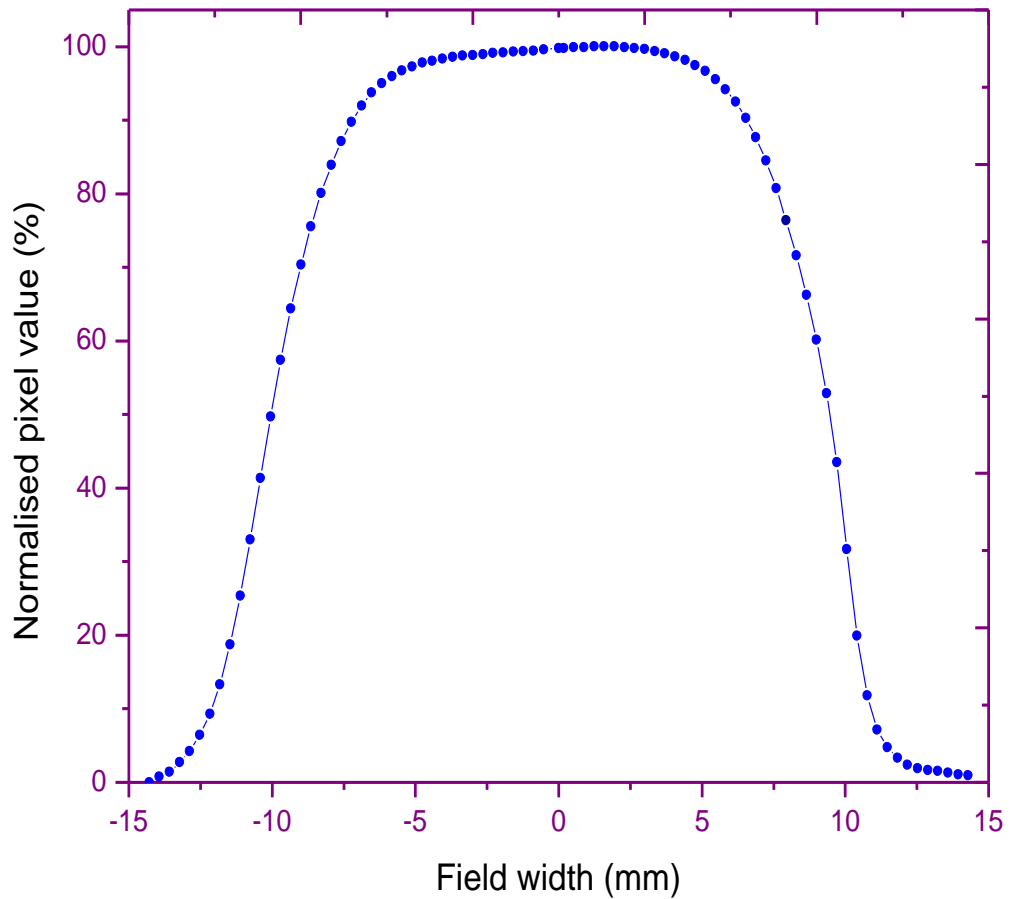
Figure 4.14. Activity distribution along the radial distance of ^{177}Lu patch source based on autoradiograph taken on EBT3 film.

Figure 4.15 presents the profile of ^{177}Lu source generated using EBT3 film to determine uniformity of activity distribution in the source. The values of $\dot{D}_{max}$, $\dot{D}_{min}$ and $\dot{D}_{avg}$ were estimated from the figure 4.15. The uniformity parameter (ICRU report 2004, Soares and McLaughlin 1993) is known as source non-uniformity (U) was estimated using equation

(4.1) and found to be 2.2%, which is much much less than 20% limit for planar and concave sources (ICRU report 2004).
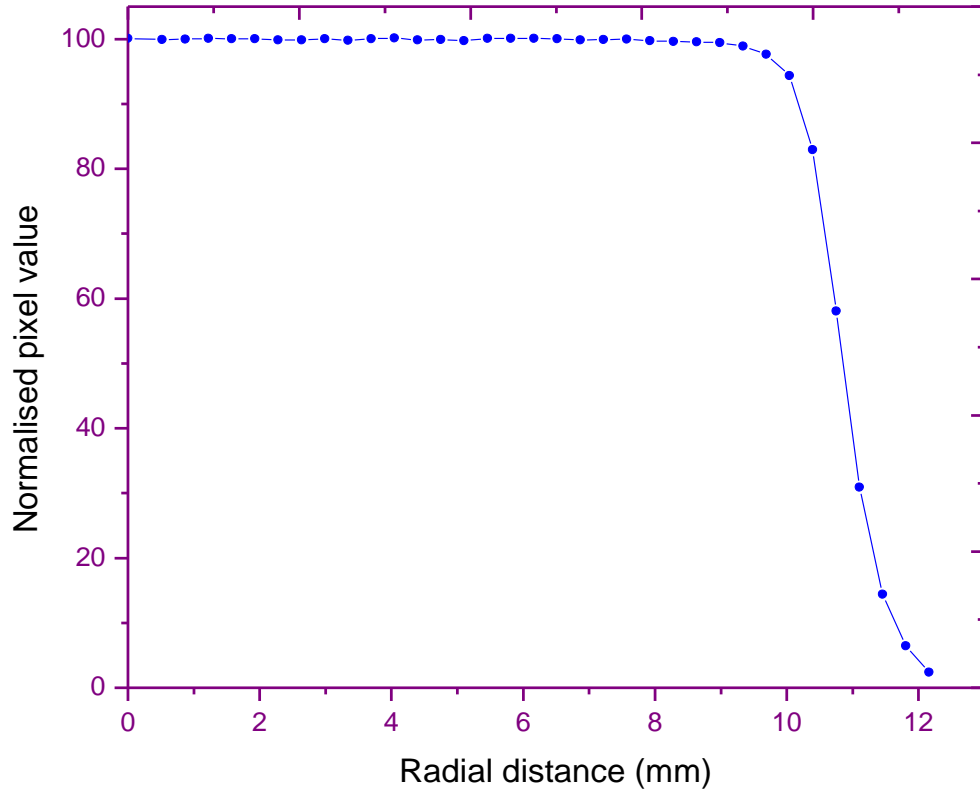
Figure 4.15. Profile of ^{177}Lu patch source generated using EBT3 film to determine uniformity of activity distribution in the source.

4.3.2.3. Surface dose rate to water

For the calculation of surface dose rate to water, equation (4.5) was used. The calculated value of $(S/\rho)_a^w$ at 5 µm depth is 1.14 ± 0.01%. Table 4.5 presents the k_{wall} correction factor for l = 0.75, 2 and 2.5 mm. The value of k_{wall} in the calculation is 1.03, which is observed to be independent of l (Table 4.5).

Table 4.5.Monte Carlo-calculated values of k_{wall}

Cavity length, l (mm)	$k_{wall} \pm 1\sigma$ in %
0.75	1.03 ± 0.30
2.0	1.03 ± 0.20
2.5	1.03 ± 0.44

Figure 4.16 presents plot of corrected net current as a function of l in the range of 0.7 - 2.5 mm. The slope obtained from the linear fit of the plot was used in the calculation of surface dose rate to water in equation (4.5).
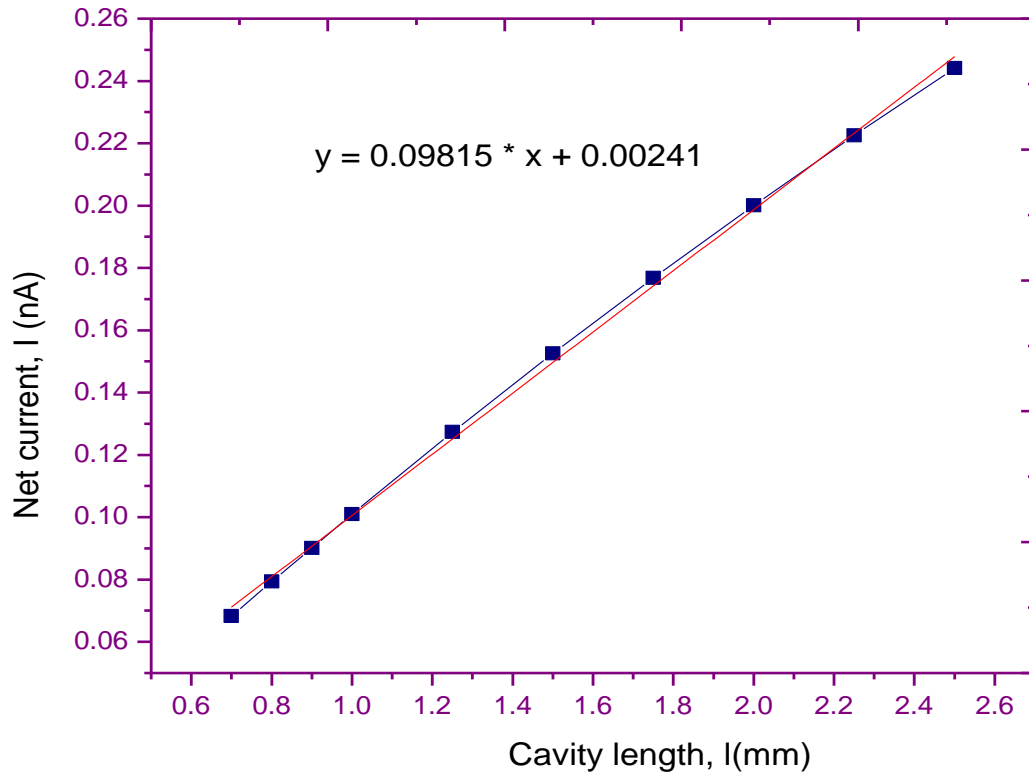
Figure 4.16. Plot of net current (I) versus cavity length (l) of the extrapolation chamber.

Table 4.6 presents the measured and calculated values of surface dose rate to water (dose rate at 5 μm depth) for ^{177}Lu patch source of unit activity.

Table 4.6.Measured and Monte Carlo-calculated on-axis dose rates per unit activity (in Gy h^{-1} mCi^{-1}) at 5 μm depth in water for ^{177}Lu patch source.

Dose rate (Gy h^{-1} mCi^{-1})		
Extrapolation chamber	Monte Carlo	Difference (%)
9.9 ± 0.7	8.7 ± 0.2	14

To compare the Monte Carlo-calculated dose rate value with that of the extrapolation chamber-based measurements, additional Monte Carlo simulations were carried out by setting the scoring radius of the simulation as 10.5 mm. Comparison of the calculated dose rate values using 1.5 mm and 10.5 mm scoring radii agreed to within 0.15%. The large deviations (14%) in extrapolation chamber-based result may be attributed to systematic uncertainty present in the extrapolation chamber measurements as the source size is smaller than sensitive volume of the chamber.

Figure 4.17 presents the Monte Carlo-calculated lateral dose rate profiles of the ^{177}Lu patch source at 5 μm and 1 mm depths in water. The profile at each depth indicates dose is uniform up to 0.95 cm and thereafter dose falls off sharply. Figure 4.18 presents the calculated dose rate per mCi in water as a function of depth in water along the central axis of the source.

For the treatment of superficial layer of skin, the time required to deliver a typical therapeutic dose of 30 Gy for a 20 mm diameter ^{177}Lu patch source containing 1 mCi of

radioactivity is about 3.45 hours. Figure 4.18 also shows that dose at 1 mm depth is negligible (0.2%) which implies dose received by normal tissue will be insignificant and it also justifies our method of measuring dose rate at 5 µm.
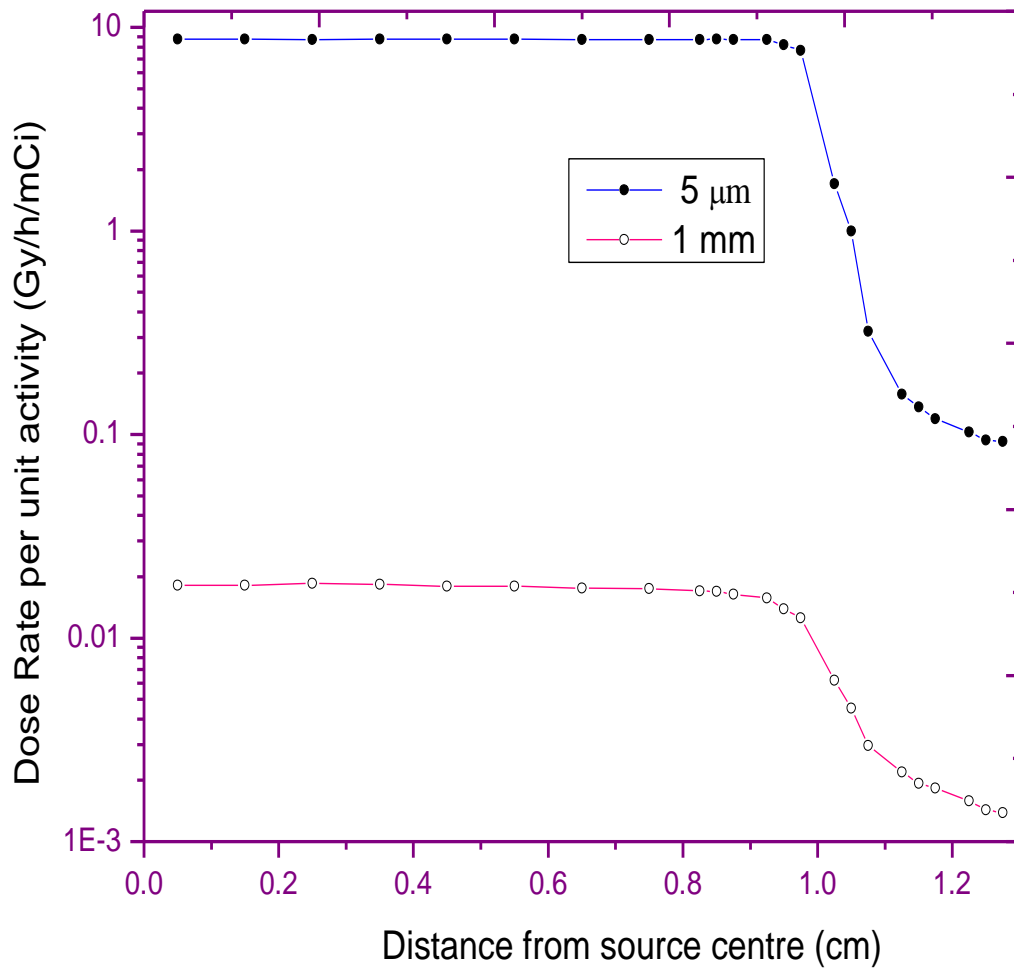
Figure 4.17. Monte Carlo-calculated dose rate profiles at surface (5 µm) and 1 mm depths in water due to 1 mCi ^{177}Lu patch source.
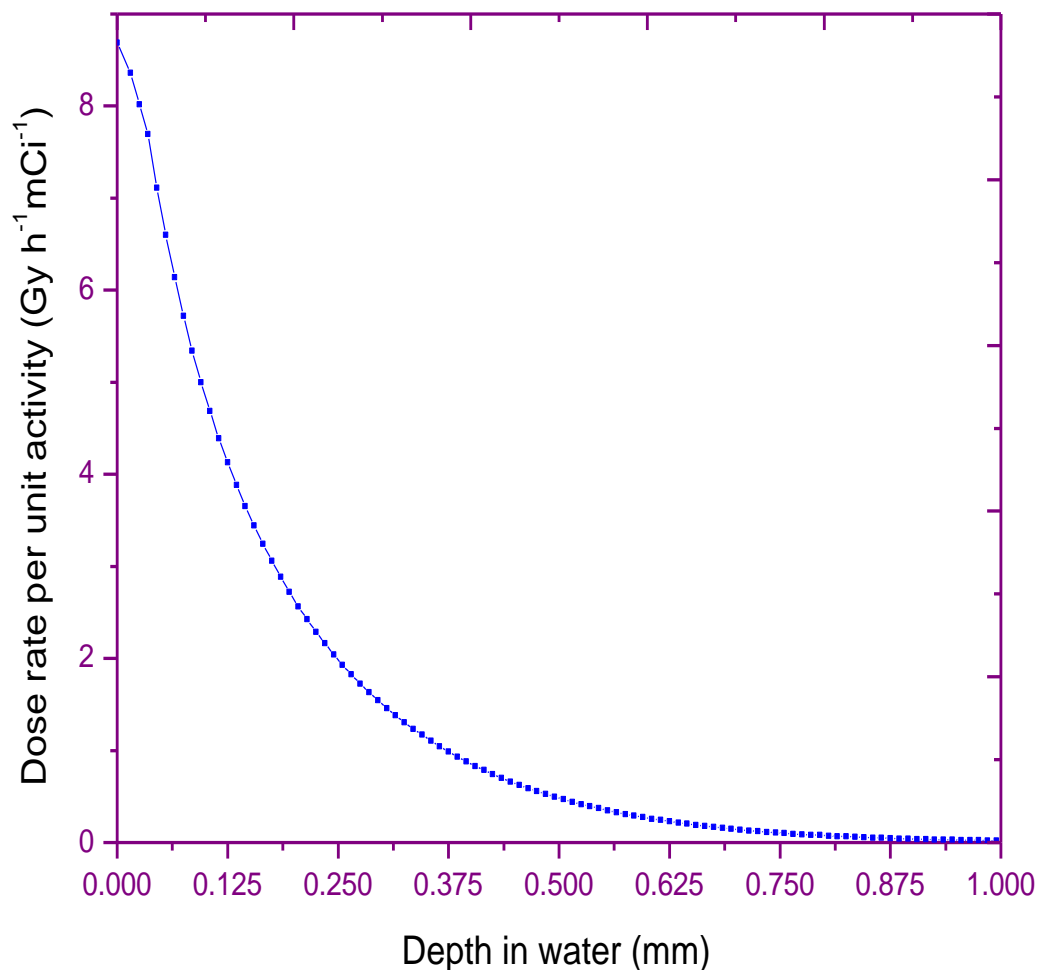
Figure 4.18. Monte Carlo-calculated on-axis dose rate in water shown as a function of depth in water due to 1 mCi ^{177}Lu patch source.

4.3.2.4. Estimation of surface dose using EBT3 films

A stack of two EBT3 films was irradiated for 20 minute in contact geometry with ^{177}Lu source placed over 5 mm-thick Perspex sheet. This measurement was again repeated for 20 minute using fresh films. The water-equivalent thickness of EBT3 film is 0.32 mm.

Since the active radiochromic layer is positioned at the centre of the film, the average dose measured by the first film is the dose at 0.16 mm depth, which is 3.61 Gy. The second EBT3 film measures the dose at a depth of 0.48 mm, which is 56.8 cGy.

From the Monte Carlo-calculated depth dose plot (Figure 4.18), the dose rates obtained at depths of 0.16 and 0.48 mm are 3.34 and 0.54 Gy h^{-1} mCi^{-1}, respectively. For an activity of 3.46 mCi and 20 min of exposure, the calculated values of doses at 0.16 and 0.48 mm depths are 3.85 Gy and 62.5 cGy, respectively. The calculate dose data at the above depths are in good agreement (within 7 - 10%) with the corresponding EBT3-based measured values of 3.61 Gy and 56.8 cGy.

The Monte Carlo-calculated dose rate at 0.16 mm depth is 38% of the dose rate at surface (5 μm). Therefore, EBT3-based surface dose rate (5 μm) will be 8.2 ± 0.1 Gy h^{-1} mCi^{-1}, which agrees within 6% with the Monte Carlo-based value of 8.7 ± 02 Gy h^{-1} mCi^{-1} (Table 4.6).

4.3.2.5. Uncertainty analysis

Total uncertainty in the extrapolation chamber measurement is due to uncertainty in *w/e* value, *dI/dl*, a_{eff}, k_{wall}, $(S/\rho)_a^w$ and u_A where u_A is the uncertainty in the activity of the ^{177}Lu patch source.

Table 4.7 presents uncertainty of the individual quantities used in the dose calculation. Final uncertainty on dose rate measured using extrapolation chamber is based on addition

in quadrature which is 6.6%. The statistical uncertainty in the Monte Carlo-calculated dose rate is 2.7%.

The total uncertainty in film measurements using the calibration curve was 1.5% which includes uncertainties in the film orientation, scanner uniformity, film reproducibility, curve fitting used to convert NOD to dose and film calibration using 4 MeV electron beam.

Table 4.7. Uncertainty of the individual quantities used in the dose calculation.

Sr. No.	Quantities	Uncertainty (%)
1[a]	*w/e* value	0.4
2[b]	*dI/dl*	0.05
3[b]	a_{eff}	6.6
4[c]	k_{wall}	0.44
5[c]	$\left(S/\rho\right)_a^w$	0.01
6	u_A	0.14

[a]Soares 1991, [b]measurement uncertainty, [c]Monte Carlo uncertainty

4.4. Conclusions

Dose distributions for the indigenously developed 1 cm x 1 cm ^{32}P-nafion skin patch source are calculated using the Monte Carlo-based EGSnrc code system. The calculated treatment time for delivering therapeutic dose of 30 Gy at 1 mm depth along the central axis of the source involving 37 MBq activity is about 2.7 hours. Hence, the ^{32}P-nafion-

patch source (1 cm x 1 cm) is effective for treatment of skin lesions approximately of size 6.5-7.0 mm.

^{177}Lu patch source was developed in-house at Bhabha Atomic Research Centre to study its dosimetric characteristics for clinical application in the treatment of superficial cancer. A ^{177}Lu patch source containing 3.46 ± 0.01 mCi of activity based on HPGe detector, was used in this study.

Absorbed dose rate at 5 µm depth in water (surface dose rate) measured using an extrapolation chamber and EBT3 Gafchromic film were 9.9 ± 0.7 and 8.2 ± 0.1 Gy h^{-1} mCi^{-1} respectively. The correction factors such as Bragg-Gray stopping power ratio of water-to-air and wall materials being different from water needed to establish the surface dose rate were calculated using Monte Carlo methods.

The Monte Carlo-calculated value of surface dose rate is 8.7 ± 0.2 Gy h^{-1} mCi^{-1}, which agrees to within 6% with the EBT3 film-based measurement and 14% with the extrapolation chamber-based measurement. In addition, on-axis depth dose and lateral dose profiles were also calculated.

CHAPTER 5

DOSIMETRY OF INDIGENOUSLY DEVELOPED ^{125}I SEED SOURCE FOR INTRAOCULAR TUMOURS

5.1. Introduction

Plaque brachytherapy has been successfully used for treatment of ocular melanomas, retinoblastoma and some metastatic ocular tumours. Plaque brachytherapy offers equivalent tumour control while allowing eye preservation and vision retention (Chiu-Tsao et al 2012). Radiation therapy in combination with chemotherapy is a suitable treatment option to save the eye with some vision (Char et al 1996 and Melia et al 2001). Low energy sources such as ^{125}I, ^{103}Pd, ^{106}Ru and ^{90}Sr/^{90}Yt etc. kept in the close contact with tumours is a proven and effective method for such type of cancers (ABS-OOTF 2014). Typically plaques are made of gold or stainless steel or silver and are concave in shape to fit to the eye. These plaques are embedded with 12 - 15 seeds during clinical application. The Collaborative Ocular Melanoma Study (COMS) design is more popular and uses gold alloy backing as plaque material (Chiu-Tsao et al 2012, Thomson and Rogers 2010). The Radiation Oncology Physics and Engineering Services Australia (ROPES) design uses stainless steel (Granero et al 2004, Saidi et al 2011) and IBt/Bebig design uses silver as plaque material (Sanchez-Reyes et al 1998).

Accurate dose measurement in eye-plaque dosimetry is challenging due to steep dose gradient in the eye and presence of critical structures such as retina, optic nerve, eye lens etc close to the radioactive source (Chaudhary et al 2008). A number of dosimetry studies

for COMS (Thomson and Rogers 2010, Acar et al 2013, Chiu-Tsao et al 1993, Rivard et al 2008, Knutsen et al 2001, Krintz et al 2002 and Shanta et al 2005) and ROPES plaque designs (Granero et al 2004, Poder and Corde 2013 and Poder et al in 2013) using different sources have been reported in literatures using measurements and Monte Carlo simulations.

Thomson and Rogers (2010) and Acar et al (2013) calculated and compared the dose distributions for ^{125}I seed models in the COMS eye plaque using the Monte Carlo code. Dosimetry data for standard COMS-plaque using ^{125}I sources were generated by Chiu-Tsao et al in 1993, Rivard et al in 2008 and Knutsen et al in 2001. Krintz et al (2002) also measured the dose distribution for COMS plaques, loaded with ^{125}I seeds in a solid water phantom using radiochromic (model MD55-2) film. Dosimetric study was carried out by Granero et al (2004) for ROPES eye plaque design loaded with ^{125}I seeds using the GEANT4 Monte Carlo code. Similarly, Poder and Corde in 2013 used Gafchromic EBT3 films for dosimetry of eye plaque and compared the data with 3D treatment planning system. In a recent study, Poder et al (2013) used PRESAGE^m 3-D type dosimeter for ROPES eye plaques embedded with 6711 model ^{125}I seeds and observed up to 2% variations in central axis depth dose distributions for all ROPES plaque models and depths of interest.

Morrison et al (2014), Acar et al (2013) and Heilemann et al (2015) used EBT3 Gafchromic film for dosimetry of ^{125}I sources. Chaudhary et al (2008) shared their treatment planning experience in dosimetry of Ocuprosta source and quality assurance of a patient treated for ocular metastasis in eye plaque therapy.

Several publications cited above discuses the use of radiochromic films for dosimetry purpose in radiotherapy. The important advantages of film dosimetry are higher spatial resolutions (0.1 mm), low energy dependency and it is a permanent record of measurement (Arjomandy et al 2010, Martisikova et al 2008, Buston et al 2006). Other important parameters of radiochromic film are the dynamic range, small dimension and easy in handling make it an ideal tool for dosimetry application.

In this Chapter, Gafchromic EBT3 film (Ashland ISP Advanced Materials, NJ, USA) was used for dose measurement of silver plaque using ^{125}I sources. The energy response of the EBT3 Gafchromic film was studied by calibrating the films at ^{125}I and ^{60}Co energy. Dose values were measured at different depths from a single ^{125}I source in a solid water phantom and results were compared with the values obtained at similar depth using EGSnrc-based Monte Carlo code system (Kawrakow et al 2013). In an another experiment, thirteen number of OcuProsta sources were embedded in a 14 mm diameter silver plaque and this plaque was used to irradiate a stack of EBT3 films. These films were read using EPSON Expression 10000 XL scanner. The films were analyzed using ImageJ software (NIH, ImageJ software) and commercial software (FilmQA Pro Ashland ISP Advanced Materials, NJ, USA). The absorbed dose rate and central axis depth dose were measured. The off-axis and isodose profiles were generated.

5.2. Materials and methods

5.2.1. Design of OcuProsta^{125}I seed source and silver plaque

Bhabha Atomic Research Centre, India indigenously developed ^{125}I seed source, known as OcuProsta, for treatment of prostate cancer and ocular diseases. The source consists of

0.5 mm diameter and 3.0 mm long silver rod coated with palladium and on which ^{125}I is adsorbed. It is encapsulated in a hollow cylindrical titanium tube of 0.05 mm thick wall. The external dimension of the seed is 0.8 mm diameter and 4.75 mm length. Titanium, in addition to being inert towards source matrix, assures good tissue compatibility. The cap end of the cylinder is sealed by laser welding. Schematic cross sectional view of an OcuProsta[125]I source is shown in Figure 5.1. The activity per seed is 3.1 mCi. Hence the air-kerma strength per ^{125}I seed is about 3.94 U, assuming 1 mCi = 1.27 U (Sharma et al 2004) where, 1 U = 1 μGy m^2 h^{-1} = 1 cGy cm^2 h^{-1}.

0.05 mm Titanium encapsulation

0.5

I-125 adsorbed on palladium coated silver rod

0.8

3

4.75
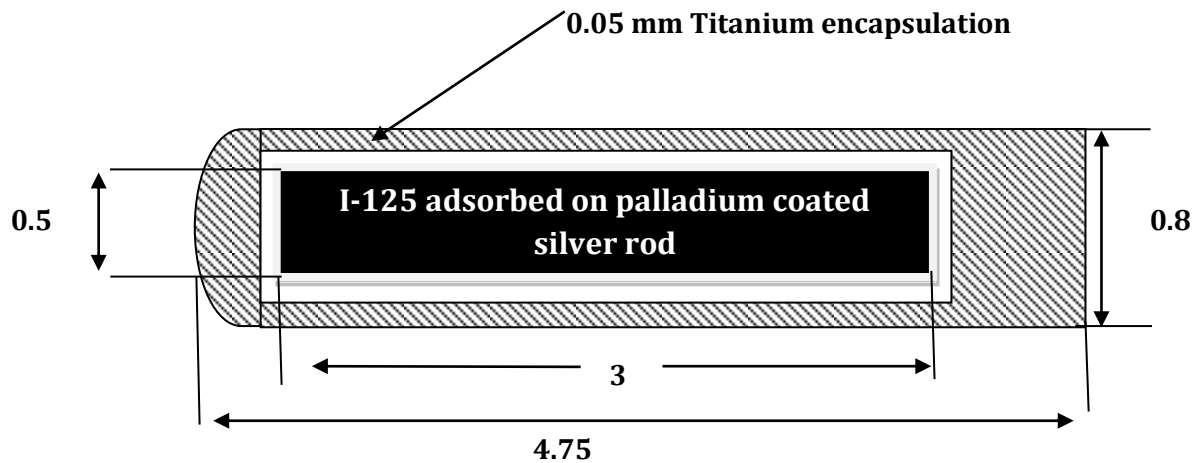
Figure 5.1. Schematic diagram of OcuProsta ^{125}I source.

Generally, eye plaques are available from 10 - 22 mm diameter with 2 mm increments. Selection of plaque depends on the size of tumour base (Chiu-Tsao et al 2012). 14 mm plaque was used in this measurement, because it is commonly used and it will cover the tumour volume (Chaudhari et al 2008). A silver plaque of 14 mm in diameter (D) and 0.5 mm in thickness (W) was fabricated locally. Its radius of curvature (R) and height (H) are

15 and 2.2 mm respectively. Depth of the plaque is the difference of its height and thickness and is 1.7 mm. Figure 5.2 presents the schematic diagram of the silver plaque.

EBT3 films.
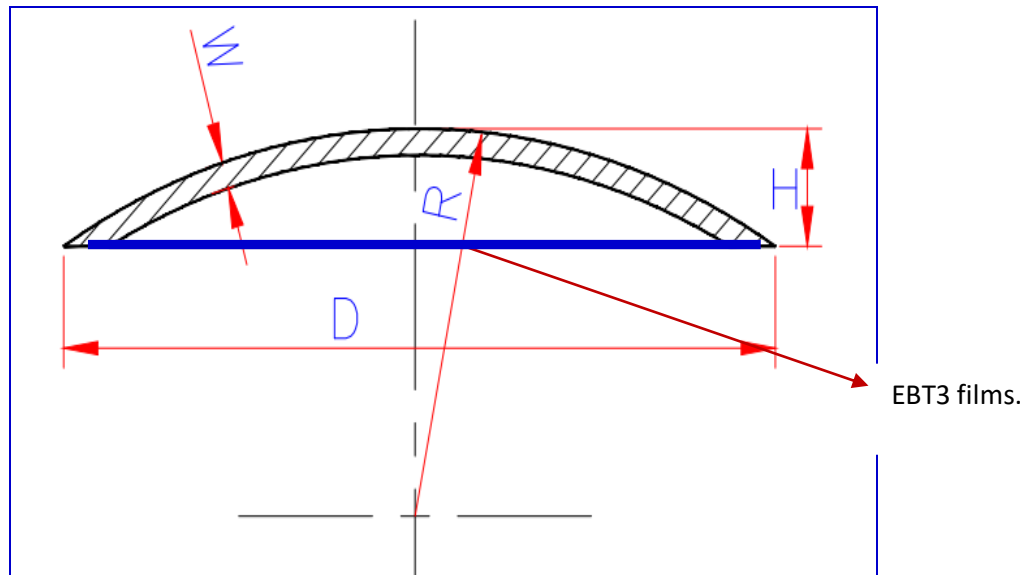
Figure 5.2. The geometry of the 14 mm diameter silver plaque. D is diameter, W is thickness, R is radius of curvature and H is height of plaque. Dimensions are not to scale. The dark blue lines represent films. Films are in contact with plaque as shown in figure.

5.2.2. Energy response of EBT3 Gafchromic film

The structural details of Gafchromic EBT3 film manufactured by Ashland ISP Advanced Materials, NJ, USA were discussed in Section 4.2.3.4 of Chapter 4. The energy response of the EBT3 Gafchromic film has been investigated by various research groups as discussed below. Devic et al (2012) reported a functional form of the dose–response relationship of the EBT, EBT2, and EBT3 radiochromic films and concluded that the relative dosimetry can be conveniently performed in radiochromic film without the need of establishing a calibration curve. Brown et al in 2012 investigated the dose-response

curves of Gafchromic EBT, EBT2 and EBT3 radiochromic films using synchrotron-produced monochromatic x-ray beams of energy 25, 30, and 35 keV and they concluded that EBT3 film has weak energy dependence, for kV x-ray beams. Arjomandy et al (2010) studied the response for EBT2 film over a wide range of photon, electron and proton beam and reported that the EBT2 film is most suitable for clinical dosimetry due to its weak energy dependence. Villarreal-Barajas et al (2014) compared the energy response of the EBT3 films for 70 kVp (HVL = 3.0 mm Al) x-ray with ^{60}Co energy and observed more than 20% under-response for 70 kVp with respect to ^{60}Co energy.

Massillon et al (2012) compared the dose response curves for KV and MV x-ray beams and concluded that the EBT3 film were weakly dependent on the energy of photon beams (6-15 MV) and observed a variation of more than 11% due to energy dependence for 50 kV x-ray. Andres et al (2010) studied the EBT2 film characteristics such as ambient light sensitivity, effect of color channels, post irradiation development, high dose behavior, and reported that the green channel can be used up to 35 Gy and the red channel can be used up to 10 Gy. The EBT3 film is recommended for dose evaluations up to 8 Gy in red channel and from 8 to 40 Gy in the green channel (Villarreal-Barajas et al 2014).

5.2.3. Calibration of EBT3 Gafchromic films at x-ray and ^{60}Co energy

The EBT3 Gafchromic films (Lot # 10251702) were used in this study. The EBT3 films were cut in to strips of 3 cm x 20 cm in size. Each film was placed at the centre of 10×15 cm^2 x-ray field, generated using a lead collimator, one at a time, at 1 m distance from the focal spot. A dosimetry grade YXLON MG325 x-ray machine, having inherent filtration of 3 mm beryllium was used for irradiation. The operating parameters, tube potential and

tube current were 70 kV, 30 mA with added filtration of 2 mm aluminum giving half value layer (HVL) of 2.4 mm of aluminum. The air-kerma rate of the x-ray machine was measured using a Free Air Ionization Chamber, an absolute standard for air-kerma measurement and was found to be 0.115 Gy min^{-1} at 1 m. The films were irradiated to doses of 50, 100, 214 and 510 Gy. Since the EBT3 films were irradiated in air, a value of $\left(\mu_{en}/\rho\right)_{air}^{water}$ = 1.015 was used to convert the air-kerma into absorbed dose to water (Massillon et al 2012). The effective energy of the x-ray beam is 30.5 keV, which is comparable to the mean energy of the ^{125}I OcuProsta seed, 28.37 keV.

A telecobalt unit (Theratron 780-E) available at our research centre was used to calibrate the EBT3 films. ^{60}Co source was considered due to its well-known decay characteristics and stable dose rate (Villarreal-Barajas et al 2014). The output of the telecobalt unit (D$_w$) at 80.5 cm was 1.98 Gy min^{-1}. The size of EBT3 films are 3 cm x 20 cm. The EBT3 films were as kept below a perspex slab of 5 mm thickness to give necessary build up. Films were irradiated at the centre of a perspex phantom at a depth of 5 mm for a 10×10 cm^2 field size. To provide adequate backscatter in this ^{60}Co irradiation, 20 cm perspex slabs were placed below the EBT3 films. The films were irradiated to doses of 50, 100, 214, 510, 946, 1654 and 3000 cGy. These sequence of doses to be delivered to the films were derived from the Film QA Pro software.

5.2.4. Irradiation of films using a single seed in Solid Water^{TM} phantom

Irradiation of EBT3 films were carried out using a single ^{125}I OcuProsta seed of *S$_K$ 2.94 U* (Figure 5.3) in Solid Water^{TM} phantom of size 17.5 cm x 30 cm x 30 cm. The middle

piece of the phantom was a 5 mm Solid Water^{TM} slab, with a groove to hold a single ^{125}I

seed. Additional 8 cm of Solid Water^{TM}slab were placed below the 5 mm slab and 9 cm

above the 5 mm slab to get full scatter condition. EBT3 films of 3 cm x 3 cm size were

placed inside the Solid Water^{TM} phantom at 1, 5, 7, 9 and 10 mm distance from the seed.

Films were irradiated for 20.58 hours. Films were analyzed and dose measured at each

depth was compared with the values calculated using DOSRZnrc user-code.
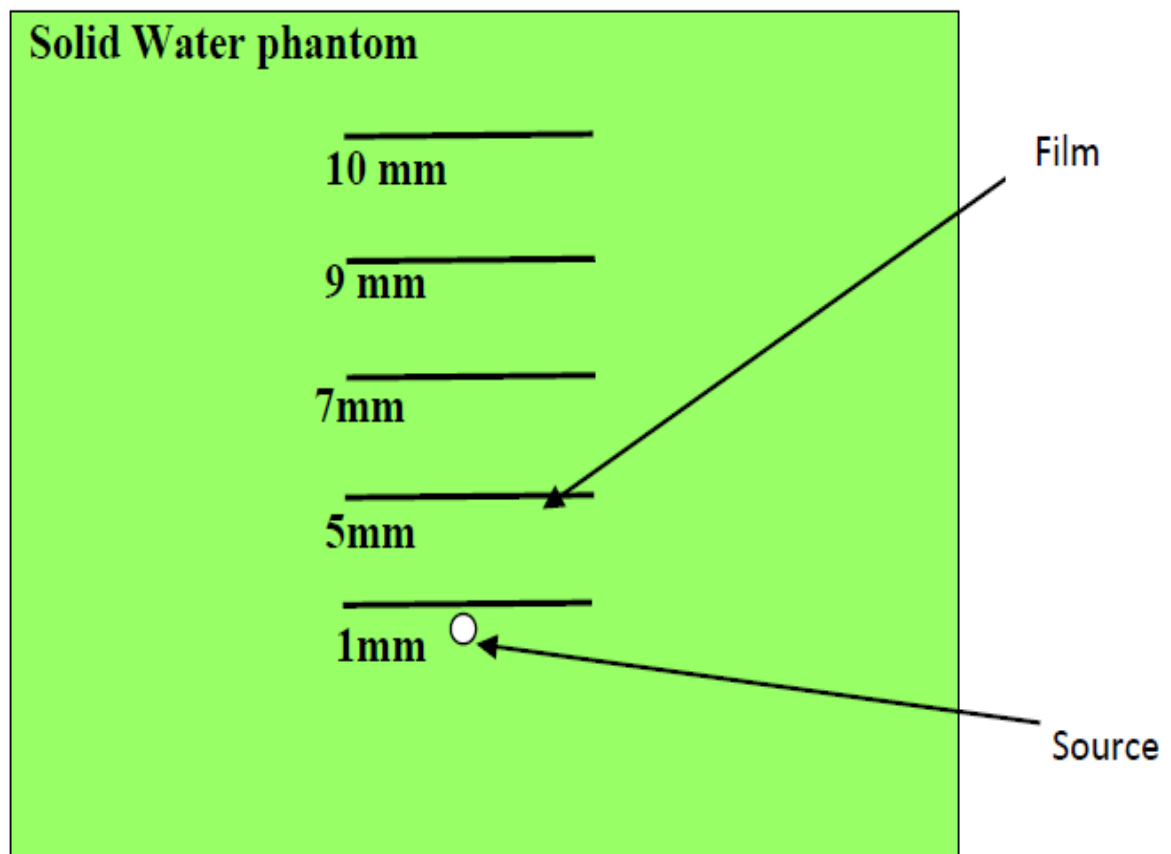
Figure 5.3. Schematic diagram of single ^{125}I OcuProsta seed in Solid Water^{TM} phantom. EBT3 Gafchromic films were placed at 1, 5, 7, 9 and 10 mm distance from the seed of S_K 2.94 U (not to scale).

5.2.5. Monte Carlo calculations

The DOSRZnrc user-code (Rogers et al 2010) was utilized in the dose calculation involving single ^{125}I seed. The ^{125}I seed was simulated at the centre of a cylindrical water phantom (20 cm diameter x 20 cm height) and the absorbed dose was scored in 0.1 mm x 0.1 mm voxel at a distance of 1, 5, 7, 9 and 10 mm from the centre of the source. The Monte Carlo calculation, transport parameters, photon, electron cut-off parameters are described in Section 2.3 of Chapter 2.

5.2.6. Dose measurement for a silver plaque loaded with 13 seeds

EBT3 films were cut into 3 cm × 3 cm square pieces. A film stack of height 1.2 cm was made by keeping 37 such pieces one above the other and placed at the centre of a wax phantom of size 10 cm × 10 cm × 3 cm. As per the COMS design, 14 mm plaque can hold a maximum of 13 seeds (Chiu-Tsao et al 2012). The 13 seeds were embedded in a 14 mm diameter plaque (Figure 5.4) with the help of adhesive glue and kept above the film stack (Figure 5. 5). The film stack was irradiated for a period of 6.067 hours. Air-kerma strength of each seed used in this study was 2.94 U.

5.2.7. Film scanning

The irradiated films were scanned in transmission mode using the EPSON Expression 10000 XL scanner with a resolution of 72 dpi after 24 hours of exposure. Films were analyzed using ImageJ software (NIH, ImageJ software). The data of red channel were used to determine optical density. Films were scanned prior to irradiation to measure the optical density of the background film.

Figure 5.4. A 14 mm diameter silver plaque embedded with 13 ^{125}I OcuProsta sources. S_K of each seed is 2.94 U.

All film pieces were scanned in the same orientation throughout scanning and measurement and hence eliminating the polarization effects (Butson et al 2009, Niroomand-Rad et al 1998 TG55). The films were positioned at the center of the flatbed scanner to avoid off-axis scanner non-uniformity (Menegotti et al 2008).

Figure 5.5. 14 mm diameter silver plaque embedded with 13 ^{125}I OcuProsta seeds, placed over EBT3 Gafchromic film. Films are in the centre of wax phantom. S_K of each seed is 2.94 U.

Change in optical density was calculated by subtracting the optical density of an unexposed film piece from the optical density from exposed film.

$$NOD = OD_{exp} - OD_{unexp} = log\left(\frac{PV_{unexp}}{PV_{exp}}\right) \qquad (5.1)$$

Where PV_{unexp} corresponds to averaged pixel value of the scanned film prior to exposure and PV_{exp} corresponds to average pixel value of the scanned film after irradiation.

The energy response, R is the ratio of the net optical density (NOD) for a given dose of the 70 kV x-ray beam and the NOD for the same dose for ^{60}Co beam.

$$R = \frac{NOD(D_w, 70kV\ X-ray)}{NOD(D_w, Co-60)} \qquad (5.2)$$

5.3. Results and discussion

5.3.1. Film Calibration

Figure 5.6 presents the NOD comparison of EBT3 films irradiated at ^{60}Co and 70 kV x-ray energy as a function dose to water. At 70 kV x-ray energy, the films were irradiated for doses up to 510 cGy because of exposure time limitations of the x-ray tube. The value of R is 0.92 for 50 cGy dose and 0.98 for dose range of 100 - 510 cGy (Table 5.1). The results indicate that the dose response is within 2% for ^{60}Co and 70 kV x-ray energy for dose range of 100 - 510 cGy. The variation up to 8% was observed for dose of 50 cGy. Higher variation at lower doses may be attributed to lower sensitivity of EBT3 films. Brown et al (2012) reported the value of R varies between 0.97 - 0.99 for monochromatic x-rays of 25 - 35 kV. Arjomandy et al in 2010 also reported the energy dependence of EBT2 film is weak, up to 4.5% over a wide range of energies (75 kV - 18 MeV photons). Hence EBT3 films calibrated at ^{60}Co energy with higher dose (more than 50 cGy) is suitable for dosimetry of ^{125}I sources.

5.3.2. Dose measurement for a single seed

The scanned images of irradiated films were analyzed using commercial software (FilmQA Pro Ashland ISP Advanced Materials, NJ, USA) and the dose values were estimated using the calibration curve given in Figure 5.6.
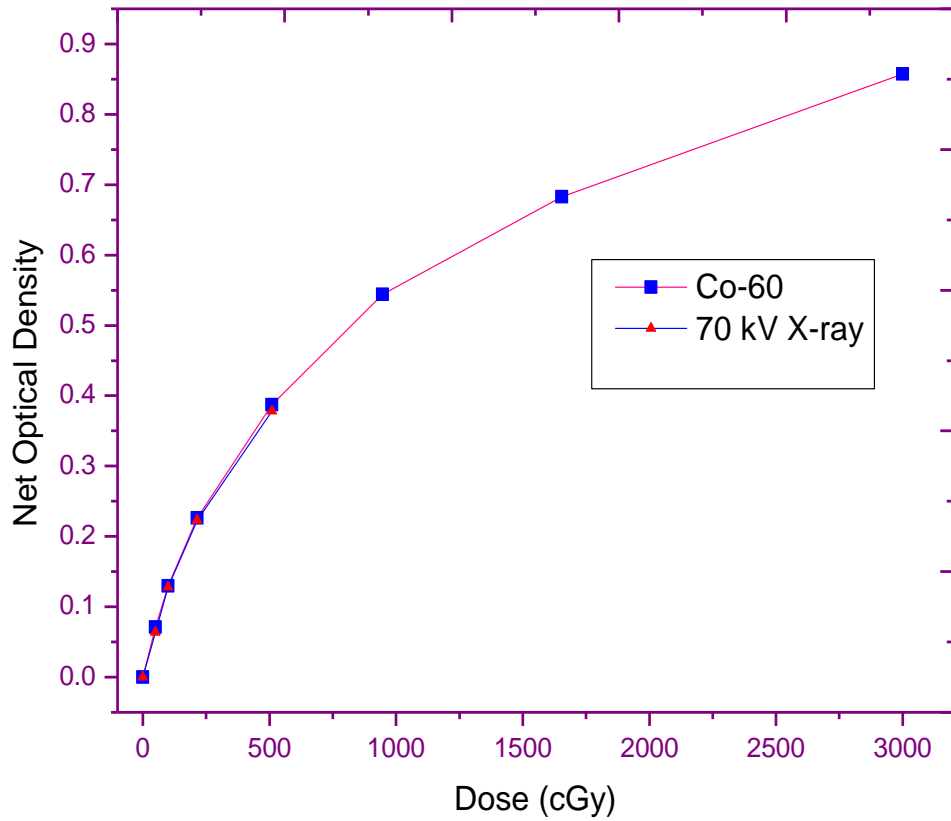
Figure 5.6. Dose response of EBT3 Gafchromic films for ^{60}Co energy and 70 kV x-ray.

Table 5.1. Energy response ratio, R = NOD (70 kV) / NOD (^{60}Co).

Dose (cGy)	R
50	0.92
100	0.98
214	0.98
510	0.98

The dose values at five depths, were compared with DOSRZnrc user-code calculated values for a given exposure time of 20.58 hours (Table 5.2). Agreement between the single seed EBT3 film measurements and DOSRZnrc user-code calculated doses were within 2 - 11%.

Table 5.2. Dose (cGy) for a single ^{125}I seed of S_K 2.94 U measured using EBT3 films in Solid Water phantom compared against DOSRZnrc user-code values.

Depth (mm)	Dose (cGy)		
	EBT3 Gafchromic film	DOSRZnrc user-code	Dose ratio (%)
1	3125	3499	11
5	215	204	5
7	105	103	2
9	63	61	3
10	46	48	4

5.3.3. Dose measurement for plaque loaded with 13 seeds

5.3.3.1. Central axis depth dose

Total S_K used in the 14 mm diameter plaque for the measurement of central axis depth dose was 38.22 U. The EBT3 film stack was exposed for a period of 6.067 hours. The central axis depth dose was measured using EBT3 film and is presented up to a depth of 12 mm in Table 5.3. Films were in contact with the plaque (Figure 5.2) and the depth given in Table 5.3 is the distance from the diameter of the silver plaque. For example, the minimum depth of measurement is 0.16 mm, which is the mid-point of first EBT3 film (water equivalent thickness is 0.32 mm).

Table 5.3. Depth dose for 14 mm diameter silver plaque embedded with 13 seeds (total S_k was 38.22 U) measured using EBT3 film.

Depth (mm)	Dose (cGy)	Depth (mm)	Dose (cGy)
0.16	2027	5.6	474
0.48	1822	5.92	455
0.8	1694	6.56	397
1.12	1479	7.2	338
1.44	1335	7.52	316
1.76	1171	8.16	287
2.08	1035	8.48	269
2.4	958	9.12	233
3.04	836	9.44	218
3.68	773	10.08	201
4	714	11.04	181
4.64	606	11.68	153
4.96	536	12	142

These depth dose data was fitted to a 12th order orthogonal polynomial using three-term recurrence relation to get depth dose at standard depths like 1, 2, 3 mm etc. Table 5.4 presents the coefficients of orthogonal polynomial of order of 12 used for fitting the depth dose data of 14 mm diameter silver eye plaque obtained using EBT3 film. Figure 5.7 presents the central axis depth dose for 14 mm diameter silver plaque was measured using EBT3 film and 12th order orthogonal polynomial fitted to this depth dose data.
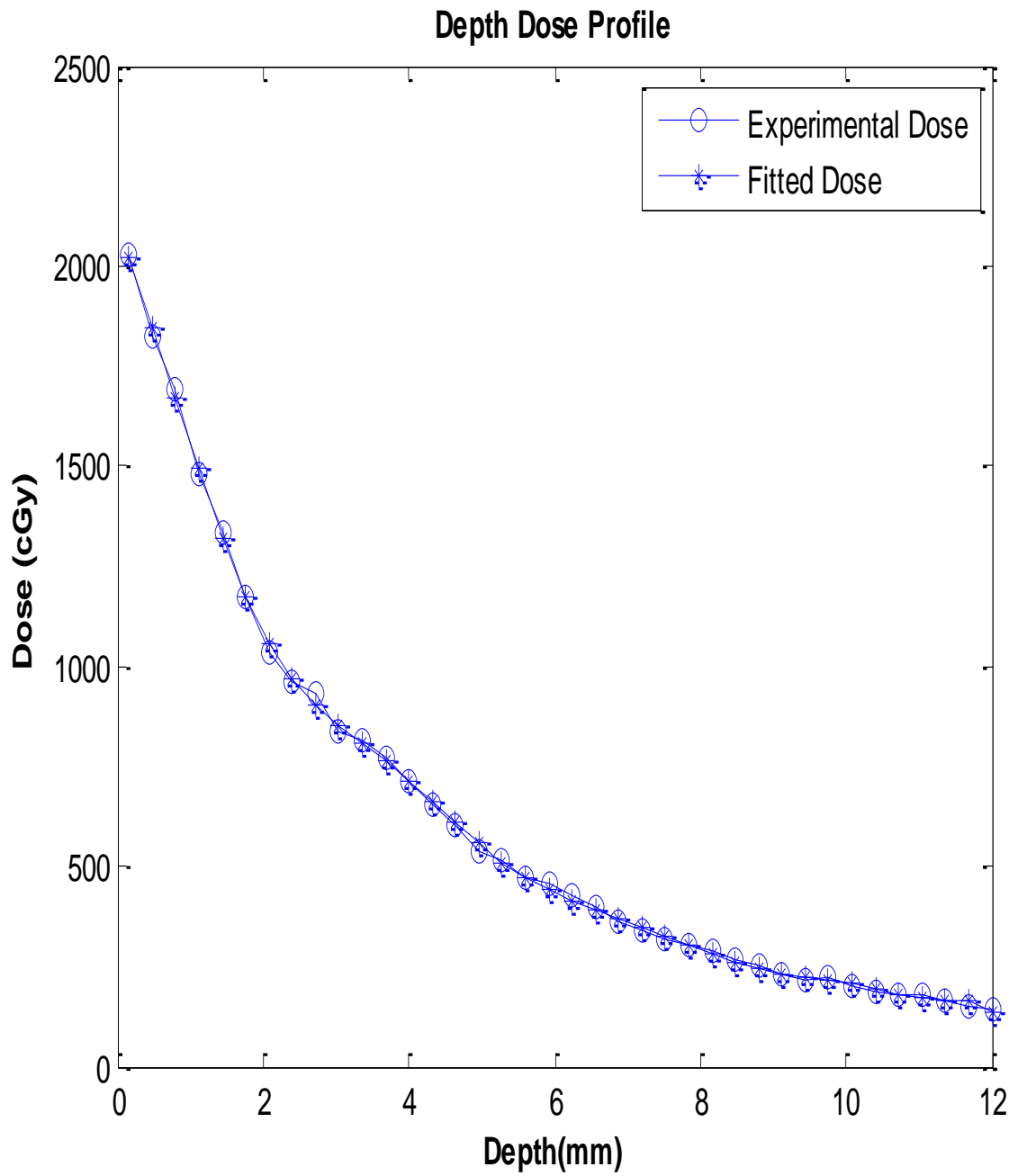
Figure 5.7. The central axis depth dose for 14 mm diameter silver plaque embedded with 13 seeds measured using EBT3 Gafchromic film. The fitted dose is estimated using 12th order orthogonal polynomial fit.

Table 5.4. The coefficients of orthogonal polynomial of order of 12 used
for fitting the depth dose data of 14 mm diameter silver eye plaque.

	B	C	d
1	6.08	0	6.23E+02
2	6.08	12.314	-1.28E+02
3	6.08	9.830	1.76E+01
4	6.08	9.446	2.17E+00
5	6.08	9.284	3.04E-01
6	6.08	9.173	-4.99E-02
7	6.08	9.074	2.69E-04
8	6.08	8.974	2.91E-03
9	6.08	8.867	-1.30E-03
10	6.08	8.750	2.39E-04
11	6.08	8.623	2.94E-05
12	6.08	8.485	-3.39E-05

Table 5.5 presents the dose values at depths of 1 - 12 mm from the surface of the 14 mm
diameter silver plaque. The values were calculated using the coefficients of the 12th order
orthogonal polynomial fit.

Table. 5.5. The dose values at depths of 1 - 12 mm from the surface of the 14 mm diameter silver plaque. The values were calculated using the coefficients of 12th order orthogonal polynomial fit.

Depth (mm)	Dose (cGy)
1	1558.47
2	1081.27
3	857.83
4	713.00
5	550.80
6	433.20
7	363.35
8	292.39
10	212.10
11	179.52
12	142.00

5.3.3.2. Off-axis profiles and isodose lines

Off-axis dose distribution profiles in planes at depths of 4, 5.9 and 7.2 mm from the plaque surface are shown in Figures 5.8, 5.9 and 5.10 respectively. The absolute values of isodose line are given in the respective plots. The isodose distribution at 4 mm depth as shown in Figure 5.8 indicates that, the central area of 5.6, 8.4, 17, 20 and 25 mm diameter are receiving 700, 600, 300, 200 and 100 cGy respectively. Figure 5.9 represents the isodose distribution at a plane which is at 5.9 mm. This shows the coverage of central

area of 5, 14.8, 20 and 25 mm diameter by 500, 300, 200, and 100 cGy respectively. Figure 5.10 represents the isodose distribution at a plane which is at 7.2 mm. This shows the coverage of central area of 4, 11, 18 and 25 mm diameter by 380, 300, 200 and 100 cGy respectively.

From these isodose distributions, it is clear that, as the depth increasing from plaque surface, dose values and the area covered by the same dose are decreasing. For a dose of 300 cGy, the central area covered at planes which are at depths 4, 5.9 and 7.2 mm are 17, 14.8 and 11 mm respectively. Hence it can be concluded that as depth increases, the central area covered by isodose lines decreases gradually.

5.4. Uncertainty calculation

The combined uncertainty in the film measurements for ^{125}I seed source was obtained by summing the quadratures of the uncertainties associated with the individual components. The total uncertainties in film measurements using the calibration curve are due to the following three components: (1) total contribution in the uncertainty due to film was 1.45% which includes (a) 1.10% in film orientation, (b) 0.59% in scanner uniformity (c) 0.01% in film reproducibility (Sorriaux et al 2013) and (d) 0.74% in the uncertainty from the curve fitting (Poder and Corde 2013) used to convert NOD to dose, (2) 0.5% uncertainty in the film calibration using ^{60}Co beam and (3) 10% uncertainty in the activity measurement of ^{125}I seeds.

The total uncertainties obtained in the dose measurement, using error propagation method is about 10%.
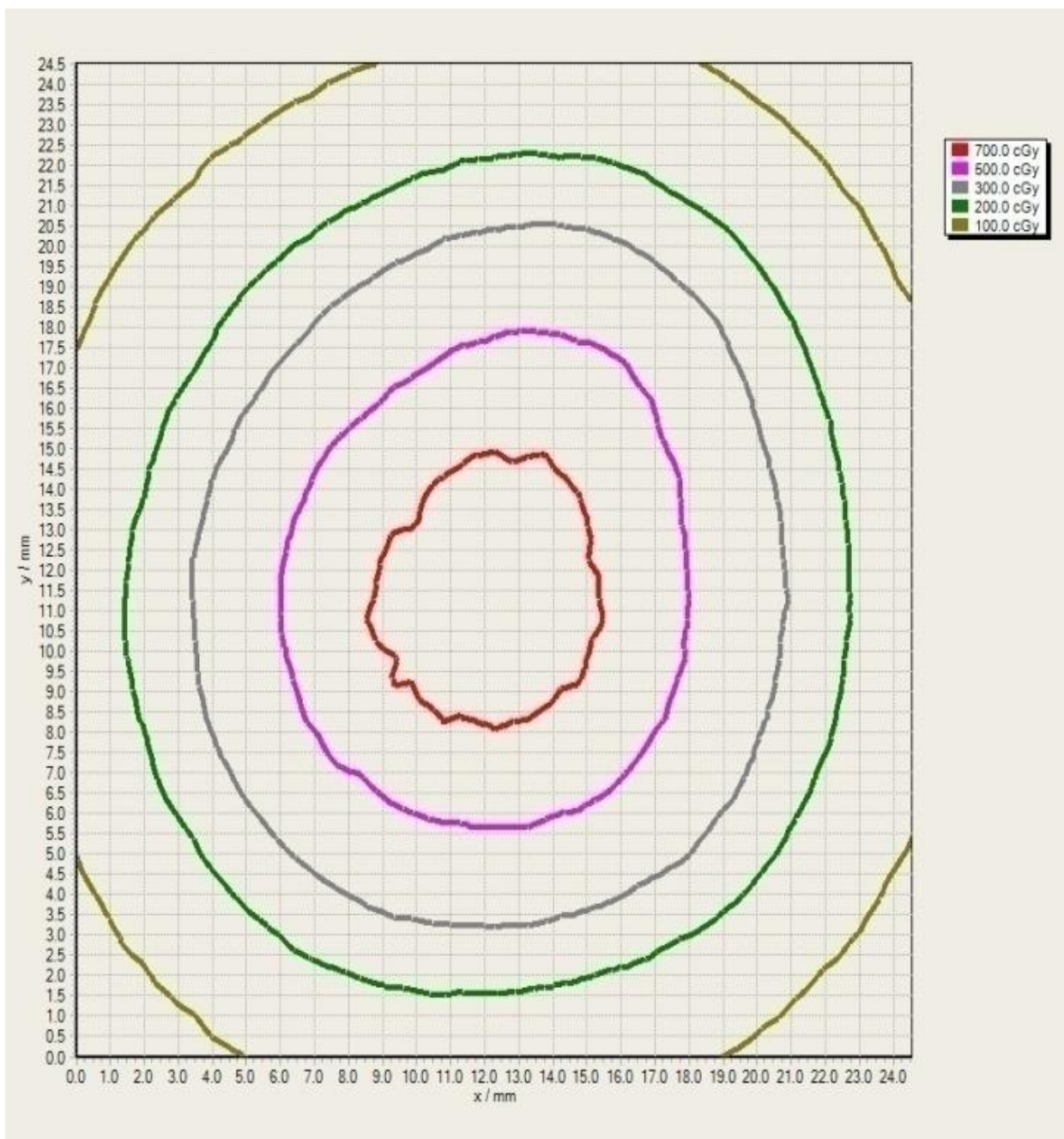
Figure 5.8. The isodose plot for 14 mm diameter silver plaque measured using EBT3 film at 4 mm from the surface of the plaque.
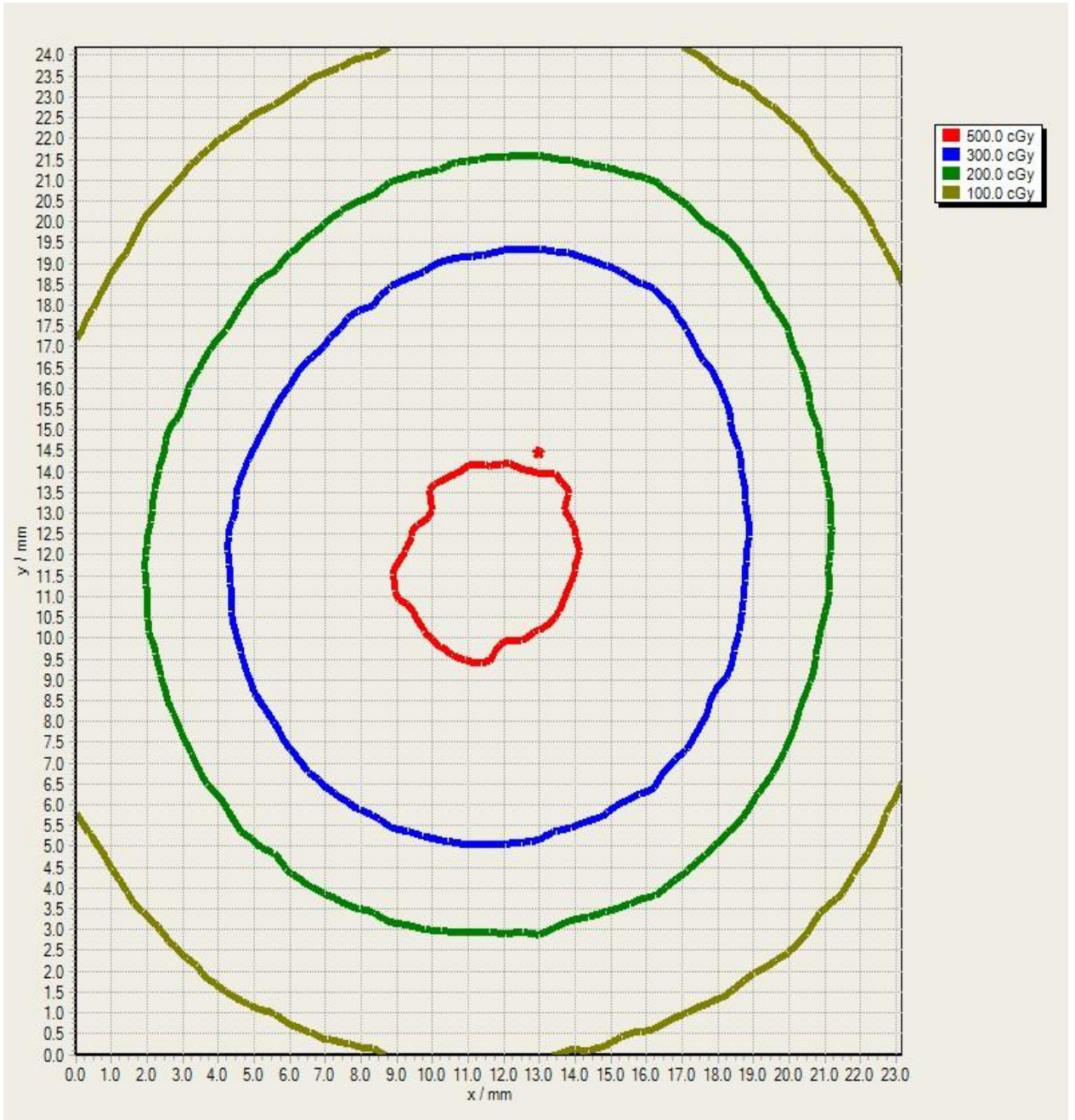
Figure 5.9. The isodose plot for 14 mm diameter silver plaque measured using EBT3 film at 5.9 mm from the surface of the plaque.
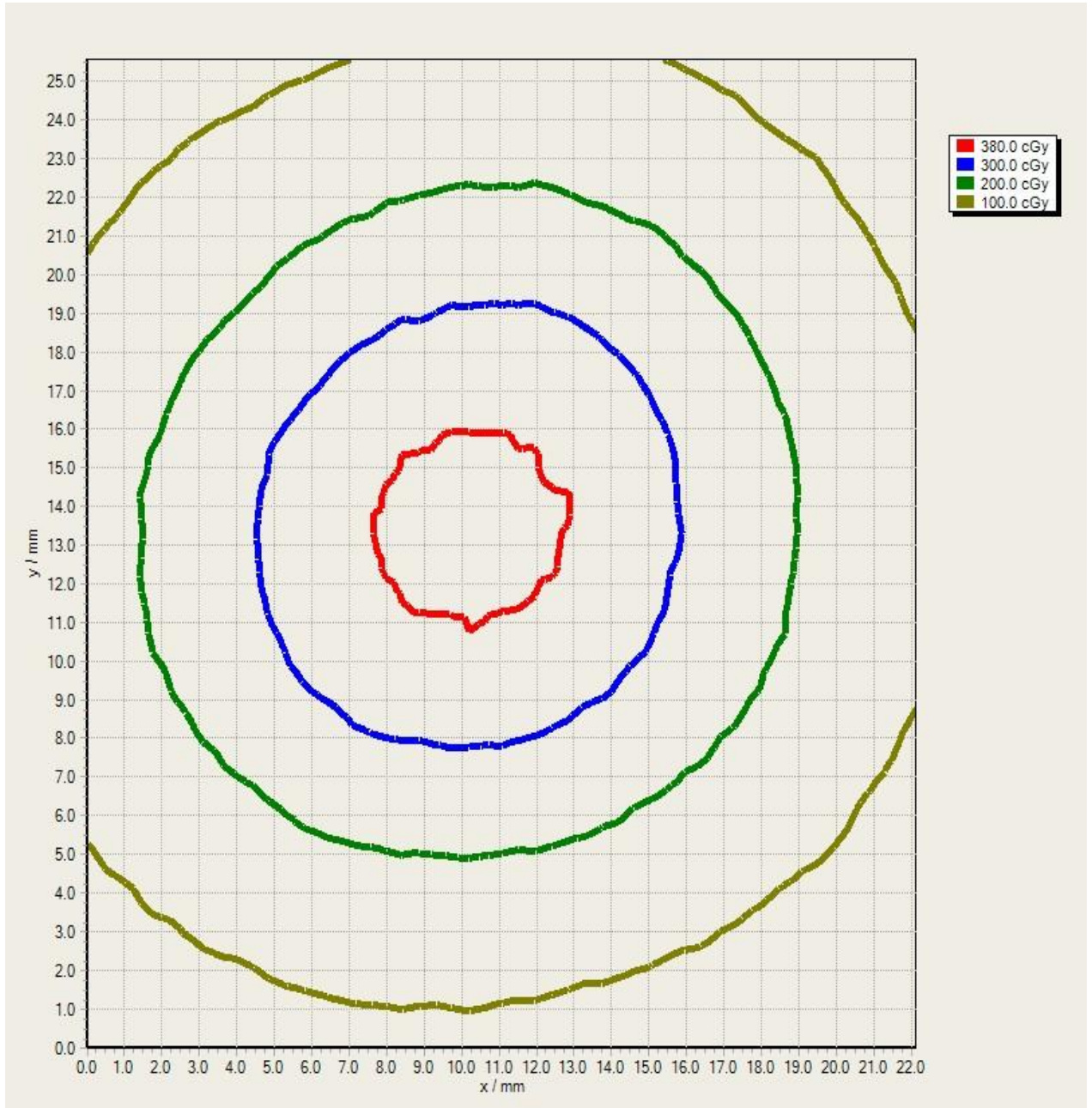
Figure 5.10. The isodose plot for 14 mm diameter silver plaque measured using EBT3 film at 7.2 mm from the surface of the plaque.

5.5. Conclusions

The energy response for the EBT3 Gafchromic film was studied at 70 kV x-ray and ^{60}Co energy. It was observed that the dose response of EBT3 film is within 2% for ^{60}Co and 70 kV x-ray energy for dose range of 100 - 510 cGy. Variations up to 8% were observed for dose of 50 cGy.

This higher variation at lower dose may be attributed to lower sensitivity of EBT3 films. Hence EBT3 films calibrated at ^{60}Co energy with higher dose (more than 50 cGy) is suitable for dosimetry of ^{125}I sources.

Dose measurement for a single ^{125}I seed in Solid Water phantom was carried out using EBT3 films and the values compares well (within 2 - 11%) with the values calculated using EGSnrc Monte Carlo methods.

Central axis depth dose and off-axis profile data were measured using EBT3 films, for a 14 mm diameter silver eye plaque loaded with 13 ^{125}I seeds. The dose profiles are presented. The isodose curve will help to estimate dose to critical structure during planning. The dose rate will be useful for treatment time calculation for a silver eye plaque of similar design.

CHAPTER 6

DOSIMETRY OF ^{125}I AND ^{131}Cs BRACHYTHERAPY SOURCES DUE TO NON-UNIFORM SCATTER CONDITION

6.1. Introduction

The AAPM TG-43 report (Nath et al 1995) and TG-43U1 (Rivard et al 2004) on brachytherapy dose calculations are well accepted by medical physics community. These reports describe the dose calculation methodology for low energy photon sources such as ^{125}I, ^{103}Pd etc. used in brachytherapy. The TG-43 formalism provides the methodology of dose distribution around a single brachytherapy source positioned at the centre of a spherical liquid water phantom. These dosimetry data are generated either by measurements using thermoluminescent dosimeter or Monte Carlo calculations and are strictly valid only for a homogeneous water phantom of the size and shape used in the simulation or measurement.

Brachytherapy treatment planning system utilizes these dose distribution data. The doses are calculated by superposing the pre-calculated dose distributions for single sources in water according to the pattern of the source placement (Beaulieu et al 2012). However, the influence of tissue composition differing from liquid water, interseed attenuation (absorption and scattering of photons by neighboring seeds), and finite patient dimensions are all ignored (Meigooni and Nath 1992b, Chibani and Williamson 2005a). Hence differences in the dose distribution occurs, when these TG-43 dosimetry data is used to plan a patient in brachytherapy.

The photoelectric effect dominates for low energy brachytherapy sources (< 50 keV). For high energy sources, Compton scattering interaction is predominant. The photoelectric interaction strongly depends on atomic number of the material. Due to predominance of the photoelectric process, the energy deposition and differences in mass-energy absorption coefficients between various tissues and water may result in significant dose differences for low energy sources. These dose differences also significantly depend on the medium chosen for radiation transport, during Monte Carlo simulation.

Several research groups published the effect of tissue inhomogeneities present in the treatment volume and their impact on dosimetry (Lee 2014, Rivard et al 2009, Taylor 2006, Thomson et al 2008, Chibani and Williamson 2005b, Carrier et al 2007, Yang and Rivard 2011, Huang et al 1990, Demarco et al 1999, Sutherland et al 2012). The dose differences arise between dose to the medium and dose to water by accounting all inhomogeneities present in the treatment volume.

During planning, dose differences occur because of tissue heterogeneities differing from water, less scatter due to finite patient size and interseed attenuation (Meigooni and Nath 1992b). In order to reduce the dosimetric uncertainties and improve the accuracy of the calculation, especially for low-energy emitters, simulation was carried out examining the effect of brachytherapy source photon interactions in a real life heterogeneous, bounded medium.

Permanent seed-implant using low energy radio-isotopes such as ^{125}I and ^{131}Cs is a well established treatment modality for early-stage prostate cancer and it is comparable to

external-beam radiation therapy and prostatectomy (Stokes et al 1997). Several dosimetry studies are available utilizing the well established EGSnrc and MCNP Monte Carlo codes. However, application of FLUKA Monte Carlo code in this low energy brachytherapy domain is limited.

In this Chapter the FLUKA Monte Carlo code (Ferrari et al 2005) was used to calculate the TG-43 dosimetry parameters for ^{125}I OcuProsta seed and ^{131}Cs Cs-1 Rev-2 seed model (Tailor et al 2008). The dose variation in the prostate due to tissue composition was estimated. The study was also extended to calculate (i) dose distribution in prostate, bladder and rectum using 39 seeds, (ii) interseed attenuation and (iii) the under-dosage due to the lack of scatter environment.

6.2. Materials and methods

6.2.1. Radioactive sources

OcuProsta ^{125}I source developed by BARC for treatment of ocular diseases and prostate cancer was simulated in this study. The schematic diagram along Cartesian co-ordinate system used in the FLUKA Monte Carlo simulation was presented in Figure 6.1 (a). Schematic drawing of the ^{131}Cs Seed CS-1 model was also shown in Figure 6.1 (b). The active part is uniformly distributed with inorganic substrate to which ^{131}Cs is chemically bound and it is surrounding a gold wire (19.3 g cm^{-3}) of 0.25 mm diameter, which serves as a radio-opaque marker. The seed is encapsulated in a titanium capsule (4.54 g cm^{-3}) with argon (0.001784 g cm^{-3}) filled in its inner spaces. Active length of source is 4 mm. ^{131}Cs is suitable for permanent interstitial implants because of its physical characteristics. It is a pure electron capture isotope. ^{131}Cs is produced by neutron capture in ^{130}Ba. ^{131}Cs

decays by electron capture to ^{131}Xe yielding gamma rays (33.6 keV), K$_\alpha$ x-rays (29.5 and 29.8 keV) and K$_\beta$ x-rays (33.6, 44.4 keV) with a mean photon energy of approximately 30.4 keV (Wittman and Fisher 2007). The half-life of ^{131}Cs source is 9.7 days. The short half-life enables production of higher dose rate sources and shortening the dose delivery time.
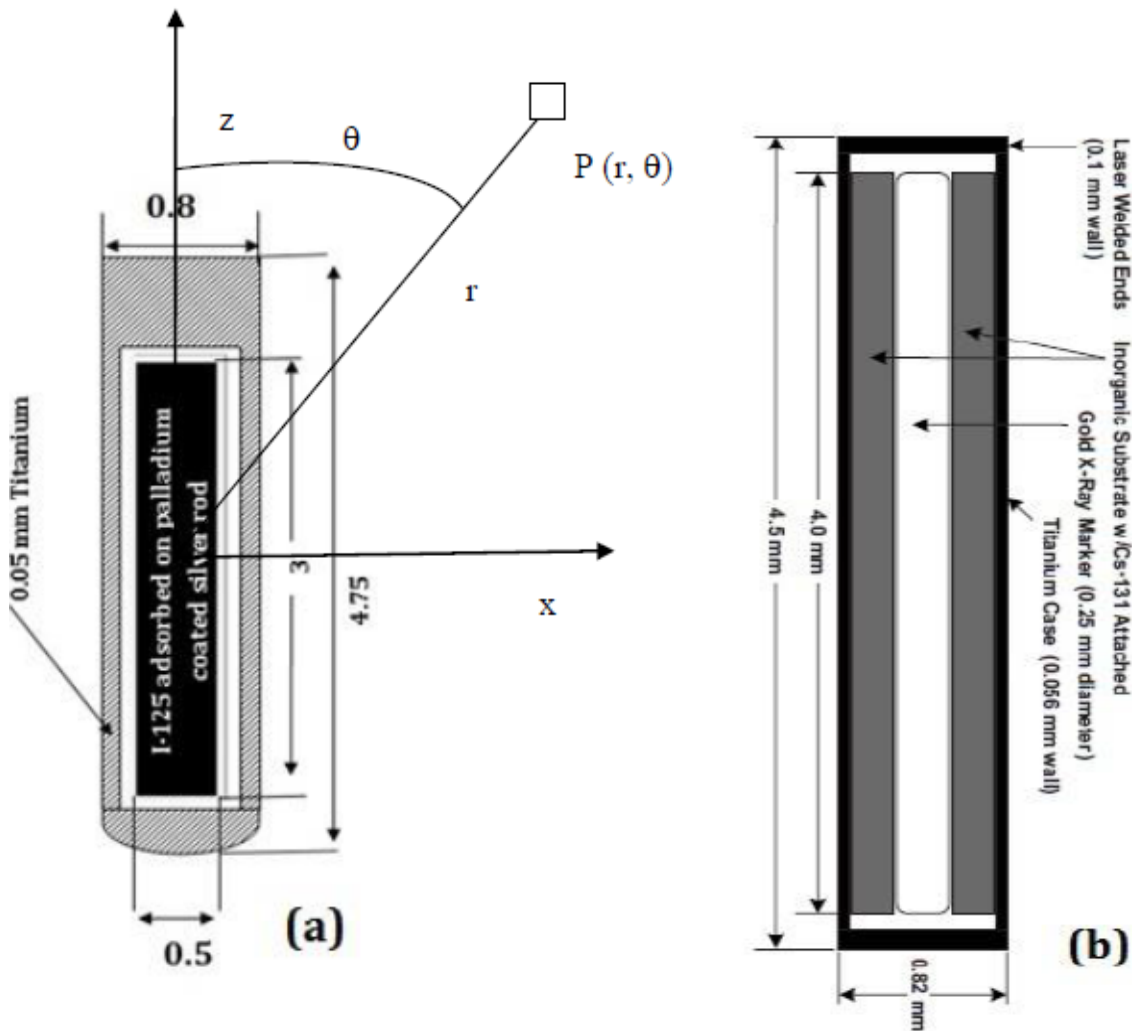
Figure 6.1. Schematic diagram of (a) ^{125}I source (OcuProsta) and (b) ^{131}Cs source (Cs-1 Rev-2 model) (Picture courtesy: Tailor et al 2008) with the cartesian co-ordinate system used in the FLUKA Monte Carlo simulation. Dimensions shown are in millimeters (not to scale). The origin of the co-ordinate system is chosen at the center of the active source.

The dosimetry parameters of ^{131}Cs Cs-1 Rev-2 seed model were already by calculated by Wittman and Fisher (2007), Murphy et al (2004) using MCNP code and measured by Tailor et al (2008) using LiF TLD detector.

6.2.2. Monte Carlo simulations

FLUKA Monte Carlo code version 2011.2c was used in this dosimetry study (Ferrari et al 2005). Anjomrouz et al in 2013 used FLUKA Monte Carlo code for dosimetry of ^{169}Yb source. In the simulation, the source was positioned at the centre of a spherical water phantom of 30 cm diameter and density 0.998 g cm^{-3} and water-kerma was calculated along the transverse axis of the source. As charged particle equilibrium exists at ^{125}I and ^{131}Cs energies, collision kerma was approximated as absorbed dose. EM-CASCA default card was used for all the simulations. Production and transport cut-off energy for both electron and photon were set as 1 keV everywhere. About 1 x 10^8 particles were simulated to achieve relative uncertainty below 1%. Dose at different locations were scored using USRBIN detector and then was scaled with appropriate factor to get dose rate per mCi.

For S_k simulation, the source was placed in a sphere of 5 meter radius filled with air. Production and transport cut-off energy for electron was set as the maximum incident photon energy of the source-spectrum everywhere whereas for photon they were kept 1 keV. Dose was scored at 1 meter using USRBIN detector. Air-kerma per initial photon was then converted to S_k per contained activity of A_c =1 mCi, S_k/A_c (cGy cm^2 h^{-1} mCi^{-1}).

The dosimetric parameters such as S_k, Λ and $g(r)$ for both ^{125}I and [131]Cs sources were generated as per the recommendations given in AAPM TG-43U1 report.

6.2.3. Effect of prostate tissue composition on dose calculation

Three prostate compositions and water were simulated as dose scoring medium in FLUKA code to study the effect of tissue composition on the dose distribution in the prostate brachytherapy using single seed ^{125}I and [131]Cs source. The prostate tissue compositions considered were ICRP prostate tissue, IPT (ICRP 23), average male soft tissue, AMST (ICRU44 1989) and skeletal muscle, SM (Snyder et al 1974). The densities and elemental compositions of prostate tissues were given in Table 6.1 (Hanada et al 2011). Since, shape of prostate was spherical with 3 - 4 cm in diameter, the dose values were estimated for distances 0.1 - 2 cm only for three prostate tissue compositions and compared with dosimetry data computed in water.

Table 6.1. The density and compositions of three prostate tissues and water.

	Weight fraction (%)												Density
	H	C	N	O	Na	P	S	Cl	K	Ca	Zn	Mg	(g cm^{-3})
AMST	10.5	25.6	2.7	60.2	0.1	0.2	0.3	0.2	0.2	-	-	-	1.030
SM	10.2	14.3	3.4	71.0	0.1	0.2	0.3	0.1	0.4	-	-	-	1.050
IPT	9.76	9.11	2.47	78.1	0.21	0.1	-	-	0.2	0.023	0.008	0.019	1.045
Water	11.1	-	-	88.9	-	-	-	-	-	-	-	-	1.000

6.2.4. Dose distribution in prostate implant

In the Monte Carlo simulation, the geometry of prostate, bladder was assumed as spherical and rectum was cylindrical (Figure 6.2(a)), as the shapes of these organs were vary clinically from patient to patient. Prostate was considered as a sphere of radius 1.5 cm and contains prostate tissue of density 1.045 g cm^{-3} (ICRP 23). Bladder was considered as a 5 cm water sphere (inner radius 4.5 cm, wall thickness 0.5 cm). Rectum was considered as a cylinder (length 12 cm, radius 1.5 cm and 2 mm rectal wall). The rectum was considered as soft tissue with density = 1 g cm^{-3}. Rectum was inclined at an angle of 55^0 with X-axis. Origin of the co-ordinate system coincides with the centre of prostate.

Figure 6.2 (a) presents a cross sectional view of prostate along with bladder and rectum. In the simulation, 39 seeds were arranged in three planes. 21 seeds in central XY-plane (Z = 0) and 9 seeds each in the top (Z = 1) and bottom plane (Z = -1) were presented in Figure 6.3 (a) and (b). The longitudinal axis of the seed was simulated along Z-axis. Figure 6.2 (b) is a magnified picture of prostate where only five seeds in the central plane and three seeds each in top and bottom plane are visible.

Inner circle (r = 0.5 cm) contains 9 seeds at an interval of 45^0 including one seed at the centre and outer circle (r = 1 cm) contains 12 seeds at an interval of 30^0. About 5 x 10^7 particles were simulated to achieve relative uncertainty below 0.1%. Simulations were carried out for both ^{125}I and ^{131}Cs sources. Doses at various points in prostate, bladder, bladder wall, rectum and rectum wall were calculated.
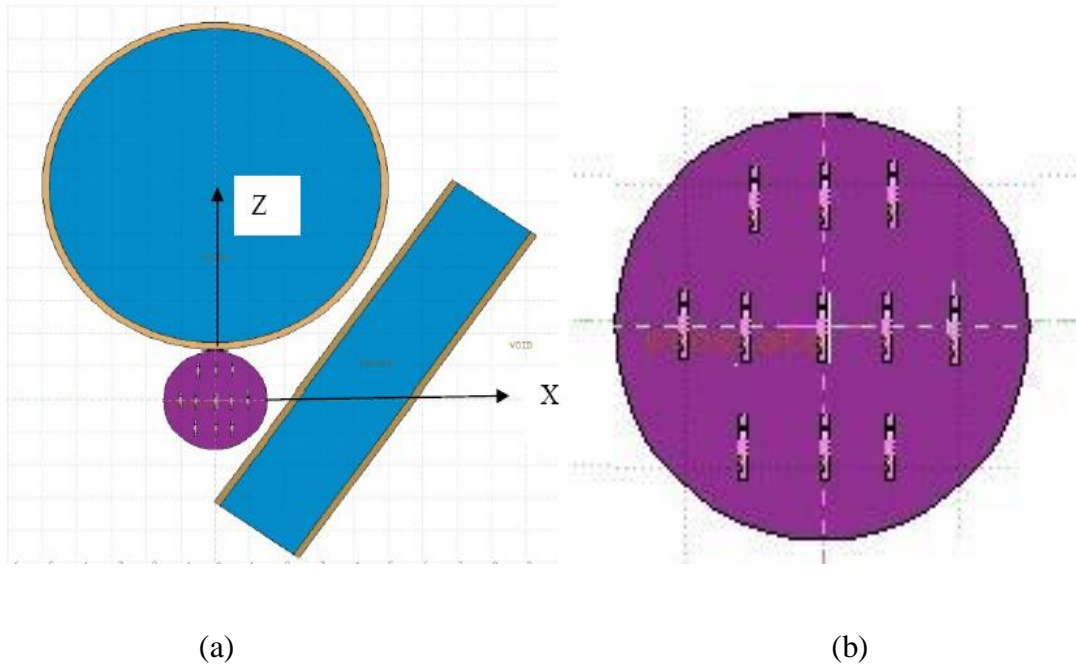
(a)   (b)

Figure 6.2. (a) Cross sectional view of prostate implant in the MC simulation along with bladder and rectum using 39 seeds. Origin of the co-ordinate system coincides with centre of prostate and contains one seed. (b) Magnified picture of prostate. Five seeds in the central plane and three seeds each in top and bottom plane are visible.

(a)   (b)
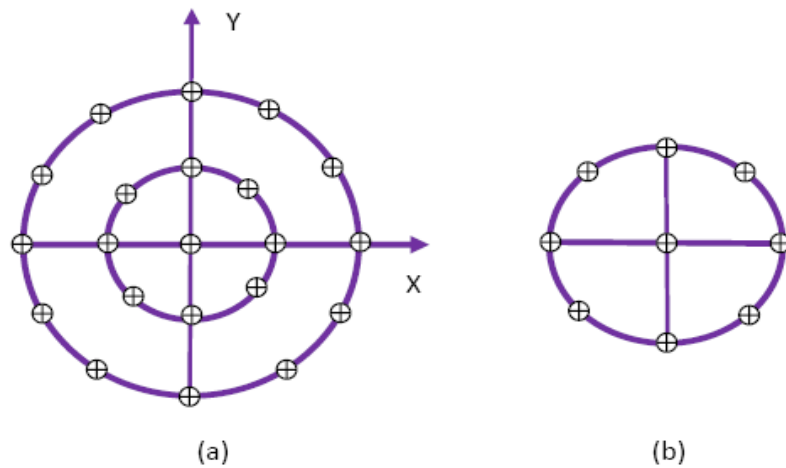
Figure 6.3. Figure represents transverse plane. (a) 21 seeds (9 inner circle + 12 outer circle) in the central XY-plane (Z=0). (b) 9 seeds each were arranged at Z=1 cm and Z=-1 cm. This makes 39 seeds.

6.2.5. Effect of interseed attenuation

Interseed attenuation was first defined by Meigooni et al (1992a) and it is the dose attenuation of one seed by the presence of other seeds, located in the path of its photons, before reaching interaction points in the tissue. It is defined as the ratio of the sum of the doses at a point due to individual seeds in the implant to the dose at that point due to the contributions from all seeds in the implant.

Interseed attenuation was estimated at three points on transverse axis 0.25, 0.75 and 1.25 cm using superposition technique. The distance and angle subtended at by the longitudinal axis of each seed, at these three points were calculated. Interpolation technique using geometry factor $G(r,\theta)$ was used to find dose rate at point from the known dose rate at nearest point. The contributions of individual seeds at these points were summed up to get the dose rate from all seeds. This dose rate was divided by the dose rate obtained in a multi-seed simulation to give the value of interseed attenuation. Interseed attenuation was calculated for both ^{125}I and ^{131}Cs sources.

6.2.6. Uniform scatter and non-uniform scatter condition

Brachytherapy treatment planning system calculates dose distribution in an unbounded phantom or in a full scatter medium, surrounding the source (Raina et al 2005). In some treatment situations like IORT treatment, the source is placed near to the skin. This is a non-uniform scatter condition and the medium is not getting adequate amount of scatter due to presence of less scattering medium. This is caused by a lack of backscattered photons at the border of the phantom.

In this study, the dose differences between uniform scatter and non-uniform scatter condition, due to lack of backscattering photon were estimated. Figure 6.4 (a) presents the uniform scatter condition, where a single seed was simulated at the centre of the water phantom of radius 15 cm. Figure 6.4 (b) presents the non-uniform scatter condition, where the same source was placed at distances r = 0.5, 1, 1.5 and 2 cm from the surface of the water phantom The ratio between dose values in both cases will give the effect of scatter contribution. The simulations were carried out for both ^{125}I and ^{131}Cs sources.
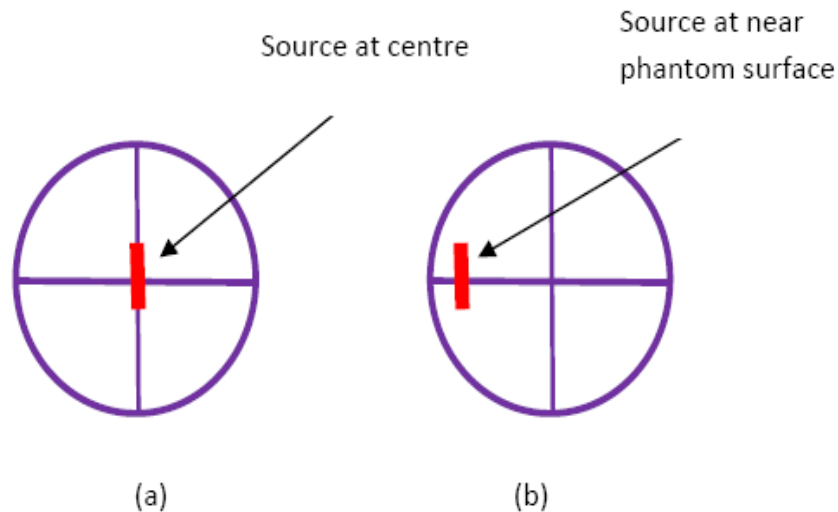
Figure 6.4. (a) Uniform scatter condition and (b) Non-uniform scatter condition.

6.3. Results and discussion

6.3.1. TG-43 dosimetry data

6.3.1.1. ^{125}I OcuProsta source

The FLUKA Monte Carlo calculated dose rate at 1 cm is 0.776 cGy h^{-1} mCi^{-1}.The values of S_k and Λ for ^{125}I OcuProsta seed calculated using FLUKA Monte Carlo code were

presented in Table 6.2. The Table also presents the values of S_k and Λ for source models of same active length and the values are in good agreement (within 2 - 3%) with each other. The uncertainties shown were only statistical and do not include uncertainty in the cross-section and source geometry.

The value of S_k excludes the contribution of low energy ($\sim$ 5 keV) titanium K-x-rays (Kubo 1985, Williamson 1988). These x-rays are clinically insignificant as they are largely absorbed by tissue or water within 1 mm of the source (the mean free path of 5-keV photons in water is 0.23 mm). They can affect S_k measurement and change the value of Λ of the source and should be excluded from the measurement. The contribution of Ti K x-rays to S_k was about 18% (Sahoo and Selvam 2009) which agrees with the value of 22% reported Meinegra et al (1998) for the 6702 source model. Taylor and Rogers (2008) presented the TG-43 database for low-energy photon-emitting brachytherapy sources using the BrachyDose code (Yegin et al 2006). The calculated values of Λ of OcuProsta seed agree within 3 - 4% with measured values (Sharma et al 2005), computed values (Sahoo and Selvam 2009) and with 6711 seed model (Taylor and Rogers 2008, Heintz et al 2001, Hanada et al 2011).

Table 6.3 presents the values of $g_L(r)$ calculated for distances r = 0.1 - 7 cm for OcuProsta ^{125}I source along with the values of 6711 and Echoseed 6733 models. The values of $g_L(r)$ for three sources models agree (within 2 - 3%) with each other.

Table 6.2. The values of S_k and Λ for three ^{125}I sources of same active length (OcuProsta seed, 6711 and Echoseed 6733 model). The values of 6711 Oncura model (active length 2.8 mm was included for comparison).

^{125}I seed models	S_K (U mCi^{-1})	Λ(cGy h^{-1} U^{-1})
OcuProsta	$0.801^{a} \pm 0.005$	$0.969^{a} \pm 0.009$
(BARC)	$0.800^{b} \pm 0.001$	$0.955^{b} \pm 0.007$
AL=3 mm		$0.95^{c} \pm 0.065$
		$0.972^{d} \pm 0.005$
6711 Oncoseed (Amersham)		0.980 (Heintz et al 2001)
		0.964 (Hanada et al 2011)
AL=3 mm		0.965 (Rivard et al TG43U1 2004)
6711 Oncura model (GE Healthcare)	$0.744^{b} \pm 0.001$	$0.931^{b} \pm 0.004$
	$0.763^{e} \pm 0.010$	$0.971^{c} \pm 0.061$
(Dolan et al 2006)		$0.942^{e} \pm 0.018$
AL=2.8 mm		$0.942^{f} \pm 0.003$
		0.956 ± 0.009 (Wittman & Fisher 2007)
EchoSeed	$0.778^{b} \pm 0.001$	$0.972^{b} \pm 0.017$
Model 6733		$0.947^{f} \pm 0.003$
(Amersham)		$0.990^{c} \pm 0.08$ (Meigooni et al 2002)
(Sowards and Meigooni 2002)		$0.970^{g} \pm 0.03$
AL=3 mm		

[a]Calculated using FLUKA Monte Carlo Code (present study)

[b]Calculated using DOSRZnrc user-code (Sahoo and Selvam 2009)

[c]Measurement using TLD detectors (Sharma et al 2005)

[d]Based on MCNP 3.1 code

[e]Based on DLC-146 updated photon cross-section data library

[f]Taylor & Rogers (2008)

[g]Based on DLC-99 photon cross-section data library using PTRAN code

Table 6.3. The Monte Carlo calculated $g_L(r)$ values of OcuProsta ^{125}I source compared with 6711 (GE Healthcare) and Echoseed 6733 source models.

r (cm)	OcuProsta	[a]6711 GE Healthcare	[b]EchoSeed 6733
0.1	1.106	1.081	1.095
0.2	1.116	1.109	1.110
0.3	1.106	1.106	1.103
0.4	1.094	1.096	1.091
0.5	1.08	1.083	1.078
0.6	1.065	1.067	1.063
0.7	1.050	1.051	1.048
0.8	1.034	1.035	1.033
0.9	1.015	1.019	1.015
1	1	1.000	1.000
1.5	0.903	0.906	0.908
2	0.809	0.804	0.812
2.5	0.714	0.712	0.722
3	0.629	0.624	0.634
3.5	0.549	0.544	0.552
4	0.476	0.473	0.481
4.5	0.416	0.409	0.418
5	0.359	0.353	0.362
6	0.265	0.260	0.269
7	0.197	0.192	0.200

[a]Sahoo and Selvam 2009, [b]Sowards and Meigooni 2002

6.3.1.2. ^{131}Cs radioactive source

Monte Carlo calculated dose rate at 1 cm and S_K were found to be 0.423 cGy h^{-1} mCi^{-1} and 0.398 U mCi^{-1} respectively for ^{131}Cs Cs1 Rev2 source. The value of Λ was 1.063 cGy h^{-1} U^{-1} which compares well (within 2%, except the value calculated by Murphy et al 2004) with the values published in literature (Table 6.4).

Table 6.4.The values of Λ for ^{131}Cs Cs1 Rev2 source model.

Investigator	Λ (cGy h^{-1} U^{-1})
This study	1.063 ± 0.006
[a]Murphy et al 2004 (MCNP 4C)	0.915 ± 0.020
Wittman & Fisher 2007 (mcnp5)	1.042 ± 0.017
Chen et al 2005 (gamma spectroscopy)	1.066 ± 0.064
Chen et al 2005 (TLD dosimetry in solid water)	1.058 ± 0.106
Rivard 2007 (mcnp5)	1.046 ± 0.019

[a]Used an earlier design of this source.

The Monte Carlo code calculated values of $g_L(r)$ for ^{131}Cs seed computed in water were presented in Table 6.5 along with the data reported by Murphy et al 2004, Tailor et al 2008 and Rivard (2007) for comparison. The values of $g_L(r)$ calculated by FLUKA and MCNP5 agrees well within 3% with each other. Differences up to 15% were observed when compared with TLD-based measurement values. The Monte Carlo code calculated

values of $g_L(r)$ for ^{125}I and ^{131}Cs source models were presented in Figure 6.5 for comparison.

6.3.2. Effect of tissue composition

Dose distribution was calculated in water and three different types of prostate tissue compositions for ^{125}I and ^{131}Cs sources for distances $0.1 - 2$ cm. This simulation involved single seed. Differences up to 4% for ^{125}I source and 3% for ^{131}Cs source were observed up to 2 cm from these sources. The values of Λ (cGy h^{-1} U^{-1}) for three prostate tissue compositions were given in Table 6.6.

Table 6.5. The line-source based $g_L(r)$ values for ^{131}Cs Cs1 Rev2 source calculated with FLUKA Monte Carlo code in water and compared with the data reported by Murphy et al (2004), Tailor et al (2008) and Rivard (2007).

	FLUKA	MCNP5	MCNP4C, water	SW, TLD	TLD
r(cm)	This study	Rivard	Murphy et al	Murphy et al	Tailor et al
0.05	1.080	1.051			
0.075	0.964	0.965			
0.1	0.958	0.96			
0.25	0.988	0.989			
0.5	1.004	1.006	1.003	1.023	0.998
0.75	1.007	1.009			1.009
1.0	1.000	1.000	1.000	1.000	1.000
1.5	0.959	0.962			0.952
2	0.908	0.908	0.923	0.864	0.909

2.5	0.852	0.845			0.845
3	0.777	0.777	0.806	0.736	0.780
4	0.643	0.642	0.679	0.586	0.645
5	0.520	0.518	0.558	0.462	0.515
6	0.408	0.411	0.454	0.361	0.42
7	0.321	0.323	0.361	0.274	0.344
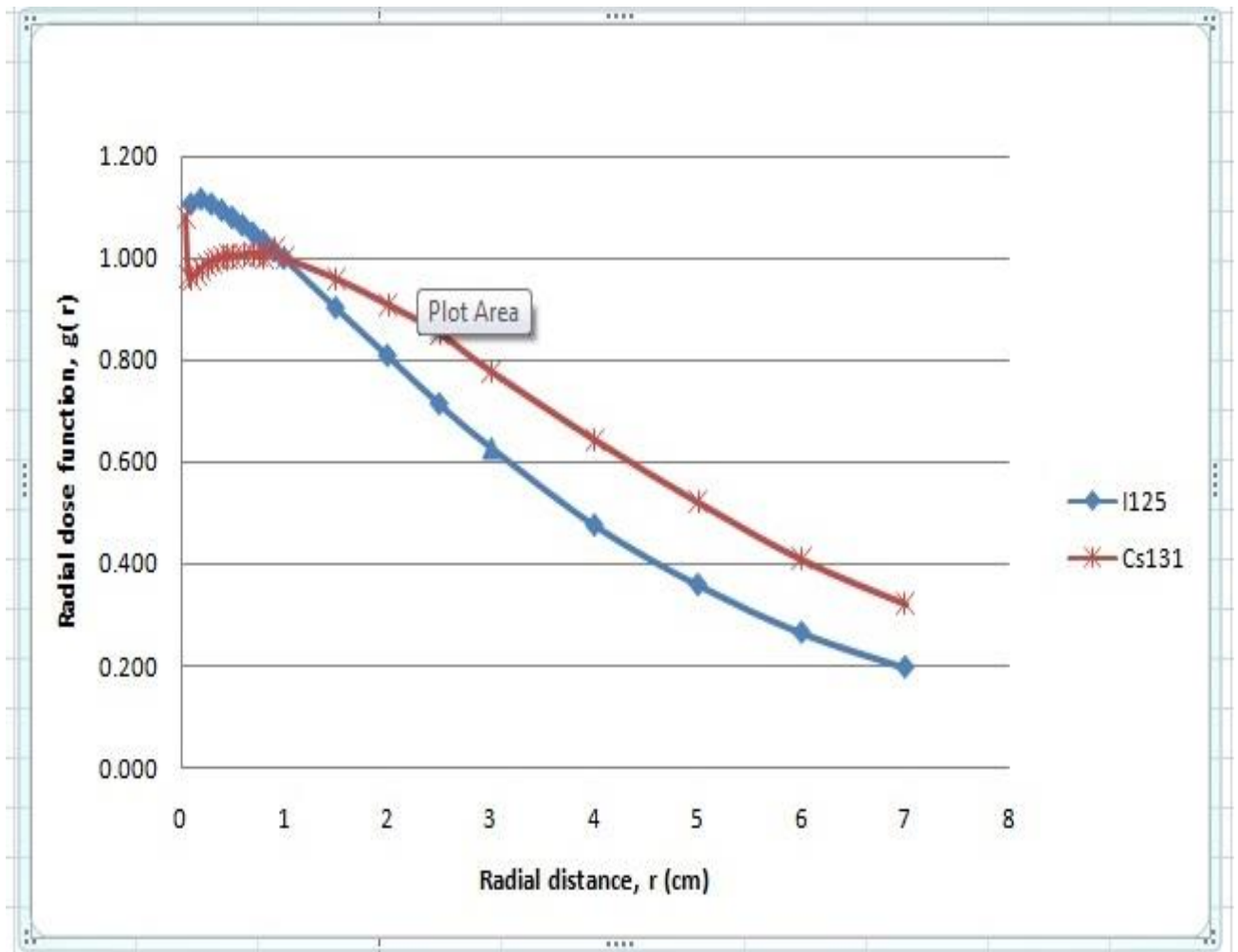
Figure 6.5.The Monte Carlo code calculated values of $g_L(r)$ for ^{125}I OcuProsta and ^{131}Cs Cs1 Rev2 sources.

Table 6.6. The values of Λ (cGy h⁻¹U⁻¹) in water and three prostate tissue compositions calculated for ^{125}I OcuProsta and ^{131}Cs Cs1 Rev2 sources.

	^{125}I OcuProsta source	^{131}Cs Cs1 Rev2 source
Water	0.969 ± 0.009	1.063 ± 0.006
AMST	0.988 ± 0.007	1.078 ± 0.008
SM	0.956 ± 0.008	1.054 ± 0.009
IPT	0.963 ± 0.005	1.058 ± 0.006

6.3.3. Dose to organs and interseed attenuation

The dose rate at selected points in prostate (X = 0.25, 0.75, 1.25 cm), bladder (Z = 1.85, 2.3 cm), rectum and rectum wall were presented in Table 6.7. These dose scoring points were selected since they are near to implanted sources. The dose values are due to thirty nine sources of 1 mCi activity used in the Monte Carlo simulation.

Table 6.7. Dose rate (mGy h⁻¹) in prostate, bladder, rectum and rectum wall due to 39 sources of 1 mCi activity each.

	^{125}I OcuProsta source	^{131}Cs Cs1 Rev2 source
Prostate (X = 0.25, 0.75, 1.25 cm)	60, 49, 24	31, 25, 13
Bladder (Z = 1.85, 2.3 cm)	7.5, 3.5	5.4, 2.7
[a]Rectum	1.8 - 4.2	1.3 - 2.8
[a]Rectum wall	5.6 - 7.0	3.3 - 4.5

[a]doses were scored at five positions on the rectum wall and rectum near to the sources

Table 6.8 presents the values of interseed attenuation in the prostate at 0.25, 0.5 and 1.25 cm due to 39 sources of 1 mCi activity each. The interseed attenuation was found to be about 6 - 9% for points inside the implant volume (r = 0.25, 0.75 cm) for both these sources, but was about 16% for r = 1.25 cm.

Table 6.8. Interseed attenuation in the prostate due to 39 sources of 1 mCi activity each.

	^{125}I OcuProsta source	^{131}Cs Cs1 Rev2 source
0.25 cm	1.06	1.09
0.75 cm	1.08	1.07
1.25 cm	1.16	1.15

Similar interseed attenuation values 6 - 12% were also reported by Meigooni et al (1992a) for two-plane implants of ^{125}I sources in a solid water phantom. Mobit and Badragan (2004) also reported about 10% interseed attenuation in an implant using 27 ^{125}I sources.

Carrier et al (2006) studied the dose differences between full Monte Carlo and superposition Monte Carlo in a prostate implant and showed interseed attenuation causes a drop of more than 6% in the dose to 90% volume (D_{90}). The interseed effect is dependent many parameters such as seed composition, configuration, seed density i.e. no. of seeds per unit implant volume, orientation and seed-to-seed distances.

6.3.4. Uniform scatter and non-uniform scatter

The dose values at different distances were estimated in uniform scatter (unbound) scatter condition by keeping the source at centre of the water phantom of 30 cm diameter. Similarly, the dose values at different distances were estimated, by keeping the source at 0.5, 1, 1.5 and 2 cm from the surface of the water phantom. This is a case of non-uniform (bound) condition. Separate simulations were carried out for ^{125}I and ^{131}Cs sources. Dose variations up to 10% and 8% were observed for ^{125}I and ^{131}Cs sources respectively.

6.4. Conclusions

The FLUKA Monte Carlo code was used to calculate the AAPM TG-43 dosimetry parameters for ^{125}I OcuProsta and ^{131}Cs Cs-1 Rev-2 sources. The dosimetry parameters were comparable (within 2 - 3%) with the published studies of similar source models. The dose distribution in the prostate due different tissue composition (inhomogeneous) and water (homogeneous), involving single seed was estimated. Variations in the dose values up to 4% and 3% were observed up to 2 cm from ^{125}I and ^{131}Cs sources respectively.

A comparable prostate implant was simulated using 39 seeds in 3 planes and dose distribution in prostate, bladder and rectum were estimated. Interseed attenuation in the prostate was estimated using the superposition approach using the result of a single seed and Monte Carlo simulation using all seeds. Interseed attenuation was found to be about 6 - 9% at points lying inside the implant volume and about 16% at points lying in the prostate boundary. These values were in good agreement with the values reported by Meigooni et al (1992a), Mobit and Badragan (2004) and Carrier et al (2006).

The under-dosage due to the lack of scatter environment was estimated by simulating the source in full scatter condition and non-uniform scatter condition. Variations up to 10% and 8% in dose values were observed for ^{125}I and ^{131}Cs sources respectively.

The effect of interseed attenuation and tissue composition has a significant contribution in the brachytherapy dose parameters specifically at low energy. Since, the TPS utilizes TG-43 data calculated in homogeneous medium (water), dose is overestimated by few percent than the actual dose delivered during treatment The actual dose difference between the TG-43 formalism and the model based Monte Carlo simulation using patient heterogeneity varies from case to case. The dosimetry accuracy is highly dependent on scatter conditions and photoelectric effect cross-sections relative to water, which is dominant mode of interaction. The recent AAPM Task Group 186 report (TG-186) by Beaulieua et al (2012) provides necessary guidance for accurate dose calculations in brachytherapy using model-based dose calculation algorithms (MBDCA).

THE RESPONSE OF WELL CHAMBER TO PRESSURE VARIATIONS AT HIGH ALTITUDES FOR ^{131}Cs AND ^{169}Yb SOURCES USING MONTE CARLO SIMULATION TECHNIQUES

7.1. Introduction

Application of low energy brachytherapy sources such as ^{125}I and ^{131}Cs has increased significantly for the treatment of ocular cancers and early-stage prostate cancer as permanent implant due to better treatment result (Murphy et al 2004, Prestidge et al 2005, Ravi et al 2011, Yan et al 2010, Rivard et al 2008). Air-kerma strength, S_K of these sources is an important dosimetry parameter, to be determined accurately. The AAPM Task Group 40 and 56 report states that the manufacturer stated source strength should be independently verified before its patient use (Kutcher et al 1994, Nath et al 1997). Well-type ionization chambers traceable to national standards laboratory are routinely used to measure S_K of brachytherapy sources at hospitals. The advantages of using the well chamber are (a) having a large volume, (b) reproducible geometry (c) nearly 4π geometry when the source is at the position of maximum response (Goetsch et al 1991a). S_K is the internationally recommended quantities for the specification of brachytherapy source strength (Nath et al 1995, Rivard et al 2004).

7.2. Effect of altitudes on air pressure

Usually, these well-type ionization chambers have a small hole (vent) to communicate with the atmosphere. The vented chamber causes the pressure inside the well chamber to

equilibrate to the pressure of the room. The air pressure, *P* is directly proportional to air density, ρ at a constant temperature, *T*. Since, *P* decreases with altitude above the earth's surface and there will be less air at high altitude compared to the amount of air at sea level.

P falls exponentially with height, *h* (m) above sea level and is given by the law of atmospheres or Barometric formula (Bohm et al 2005)

$$P = P_0 \, e^{\frac{-Mgh}{R(T+273.15)}} \qquad\qquad (7.1)$$

Where P_0 is standard pressure (1013.2 mbar) at *h* = 0, *M* is molecular mass (29 g mol^{-1}) of air, *g* is the acceleration due to gravity (9.8 m s^{-2}), *R* is the universal gas constant (8.314 J mol^{-1} ^{0}K^{-1}), and *T* is temperature in ^{0}C. For example, the ρ at Shimla (an Indian city) which is situated *h* = 2276 m above sea level is 0.94 kg m^{-3}, which is about 78% of standard air density, ρ_{std} of 1.197 kg m^{-3}.

Therefore, during routine measurements, a temperature and pressure correction factor, K_{TP} is applied to account for the change of ρ in chamber volume due to change in *P*. The K_{TP} *factor* is given by following expression.

$$K_{TP} = \frac{(T+273.15)\,P_0}{(T_0+273.05)\,P} \qquad\qquad (7.2)$$

Where P_0 is usually taken as 1013.25 mbar and T_0 as 22°C hereafter referred to as the standard reference condition.

The EGSnrc Monte Carlo code is of golden standard code (Kawrakow et al 2013) and it is widely used in medical physics and dosimetry applications. Bohm et al (2005 and 2007)

studied the response of the well chamber at high altitudes is using Monte Carlo calculations and measurements and reported 10 - 20% over-response at high altitudes for low photon energies (20 - 40 keV). Griffin et al (2005) designed a pressure vessel for range of pressure corresponding to height 2590 m above sea level to 610 m below sea level. They measured this over-response for three models of air-communicating well chambers for low-energy photon sources at high altitudes and proposed an additional correction factor. Russa and Rogers (2006 and 2007) investigated the validity of the K_{TP} correction factor for kilovoltage X- rays for different ion chambers using the EGSnrc Monte Carlo code and measurements. They also reported that the standard K_{TP} correction factor breaks down at kV energies.

In summary, the EGSnrc Monte Carlo code accurately estimates the response of ionization chamber at low photon energies (Bohm et al 2005 and 2007) and kilo-voltage X- rays (Russa and Rogers 2006 and 2007). In this Chapter, a well chamber was simulated using the CAVRZnrc user-code (Rogers et al 2010) of the EGSnrc code system (Kawrakow et al 2013). The K_{TP} corrected normalized response of the well chamber at high altitudes was calculated using above user-code. In order to establish the suitability of FLUKA Monte Carlo code at low photon energies, a well-type ionization chamber was simulated in this study. The K_{TP} corrected normalized response was estimated and compared with the value obtained using CAVRZnrc user-code.

The ^{131}Cs source model (Cs-1 Rev-2 model) used in permanent implant (Tailor et al 2008),^{169}Yb (4140 model) developed for high dose rate (HDR) application (Medich et al

2006) and photon energies in the 20 - 100 keV range are considered in this work. Response is estimated for well-type ionization chambers made with aluminum wall material and other hypothetic ionization chambers made with graphite, copper and C-552 materials.

7.3. Material and methods

7.3.1. Well chamber

A cylindrical well chamber is modeled as per the specifications available in literature (Bohm et al 2005). It is 10 cm in diameter and 16 cm in height, made of an aluminum foil on the butyrate inner wall, an aluminum collecting electrode and outer body is aluminum. This chamber is a vented chamber. The air-filled inner active volume is 5.4 mm thick and the air-filled outer active volume is 7.6 mm thick. The schematic diagram of well chamber is given in Figure 7.1. The thickness of butyrate inner wall, aluminum foil and collecting electrode is not known. We varied the thickness of butyrate inner wall from 0.5 mm to 1 mm and fixed at 0.8 mm after observing the response. Similarly the thickness of aluminum foil and collecting electrode kept at 0.1 mm.

The position of maximum response of the well chamber is determined by calculating the chamber response as a function of seed position using CAVRZnrc user-code. Well chamber along with the ^{131}Cs source (Cs-1 Rev-2 model) and ^{169}Yb (4140 model) were simulated, at the position of maximum response in the CAVRZnrc user-code and Fluka Monte Carlo code (Ferrari et al 2005). In addition, point photon sources in the energy range 20-100 keV were also simulated. Studies carried out for $\rho = 0.862$ kg m^{-3} (h = 3048 m) to 1.197 kg m^{-3} (standard air density), which covers all high altitude Indian cities

mentioned in Table 7.1. Mexico was also included in this study as its height above sea level is 2240 m.
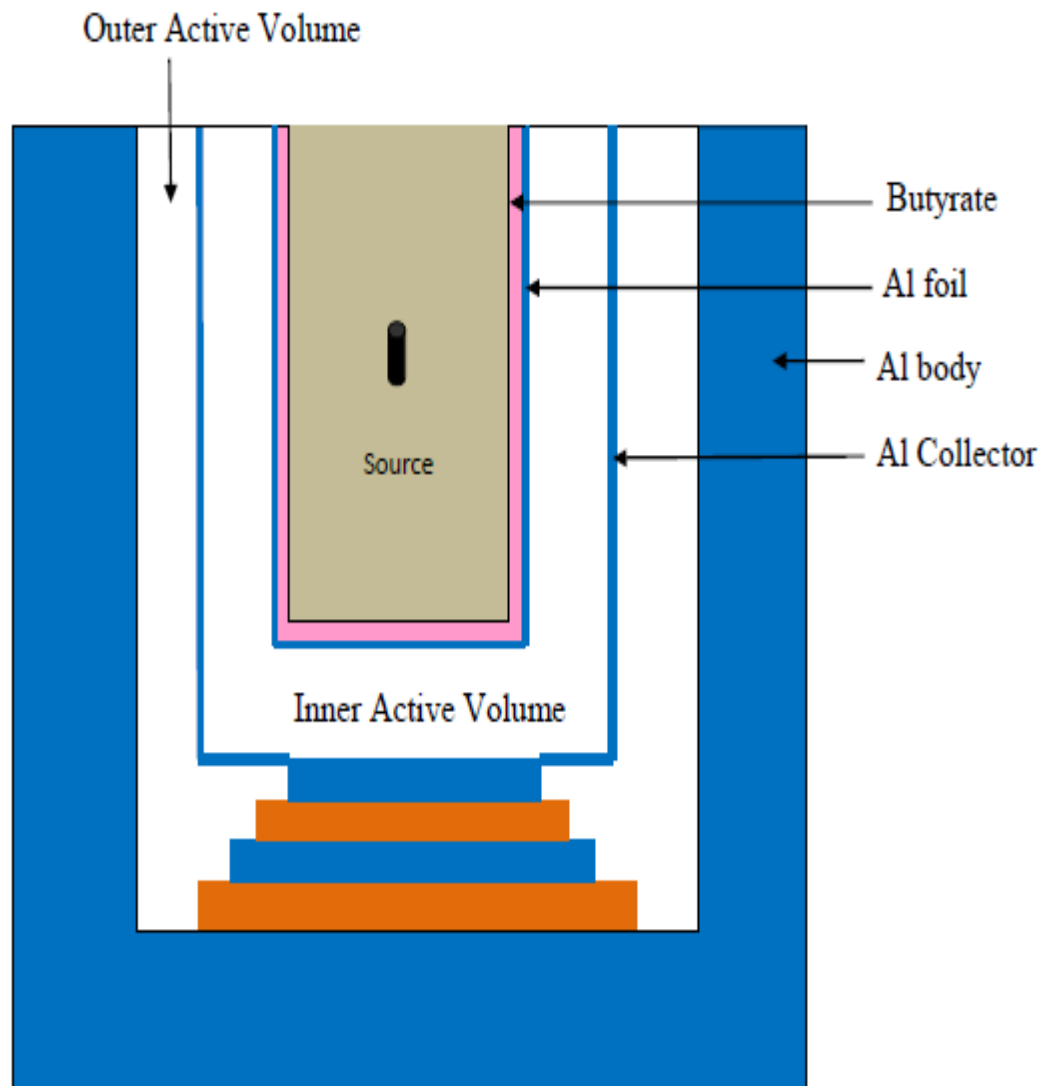
Figure 7.1. A simplified schematic diagram of a well-type ionization chamber.

Table 7.1. Height and air density of high altitude Indian cities. The Table also includes Mexico.

City	Height (m) above sea level	Air density (kg m^{-3})
Shimla	2276	0.937
Mexico	2240	0.940
Darjeeling	2042	0.961
Srinagar	1585	1.009
Bengaluru	920	1.084
Pune	560	1.127

7.3.2. Source models investigated (^{131}Cs and ^{169}Yb)

The ^{131}Cs source (Cs-1 Rev-2 model) produced by IsoRay Medical, Inc. is studied because of its suitability for permanent interstitial implants (Tailor et al 2008). The ^{131}Cs source has half-life of 9.7 days and it decays by electron capture to ^{131}Xe yielding gamma rays and x-rays with average photon energy of approximately 30.4 keV. Figure 7.2 presents the geometry of the source.

The ^{169}Yb source (4140 model) developed by Implant Sciences Corporation for HDR application is considered in this work (Medich et al 2006). The ^{169}Yb source has a 32 day half-life and average energy of 93 keV. The geometry of the source is given in Figure 7.3.
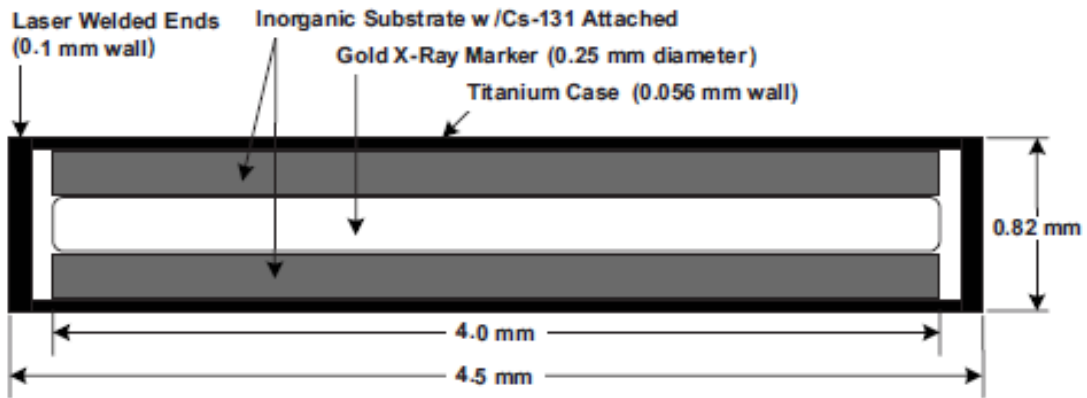
Figure 7.2. Geometry of ^{131}Cs source (Cs-1 Rev-2 model) used in the Monte Carlo simulation (Picture courtesy: Tailor et al 2008).
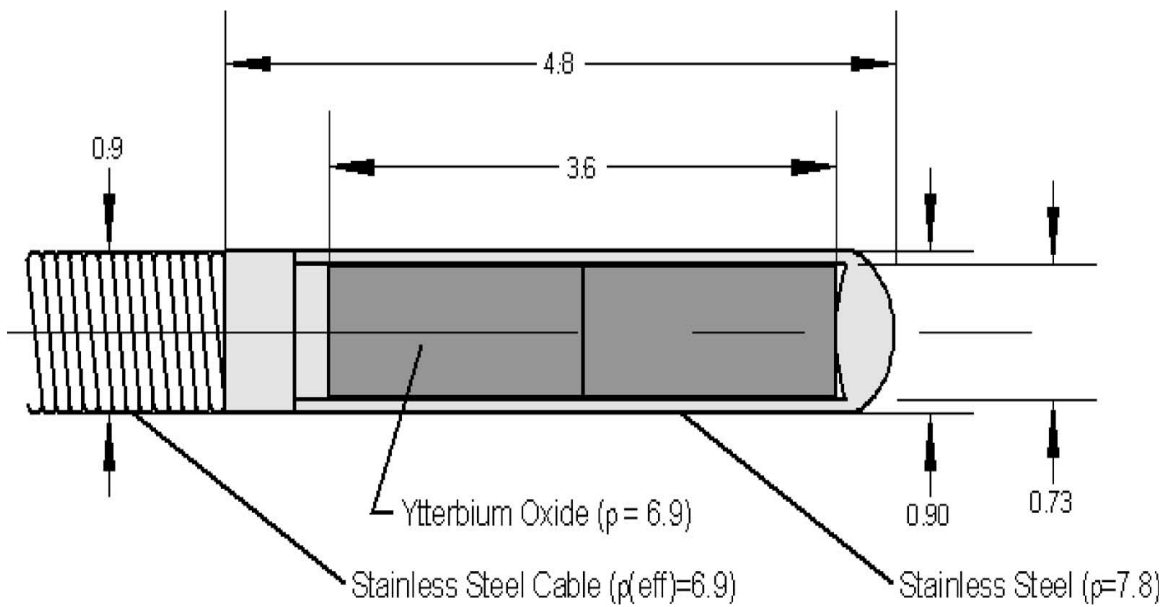
Figure 7.3. Geometry of ^{169}Yb (4140 model) used in the Monte Carlo simulation (Picture courtesy: Medich et al 2006).

7.3.3. Monte Carlo Techniques

7.3.3.1. Simulations using CAVRZnrc user-code

The CAVRZnrc user-code (Rogers et al 2010) scores a variety of quantities of dosimetric interest for an ion chamber. The geometry block of this user-code contains all the necessary inputs like thickness of planes and radius of cylinders for defining well-type ionization chamber, along with the radio isotope. A PEGS4 data file is created for the all media present in the regions and linked to the input file. All the scoring regions comprising the cavity are entered in the cavity block of the user-code. The material described in the cavity is air.

This user-code gives the total energy deposited in the cavity by electrons generated by primary photons and the energy deposited in the cavity by the scatter component that contains the dose due to scattered photons as well as the dose due to bremsstrahlung, fluorescent and annihilation photons, whatever their origin (Bielajew1986). The output of this user-code is normalized to per starting particle. The transport parameters were already discussed in Chapter 2. Up to 10^8 particle histories were simulated and statistical uncertainties are in the range of 0.6 - 0.8%.

The response of the well chamber is the energy deposited in the active volume, i.e. air cavity in the simulation and it is the product of the output (Gy/particle) of the simulation and ρ. This energy response is normalized with respect to ρ_0. We assume $T = T_0 = 22\ ^0$C, then $K_{TP} = \frac{P_0}{P}$. The product of K_{TP} and normalized response is known as K_{TP} corrected normalized response. Inner wall of well chamber is always simulated as butyrate material

of thickness 0.8 mm. The response of aluminum chamber (outer wall, foil, collecting electrode made of aluminum) compared with well chamber made of copper or C-552 or graphite material.

7.3.3.2. Simulation using FLUKA Monte Carlo code

FLUKA Monte Carlo code version 2011.2c is used in present study (Ferrari et al 2005). The well-type ionization chamber and source geometry were modeled in Monte Carlo code. The energy spectra of the sources involved in this study were linked with the input files through SOURCE.f subroutine. EM-CASCA defaults card was used for all the simulations. Transport and production cut-off for both electrons and photons were set at 1 keV everywhere. Single scattering at boundaries or for too short steps were activated through MULSOPT card. Air densities inside the active region of chamber were varied and corresponding energy deposition inside that active region was scored using USRBIN card on region basis. Total energy deposited inside active region was divided by the volume of the active region to get energy deposited per unit volume of the active region of the chamber. Around 10^7 particles were simulated to achieve relative uncertainty below 1% at energy deposition level.

7.4. Results and Discussion

7.4.1. Comparison of response in CAVRZnrc and FLUKA

Monte Carlo simulations carried out to estimate the normalised response of the well chamber as a function of air density in the photon energy range 20 - 100 keV. The air density (kg m^{-3}) considered in the simulations are 0.862 (3048 m), 0.983 (1829 m), 1.05

(1219 m), 1.184 (100 m) and 1.197 (sea level). It is observed that, for air density 0.862 kg m^{-3}, which corresponds to 3048 m height, the normalized response is 12% and 26% lower than unity for 20 and 100 keV respectively. Hence the normalized response decreases.

In order to correct the response of the chamber, K_{TP} factor is multiplied with normalized response. At high altitudes and for low photon energies, a significant deviation in the K_{TP} corrected normalized response was observed. At 3048 m, the K_{TP} correction factor overcorrects the response by 22%, 15%, and 6% for 20, 30 and 50 keV photon energies respectively. At 100 keV, K_{TP} corrected normalized response is much closer to unity. This is because, at higher altitudes, the pressure and hence the number of air molecules in the chamber cavity decreases. The results obtained were in good agreement with the values published by Bohm et al (2005).

The normalized response of aluminum-walled chamber for 20 and 100 keV photon energy was calculated using CAVRZnrc and FLUKA Monte Carlo code and presented in Figure 7.4. The response calculated using both the codes is in good agreement with each other.

The continuous slowing down approximation (CSDA) ranges for 20 - 100 keV electrons in dry air are presented in Table 7.2 calculated using ESTAR Computer program (version 1.2.3) available online at National Institute of Standards and Technology website (Berger et al 2005). The range of electrons generated by 20 keV photons are of same order compared to the inner cavity (5.4 mm) and outer cavity (7.6 mm) dimension of the well

chamber and many of the generated electrons that reach the active volume will stop in the cavity volume.
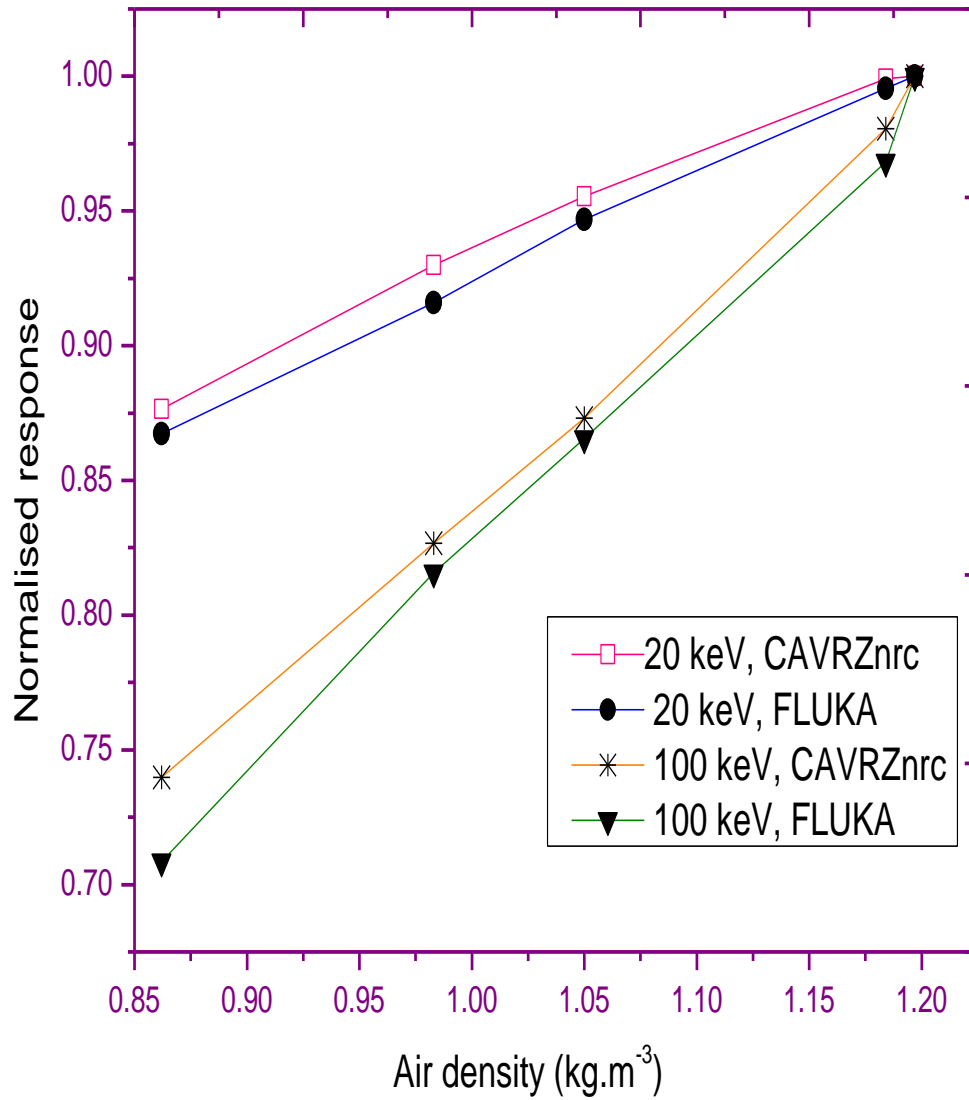
Figure 7.4. Normalized response of the well-type ionization chamber (aluminum wall) with air density for 20 and 100 keV photon energy calculated using CAVRZnrc and FLUKA Monte Carlo code.

Table 7.2. Continuous slowing down approximation (CSDA) ranges (mm) for 20 - 100 keV electrons in dry air (Berger et al 2005).

Energy (keV)	Range (mm) $\rho_{air} = 0.862$ kg m^{-3}	Range (mm) $\rho_{std} = 1.197$ kg m^{-3}
0	11.3	8.2
30	23.2	16.7
50	57.0	41.0
100	188.3	135.6

In the measurement of air-kerma strength, air-communicating chambers are considered as Bragg-Gray cavities. Bragg-Gray cavity theory tells that the entire dose is delivered by charged particles crossing the cavity and depositing energy along the way. It is assumed that no particles stop in the chamber.

Therefore, the application of the K_{TP} correction factor is not suitable in low energy photon energy range, when the electrons stop in the active volume of the cavity. For 100 keV photon, the CSDA range of electrons in air is much higher than the cavity dimension. A large fraction of electrons will cross the cavity, and only few percent of electrons will stop in the cavity.

7.4.2. Response of the well-type chamber for ^{131}Cs source

Figure 7.5 presents CAVRZnrc Monte Carlo code calculated K_{TP} corrected normalized response of the well-type ionization chamber with air density for ^{131}Cs source. Inner wall of well chamber is always simulated as butyrate material, where as outer wall, foil,

collecting electrode of the well chamber were simulated as aluminum or copper or C-552 or graphite material.

Figure 7.5 shows that the response is higher for chamber made with high atomic number material (Z) than chambers with low Z material walls. For $\rho_{air} = 0.862$ kg m^{-3}, which correspond to h = 3000 m, the K_{TP} corrected normalized response is 30% and 17% higher than unity for copper and aluminum chamber, respectively. Similarly, this response is 10% and 5% lower than unity for graphite and C-552 chamber, respectively.

Figure 7.5. CAVRZnrc user-code calculated K_{TP} corrected normalized response of the well-type ionization chamber with air density for ^{131}Cs source.

This response is dependent on Z and photon cross section of the chamber material. More electrons are generated by photons in copper and aluminum chamber, hence more response in copper and aluminum chamber. Fewer electrons are generated in C-552 and graphite (low Z material), hence lesser response.

Secondly, the photon cross section at ^{131}Cs energy is much larger for aluminum and copper than for C-552 and graphite, thereby generating more electrons. Hence, low-Z materials have lower response and high-Z materials have higher response.

The K_{TP} corrected normalized response obtained from separate simulations using CAVRZnrc user-code and FLUKA Monte Carlo code. Their ratio, $[K_{TPNR}]_{FLUKA}^{CAVRZnrc}$ were presented in Table 7.3 for ^{131}Cs source in different chamber materials simulated at different air densities. The ratio is within 2%, which shows that FLUKA Monte Carlo code can accurately model the response of well-type ionization chamber.

Table 7.3. $[K_{TPNR}]_{FLUKA}^{CAVRZnrc}$ for ^{131}Cs source in different chamber materials.

Air density (kg m^{-3})	Copper	Aluminum	C-552	Graphite
0.862	1.02	0.98	0.99	1.01
0.983	1.00	0.99	0.99	1.01
1.050	1.02	0.99	1.00	1.00
1.184	1.02	1.00	0.99	0.99
1.197	1.00	1.00	1.00	1.00

Table 7.4 presents the CAVRZnrc user-code calculated K_{TP} corrected normalized response for aluminum made well chamber for [131]Cs and [169]Yb source for cities at high altitudes. For [131]Cs source, this response is about 3 - 13% higher than unity.

7.4.3. Response of the well-type chamber for [169]Yb source

Figure 7.6 presents CAVRZnrc user-code calculated K_{TP} corrected normalized response of the well-type ionization chamber with air density for [169]Yb source for standard aluminum well chamber as well as for copper, C-552 and graphite materials.

For air density 0.862 kg m^{-3}, which corresponds to 3000 m height, this response is 9% and 4% higher than unity for copper and aluminum chamber, respectively. The response is about to unity for C-552 chamber and 1 - 2% lower than unity for graphite chamber.

Table 7.4. K_{TP} corrected normalized response of aluminum made well chamber for [131]Cs and [169]Yb sources for cities at high altitudes calculated using the CAVRZnrc user-code.

City	Height (m) above sea level	Air density (kg m^{-3})	K_{TP} corrected normalized response for aluminum chamber	
			[131]Cs	[169]Yb
Shimla	2276	0.937	1.13	1.03
Mexico city	2240	0.940	1.13	1.03
Darjeeling	2042	0.961	1.12	1.03
Srinagar	1585	1.009	1.09	1.02
Bengaluru	920	1.084	1.05	1.01
Pune	560	1.127	1.03	1.01

This response is about 1 - 3% higher than unity for the high altitude cities given in Table 7.4, which is again due to the range of electrons is higher than cavity dimension and few electrons will stop in the cavity. The K_{TP} corrected normalized response is higher because of high Z and higher photon cross section in aluminum and copper than for C-552 and graphite. The response of a well-type ionization chamber is influenced by many parameters, such as photon energy, size of the active volume, and chamber wall material.

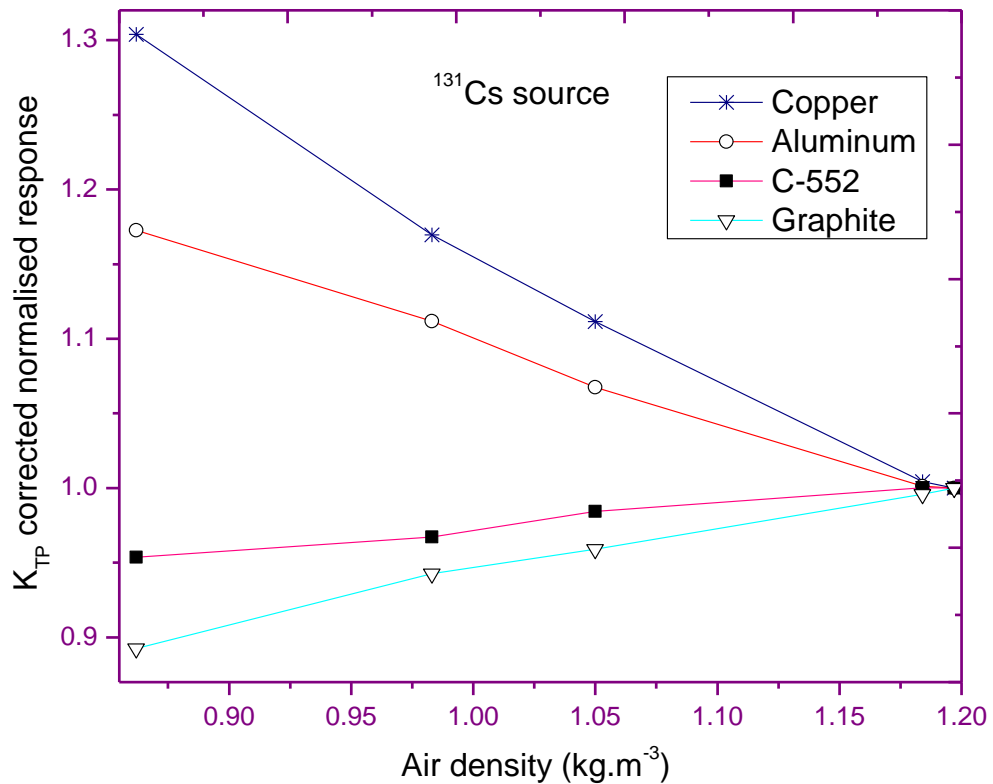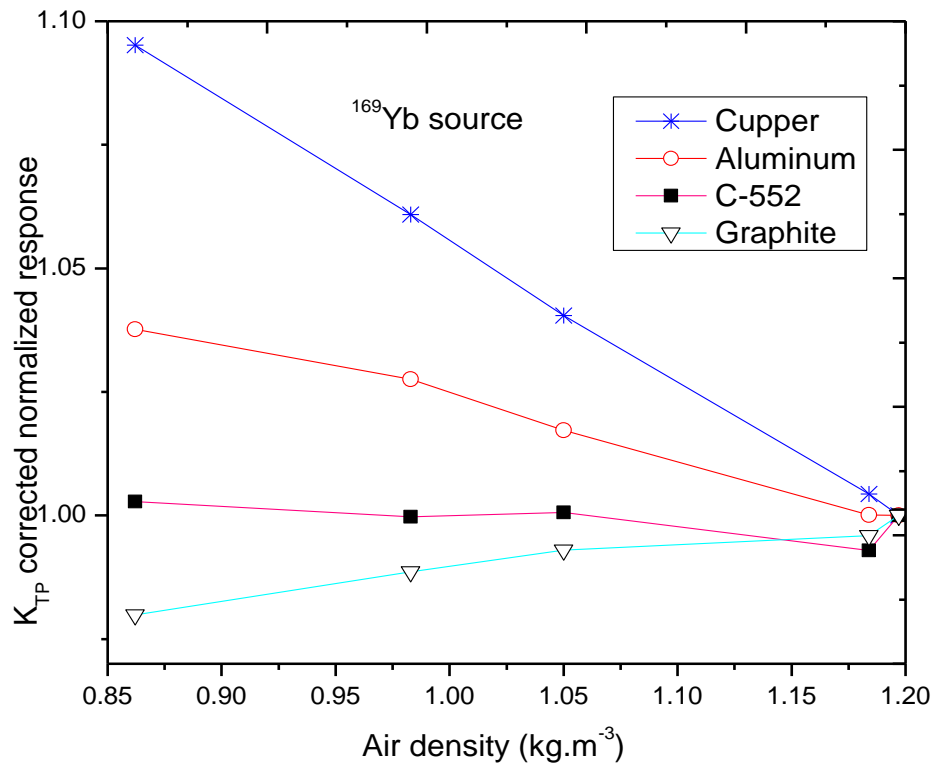

Figure 7.6. CAVRZnrc calculated K_{TP} corrected normalized response of the well-type ionization chamber with air density for ^{169}Yb source.

Table 7.5 presents the K_{TP} corrected normalized response ratio $[K_{TPNR}]_{FLUKA}^{CAVRZnrc}$ for ^{169}Yb source for different well chamber materials, simulated at different air densities. The ratio is within 3%.

Table 7.5. $[K_{TPNR}]_{FLUKA}^{CAVRZnrc}$ for ^{169}Yb source in different chamber materials.

Air density (kg m^{-3})	Copper	Aluminum	C-552	Graphite
0.862	0.99	0.97	1.02	1.02
0.983	1.00	1.01	1.00	1.03
1.050	1.00	1.01	1.00	1.01
1.184	1.00	1.00	0.99	1.01
1.197	1.00	1.00	1.00	1.00

7.5. Conclusions

The K_{TP} corrected normalized response of the well-type ionization chamber as a function of air density is calculated using the EGSnrc Monte Carlo code system and FLUKA Monte Carlo code. At high altitudes, this K_{TP} factor results an over-response in the chamber for low energy photon sources. This over-response is because for low energy sources, the range of the electrons in the active volume of the well chamber is nearly equal to the dimension of the active volume and the well chamber does not behave as a small cavity dosimeter.

Well chambers are modeled with aluminum and other materials like graphite, C-552, copper. It is understood that, the response is dependent on Z and photon cross section of

the chamber material. Over-response is observed in copper and aluminum chamber because of high Z material. Chamber wall material made of high Z material, backscatter a large fraction of incident electrons and hence over-response is observed. Hence it is suggested that K_{TP} correction factor must be modified to appropriately to correct the change in chamber response.

The K_{TP} corrected normalized response ratio $[K_{TPNR}]_{FLUKA}^{CAVRZnrc}$ was obtained using ^{131}Cs and ^{169}Yb source using CAVRZnrc user-code and FLUKA Monte Carlo code for copper, aluminum, C-552 and graphite well chamber at different air densities. The ratio is within 2 - 3%, which shows that FLUKA Monte Carlo code can also accurately model the response of well-type ionization chamber at high altitudes.

CHAPTER 8

SUMMARY AND CONCLUSIONS

8.1. Summary and Conclusions

Brachytherapy is a well established treatment modality for the treatment of gynaecologic cancers, oral cancers, sarcomas, breast and prostate cancers etc. It allows conformal treatment without heavy technological involvement and treatment cost. Brachytherapy treatments have many advantages, it is patient friendly and the depth dose characteristics are compared to 3-Dimensional conformal radiotherapy (3D-CRT) or intensity modulated radiotherapy (IMRT).

About 30 low-energy photon source models (^{125}I, ^{103}Pd, and ^{131}Cs) are available for permanent and temporary brachytherapy. ^{131}Cs, a new low energy isotope along with transrectal ultrasound (TRUS) image guidance, is popular treatment technique for the early stage prostate cancer. In addition, an electronic brachytherapy source (EBS) i.e. a miniaturized 50 kVp x-ray tube has been developed. In the last decade, several beta emitting sources (^{32}P, ^{106}Ru, ^{90}Sr, and ^{90}Y) are used in intravascular brachytherapy for prevention of restenosis, eye applicator for choroidal melanoma and surface brachytherapy.

About 10 ^{192}Ir HDR source models and 4 ^{60}Co HDR sources are available worldwide in remote afterloading technology systems. BARC / BRIT, India has developed a ^{192}Ir HDR source for indigenous Karknidon HDR machine; ^{125}I source (OcuProsta) for ocular and prostate cancers and ^{32}P, ^{177}Lu skin patch sources for skin applications.

Source strength determination (source calibration) in terms of air-kerma strength (AKS) is utmost important for accurate dose delivery. In some planning systems, the traditional source strength quantities such as activity (curie, Ci) are still used. It is preferable that TPS to be modified to operate on the NIST traceable quantity of air-kerma strength.

Accurate dose determination for a new source design is essential for its clinical applications. In this regard, AAPM Task Group published TG-43 report in 1995 and TG-43U1 in 2004 reports for low energy sources (Nath et al 1995, Rivard et al 2004). Recently in 2012 AAPM published similar recommendations and guidelines for high-energy photon sources with average energy higher than 50 keV (Perez-Calatayud et al 2012). It is recommended to measure the dosimetry parameters directly in the water phantom and/or calculate the dose distribution using Monte Carlo techniques.

Recently, application of the Monte Carlo techniques in clinical dosimetry has increased due to availability of several user-friendly Monte Carlo codes and advanced high speed computers. Therefore it is widely used and accepted dosimetry tool for radiotherapy users. The users should utilize these codes with updated cross-section data to generate reference dose distribution and check the result for its accuracy.

The dosimetry parameters of the ^{192}Ir HDR source were generated using the EGSnrc Monte Carlo code and the results are in good agreement with other similar ^{192}Ir HDR sources. The calculated data of the ^{192}Ir HDR source are utilized for the development of the brachytherapy treatment planning software.

Central axis depth dose and dose profiles of in-house developed ^{32}P patch source for skin applications were calculated using Monte Carlo code. Based on the calculated dose rate, the treatment time to deliver a therapeutic dose at reference depth (1 mm) is calculated.

Surface dose and dose profiles for a ^{177}Lu patch source for skin applications were calculated using Monte Carlo code and compared with extrapolation chamber and EBT3 film-based measurements. EBT3 films were used to estimate the source uniformity (ICRU report 2004) and measure surface dose using electron beam calibration. The study also includes (i) determination of activity of the ^{177}Lu patch source using the HPGe detector, (ii) estimation of Bragg-Gray stopping power ratio of water-to-air and chamber wall correction factor needed to be applied on measurements for establishing the dose rate at 5 μm depth using the Monte Carlo methods.

The dose response for the EBT3 film was studied at 70 kV x-ray and ^{60}Co energy. The variations are within 2% for dose range of 100 - 510 cGy and 8% for dose of 50 cGy. Hence EBT3 film calibrated at ^{60}Co energy is suitable for dosimetry of ^{125}I sources for doses more than 50 cGy. Dose rate values measured along transverse axis for a single ^{125}I seed are in good agreement with the values obtained using EGSnrc Monte Carlo methods. Central axis depth dose and off-axis profiles were measured using EBT3 films, for a 14 mm diameter silver eye plaque loaded with 13 ^{125}I seeds. The dosimetry data will be useful for treatment time calculation for a silver eye plaque of similar design and to estimate dose to critical structure during planning.

Brachytherapy treatment planning system uses the TG-43 dosimetry data calculated around a single source positioned at the centre of a liquid water or solid phantom. The dose distribution in the planning system is calculated by superposing the TG-43 dose distributions according to the pattern of the source placement. However, the influence of tissue composition differing from liquid water, interseed attenuation (absorption and scattering of photons by neighboring seeds), and finite patient dimensions are all ignored.

The dose distribution in the prostate due to effect of tissue composition involving single seed was estimated for ^{125}I OcuProsta and ^{131}Cs Cs-1 Rev-2 sources using FLUKA Monte Carlo code. Variations in the dose values up to 4% and 3% are observed for close distances from ^{125}I and ^{131}Cs sources respectively.

Dose distribution in prostate, bladder and rectum were estimated using Monte Carlo simulation for a prostate implant loaded with 39 seeds in 3 planes. Interseed attenuation was estimated using the superposition approach and is about 6 - 9% at points lying inside the implant volume and about 16% at points lying in the prostate boundary. The under-dosage due to the lack of scatter environment was estimated. Variations up to 10% and 8% in dose values are observed for ^{125}I and ^{131}Cs sources respectively.

The response of well chamber to pressure variations at high altitudes for ^{131}Cs and ^{169}Yb sources was studied using Monte Carlo simulation techniques. The K_{TP} factor results an over-response 3 - 13% for ^{131}Cs source and 1 - 3% for ^{169}Yb source higher than unity.

The highlights the major contributions and achievements made in this research work were listed as follows:

- Dosimetry of indigenously developed ^{192}Ir HDR brachytherapy source developed for Karknidon and its application in radiotherapy treatment planning system.

- Dosimetry of ^{32}P and ^{177}Lu patch sources used in superficial brachytherapy applications.

- Dosimetry of indigenously developed ^{125}I source for intraocular tumours.

- Dosimetry of ^{125}I and ^{131}Cs brachytherapy sources due to non-uniform scatter condition

- Response study of well chamber to pressure variations at high altitudes for ^{131}Cs and ^{169}Yb sources using Monte Carlo simulation techniques.

8.2. Future scope

Significant research studies were already carried out in the field of brachytherapy dosimetry using Monte Carlo techniques. The brachytherapy dosimetry accuracy for low energy photon sources is highly dependent on scatter conditions and photoelectric effect cross-sections relative to water, which is dominant mode of interaction. The recent AAPM Task Group 186 report (TG-186) provides necessary guidance for accurate dose calculations in brachytherapy using model-based dose calculation algorithms (MBDCA) (Beaulieua L et al 2012).

The ^{32}P and ^{177}Lu patch sources were prepared by immersing the nafion membrane in a solution of known activity. The activity of the these sources was estimated using NaI(Tl) counter by subtracting the residual activity in the reaction volume from the initial added

^{177}Lu activity in the reaction volume. Parameters for characterization of source uniformity as per ICRU report 2004 may be determined using radiochromic films.

Accordingly, following studies can be initiated as continuation of the works presented in this thesis:

- Patient-specific dose distributions based upon the actual locations of the sources, applicator heterogeneities, interseed attenuation, patient size, and can account for tissue heterogeneities using Monte Carlo techniques. Such detailed studies may be clinically useful.

- Development of calibration standard for ^{32}P and ^{177}Lu patch sources and characterization of source in terms of reference absorbed-dose rate, contained activity and source uniformity (ICRU report 2004).

REFERENCES

AAPM 1987 Specification of Brachytherapy Source Strength *Report 32 of American Association of Physicists in Medicine American Institute of Physics* (New York)

ABS OOTF 2014 The American Brachytherapy Society consensus guidelines for plaque brachytherapy of uveal melanoma and retinoblastoma The American Brachytherapy Society - Ophthalmic Oncology Task Force *Brachytherapy* **13** 1-14

Acar H, Chiu-Tsao S T, Özbay I, Kemikler G and Tuncer S 2013 Evaluation of material heterogeneity dosimetric effects using radiochromic film for COMS eye plaques loaded with 125I seeds (model I25.S16) *Med. Phys.* **40** 011708-13

AERB 2001 Testing and classification of sealed radioactive sources. Safety Standard no: AERB/SS/3 (Rev.1) Atomic Energy Regulatory Board Mumbai India

Agostinelliae S *et al.* 2003 Geant4 - A simulation tool kit *Nuc. Instr. and Methods. in Phys. Resea. A* **506** 250-303

Ali M M and Khan F M 1990 Determination of surface dose rate from a 90Sr ophthalmic Applicator *Med. Phys.* **17** 416-21

Anagnostopoulos G, Baltas D, Pantelis E, Papagiannis P and Sakelliou L 2004 The effect of patient inhomogeneities in oesophageal ^{192}Ir HDR brachytherapy: a Monte Carlo and analytical dosimetry study *Phys. Med. Biol.* **49** 2675-2685

Andreo P 1991 Monte Carlo techniques in medical radiation physics *Phys. Med. Biol.* **36** 861-920

Andres C, Castillo A D, Tortosa R, Alonso D and Barquero R 2010 A comprehensive study of the Gafchromic EBT2 radiochromic film: A comparison with EBT *Med. Phys.* **37** 62-71

Angelopoulos A, Baras P, Sakelliou L, Karaiskos P and Sandilos P 2000 Monte Carlo dosimetry of a new ^{192}Ir high dose rate brachytherapy source *Med. Phys.* **27** 2521-27

Anjomrouz M, Sadeghi M and Haddadi A 2013 Monte Carlo characterization of ^{169}Yb as a high-dose-rate source for brachytherapy application by FLUKA code *J. of Appl. Clini. Med. Phys.* **14** (4) 196-205

Arjomandy B, Tailor R, Anand A, Sahoo N, Gillin M, Prado K and Vicic M 2010 Energy dependence and dose response of Gafchromic EBT2 film over a wide range of photon, electron, and proton beam energies *Med. Phys.* **37** (5) 1942-47

Attix F H 1986 *Introduction to Radiological Physics and Radiation Dosimetry (*New York: John Wiley and Sons)

Bakshi A K, Vandana S, Palani Selvam T, Chougaonkar M P and Mayya Y S 2013 Measurement of the output of ISO recommended beta sources with an extrapolation chamber *Radiat. Meas.* **53-54** 50-55

Bakshi A K, Vandana S, Palani Selvam T and Rama P 2014 Study on the characteristics of indigenously developed ^{106}Ru/^{106}Rh source *Radiat. Meas.* **64** 23-28

Bakshi A K, Rama P, Chinnaesakki S, Rupali P, Deepa S, Ajay D, Palani Selvam T, Sapra B K and Datta D 2017 Measurements of background radiation levels around Indian station Bharati during 33rd Indian Scientific Expedition to Antarctica *J. of Envir. Radioactivity* **167** 54-61

Ballester F, Hernandez C, Perez-Calatayud J and liso F 1997 Monte Carlo calculation of dose rate distributions around ^{192}Ir wires *Med. Phys.* **24** 1221- 8

Ballester F, Puchades V, Lluch J L, Serrano-Andres M A, Limami Y and Perez-Calatayud J 2001 Technical note: Monte-Carlo dosimetry of the HDR 12i and Plus ^{192}Ir Sources *Med. Phys.* **28** 2586-91

Ballester F, Granero D, Perez-Calatayud, Casal E, Agramunt S and Cases R 2005 Monte Carlo dosimetric study of the BEBIG ^{60}Co HDR source *Phys. Med. Biol.* **50** (21) N309-N316

Ballester F, Granero D, Perez-Calatayud J, Melhus C S and Rivard M J 2009 Evaluation of high-energy brachytherapy source electronic disequilibrium and dose from emitted electrons. *Med. Phys.* **36** (9) 4250-56

Ballester F, Granero D, Perez-Calatayud J and Venselaar J L M and Rivard M J 2010 Study of encapsulated ^{170}Tm sources for their potential use in brachytherapy *Med. Phys.* **37** (4) 1629-1637

Baltas D, Karaiskos P, Papagiannis P, Sakelliou L, Loeffler E and Zamboglou N 2001 Beta versus gamma dosimetry close to ^{192}Ir brachytherapy sources *Med. Phys.* **28** 1875-82

Baltas D, Sakelliou L and Zamboglou N 2007 Monte Carlo-Based Source Dosimetry (Ch-9) *Physics of Modern Brachytherapy for Oncology Oncology* (New York: Taylor & Francis)

Baro J, Sempau J, Fernandez-Varea J M, Salvat F 1995 PENELOPE: an algorithm for Monte Carlo simulation of the penetration and energy loss of electrons and positrons in matter. *Nucl. Instrum. Methods* B **100** 31 46

Baum R P, Kulkarni H R, Schuchardt C, Singh A, Wirtz M et al 2016 ^{177}Lu-Labeled Prostate-Specific Membrane Antigen Radioligand Therapy of Metastatic Castration-Resistant Prostate Cancer: Safety and Efficacy *J. Nucl. Med.* **57**(7) 1006-13

BCRU 1984 Specification of brachytherapy sources: Memorandum from the British Committee on Radiation Units and Measurements *Br. J. Radiol.* **57** 941-42

Beaulieua L, Tedgren A C, Carrier J F, Davis S D, Mourtada F, Rivard M J, Thomson R M, Verhaegen F, Wareing T A and Williamson J F 2012 Report of the Task Group 186 on model-based dose calculation methods in brachytherapy beyond the TG-43 formalism: Current status and recommendations for clinical implementation *Med. Phys.* **39** (10) 6208-36

Berger M J 1963 Monte Carlo calculation of the penetration and diffusion of fast charged Particles *Methods Comput. Phys.***1** 135-215

Berger M J 1968 MIRD Pamphlet 2: Energy deposition in water by photons from point isotropic sources *J. Nucl. Med.* **9**(Suppl. 1) 17-25

Berger M J, Hubbell J H, Seltzer S M, Chang J, Coursey J S, Sukumar R, Zucker D S and Olsen K 1987 XCOM Photon Cross Sections on a Personal Computer NIST Report No. NBSIR 87-3597. http://www.nist.gov/pml/data/xcom/. (accessed June 06, 2017)

Berger M J 1993 Proton Monte Carlo Transport Program PTRAN   NISTIR 5113

Berger M J, Coursey J S, Zucker M A and Chang J 2005. ESTAR, PSTAR, and ASTAR: Computer programs for calculating stopping-power and range tables for electrons, protons, and helium ions (version 1.2.3). (Online) Available http://physics.nist.gov/Star (2018.04.02). National Institute of Standards and Technology (Gaithersburg, MD)

Bhabha H J 1935 Proc. Royal Society London A154 – 195

Biggs F, Mendelsohn L B and Mann J B Hartree-Fock 1975 Compton profiles for the elements At. Data Nucl. Data Tables **16** 201 - 309

Bhola S, Selvam T P, Sahoo S and Vishwakarma R S 2012 An analytic approach to the dosimetry of a new BEBIG ^{60}Co HDR brachytherapy source *J. Med. Phys.* **37** 129-37

Bielajew A F 1986 Ionization cavity theory: a formal derivation of perturbation factors for thick-walled ion chambers in photon beams *Phys. Med. Biol.* **31** 161-170

Bohm T D, Mourtada F A and Das R K 2001 Dose rate table for a ^{32}P intravascular brachytherapy source from Monte Carlo calculations *Med. Phys.* **28** 1770-1775

Bohm T D, DeLuca P M and DeWerd L A 2003 Brachytherapy dosimetry of ^{125}I and ^{103}Pd sources using an updated cross section library for the MCNP Monte Carlo transport code *Med. Phys.* **30** 701-11

Bohm T D, Griffin S L, DeLuca P M Jr and DeWerd L A 2005 The effect of ambient pressure on well chamber response: Monte Carlo calculated results for the HDR 1000 Plus *Med. Phys.* **32** 1103-14

Bohm T D, John A. Micka, and Larry A. DeWerd 2007 Monte Carlo aided design of an improved well-type ionization chamber for low energy brachytherapy sources *Med. Phys.* **34** 1274-85

Boman E, Tervo J and M Vauhkonen M 2005 Modelling the transport of ionizing radiation using the finite element method *Phys. Med. Biol.* **50** 265-280

Borca V C, Pasquino M, Russo G, Grosso P Cante D, Sciacero P, Girelli G, Porta M RL and Tofani S 2013 Dosimetric characterization and use of GAFCHROMIC EBT3 film for IMRT dose verification *J. Appl. Clin. Med. Phys.* **2** 158-171

Boutilon M and Perroche-Rous A M 1987 Re-evaluation of the W value for electrons in dry air *Phys. Med. Biol.* **32** 213-291

Briesmeister J F 1993 MCNP-a general Monte Carlo N-particle transport code. Version 4A Los Alamos, NM: Los Alamos National Laboratory

Brown T A D, Hogstrom K R, Alvarez D, Matthews K L II, Ham K and Dugas J P 2012 Dose-response curve of EBT, EBT2, and EBT3 radiochromic films to synchrotron-produced monochromatic x-ray beams *Med. Phys.* **39** 7412-17

Butson M J, Cheung T and Yu P K 2009 Evaluation of the magnitude of EBT Gafchromic film polarization effects *Australas. Phys. Eng. Sci. Med.* **32** 21-25

Capote R, Mainegra E and Lopez E 2001a Anisotropy function for ^{192}Ir low-dose-rate brachytherapy sources: an EGS4 Monte Carlo study *Phy. Med. Bio.* **46** 1487-1489

Capote R, Mainegra E and Lopez E 2001b Anisotropy functions for low energy interstitial brachytherapy sources: An EGS4 Monte Carlo study *Phys. Med. Biol.* **46** 135-150

Carrier J F, Beaulieu L, Therriault-Proulx F and Roy R 2006 Impact of interseed attenuation and tissue composition for permanent prostate implants *Med. Phys.* **33** 595-604

Carrier J F, D'Amours M, Verhaegen F, Reniers B, Martin A G, Vigneault E and Beaulieu E 2007 Postimplant dosimetry using a Monte Carlo dose calculation engine: A new clinical standard *Int. J. Radiat. Oncol. Biol. Phys.* **68** 1190-98

Cember H and Johnson T E 2009 *Introduction to Health Physics*, 4th Edition (New York: MC Graw Hill Medical Publication)

CFMRI 1983 Recommendations pour la determination des doses absorbé´es en curie´ Therapie *Report 1 of the Comite Francais Measure des Rayonments Ionizants Bureau National de Me´ Trologie* (Paris)

Chang H C, Seongmoon J, Kanghyuk C, Kwang-Jae S, Lee J S and Ye S J 2016 Radioactivity determination of sealed pure beta-sources by surface dose measurements and Monte Carlo simulations; *Nuc. Instr. and Meth. in Phy. Research* A **816** 87-95

Char D H, Kroll S, Quivey J M, Castro J 1996 Long term visual outcome of radiated uveal melanomas in eyes eligible for randomization to enucleation versus brachytherapy. *Br. J. Ophthalmol.* **80** 117-124

Chaudhari S, Deshpande S, Anand V, De S, Saxena S, Dash A, Basu M, Samant P and Kannan V 2008 Dosimetry and treatment planning OcuProsta ^{125}I seeds for intraocular lesions *J. Med. Phys.* **33** (1) 14-18

Chen Z and Nath R 2001 Dose rate constant and energy spectrum of interstitial brachytherapy source. *Med. Phys.* **28** (1) 86-96

Chen Z, Bonziorni P and Nath R 2005 Dose rate constant of a new Cesium131 interstitial brachytherapy seed measured by thermoluminescent dosimetry and gamma-ray spectroscopy *Med. Phys.* **32** 3279-85

Chibani O and Williamson J F 2005a MCPI: A sub-minute Monte Carlo dose calculation engine for prostate implants *Med. Phys.* **32** 12 3688 -3698

Chibani O, Williamson J F and Todor D 2005b Dosimetric effects of seed anisotropy and interseed attenuation for 103Pd and 125I prostate implants *Med. Phys.* **32** 2557-66

Chiu-Tsao S T, Anderson L L, O'Brien K, Stabile L and Liu J C 1993 Dosimetry for ^{125}I seed (model 6711) in eye plaques *Med. Phys.* **20** 383-89

Chiu-Tsao S T, Medich D, and Munro III J 2008 The use of new GafChromic EBT film for 125I seed dosimetry in Solid Water phantom *Med. Phys.* **35** 3787-99

Chiu-Tsao S T *et al.* 2012 Dosimetry of ^{125}I and ^{103}Pd COMS eye plaques for intraocular tumors: Report of Task Group 129 by the AAPM and ABS *Med. Phys.* **39** 6161 - 84

Cohen V M L, Papastefanou V P, Liu S, Stoker I and Hungerford J L 2013 The Use of Strontium-90 Beta Radiotherapy as Adjuvant Treatment for Conjunctival Melanoma J. Oncol. Article ID 349162 (http://dx.doi.org/10.1155/2013/349162)

Crijns W, Maes F, Heide U A van der and Van den Heuvel F 2013 Calibrating page sized Gafchromic EBT3 films *Med. Phys.* **40** 012102-1

Cullen D E, Perkins S T and Rathkopf J A 1990 The 1989 Livermore Evaluated Photon Data Library (EPDL), Lawrence Livermore National Laboratory Report UCRL-ID-103424 (Livermore, California)

Danthala M, Kallur K G, Prashant G R, Rajkumar K and Rao M R 2014 ^{177}Lu-DOTATATE therapy in patients with neuroendocrine tumours: 5 years' experience from a tertiary cancer care centre in India *Eur. J. Nucl. Med. Mol. Imaging.* **41** (7) 1319-1326

Das R K and Thomadsen B R 2005 High Dose Rate Sources and Delivery Systems *Brachytherapy Physics* 2nd edn ed B R Thomadsen, M J Rivard and W M Butler (Madison, WI: Medical Physics Publishing) pp 59-74

Daskalov G M, Loffler E and Williamson J F 1998 Monte Carlo-aided dosimetry of a new high dose-rate brachytherapy source *Med. Phys.* **25** 2200-08

Deasy J O and Soares C G 1994 Extrapolation chamber measurements of ^{90}Sr+^{90}Y beta-particle ophthalmic applicator dose rates *Med. Phys.* **21** 91-99

Demarco J J, Smathers J B, Burnison C M, Ncube Q K and Solberg T D 1999 CT-based dosimetry calculations for 125I prostate implants *Int. J. Radiat. Oncol. Biol. Phys.* **45** 1347-1353

Devic S, Tomic N, Aldelaijan S, DeBlois F, Seuntjens J, Chan M F and Lewis D 2012 Linearization of dose–response curve of the radiochromic film dosimetry system. *Med. Phys.* **39** (8) 4850-57

Dolan J, Li Z and Williamson J F 2006 Monte Carlo and experimental dosimetry of an 125I brachytherapy seed *Med. Phys.* **33**(12) 4675-84

Duggan D and Johnson B L 2004 Improved radial dose function estimation using current version MCNP Monte Carlo simulation: Model 6711 and ISC3500 125I brachytherapy sources Appl. Radiat. Isot. **61** 1443-50

Eckhardt R 1987 Stan Ulam, John Von Neumann, and the Monte Carlo method Los Alamos Science Special Issue 131 (http://www-star.st-and.ac.uk/~kw25/teaching/mcrt /MC_history_3.pdf). Last assessed 06.08.2018

Enger S A, D'Amours M and Beaulieu L 2011 Modeling a hypothetical ^{170}Tm source for brachytherapy applications *Med. Phys.* **38** (10) 5307-5311

Enger S A, LundqvistH, D'Amours M and Beaulieu L 2012 Exploring ^{57}Co as a new isotope for brachytherapy applications *Med. Phys.* **39** 2342-2345

ESTRO 2004 European Guidelines for Quality Assurance in Radiotherapy, A Practical Guide to Quality Control of Brachytherapy Equipment Booklet No 8 , J. Venselaar and J. Perez-Calatayud, eds. (Belgium)

Ferrari A, Sala P, Fasso A and Ranft J 2005 FLUKA: a multi-particle transport code. CERN-2005-10, INFN/TC_05/11, SLAC-R-773

Gao W, Liu L, Liu Z Y, Li Xu-Dong and Chen L 2009 Interstitial injection of ^{32}P-chromic phosphate during lung cancer resection to treat occult lymphatic metastasis *Nucl. Med. Commun.* **30** 420-426

Gentle J E 1998 *Random Number Generation and Monte Carlo Methods* (New York: Springer-Verlag)

Gleckler M, Valentine J D and Silberstein E B 1998 Calculating lens dose and surface dose rates from ^{90}Sr ophthalmic applicators using Monte Carlo modeling *Med. Phys.* **25** 29-36

Goetsch S J, Attix F H, Pearson D W and Thomadsen B R 1991a Calibration of ^{192}Ir high dose rate afterloading system *Med. Phys.* **18** 462-7

Goetsch S J and Sunderland K S 1991b Surface dose rate calibration of Sr-90 plane ophthalmic applicators *Med. Phys.* **18** 161-66

Granero D, Perez-Calatayud J, Ballester F, Casal E and de Frutos J M 2004 Dosimetric study of the 15mm ROPES eye plaque *Med. Phys.* **31** 3330-36

Granero D, Perez-Calatayud J, Ballester F 2005 Monte Carlo calculation of the TG-43 dosimetric parameters of a new BEBIG Ir-192 HDR source *Radiotherapy and Oncology* **76** 79-85

Granero D, Perez-Calatayud J, Casal E, Ballester F and Venselaar J 2006 A dosimetric study on the Ir-192 high dose rate Flexisource *Med. Phys.* **33** 4578-82

Granero D, Perez-Calatayud J and Ballester F 2007 Technical note: Dosimetric study of a new ^{60}Co source used in brachytherapy *Med. Phys.* **34** (9) 3485-88

Granero D, Pérez-Calatayud J, Pujades-Claumarchirant M C, Ballester F, Melhus C S, Rivard M J 2008 Equivalent phantom sizes and shapes for brachytherapy dosimetric studies of ^{192}Ir and ^{137}Cs *Med. Phys.* **35** 4872-7

Granero D, Vijande J, Ballester F and Rivard M J2011 Dosimetry revisited for the HDR 192Ir brachytherapy source model mHDR-v2 *Med. Phys.* **38** 487-494

Griep C, Davelaar J, Scholten A N, Chin A and Leer J W 1995 Electron beam therapy is not inferior to superficial X-ray therapy in the treatment of skin carcinoma *Int. J. Radiat. Oncol. Bio. Phys.* **32**(5) 1347-50

Griffin S L, DeWerd L A, Micka J A and Bohm T D 2005 The effect of ambient pressure on well chamber response: Experimental results with empirical correction factors *Med. Phys.* **32** 700-9

Guix B, Finestres F, Tello J, Palma C, Martinez A, Guix J and Guix R 2000 Treatment of skin carcinomas of the face by high-dose-rate brachytherapy and custom-made surface molds *Int. J. Radiat. Oncol. Biol. Phys.* **47** (1) 95-102

Gupta P, Malhotra A, Saxena S K, Gupta S, Bandhopadhyaya G P, Venkatesh M and Pandey U 2009 Radionuclide therapy of basal cell carcinoma with Phosphorus-32 skin patch *J. Nucl. Med.* **50** (Supplement 2) 158

Hanada T, Yorozu A, Ohashi T, Shigematsu N, Saito K, Maruyama K 2011 The effect of tissue composition of the prostate on the dose calculation for ^{125}I brachytherapy *Kitasato. Med. J*. **41** 136-144

Heilemann G, Nesvacil N, Blaickner M, Kostiukhina N and Georg D 2015 Multidimensional dosimetry of 106Ru eye plaques using EBT3 films and its impact on treatment planning *Med. Phys.* **42** (10) 5798-5808

Heintz B H, Wallace R E and Hevezi J M 2001 Comparison of I-125 sources used for permanent interstitial implants *Med. Phys.* **28** (4) 671-682

Hendee W R and Ibbott G S 1999 *Radiation Therapy Physics* Mosby St. Louis USA

Huang D C, Schell M C, and Weaver K A 1990 Dose distribution of ^{125}I sources in different tissues *Med. Phys.* **17** 826-832

Hubbell J H and Seltzer S M 1995 Tables of x-ray mass attenuation coefficients and mass energy-absorption coefficients 1 keV to 20 MeV for elements Z=1 to 92 and 48 additional substances of dosimetric interest. NIST Interagency Report No. 5632

Hubbell J H 2006 Review and history of photon cross section calculations *Phys. Med. Biol.* **51** R245-R262

IAEA 1989 Measurement of radionuclides in food and environment *Technical Report Series no. 295 of International Atomic Energy Agency* (Vienna)

IAEA 1999 Calibration of Brachytherapy Sources Guidelines on Standardized Procedures for the Calibration of Brachytherapy Sources at SSDLs and Hospitals *TECDOC-1079 of International Atomic Energy Agency* (Vienna)

IAEA 2002a Calibration of Photon and Beta Ray Sources Used in Brachytherapy Guidelines on Standardized Procedures at Secondary Standards Dosimetry Laboratories (SSDLs) and Hospitals *TECDOC-1079 of International Atomic Energy Agency* (Vienna)

IAEA 2002bCalibration of photon and beta ray sources used in brachytherapy *TECDOC 1274 of International Atomic Energy Agency* (Vienna)

IAEA 2004 Quantifying Uncertainty in Nuclear Analytical Measurements *TECDOC No.1401 of International Atomic Energy Agency* (Vienna)

ICRU 1976 Determination of absorbed dose in a patient irradiated by beams of x or gamma rays in radiotherapy procedures *Report 24 of the Int. Commission on Radiation Units and Measurements* (Bethesda, MD)

ICRU 1985 Dose and Volume Specification for Reporting Intracavitary Therapy in Gynecology *Report 38 of the Int. commission on Radiation Units and Measurements* (Bethesda, MD)

ICRU 1989 Tissue substitutes in radiation dosimetry and measurements *Report 44 of the Int. Commission on Radiation Units and Measurements* (Bethesda, MD)

ICRU 1997 Dosimetry of external beta rays for radiation protection *Report 56 of the Int. Commission on Radiation Units and Measurements* (Bethesda, MD)

ICRU1997Dose and Volume Specification for Reporting Interstitial Therapy *Report 58 of Int. Commission on Radiation Units and Measurements* (Bethesda, MD)

ICRU 1998 Fundamental Quantities and Units for Ionizing Radiation *Report 60 of the Int. Commission on Radiation Units and Measurements* (Bethesda, MD)

ICRU report 2004 Dosimetry of beta rays and low-energy photons for brachytherapy with sealed sources Report 72 *of the Int. Commission on Radiation Units and Measurements* (Bethesda, MD)

Janicki C, Duggan D M, Coffey C W, Fischell D R and Fischell T A 1997 Radiation dose from a phosphorous-32 impregnated wire mesh vascular stent *Med. Phys.* **24** 437-445

Jeong J M, Lee Y J, Kim E H Chang Y S, Kim Y J, Son M, Lee D S, Chung J and Myung Chul Lee 2003 Preparation of [188]Re labeled paper for treating skin cancer *Appl. Radiat. Isot.* **58** 551-555

Karaiskos P, Sakeliou L, Sandilos P and Vlachos L 2000a Limitations of the point and line source approximations for the determination of geometry factors around brachytherapy sources *Med. Phys.***27** 124-28

Karaiskos P, Angelopoulos A, Baras P, Rozaki-Mavrouli H, Sandilos P, Vlachos L and Sakelliou L 2000b Dose rate calculations around ^{192}Ir brachytherapy sources using a Sievert integration model *Phys. Med. Biol.* **45** 383-98

Karaiskos P, Angelopoulos A, Pantelis E, Papagiannis P, Sakelliou L, Kouwenhoven E and D. Baltas 2003 Monte Carlo dosimetry of a new ^{192}Ir pulsed dose rate brachytherapy source *Med. Phys.* **30** 9-16

Kawrakow I 2000 Accurate condensed history Monte Carlo simulation of electron transport. EGSnrc, the new EGS4 version *Med. Phys.* **27** 485-498

Kawrakow I, Mainegra-Hing E, Rogers D W O, Tessier F and Walters B R B 2013 The EGSnrc code system: Monte Carlo simulation of electron and photon transport *Technical Report* PIRS-701 National Research Council of Canada

Khan F M 2010 *The Physics of Radiation Therapy* 4th Edition (Philadelphia: Lippincott Williams & Wilkins)

Kirov S and Williamson J F 2001 Monte Carlo-aided dosimetry of the Source Tech Medical model STM1251 I-125 interstitial brachytherapy source *Med. Phys.* **28** 764-72

Knutsen S, Hafslund R, Monge O R, Valen H, Muren L P, Rekstad B L, Krohn J and Dahl O 2001 Dosimetric verification of a dedicated 3D treatment planning system for episcleral plaque therapy *Int. J. Radiat. Oncol. Biol. Phys.* **51** 1159-66

Koneru B, Shi Y, Munaweera I, Wight-Carter M, Kadara H, Yuan H, Di Pasqua A J and Balkus K J Jr 2016 Radiotherapeutic bandage for the treatment of squamous cell carcinoma of the skin *Nucl. Med. Biol.* **43** (6) 333-38

Kopf AW 1979 Computer analysis of 3531 basal cell carcinomas of the skin *J. Dermatol.* **6** 267-281

Krintz A, Hanson W F, Ibbott G S and Followill D S 2002 Verification of plaque simulator dose distributions using radiochromic film *Med. Phys.* **29** 1220-21

Krishnaswamy V 1972 Dose distribution about ^{137}Cs sources in tissue *Radiology* **105** 181-4

Krishnaswamy V 1979 Dose tables for ^{125}I seed implants *Radiology* **132** 727-30

Kubo H 1985 Exposure contribution from Ti K x rays produced in the titanium capsule of the clinical ^{125}I seed *Med. Phys.* **12** (2) 215-20

Kutcher G J, Coia L, Gillin M, Hanson W F, Leibel S, Morton R J, Palta J R, Purdy J A, Reinstein L E, Svensson G K, Weller M, and Wingfield L 1994 Comprehensive QA for radiation oncology: Report of AAPM Radiation Therapy Committee Task Group 40 *Med. Phys.* **21** 581-618

Landau L D, Pomeranchuk I Y 1953 The limits of applicability of the theory of bremsstrahlung by electrons and of creation of pairs at large energies (In Russian) *Dokl. Akad. Nauk* SSSR **92** 535

Lee J D, Park K K, Lee M G, Kim E H, Rhim K J, Lee J T, Yoo H S, Kim Y M, Park K B and Kim J R 1997 Radionuclide therapy of skin cancers and Bowen's disease using a specially designed skin patch *J. Nucl. Med.* **38** 697-701

Lee C D 2014 Recent developments and best practice in brachytherapy treatment planning *Br. J. Radiol.* **87** 20140146

Lewis D, Micke A, Yu X and Chan M 2012 An efficient protocol for radiochromic film dosimetry combining calibration and measurement in a single scan *Med. Phys.* **39** 6339-50

Li Z, Das R K, DeWerd L A, Ibbott G S Meigooni A S, Pérez-Calatayud J, Rivard M J, Sloboda R S and Williamson J F 2007 Dosimetric prerequisites for routine clinical use of photon emitting brachytherapy sources with average energy higher than 50 keV. *Med. Phys.* **34** 37-40

Lorence L J Jr and Beutler D E 1997 Radiation transport phenomena and modeling. Part A: codes *Technical Report* Sandia Report

Mainegra E, Capote r and Lopez E 1998 Dose rate constants for 103Pd, 125I, 196Yb, 192Ir, brachytherapy sources: An EGS4 Monte Carlo study *Phys. Med. Biol.* **43** 1557-66

Mallath M K *et al.* 2014 The growing burden of cancer in India: epidemiology and social context *Lancet. Oncol.* **15** 205-12

Martisikova M, Ackermann B and Jakel O 2008 Analysis of uncertainties in Gafchromic EBT film dosimetry of photon beams *Phys. Med. Biol.* **53** 7013-27

Massillon-JL G, Chiu-Tsao S T, Domingo-Munoz I and Chan M F 2012 Energy dependence of the new GafChromic EBT3 film: Dose response curves for 50 kV, 6 and 15 MV x-ray beams *Int. J. Med. Phys. Clin. Eng. Radiat. Oncol.* **1** 60-65

MCNP 5 2003 X-5 Monte Carlo TeamA General Monte Carlo N-Particle Transport Code Version 5Los Alamos National Laboratory (Los Alamos, NM, USA)

Medich D C, Tries M A and Munro J J 2006 Monte Carlo characterization of an ytterbium-169 high dose rate brachytherapy source with analysis of statistical uncertainty *Med. Phys.* **33** 163-72

Medich D C and Munro J J 2010 Dependence of Yb-169 absorbed dose energy correction factors on self-attenuation in source material and photon buildup in water *Med. Phys.* **37** (5) 2135-44

Meisberger L L, Keller R J and Shalek R J 1968 The effective attenuation in water of the gamma rays of Au-198, Ir-192, Cs-137, Ra-226, and Co-60 *Radiol.* **90** 953-57

Meigooni A S, Meli J A and Nath R 1992a Interseed effects on dose for ^{125}I brachytherapy implants *Med. Phys.* **19** 385-90

Meigooni A S and Nath R 1992bTissue inhomogeneity correction for brachytherapy sources in a homogeneous phantom with cylindrical symmetry *Med. Phys.* **19** 401-407

Meigooni A S, Dini S A, Sowards K, Hayes J L and Al-Otoom A *2002* Experimental determination of the TG-43 dosimetric characteristics of Echo Seed model 6733 ^{125}I brachytherapy source *Med. Phys.* **29** 939-42

Meigooni A S, Rachabatthula V, Awan S B and Koona R A 2005 Comment on 'Update of AAPM Task Group No. 43 Report: A revised AAPM protocol for brachytherapy dose calculations *Med. Phys.* **32** (6) 1820-1821

Melia B M, Abramson D H, Albert D M, Boldt H C, Earle J D, Hanson W F et al 2001 Collaborative Ocular Melanoma Study (COMS) randomized trial of 125I brachytherapy for medium choroidal melanoma. I. Visual acuity after 3 years. COMS report no. 16. *Ophthalmol.* **108** 348-66

Menegotti L, Delana A, and Martignano A 2008 Radiochromic film dosimetry with flatbed scanners: A fast and accurate method for dose calibration and uniformity correction with single film exposure *Med. Phys.* **35**, 3078-85

Meridith W J 1947 *Radium Dosage: The Manchester System* (Edinburg, UK: Livingston Ed.)

Mobit P and Badragan Iulian 2004 Dose perturbation effects in prostate seed implant brachytherapy with I-125 *Phys. Med. Biol.* **49** 317 -78

Moller C 1932 Zur Theorie des Durchgangs schneller Elektronen durch Materie. *Ann.Phys.* **406** 531 - 585

Montagna W and Carlisle K J 1991 The architecture of black and white facial skin *Am. Acad. Dermatol.* **24** 929-37

Morrison H, Geetha Menon and Ron S. Sloboda 2014 Radiochromic film calibration for low-energy seed brachytherapy dose measurement *Med. Phys.* **41** (7) 072101-1

Mukherjee A, Pandey U, Sarma H D, Pillai M R A and Venkatesh M 2002 Preparation and evaluation of ^{90}Y skin patches for therapy of superficial tumours in mice *Nucl. Med. Commun.* **23** 243-47

Mukherjee A, Pandey U, Sarma H D, Gupta S K, Ingle A D, Pillai M R A and Venkatesh M 2003 Bioevaluation of radioactive bandages in a murine model of melanoma *Int. J. Radiat. Biol.* **79** 839 - 45

Munro J J, Medich D and Mutyala S 2008 Intraoperative high dose rate brachytherapy using Thulium-170 radiation sources *Brachytherapy* **7** 160

Murphy M K, Piper R K, Greenwood L R, Mitch M G, Lamperti P J, Seltzer S M, Bales M J and Phillips M H 2004 Evaluation of the new cesium-131 seed for use in low-energy x-ray brachytherapy *Med. Phys.* **31** 1529-38

Nag S, Beyer D, Friedland J, Grimm P and Nath R 1999 American Brachytherapy Society (ABS) recommendations for transperineal permanent brachytherapy of prostate cancer *Int. J. Radiat. Oncol. Biol. Phys.* **44** 789-799

Nag S, Bice W, DeWyngaert K, Prestidge B, Stock R and Yu Y 2000 The American Brachytherapy Society recommendations for permanent prostate brachytherapy post implant dosimetric analysis. *Int. J. Radiat. Oncol. Biol. Phys.* **46** 221-230

Nath R, Meigooni AS, Muench P and Melillo A 1993 Anisotropy functions for ^{103}Pd, ^{125}I and ^{192}Ir interstitial brachytherapy sources *Med. Phys.* **20** 1465-73

Nath R, Anderson L L, Luxton G, Weaver K A, Williamson J F and Meigooni A S 1995 Dosimetry of interstitial brachytherapy sources: Recommendations of the AAPM Radiation Therapy Committee Task Group No. 43 *Med. Phys.* **22** 209-34

Nath R, Anderson L L, Meli J A, Olch A J, Stitt J A and J. F. Williamson 1997 Code of practice for brachytherapy physics: Report of the AAPM Radiation Therapy Committee Task Group No. 56 *Med. Phys.* **24** 1557-98

Nath R *et al.* 1999a Intravascular brachytherapy physics: Report of the AAPM Radiation Therapy Committee Task Group No. 60 *Med. Phys.* **26** 119-152

Nath R, Yue N, and Liu L 1999b On the depth of penetration of photons and electrons for intravascular brachytherapy *Cardiovasc. Radiat . Med*. **1** (1) 72-79

Nath R 2005 Sources and Delivery Systems I: Radionuclides *Brachytherapy Physics* 2nd edn ed B R Thomadsen, M J Rivard and W M Butler (Madison, WI: Medical Physics Publishing) pp 25-30

NICPR 2018 National Institute of Cancer Prevention and Research under *Indian Council of Medical Research (ICMR),* accessed 10 July 2018 (http://cancerindia.org.in/ statistics/)

NIH, ImageJ software, National Institute of Health (Bethesda, MD), (http://rsbweb.nih.gov/ ij/docs/faqs.html)

NNDC 2003 Lu177 spectrum National Nuclear Data Center, Brookhaven National Laboratory (www.nndc.bnl.gov /nudat2, dataset#1, F.G. Kondev Nuclear Data Sheets 98 80

Niroomand-Rad A, Blackwell C R, Coursey B M, Gall K P, Galvin J M, McLaughlin W L, Meigooni A S, Nath R, Rodgers J E and Soares C G 1998 Radiochromic film dosimetry: Recommendations of AAPM Radiation Therapy Committee Task Group 55 *Med. Phys.* **25** 2093-2115

Panda S 2010 Nonmelanoma Skin Cancer in India: Current Scenario *Indian J. Dermatol.* **55**(4) 373-8

Pandey U, Saxena S K, Sarma H D, Tandon P, Rama R, Samuel G, Dash A and Venkatesh M 2008 Bioevaluation studies of ^{32}P incorporated mould brachytherapy sources for potential application in treatment of superficial tumors *Nucl. Med. Commun.* **29** 717-723

Papagiannis P, Angelopoulos A, Pantelis E, Sakelliou L, Baltas D, Karaiskos P, Sandilos P and Vlachos L 2002 Dosimetry comparison of ^{192}Ir sources *Med. Phys.* **29** (10) 2239 - 46

Papagiannis P, Angelopoulos A, Pantelis E, Sakelliou L, Karaiskos P and Shimizu Y 2003 Monte Carlo dosimetry of ^{60}Co HDR brachytherapy sources *Med. Phys.* **30** 712–21

Park Y K, Ye S J, Kim I H, Wee W R, Kim M K, Han H S, Son K and Park U J 2008 Potential use of ^{32}P ophthalmic applicator: Monte Carlo simulations for design and dosimetry *Med. Phys.* **35** 1854-1858

Pérez-Calatayud J, Ballester F, Serrano-Andre s M A, Puchades V, Lluch J L, Limami Y and Casal F 2001 Dosimetry characteristics of the Plus and 12i GammaMed PDR ^{192}Ir sources *Med. Phys.* **28** 2576-85

Perez-Calatayud J, Granero D, and Ballester F 2004 Phantom size in brachytherapy source dosimetric studies *Med. Phys.* **31** (7) 2075-2081

Perez-Calatayud J, Granero D C, Ballester F P 2009 Monte Carlo Application in Brachytherapy Dosimetry. Y. Lemoigne and A. Cancer (Eds.) *Radiotherapy and Brachytherapy* (New York: Springer Science) p-239

Perez-Calatayud J, Ballester F, Das R K, Dewerd L A, Ibbott G S, Meigooni A S, Ouhib Z, Rivard M J, Sloboda R S and Williamson J F 2012 Dose calculation for photon-emitting brachytherapy sources with average energy higher than 50 keV: Report of the AAPM and ESTRO *Med. Phys.* **39** 2904-2929

Poder J and Corde S 2013a I-125 ROPES eye plaque dosimetry: Validation of a commercial 3D-ophthalmic brachytherapy treatment planning system and independent dose calculation software with GafChromic ® EBT3 films *Med. Phys.***40** (12), 121709-1

Poder J, Annabell N, Geso M, Alqathami M and Corde S 2013b ROPES eye plaque dosimetry: commissioning and verification of an ophthalmic brachytherapy treatment planning system *J. Phys.Conf. Ser.* **444** 012102 (doi:10.1088/1742-6596/444/1/012102)

Podgorsak E B and Podgorsak M B 2005 Special Procedures and Techniques in *Radiotherapy Radiation Oncology Physics: A Handbook for Teachers and Students* ed Podgorsak E B et al Chap 15 International Atomic Energy Agency Vienna (ISBN 92–0–107304–6)

Prestidge B, Bice W S, Jurkovic I, Walker E, Marianne S and Sadeghi A *2005* Cesium-131 permanent prostate brachytherapy: An initial report Int. J. Radiat. Oncol. Biol. Phys. **63** S336-S337

Pruitt J S 1987 Calibration of beta particle-emitting ophthalmic applicators NBS Special Publication p-250 July

Raina S, Avadhani J S, Oh M, Malhotra H K, Jaggernauth W, Kuettel M R and Podgorsak M B 2005 Quantifying IOHDR brachytherapy under dosage resulting from an incomplete scatter environment *Int. J. Rad. Onco. Biol. Phys.* **61** 1582-86

Ravi A, Keller B and Pignol J 2011 Evaluation of the radiation safety of using Cs-131 seeds for permanent breast seed implantation *Int. J. Radiat. Oncol. Biol. Phys.* **81** S720-S721

Rivard M J, Coursey B M, DeWerd L A, Hanson W F, Huq M S, Ibbott G S, Mitch M G, Nath R and Williamson J F 2004 Update of AAPM Task Group Report No.43: A revised AAPM protocol for brachytherapy dose calculations *Med. Phys.* **31** 633-74

 Rivard M J 2007 Brachytherapy dosimetry parameters calculated for a ^{131}Cs source *Med. Phys.* **34** 754-62

Rivard M J, Butler W M, DeWerd L A, Huq M S, Ibbott G S, Meigooni A S, Melhus C S, Mitch M G, Nath R and Williamson J F 2007 Supplement to the 2004 update of the AAPM Task Group No. 43 Report. *Med. Phys.* **34** (6) 2187-2205

Rivard M J, Melhus C S, Sioshansi S and Morr J 2008 The impact of prescription depth, dose rate, plaque size, and source loading on the central axis using 103Pd, 125I, and 131Cs *Brachytherapy* **7** 327-335

Rivard M J, Venselaar J L M and Beaulieu L 2009a The evolution of brachytherapy treatment planning *Med. Phys.* **36** 2136-2153

Rivard M J, Melhus C and Williamson J F 2009b Brachytherapy Dose Calculation Formalism, Dataset evaluation, and Treatment Planning System Implementation. AAPM Summer School: Clinical Dosimetry Measurements in Radiotherapy (23 June 2009) at Colorado College, CO (https://www.aapm.org/meetings/09SS/documents/13Rivard-TG-43FormalismforBrachytherapy .pdf)

Rivard M J, Buller W M, DeWerd L A, Ibbott G S, Meigooni A S, Melhus C S, Mitch M G and Nath R 2010 Erratum: Supplement to the 2004 update of the AAPM Task Group No. 43 Report: A revised AAPM protocol for brachytherapy dose calculations *Med. Phys.* **37** 2396

Roa D E, Song H, Yue N, d'Errico F and Nath R 2004 Dosimetric characteristics of the Novoste Beta-Cath 90Sr/Y source trains at sub-millimeter distances *Med. Phys.* **31** 1269

Rogers D W O and Bielajew A F 1990 Monte Carlo Techniques of Electron and Photon Transport for Radiation Dosimetry *The Dosimetry of Ionizing Radiation* ed Kase K R, Bjarngard B E and Attix F H Chapter 5, Vol. III (Academic Press)

Rogers D W O 2006 Fifty years of Monte Carlo simulations for medical physics. *Phys. Med. Biol.* **51** R287-R301

Rogers D W O, Kawrakow I, Seuntjens J P, Walters B R B and Mainegra-Hing E 2010 NRC user codes for EGSnrc Technical Report PIRS-702 (rev. B) National Research Council of Canada

RPC 2005 Radiological Physics Center The M.D. Anderson Cancer Center, Houston, TX http://rpc.mdanderson. org/rpc/htm/Home_htm/Low-energy.html (last accessed May 1, 2005)

Russa D J La and Rogers D W O 2006 An EGSnrc investigation of the P_{TP} correction factor for ion chambers in kilovoltage x-rays *Med. Phys.* **33** 4590-99

Russa D J. La, Malcolm McEwen and Rogers D W O 2007 An experimental and computational investigation of the standard temperature-pressure correction factor for ion chambers in kilovoltage x-rays *Med. Phys.* **34** 4690-99

Sahoo S and Selvam T P 2009 An EGSnrc investigation of the air-kerma strength, dose rate constant, and radial dose function of ^{125}I brachytherapy sources *Radiol. Phys. Tech.* **2** 198-204

Sahoo S, Selvam T P, Vishwakarma R S and Chourasiya G 2010 Monte Carlo modeling of ^{60}Co HDR brachytherapy source in water and in different solid water phantom materials. *J. Med. Phys.* **35** (1) 57-64

Sahoo S and Selvam T P 2014 Comment on "Design and bioevaluation of a ^{32}P-patch for brachytherapy of skin diseases (Appl. Radiat. Iso. 66, 303–309, 2008) *Appl. Radiat. Iso.* **91** 62- 63

Saidi P, Sadeghi M, Shirazi A 2011 Claudio Tenreiro ROPES eye plaque brachytherapy dosimetry for two models of 103Pd seeds *Australas. Phys. Eng. Sci. Med.* **34** 223-231

Salgueiro M J, Duran H, Palmieri M, Rosana P, Vanina M, Ricardo U, Maximo C, Jorge N and Marcela Z 2008a Bioevaluation of ^{32}P patch designed for the treatment of skin diseases *Nucl. Med. Biol.* **35** 233-37

Salgueiro M J, Duran H, Palmieri M, Pirchio R, Nicolini J, Ughetti R, Papparella M L, Casale G and Zubillaga M 2008b Design and bioevaluation of a ^{32}P-patch for brachytherapy of skin diseases *Appl. Radiat. Isot.* **66** 303-309

Salvat F, Fernandez-Varea J M, Baro J, Sempau J 1996 PENELOPE, an algorithm and Computer code for Monte Carlo simulation of electron photon showers. CIEMAT Report n. 799. Madrid

Sanchez-Reyes A, Tello J J, Guix B, Salvat F 1998 Monte Carlo calculation of the dose distributions of two 106Ru eye applicators *Radiotherapy and Oncology* **49** 191-196

Sauter F 1931 Uber den atomaren Photoeffekt bei grosser H¨arte der anregenden Strahlung *Ann. Physik* 9 217 - 247

Saxena S K, Yogendra K and Dash A 2012 Nafion-Zirconium phosphate composite membrane: A new approach to prepare ^{32}P patches for superficial brachytherapy applications *Cancer. Biother. Radiopharm.* **27**(4) 276-84

Saxena S K, Pandey U, Chakravarty R, Kumar Y, Sarma H D and Dash A 2014 On the Application of Nafion Membrane for the Preparation of 90Y Skin Patches, Quality Control, and Biological Evaluation for Treatment of Superficial Tumors *Cancer Biotherapy & Radiopharmaceuticals* **29**(5) 200-209

Saxena S K, Yogendra K, Shetty P, Dash A 2015 Studies on the development of Nafion-115 based ^{177}Lu-patches for their application in superficial brachytherapy of skin cancer Proceedings of NUCAR, 494-5

Seltzer S M, Berger M J 1985 Bremsstrahlung spectra from electron interactions with screened nuclei and orbital electrons *Nucl. Instr. Meth.* **B12** 95 – 134

Selvam T P and Rogers D W O 2008 Inclusion of Bragg-Gray Stopping Power Ratios in the EGSnrc User-code SPRRZnrc Report CLRP 06-010 Ottawa-Carleton Institute of Physics, Carleton University, Ottawa, KIS, 5B6 physics.carleton.ca/~drogers/pubs/papers/bgspr.pdf

Selvam T P, Sahoo S and Vishwakarama R S 2009 EGSnrc-based Monte Carlo dosimetry of CSA1 and CSA2 ^{137}Cs brachytherapy source models *Med. Phys.* **36** 3870-79

Selvam T P and Bhola S 2010 Technical Note: EGSnrc-based dosimetric study of the BEBIG[60]Co HDR brachytherapy sources *Med. Phys.* **37** 1365

Shanta A, Tripathi U B, Vandana S and Bhatt B C 2005 Dosimetry of ophthalmic applicator susing ^{125}I seed sources J. *Med. Phys.* **30** (1) 14 -19

Sharma S D, Shanta A, Palani Selvam T, Tripathi U B and Bhatt B C 2004 Medical physics aspects of ophthalmic brachytherapy BARC Report (BARC/2004/E/036) p-19

Sharma S D, Basu M, Shanta A, Selvam T P, Tripathi U B and Bhatt B C 2005 Dosimetry parameters of BARC OcuProsta ^{125}I seed source *Austra. Phys. Eng. Sci. Med*. **28** 14-20

Sheridan A T and Dawber R P 2000 Curettage, electrosurgery and skin cancer *Australas. J. Dermatol.* **41** 19-30

Sievert R M 1921 Die Intensitatsverteilung der primaren: Strahlung in der Nahe Medizinischer Radiumpraparate. *Acta. Radiol.* **1** 89-128

Skowronek J, Zwierzchowski G and Piotrowski T 2001 Pulsed dose rate brachytherapy – Description of a method and a review of clinical applications *Rep. Pract. Oncol. Radiother*. **6** 4

Snyder W S, Cook M J, Nasset E S et al 1974 Report of the task group on reference man. Technical Report No. 23. *ICRP (International Commission on Radiological Protection)*

Soares C G 1991 Calibration of ophthalmic applicators at NIST: A revised approach *Med. Phys.* **18** 787-93

Soares C G and McLaughlinW L1993 Measurement of radial dose distributions around Small beta particle emitters using high resolution radiochromic foil dosimetry *Radiat. Prot. Dosim.* **47** 367-372

Soares C G, Vynckier S, Jarvinen H, Cross W G, Sipila P, Fluhs D, Schaeken B, Mourtada F A, Bass G A and Williams T T 2001 Dosimetry of beta-ray ophthalmic applicators: Comparison of different measurement methods *Med. Phys.* **28** (7) 1373-1384

Sorriaux J, Kacperek A, Rossomme S, Lee J A, Bertrand D, Vynckier S and Sterpin E 2013 Evaluation of Gafchromic EBT3 films characteristics in therapy photon, electron and proton beams *Physica Medica* **29** 599 - 606

Sowards K T and Meigooni A S 2002 A Monte Carlo evaluation of the dosimetric characteristics of the EchoSeed^{TM} model 6733 ^{125}I brachytherapy source *Brachytherapy* **1** 226-232

Storm E and Israel H I 1970 Photon cross sections from 1 keV to 100 MeV for elements Z=1 to Z=100, Atomic Data and Nuclear Data Tables **7** 565-681

Stokes S H, Real J D, Adams P W, Clements J C, Wuertzer S and Kan W 1997 Transperineal ultrasound-guided radioactive seed implantation for organ-confined carcinoma of the prostate *Int. J Radiat. Oncol. Biol. Phys.* **37** 337-41

Sudhir K, Srinivasan P, Sharma S D, Saxena S K, Bakshi A K, Dash A, Babu D A R and Sharma D N 2015 Determination of surface dose rate of indigenous ^{32}P patch brachytherapy source by experimental and Monte Carlo methods *App. Rad. Iso.* **103** 120-27

Suntharalingam N, Podgorsak E B and Tölli H 2005 Brachytherapy: Physical and clinical aspects in *Radiotherapy Radiation Oncology Physics: A Handbook for Teachers and Students* ed Podgorsak E B et al Chap 13 International Atomic Energy Agency Vienna (ISBN 92–0–107304–6)

Sutherland J G H, Furutani K M, Garces Y I and Thomson R M 2012 Model-based dose calculations for ^{125}I lung brachytherapy *Med. Phys.* **39** 4365-77

Tailor R, Geoffrey I, Stephanie L, Whitney B W and Naresh T 2008 Dosimetric characterization of a ^{131}Cs brachytherapy source by thermoluminescence dosimetry in liquid water *Med. Phys.* **35** (12) 5861-68

Taylor R E P 2006 Monte Carlo calculations for brachytherapy," M.Sc. thesis, Carleton University, Ottawa, Canada

Taylor R E P, Yegin G and Rogers D W O 2007 Benchmarking BrachyDose: Voxel based EGSnrc Monte Carlo calculations of TG-43 dosimetry parameters *Med. Phys.* **34** 445-57

Taylor R E P and Rogers D W O 2008 An EGSnrc Monte Carlo-calculated database of TG-43 parameters *Med. Phys.* **35** 4228-4241

Ter-Mikaelyan M L 1954 Bremsstrahlung radiation spectrum in a medium *Dokl. Akad. Nauk* SSSR **94** 1033

Thomadsen B R, Rivard M J and Butler W M 2005 (Eds.) *Brachytherapy Physics*. 2nd ed. Proceedings of the Joint AAPM and ABS Summer School. Medical Physics Publishing

Thomson R M, Taylor R E P and Rogers D W O 2008 Monte Carlo dosimetry for ^{125}I and ^{103}Pd eye plaque brachytherapy *Med. Phys.* **35** 5530-43

Thomson R M and Rogers D W O 2010 Monte Carlo dosimetry for 125I and 103Pd eye plaque brachytherapy with various seed models *Med. Phys.* **37** 368-376

Vandana S, Bakshi *A K,* Saxena S K, Arghya C, Palani Selvam T, Srivastava K, Dash A and Datta D 2016 Characterisation of ^{32}P beta source for external radiation protection *Radiat. Meas.* **89** 52-62

Villarreal-Barajas J E and Khan R F H 2014 Energy response of EBT3 radiochromic films: implications for dosimetry in kilovoltage range *J. App. Clin. Med. Phys.* **15** 331-8

Waksman R and Crocker I R 1996 Radiation for prevention of restenosis: where are we? *Int. J. Radiat. Oncol. Biol. Phys.* **36** 959-961

Wallace S A, Schumera W and Horrigan M 2002 Monte Carlo dosimetry of a tandem positioned beta-emitting intravascular brachytherapy source train *Med. Phys.* **29** 544-549

Walters B, Kawrakow I and Rogers D W O 2009 DOSXYZnrc users manual, NRCC Report PIRS-794 (rev. B) National Research Council of Canada Ottawa Canada

Wang R and Sloboda R S 1996 Accuracy of NPS calculated HDR Ir-192 source dosimetry for endobronchial brachytherapy *Med. Phys.* **23** 804 (abstract)

Wang R and Sloboda R S 1998 Monte Carlo dosimetry of the VariSource high dose rate ^{192}Ir source *Med. Phys.* **25** 415-23

Wang R and Li X A 2000 A Monte Carlo calculation of dosimetric parameters of ^{90}Sr/^{90}Y and ^{192}Ir SS sources for intravascular brachytherapy *Med. Phys.* **27** 2528-2535

Wang R and Li X A2002 Dose characterization in the near-source region for two high dose rate brachytherapy sources *Med. Phys.* **29** (8) 1678-86

WHO 2017a World Health Organisation (http://www.who.int/cancer/en/, accessed August 10, 2017)

WHO 2017b World Health Organisation Ultraviolet radiation and the INTERSUN Programme   Skin cancers, http://www.who.int/uv/faq/skincancer/en/index1. html. (accessed June 06, 2017)

Williamson J F, Morin R L and Khan F M 1983 Monte Carlo evaluation of the Sievert integral for brachytherapy dosimetry *Phys. Med. Biol.* **28** 1021-32

Williamson J F 1987 Monte Carlo evaluation of kerma at a point for photon transport Problems *Med. Phys.* **14** 567-76

Williamson J F 1988 Monte Carlo evaluation of specific dose constants in water for ^{125}I seeds *Med. Phys.* **15** (5) 686-94

Williamson J F 1991 Comparison of measured and calculated dose rates in water near I-125 and Ir-192 seeds *Med. Phys.* **18** 776-786

Williamson J F, Tomadsen B R and Nath R 1995 *Brachytherapy Physics* (Madison: Medical Physics Publishing)

Williamson J F and Li Z 1995 Monte Carlo aided dosimetry of the microSelectron pulsed and high dose-rate ^{192}Ir sources *Med. Phys.* **22** 809-19

Williamson J F 1996 The Sievert integral revisited: evaluation and extension to ^{125}I, ^{169}Yb, and ^{192}Ir brachytherapy sources *Int. J. Radiat. Oncol. Biol. Phys.* **36** 1239-50

Williamson J F, Coursey B M, DeWerd L A, Hanson W F and Nath R 1998 Dosimetric prerequisites for routine clinical use of new low energy photon interstitial brachytherapy sources *Med. Phys.* **25** 2269-70

Williamson J F 2005 Semi-empirical dose-calculation models in brachytherapy *Brachytherapy Physics* 2nd edn ed B R Thomadsen, M J Rivard and W M Butler (Madison, WI: Medical Physics Publishing) pp 201-2

Wittman R S and Fisher D R 2007 Multiple-estimate Monte Carlo calculation of the dose rate constant for a Cs-131 interstitial brachytherapy seed *Med. Phys.* **34** 49-54

Xu Y P, Yang M, Pan D H, Wang L Z, Liu Lu, Huang P and Shao G 2012 Bioevaluation study of 32P-CP-PLLA particle brachytherapy in a rabbit VX2 lung tumor model *Appl. Radiat. Isot.***70** 583-588

Yan W et al 2010 Cesium-131 brachytherapy for lung cancer: Dosimetric, safety considerations and initial experience *Int. J. Radiat. Oncol., Biol., Phys.* **78** S540-S541

Yang Y and Rivard M J 2011 Evaluation of brachytherapy lung implant dose distributions from photon-emitting sources due to tissue heterogeneities *Med. Phys.* **38** 5857-62

Dosimetry of indigenously developed ^{177}Lu patch source for surface brachytherapy— Experimental and Monte Carlo methods

Sridhar Sahoo[1,4,5]**, Vandana Shrivastava**[1]**,
T Palani Selvam**[1,4]**, A K Bakshi**[1,4]**, Rajesh Kumar**[1]**, P Rama**[1]**,
D Datta**[1,4]**, S Chinnaesakki**[2]**, S K Saxena**[3]**,
Yogendra Kumar**[3] **and A Dash**[3,4]

[1] Radiological Physics & Advisory Division, Bhabha Atomic Research Centre,
Mumbai—400 085, India
[2] Health Physics Division, Bhabha Atomic Research Centre, Mumbai—400 085, India
[3] Radiopharmaceuticals Division, Bhabha Atomic Research Centre, Mumbai—400
085, India
[4] Homi Bhabha National Institute, Mumbai—400 094, India

E-mail: barcsridhar@gmail.com

CrossMark

Abstract

This paper describes the evaluation of dosimetry characteristics of an in-house developed ^{177}Lu skin patch source for treatment of non-melanoma skin cancer. A ^{177}Lu skin patch source based on Nafion-115 membrane backbone containing 3.46 ± 0.01 mCi of activity was used. Activity measurement of the patch source was based on gamma ray spectrometry using a HPGe detector. The efficiencies of the HPGe detector were fitted using an orthogonal polynomial function. The absorbed dose rate to water at 5 μm depth in water was determined using an extrapolation chamber, EBT3 Gafchromic film and compared with Monte Carlo methods. The correction factors such as Bragg-Gray stopping power ratio of water-to-air and chamber wall material being different from water, needed to be applied on measurements for establishing the dose rate at 5 μm depth, were calculated using the Monte Carlo method. Absorbed dose rate at 5 μm depth in water (surface dose rate) measured using an extrapolation chamber and EBT3 Gafchromic film were 9.9 ± 0.7 and 8.2 ± 0.1 Gy h^{-1} mCi^{-1} respectively for the source activity of 3.46 ± 0.01 mCi. The surface dose rate calculated using the Monte Carlo method was 8.7 ± 0.2 Gy h^{-1} mCi^{-1}, which agrees reasonably well with measurement. The measured dose rate per mCi offers scope for ascertaining

[5] Author to whom any correspondence should be addressed.

Original Article

Dosimetry of indigenously developed ^{192}Ir high-dose rate brachytherapy source: An EGSnrc Monte Carlo study

Sridhar Sahoo, T. Palani Selvam, S. D. Sharma, Trupti Das[1], A. C. Dey[1], B. N. Patil[1], K. V. S. Sastri[1]

Radiological Physics and Advisory Division, Bhabha Atomic Research Centre, [1]Board of Radiation Isotope and Technology, Vashi, Navi Mumbai, Maharashtra, India

ABSTRACT

Clinical application using high-dose rate (HDR) ^{192}Ir sources in remote afterloading technique is a well-established treatment method. In this direction, Board of Radiation and Isotope Technology (BRIT) and Bhabha Atomic Research Centre, India, jointly indigenously developed a remote afterloading machine and ^{192}Ir HDR source. The two-dimensional (2D) dose distribution and dosimetric parameters of the BRIT ^{192}Ir HDR source are generated using EGSnrc Monte Carlo code system in a 40 cm dia × 40 cm height cylindrical water phantom. The values of air-kerma strength and dose rate constant for BRIT ^{192}Ir HDR source are $9.894 \times 10^{-8} \pm 0.06\%$ UBq^{-1} and $1.112 \pm 0.11\%$ cGyh^{-1}U^{-1}, respectively. The values of radial dose function ($g_L(r)$) of this source compare well with the corresponding values of BEBIG, Flexisource, and GammaMed 12i source models. This is because of identical active lengths of the sources (3.5 mm) and the comparable phantom dimensions. A comparison of $g_L(r)$ values of BRIT source with microSelectron-v1 show differences about 2% at r = 6 cm and up to 13% at r = 12 cm, which is due to differences in phantom dimensions involved in the calculations. The anisotropy function of BRIT ^{192}Ir HDR source is comparable with the corresponding values of microSelectron-v1 (classic) HDR source.

Key words: Brachytherapy; ^{192}Ir high-dose rate source; TG43; EGSnrc Monte Carlo

Introduction

In brachytherapy, sealed radioactive sources are placed near or inside a tumor, to deliver prescribed radiation dose to tumor by intracavitary, interstitial, or surface mold technique. In this treatment modality, a high radiation dose can be delivered locally to the tumor with rapid dose falloff in the surrounding normal tissue.

^{192}Ir high-dose rate (HDR) sources are widely used in brachytherapy treatment because of remote afterloading technology that reduces exposure to hospital personnel, high source activity, higher dose rate, short treatment time, and more important is comfort to patient. Many HDR ^{192}Ir source models such as microSelectron-v1 (classic), microSelectron-v2, BEBIG GmBH, VariSource (classic), VariSource (VS2000), Flexisource, and GammaMed 12i are available worldwide for clinical applications.[1-7]

Board of Radiation and Isotope Technology (BRIT) and Bhabha Atomic Research Centre (BARC) jointly developed a remote afterloading HDR machine (Karknidon) for brachytherapy treatments. Seven machines have been already

Address for correspondence:
Mr. Sridhar Sahoo,
Radiological Physics and Advisory Division, Bhabha Atomic Research Centre, Room No. 204, CT and CRS Building, Anushaktinagar, Mumbai - 400 094. Maharashtra, India.
E-mail: barcsridhar@gmail.com

Access this article online	
Quick Response Code:	**Website:** www.jmp.org.in
	DOI: 10.4103/0971-6203.181639

Monte Carlo-based dose calculation for ^{32}P patch source for superficial brachytherapy applications

Sridhar Sahoo, Selvam T. Palani, S. K. Saxena^1, D. A. R. Babu, A. Dash^1

Radiological Physics and Advisory Division, Bhabha Atomic Research Centre, ^{1}Isotope Production and Applications Division, Bhabha Atomic Research Centre, Mumbai, Maharashtra, India

ABSTRACT

Skin cancer treatment involving ^{32}P source is an easy, less expensive method of treatment limited to small and superficial lesions of approximately 1 mm deep. Bhabha Atomic Research Centre (BARC) has indigenously developed ^{32}P nafion-based patch source (1 cm × 1 cm) for treating skin cancer. For this source, the values of dose per unit activity at different depths including dose profiles in water are calculated using the EGSnrc-based Monte Carlo code system. For an initial activity of 1 Bq distributed in 1 cm^2 surface area of the source, the calculated central axis depth dose values are 3.62×10^{-10} GyBq^{-1} and 8.41×10^{-11} GyBq^{-1} at 0.0125 and 1 mm depths in water, respectively. Hence, the treatment time calculated for delivering therapeutic dose of 30 Gy at 1 mm depth along the central axis of the source involving 37 MBq activity is about 2.7 hrs.

Key words: ^{32}P patch; brachytherapy; dosimetry; nafion; skin cancer

Introduction

Basal cell carcinoma is one of the most common skin cancers, occurs mostly in middle aged people, and is more probable for the fair complexion people.[1] The treatment modalities for skin cancers are surgical excision, radiotherapy and chemotherapy. Each treatment modality has its own advantages and disadvantages. Removing the affected area by surgical excision is usually preferred in many cases, but the recurrence rates after treatment are high. Radiotherapy treatment using external beam therapy is too expensive and it also delivers unnecessary dose to underlying normal tissues. Chemotherapy has its own side effects.

Mould or superficial brachytherapy is a promising alternative treatment method for such skin cancers, where high-energy beta emitting radio-nuclides such as ^{32}P, ^{90}Sr/^{90}Y, ^{188}Re are used to overcome the disadvantages of radiotherapy and surgery. In superficial brachytherapy, prescribed dose can be delivered to the affected area without excessive damage to the neighboring normal tissues. This technique is simple, less trauma to patients, and less expensive as compared to external beam therapy.

Lee et al., introduced the treatment of skin cancer and Bowen's disease using beta emitting ^{165}Ho-impregnated patch sources.[2] Successful tumor destruction was observed both in animal and human studies. Mukherjee et al., in their studies evaluated ^{90}Y skin patches and ^{188}Re radioactive bandages for therapy of superficial tumors in mice.[3,4] Treatment of skin cancer using ^{188}Re-labeled paper patches has been reported by Jeong et al.[5]

Pandey et al., reported the use of ^{32}P cellulose-based adsorbent paper skin patches to control the tumor regression in C57BL6 mice bearing melanoma.[6] Park et al.,[7] studied the use of ^{32}P ophthalmic applicator after pterygium and glaucoma surgeries. They demonstrated that dose distributions obtained using the ^{32}P source is beneficial for reducing the incidence rate of radiation-induced cataract and it can deliver therapeutic doses to the surface of the conjunctiva while sparing the lens better than the ^{90}Sr/^{90}Y applicators. Xu et al.,[8] investigated the therapeutic effects of the chromic phosphate particle-based ^{32}P source in a

Address for correspondence:
Mr. Sridhar Sahoo,
Radiological Physics and Advisory Division, CT CRS Building,
Bhabha Atomic Research Centre, Mumbai-400 094,
Maharashtra, India.
E-mail: barcsridhar@gmail.com

Comment on "Design and bioevaluation of a ^{32}P-patch for brachytherapy of skin diseases" [Appl. Radiat. Isot. 66 (2008) 303–309]

We read with interest the article by Salgueiro et al. (2008) on the design and bioevaluation of a ^{32}P-patch for brachytherapy of skin diseases. The authors designed a ^{32}P patch source using phosphoric-^{32}P-acid and chromic ^{32}P-phosphate in combination with natural rubber or silicone. They evaluated its therapeutic efficacy (arrest of tumor growth and regression of tumors) using female Sencar mice.

The authors also carried out depth dose calculations by simulating the ^{32}P-silicone-patch source using the Monte-Carlo-based MCNP5 code (X-5 Monte Carlo Team, 2003). The density and chemical composition of the silicon patch are 1.2 g/cm^3 and SiC$_2$H$_6$O, respectively. The authors modeled the source as a cylindrical disc with dimensions 1 mm height and 5 mm diameter. ^{32}P beta particles were uniformly distributed in this disc. Skin was simulated as water of density as 1 g/cm^3. No details of scoring dimensions (radius and thickness) used in the Monte-Carlo calculations were provided in the study. Similarly, the initial beta spectrum of ^{32}P used in their calculations was also not mentioned. The activity per unit area of the ^{32}P source considered in the therapeutic studies was 10.6 MBq/cm^2. The surface area of the source is 0.19635 cm^2. Hence, the total activity of the source considered in their work was 2.081 MBq. The authors estimated the dose rate (Gy/h) at different depths (0.0001, 0.01, 4 and 7.5 mm) in water and reported the values in Table 1.

We repeated the depth dose calculations using the DOSRZnrc (Rogers et al., 2010) user-code of the EGSnrc Monte-Carlo code system (Kawrakow et al., 2010). In our calculations, the ^{32}P-silicone-patch source was positioned on a cylindrical water

phantom of dimensions 3 cm radius × 3 cm height. The source and the water phantom had a common axis. The schematic diagram of the geometry used in the Monte-Carlo simulation is shown in Fig. 1. The ^{32}P beta spectrum needed for the Monte-Carlo calculations was taken from the ICRU Report no. 56 (ICRU, 1997). Maximum energy of ^{32}P source is 1.71 MeV is considered in our simulation (Xu et al., 2012).

The PEGS4 data set needed for the Monte-Carlo calculations was generated by setting AE=0.521 MeV and AP=0.01 MeV, where the parameters AE and AP are the low energy thresholds for the production of knock-on electrons and secondary bremsstrahlung photons, respectively. We used EXACT boundary crossing algorithm and PRESTA-II electron-step algorithm in the simulations. In the Monte-Carlo calculations, absorbed dose per incident beta particle was scored, as a function of depth in water along the central axis. The scoring radius was 1 mm. The first 200 scoring slabs were of 1-μm-thick and the rest were of 10-μm-thick. The dose values in Gy/beta particle were subsequently converted to Gy/h by using the total activity of 2.081 MBq. Up to 5×10^8 particle histories were simulated. The 1σ statistical uncertainties on dose values at smaller depths were usually about 0.2%. The uncertainty on the dose value at 7.5 mm is as large as 20%.

A comparison of dose rate data against the values by Salgueiro et al. (2008) showed reasonably a good agreement for depths 0.0001 mm and 0.01 mm. For example, the EGSnrc-based values at depths 0.0001 mm and 0.01 mm are 11.57 and 11.28 Gy/h, respectively, whereas the corresponding values reported by Salgueiro et al. (2008) are 14.02 and 11.7 Gy/h. For the depths 4 mm and 7.5 mm, the published values are higher by a factor of about 22 and 3.6×10^4, respectively. In order to investigate this discrepancy, an auxiliary simulation was carried out, by assuming that the source particles were uniformly distributed on the bottom surface of the 5 mm diameter × 1 mm height silicone patch. In this calculation, the particles were distributed in 5 mm diameter × 1 μm height of the 5 mm diameter × 1 mm height silicone patch.

Table below compares the dose rate values as a function of depth in water against the published values. The number shown in the

Table 1
Comparison of Monte-Carlo-calculated dose rate (Gy/h) values for the ^{32}P-silicone-patch as a function of depth in water. The number shown in the parenthesis is the percentage error (1σ) on the calculated dose values. The published dose rate values had an uncertainty of < 1%.

Depth in water (mm)	Salgueiro et al. (2008)	This work	
		Source type 1[a]	Source type 2[b]
0.0001	14.02	11.57 (0.2%)	54.95 (0.05%)
0.01	11.7	11.28 (0.3%)	38.09 (0.05%)
4	2.3	0.11 (0.4%)	0.20 (0.3%)
7.5	1.2	3.35×10^{-5} (24%)	1.05×10^{-4} (15%)
1.4	–	2.3 (0.2%)	–
2.0	–	1.2 (0.3%)	–

[a] ^{32}P source particles uniformly distributed in silicone patch of diameter 5 mm and height 1 mm.
[b] ^{32}P source particles uniformly distributed on the bottom surface of the silicone patch of diameter 5 mm and height 1 μm.
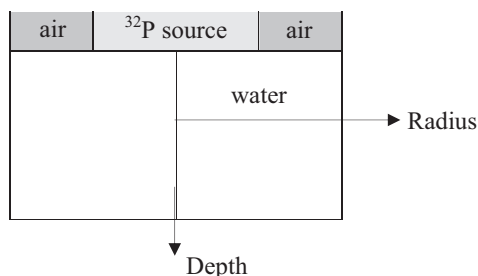

Fig. 1. Schematic diagram of the geometry used in the EGSnrc Monte-Carlo simulation. Figure also includes RZ-coordinate system (radius, depth) used in the simulation.

CALIBRATION OF EBT3 FILM FOR ITS USE AT ^{125}I ENERGIES

Sridhar Sahoo[1,3], Vandana S[1], Rajesh Kumar[1], T. Palani Selvam[1,3], Sunil Singh[2], D. Datta[1,3]

[1]*Radiological Physics & Advisory Division*
[2]*Radiation Safety Systems Division*
Bhabha Atomic Research Centre, Mumbai - 400 085, India
[3]Homi Bhabha National Institute, Mumbai- 400 094, India

Introduction: Gafchromic EBT3 film is widely used for dose measurement in radiotherapy due to its higher spatial resolutions, low energy dependency, dynamic range and easy handling. In the present study, the films were calibrated at[60]Co and 70 kV X-ray (effective energy is 30.5 keV) which is comparable to the mean energy 28.37 keV of ^{125}I source.

Materials and methods: EBT3 films (3 cm x 20 cm) were placed in air at the centre of 10×15 cm[2]X-ray field, at 1 m distance from the focal spot. The X-ray machine was operated at 70 kV potential and 30 mA tube current. The films were irradiated to doses of 0.5, 1.0, 2.14 and 5.1 Gy. A telecobalt unit was used to calibrate the EBT3 films. The output of machine was 1.98 Gy/min at 80.5 cm in water. The films (size 3 cm x 20 cm) were kept at depth of dose maximum in perspex phantom of size 30x30x20 cm[3]. Films were irradiated to doses of 0.5, 1.0, 2.14, 5.1, 9.46, 16.54 and 30 Gy using10×10 cm[2]field size.

The irradiated films were scanned using the EPSON Expression 10000 XL scanner with a resolution of 72 dpi after 24 h of irradiation. Films were scanned prior to irradiation to measure the optical density (OD) of the background image. Net optical density (NOD) was calculated by subtracting the OD of an unexposed film piece from the OD from exposed film. Films were analysed using ImageJ software. The energy response, R is the ratio of the NOD for a given dose of the 70 kV X-ray beam and the NOD for the same dose for ^{60}Co beam.

Results and discussion: The value of R is 0.92 for 50 cGy dose and 0.98 for dose range of 100-510 cGy. The dose response is within 2% for ^{60}Co and 70 kV X-ray for dose range of 100 - 510 cGy. The variation up to 8% was observed for dose of 50 cGy. Higher variation at lower dose may be attributed to lower sensitivity of EBT3 films. Hence, EBT3 films calibrated at ^{60}Co energy with higher dose (more than 50 cGy) is suitable for dosimetry of ^{125}I sources.

THE RESPONSE OF WELL CHAMBER TO PRESSURE VARIATIONS AT HIGH ALTITUDES - A MONTE CARLO STUDY FOR [169]YB SOURCE

Sridhar Sahoo[1,2], T. Palani Selvam[1,2], Arghya Chattaraj[1], D. Datta[1,2]
[1]Radiological Physics & Advisory Division
Bhabha Atomic Research Centre, Mumbai - 400 085, India
[2]Homi Bhabha National Institute, Mumbai- 400 094, India

Introduction: Well-type ionization chambers traceable to national standards laboratory are routinely used to measure air-kerma strength of brachytherapy sources. During routine measurements, a temperature and pressure correction factor (K_{TP}) is applied to account for the change of air density in chamber volume.

The air pressure, P is directly proportional to air density at a constant temperature. P falls exponentially with height, h (m) and is given by the Barometric formula $P=P_0 \exp(-Mgh/R(T+273.15))$, where P_0 is standard pressure (1013.2 mbar) at h=0, M is molecular mass (29 g/mol), g is acceleration due to gravity (9.8 m/s^2), R is the universal gas constant (8.314 J/mol. ^{0}K), and T is temperature in ^{0}C. For example, air density at Shimla (h=2276 m) is 0.94 kg/m^3, which is about 78% of standard air density of 1.197 kg/m^3.

Objectives: The K_{TP} corrected normalized response of a well chamber to air density variations at high altitudes for ^{169}Yb source is studied using the EGSnrc Monte Carlo code system. Simulations were also carried out using the FLUKA Monte Carlo code. The source model ^{169}Yb (4140 model, E_{avg}= 93 keV) developed for high dose rate application is considered in the work. In addition, the response of hypothetic well chamber made of graphite, copper and C-552 is also investigated.

Material and Methods: A cylindrical well chamber of 10 cm-diameter and 16 cm-height, made of an aluminum foil on the butyrate inner wall, an aluminum collecting electrode and outer wall. Well chamber with the investigated source is modeled in the CAVRZnrc user-code of the EGSnrc code system and FLUKA Monte Carlo code. Simulations are carried out for air densities ranging from 0.862 kg/m^3 (3048 m) to 1.197 kg/m^3. These air densities cover cities in the world at different altitudes including Indian cities mentioned in Table 1.

Beta-gamma spectrometry of indigenously developed ^{177}Lu patch source for superficial brachytherapy

Sridhar Sahoo[1], T. Palani Selvam[1], Rahul Tripathi[2], Rama P.[1], Gupta A. M.[3], Saxena S. K.[4] and Yogendra Kumar[4]

[1]Radiological Physics & Advisory Division, [2]Radiochemistry Division
[3]Health Physics Division, [4]Isotope Production & Applications Division
Bhabha Atomic Research Centre, Mumbai 400085, India

(Corresponding Author: Email: barcsridhar@gmail.com; Phone: +91-22-25598654)

Introduction: Isotope Production & Applications Division, BARC have developed Nafion-115 based ^{177}Lu patch source for its potential application in the treatment of skin cancer.[1] ^{177}Lu has a half life of 6.7 days and it emits beta particles with energies 498 keV (78.6 %), 385 keV (9.1 %) and 176 keV (12.2 %) along with low-energy photons 113 keV (6.4 %) and 208 keV (11 %). The moderate beta energy is effective in treating superficial tumor without delivering unnecessary dose to the normal tissues. Spectrum of a circular source (20 mm dia) was acquired using high resolution HPGe, Si(Li) detector and for liquid ^{177}Lu sample using liquid scintillation counting system. Measurement of activity was also carried out.

Materials and Methods: The ^{177}Lu source was produced by neutron irradiation of ^{176}LuO$_3$. ^{177}Lu activity is incorporated in a nafion membrane (130 μm thick) and immobilized with 40 μm plastic. The spectrum was generated by keeping the source at 30 cm distance from the HPGe detector for 100 secs (fig.1). The detector is calibrated using the standard gamma sources (^{60}Co, ^{137}Cs and ^{133}Ba). The activity A (mCi) of the source was derived using the equation: A = (N x 100 x 100) / (η x Pγ), Where N is the net count rate of the photo-peak of ^{177}Lu source, η is the photo peak efficiency of the detector for particular photo-peak, Pγ is the gamma emission probability.[2]

The activity concentration of a ^{177}Lu solution was measured with Hidex 300SL liquid scintillation counting system based on the triple-to-double coincidence ratio (TDCR) method. Sample was prepared with 12 ml AquaLight scintillator and 0.1 ml ^{177}Lu activity in 20 ml low-potassium borosilicate glass vial. Activity was calculated using TDCR value (0.97) and also verified with delayed counting with regular intervals. A beta spectrum generated is shown in fig.3. The spectrum was also acquired for 24 hrs using Si(Li) detector (fig.2).

Results and Discussion: A typical combined beta particle spectrum with end point energy around 498 keV was observed in the Si(Li) detector. In addition, low energy X-rays 54.6 keV, 55.8 keV, 63 keV, 63.2 keV, 64.9 keV, 112.9 keV and 208 keV gamma lines were also seen in the Si(Li) spectrum (Fig.2). The activity of ^{177}Lu patch source was found to be 0.51 and 0.50 mCi for 113 keV and 208 keV photon energies respectively from HPGe measurement. The activity of the ^{177}Lu liquid sample is found to be 13.6 kBq/ml (top curve of fig.3) and 6.4 kBq/ml (bottom curve of fig.3) after a delay of seven days. The beta spectra generated using coincidence counting will be useful for dosimetry using Monte Carlo techniques.
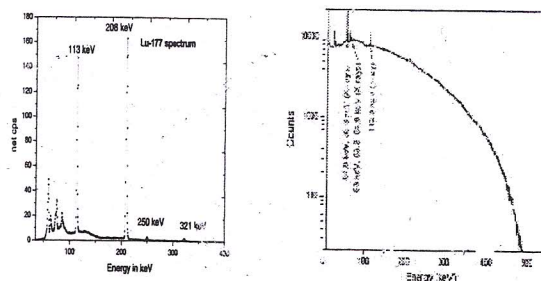

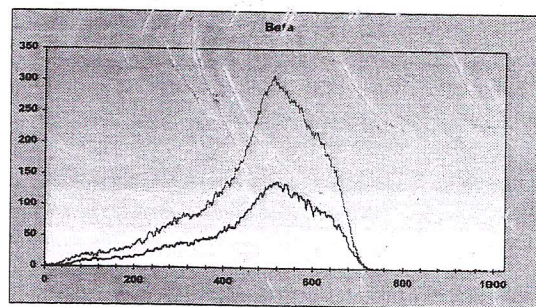**Fig.1 & 2. Gamma ray spectrum of ^{177}Lu source recorded on a coaxial HPGe and Si(Li) detector.**

Fig.3. ^{177}Lu beta spectra on liquid scintillation counting system Hidex 300SL (channel vs count).

References:

1. Saxena et .al.,(2015): Studies on the development of Nafion-115 based ^{177}Lu-patches for their application in superficial brachytherapy of skin cancer, Proceedings of NUCAR, 494-5.
2. IAEA, 1989 Regional workshop on environmental sampling and measurement of radioactivity for monitoring purpose, Kalpakam, India 85-92.

2

Dosimetry of indigenous developed ^{169}Yb brachytherapy seed source

<u>Sridhar Sahoo</u>[1], T. Palani Selvam[1], S. K. Saxena[2], A. Dash[2]

[1]Radiological Physics and Advisory Division, Bhabha Atomic Research Centre, Mumbai-400094, India
[2]Isotope Production and Applications Division, Bhabha Atomic Research Centre, Mumbai-400085, India

(Corresponding Author: Email: barcsridhar@gmail.com; Phone: +91-22-2559 8654)

Introduction: Isotope Applications & Production Division, BARC indigenously developed a procedure to fabricate ^{169}Yb seed source for the treatment of cancer.[1] This source can be prepared by encapsulating inactive Yb_2O_3 microspheres in titanium capsule and irradiating with neutrons in a reactor for a predetermined duration. The objective of this study is to calculate AAPM TG43 dosimetry parameters such as, air-kerma strength (S_k), dose rate constant (Λ), radial dose function g(r) and anisotropy function F(r,θ) for this brachytherapy source using the Monte Carlo method. [2] The calculated parameters were compared with ^{169}Yb HDR (model 4140) source. [3]

Material and Methods: The ^{169}Yb seed source was simulated using the MCNP 3.1 Monte Carlo code. The active part of the source consists of six Yb_2O_3 microspheres (0.65-mm-dia) arranged inside a 0.05-mm-thick titanium capsule (fig. 1). The active length is 3.9 mm. The total length is 4.75 mm and outer diameter is 0.8 mm. The initial photon spectrum needed for Monte Carlo calculation was taken from literature.[3] Photon cut-off energy in the simulation was 10 keV. The electron transport is not considered in the simulation. Water-kerma is calculated in a cylindrical water phantom (density = 0.998 g/cm^3) of 40 cm radius and 40 cm height. S_k is calculated in a free space sphere of radius 150 cm. 1x10^8 source photon histories are simulated in each simulation to get desired statistics. The dosimetric parameters such as Λ, g(r) and F(r,θ) were calculated as per the AAPM TG-43U1 report.

Results and Discussion: The calculated reference dose rate in water for BARC ^{169}Yb seed source is 1.38±0.09 cGy h^{-1} mCi^{-1}. The value of S_k in free space is 1.15 ±0.03 cGy h^{-1} mCi^{-1} cm^2. The value of Λ is 1.20 ± 0.1 cGy h^{-1} U^{-1}, where U is the unit of S_k (1U=1 cGy h^{-1} cm^2).

The values of $g_L(r)$ are calculated for radial distances, r=0.5-10 cm and fitted to a fifth order polynomial function, $g_L(r) = b_0+b_1r +b_2r^2+b_3 r^3+b_4r^4+b_5r^5$. The values of g(r) increases from 0.95 at r=0.5 cm to 1.19 at r=5.5 cm and falls to 1.08 at r=10 cm. Figure 2 compares the values of $g_L(r)$ for ^{169}Yb seed source (BARC) with ^{169}Yb HDR (model 4140) source for radial distances, r=0.5-10 cm. The values of F(r,θ) are calculated for radial distances, r=0.25 - 10 cm

between θ=0^0 and 180^0. Figure 3 compares the values of F(r,θ) for ^{169}Yb seed source (BARC) with ^{169}Yb HDR (model 4140) source for r=1 cm. Anisotropy is less pronounced for the BARC source when compared to the model 4140.
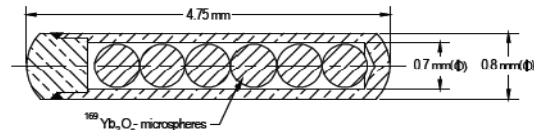
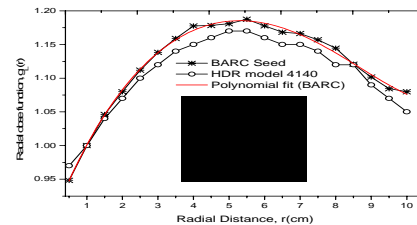

Fig. 1. Design of proposed ^{169}Yb BARC seed source.

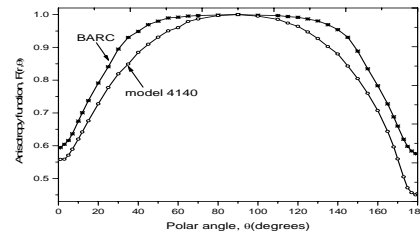**Fig. 2. Comparison of the $g_L(r)$ of ^{169}Yb BARC source with model 4140 source for r=0.5-10 cm.**

Fig. 3. Comparison of F(r,θ) of ^{169}Yb BARC source with model 4140 source for r=1 cm.

References:

1. Saxena S.K. et al. Feasibility studies for the development of ^{169}Yb-brachytherapy seeds: Emerging radiation sources for the management of cancer. Proceedings of symposium on Nuclear Analytical Chemistry, 2014; pp-352-353, Mumbai.

2. Rivard M.J. et al. Update of AAPM Task Group No. 43 Report: A revised AAPM protocol for brachytherapy dose calculations. Med Phys. 2004; 31: 633-674.

3. Medich D.C. et al. Monte Carlo characterization of an ytterbium-169 HDR brachytherapy source with analysis of statistical uncertainty. Med Phys. 2006; 33:163-172.